The use of small molecule modulators to enhance neuroplasticity through perineuronal net manipulation

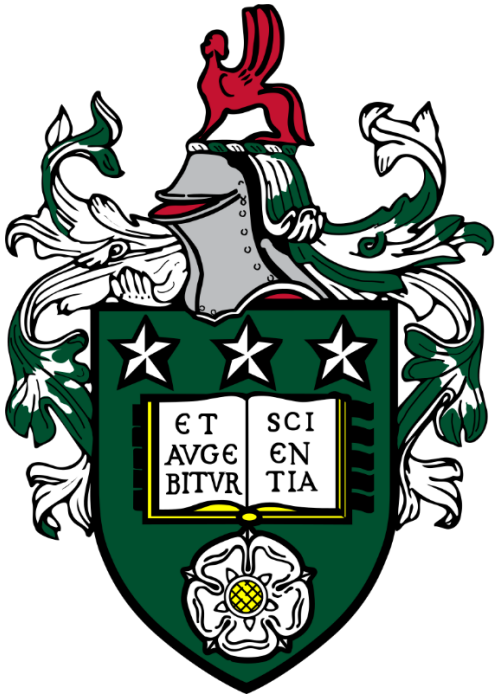

Janice Mei San Ng

Submitted in accordance with the requirements for the degree of

Doctor of Philosophy

The University of Leeds

School of Biomedical Sciences

January 2023

Intellectual Property Rights Statement

The candidate confirms that the work submitted is her own, except where stated below. The contribution of the candidate and the other authors to this work has been explicitly indicated below. The candidate confirms that appropriate credit has been given within the thesis where reference has been made to the work of others.

The 4-methylumbelliferone derivatives, termed “JD059” and “JD060”, were designed and synthesised by Dr. James Duncan in collaboration with Dr Richard Foster, School of Chemistry, University of Leeds.

Dr Jessica Kwok has a patent ‘Treatment of Conditions of the Nervous System’ (PCT/EP2020/079979) issued.

Covid-19 Statement

This work was conducted during the Covid-19 (SARS-CoV-2) pandemic of 2020. The consequent closure of the University campus, alongside national and international lockdowns in 2020 and 2021, had a significant impact on the progress of this study. To accommodate for this impact, the design and scope of the study were augmented.

Acknowledgements

There are many people who have been instrumental in my PhD journey. While I am proud of this thesis and the person I have become, my motivation and strength during the past few years are built upon the support of those around me.

I would like to thank my supervisor, Dr Jessica Kwok, for your guidance and tutorship. The first year of my PhD was tumultuous and full of uncertainty, and I am immensely grateful we stuck it out together. Thank you for allowing me to delve deeper into the world of PNNs, for encouraging critical thinking, and for helping me become a better scientist.

My sincere gratitude also goes to Prof Ronaldo Ichiyama, my co-supervisor. Thank you for your kindness, for all the laughs over silly competition shows, and for facilitating my passion in neural regeneration. Thank you to Dr James Duncan for synthesising the analogues used in this study and for helping me wade through all the chemistry involved, and a huge thanks to my colleagues who taught me invaluable technical skills.

An unwavering support system in the lab is indispensable for surviving a PhD. My biggest, most heartfelt thanks goes to Stuart, Ashleigh, and Lynda. I owe you all a debt of gratitude for consistently showering me with love and support, and for keeping me grounded. I know I have made friends for a lifetime. Special thanks to Cihan for your wonderful company; may we spend many more afternoons together chatting over Turkish desserts and coffee. Thank you to Sylvain for your encouragement, especially as I navigated through animal work. To Raphael and Josh, thank you for your friendships, and for the all the conversation over late night pints.

I could not have survived this journey without my family. My mum, sister, dad, my beloved 婆婆 and **公公**, and baby Eli—you have all been tirelessly cheering me on in all my endeavours for as long as I can remember. Thank you, endlessly, and I hope I have made you all proud. To my paternal **公公,** 爺爺 and 嫲嫲, I am sorry I did not finish in time for you to see this thesis. I will celebrate crossing this finish line with you in my heart.

Finally, to my partner, Tom. I am still searching for the words that could encapsulate your unwavering love and encouragement. Thank you for always believing in me when I (often) did not. Your love is like home to me, and you have made all the difference throughout this challenging, momentous journey.

Abstract

Perineuronal nets (PNNs) are aggregates of extracellular matrix (ECM) structures that envelope subpopulations of neurons in the adult central nervous system (CNS). They are particularly enriched in hyaluronan (HA) and chondroitin sulphate proteoglycans (CSPGs), which are imperative to PNN function. Apart from providing structural support, PNNs have been established to orchestrate the stabilisation of the mature neural circuitry and limiting neural plasticity. Removing PNNs could unlock CNS plasticity; however, non-invasive and safe methods have not been established. In this thesis, we have investigated the effects of an orally-administered, commercially available hyaluronan (HA) inhibitor, 4-methylumbelliferone (4-MU), on PNNs and plasticity, which has not been thoroughly explored. To further potentiate compound efficacy, we have collaborated with the School of Chemistry at the University and designed new derivatives of 4-MU. The effect of these novel derivatives, termed JD059 and JD060, on PNNs and plasticity have also been investigated.

To investigate the expression and morphology of PNNs, the PNN-HEK293 cell line was utilised, which has been established in the lab as an *in vitro* model of PNNs. Cells were stained with PNN markers: hyaluronan binding protein (HABP) and *Wisteria floribunda* agglutinin (WFA) to examine the effects of 4-MU, JD059, and JD060 is suppressing PNNs. Fluorescence intensity measurements show that PNNs were substantially reduced after treatment with all compounds in a dose-dependent manner. JD060 elicited the highest potency in reducing HA (96.9 ± 1.62% after 1 mM JD060 vs 82.2 ± 1.84% after 4-MU and 90.9 ± 8.20% after JD059, $p<0.05$) and WFA (43.3 ± 7.30% after 0.5 mM of JD060 vs 29.4 ± 2.36% after 4-MU and 30.6 ± 2.16% after JD059, $p<0.05$) when compared to the other two compounds. To assess the potential cytotoxic effects of the compounds, cell nuclei assessment and alamar metabolic assays were used. No adverse effects on nuclei morphology nor a reduction in metabolic rate were observed at the highest dose tested (i.e 1 mM).

4-MU binds to glucuronic acid (GlcA) and prevents its conjugation to uridine diphosphate (UDP), impeding the formation of UDP-GlcA, a key substrate for HA synthesis. While 4-MU is a known HA synthesis inhibitor, its effects on the synthesis of other glycosaminoglycans (GAGs) has not been fully investigated. To characterise the type of GAGs affected by 4-MU and its derivatives, GAGs were extracted from PNN-HEK293 cells after treatment with the small molecules. There was a significant reduction of total amount of GAGs in cells treated with all compounds. With the use of fluorophore-assisted carbohydrate electrophoresis

(FACE), the amount of GAG composition was analysed. Importantly, we reveal that 4-MU does not only attenuate the production of HA (47.6 ± 8.02% decrease after 1 mM 4-MU), but also chondroitin sulphates (CS) (28.0 ± 4.33% decrease). Similar to 4-MU, 1 mM of JD059 and JD060 caused a reduction of HA (55.1 ± 10.3 % and a 54.4 ± 3.02%, respectively) and CS (52.6 ± 9.17 % and a 62.9 ± 5.80%, respectively).

Finally, in order to assess the functional role of HA/CS reduction in axonal sprouting, an indicative *in vitro* measurement of neural plasticity, dissociated adult dorsal root ganglion (DRG) neurons were cultured on surfaces coated with GAGs isolated from PNN-HEK293 cells. DRG neurons cultured on surfaces with GAGs recovered from 4-MU-, JD059-, and JD060-treated cells showed longer neurite projections when compared to untreated conditions (367.7 ± 28.6 µm, 358.4 ± 34.9 µm, 412.2 ± 41.5 µm, respectively vs 200.9 ± 34.3 µm in untreated, $p<0.001$). This suggests that a reduction of HA/CS, inducd by the treatment of 4-MU and its derivatives, serves as favourable substrates for the sprouting of neurons.

Taken together, this thesis has shown that 4-MU, JD059, and JD060 have the capacity to ameliorate the inhibitory nature of PNNs on neural plasticity. The results provide new evidence that 4-MU is not only down-regulating HA, but also CS synthesis. The findings indicate that the small molecule inhibitors are safe and potent in reducing PNN formation for the potential enhancement of neural plasticity.

Table of Contents

List of figures and tables

Figures

Tables

Abbreviations

2-AMAC: 2-aminoacridone

4-MU: 4-methylumbelliferone

ACN: Acetonitrile

AM: acetoxymethyl

AMPAR: α-amino-3-hydroxy-5-methyl-4-isoxazolepropionic acid receptor

ANOVA: Analysis of variance

ASD: Autism spectrum disorder

BA: Basolateral

BCA: bicinchoninic acid assay

BDNF: Brain-derived neurotrophic factor

BSA: Bovine serum albumin

C4S: Chondrotin-4-sulphate

C6S: Chondroitin-6-sulphate

ChABC: Chondroitinase ABC

CNS: Central nervous system

CP: Critical period

CPC: Cetylpyridinium chloride

Crtl: Cartilage and proteoglycan link protein

CS: Chondroitin sulphate

CS56: Chondroitin sulphate 56

CS-GAG: Chondroitin sulphate glycosaminoglycan

CSPG: Chondroitin sulphate proteoglycan

CST: Corticospinal tract

DAPI: 4′,6-diamidino-2-phenylindole

DG: Dentate gyrus

DMSO: Dimethyl sulfoxide

DRG: Dorsal root ganglion

DS: Dermatan sulphate

ECL: Enhanced chemiluminescence

ECM: Extracellular matrix

EDTA: Ethylenediaminetetraacetic acid

EE: Environmental enrichments

GAG: Glycosaminoglycan

GalNAcT1: N-acetylgalactosaminyltransferase

GPI: Glycosylphosphatidylinositol

HA: Hyaluronan

HA: Hyaluronan

HABP: Hyaluronan binding protein

HAPLN: Hyaluronan and proteoglycan link protein

HAS: Hyaluronan synthase

HEK293: Human embryonic kidney 293

HRP: Horseradish peroxidase

HS: Heparin/heparan sulphate

HSPG: Heparin sulphate proteoglycan

KS: Keratin/keratan sulphate

LA: Lateral

LAR: Leukocyte common antigen-related

LDS: Lithium dodecyl sulfate

LDH: Lactate dehydrogenase

LMW: Low molecular weight

LTD: Long-term depression

LTP: Long-term potentiation

L-VDCC: L-type voltage-dependent calcium channels

MD: Monocular deprivation

mGluR: Metabotropic glutamate receptors

MMPs: Matrix metalloproteinases

MMSE: Mini-mental State Examination

NCAM: Neural cell adhesion

NDS: Normal donkey serum

NGF: Nerve growth factor

NMDAR: N-methyl-D-aspartate receptors

NPC: Neural precursor cell

NPTX: Neuronal pentraxin

OD: Ocular deprivation

Otx2: Orthodenticle Homeobox 2

PBS: Phosphate buffered saline

PFA: Paraformaldehyde

PG: Proteoglycans

PNN: Perineuronal net

PNN-HEK293: Perineuronal net-human embryonic kidney 293

4-MU: Perineuronal net inhibitor

PTPσ: Protein tyrosine phosphatase-sigma

PV: Parvalbumin

PVDF: Polyvinylidene fluoride

RGC: Retinal ganglion cells

RIPA: Radioimmunoprecipitation Assay

RPM: Revolutions per minute

SCI: Spinal cord injury

SDS-PAGE: oSdium dodecyl sulfate-polyacrylamide gel electrophoresis

SEC: Size exclusion chromatography

Sema3A: Semaphorin 3A

STED: Stimulated emission depletion

TBS: Tris buffered saline

TBS-T: Tris buffered saline with tween

TCA: Trichloroacetic acid

TEMED: Tetramethylethylenediamine

TGS: Tris-glycine SDS

TN-R: Tenascin-R

TrkB: Tropomyosin receptor kinase B

TSP: Thrombospondins

UDP: Uridine diphosphate

UGT: Glucuronyltransferase

VIP: Vasoactive intestinal peptide

WFA: *Wisteria floribunda* agglutinin

Chapter 1: Introduction

1.1 Neural plasticity

With its astonishing information-processing prowess, there is arguably nothing more complex than the human central nervous system (CNS). The CNS possesses a kaleidoscope of different cell types. This includes approximately 100 billion neurons, which are the main communication units of the CNS. Each neuron has the capacity to form hundreds of thousands of synapses with other cells. Together, these highly complex and organised neural networks are specialised for the rapid conveyance of nerve impulses precisely and accurately. It has been the endeavour of neuroscientists to decipher the dynamics of neural networks in order to understand how our CNS functions, or how dysfunction leads to disease, for decades. Whilst much progress has been made on uncovering the inner workings of the brain, substantial gaps of knowledge remain. One such example is how neural plasticity shapes CNS function, and how this capacity may be harnessed in events of CNS injury and dysfunction.

Plasticity of the CNS is a crucial component of the system to adapt to rapidly-changing internal or external stimuli. Such adaptations may be short-lasting or enduring, and can generally describe maturation and development, learning, and compensatory modifications in response to physiological losses from aging, disease, or trauma. While neural networks in the CNS have the capacity for such plasticity, there is equally several physiological "brakes" to ensure stability and consolidation of neural information, one of which being the perineuronal net (PNN), elaborated in detail below (chapter 1.5). Indeed, the CNS extracellular milieu is one of the cardinal factors that influence neural plasticity. For the purposes of this work and for brevity, we will focus on two broad forms of plasticity: synaptic and structural plasticity (including neurogenesis), both of which have been shown to be influenced by the CNS extracellular matrix (ECM) and perineuronal nets (PNNs).

1.1.1 Synaptic plasticity

Synaptic plasticity describes the modification of synaptic strength or efficacy (Citri and Malenka, 2008; Magee and Grienberger, 2020), such as altering, for example, the number of receptors of the postsynaptic site. Long-term potentiation (LTP) is a biological process by which high frequency input results in the long-lasting increase in signal transmission between

neurons (Hu and Jhamandas, 2020), and is an extensively-studied form of synaptic plasticity. LTP exhibits cooperativity, induced by the concomitant activation of numerous synapses. LTP also exhibits associativity, wherein a weak stimulus could be reinforced if associated with a strong one. In contrast, long-term depression (LTD) describes a long-lasting decrease in synaptic transmission as a result of prolonged low frequency input. LTP and LTD are triggered by the activation of *N*-methyl-D-aspartate (NMDA) receptors (NMDARs). Fast excitatory neurotransmission in the mammalian brain is mostly mediated by the AMPA (α-amino-3-hydroxy-5-methyl-4-isoxazolepropionic acid) receptor (AMPAR) at the postsynaptic membrane. During synaptic transmission, calcium influx through NMDARs and the resultant increase in calcium in the dendritic spine triggers a cascade of events that drive synaptic plasticity (Citri and Malenka, 2008; Bear *et al.*, 2016) (Figure 1).

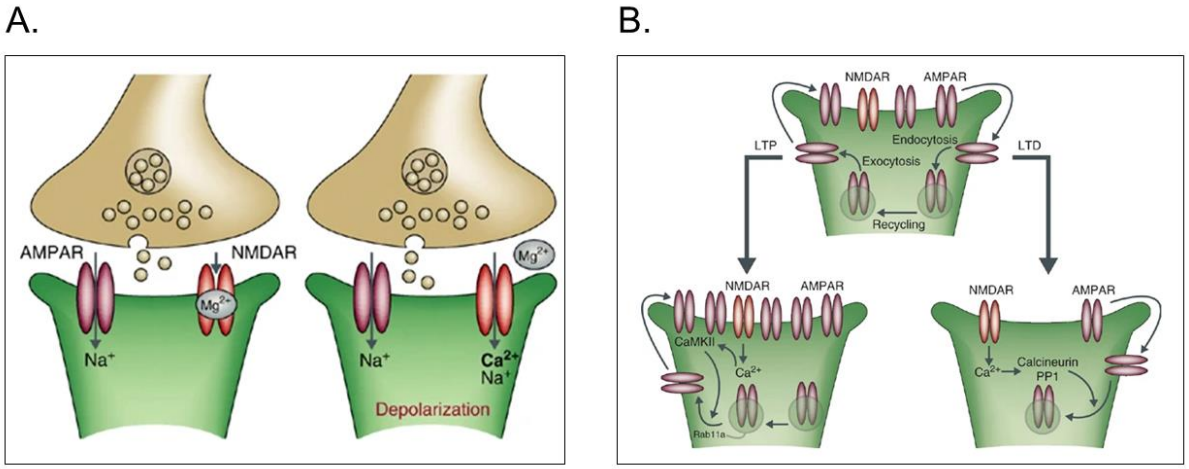

Figure 1. Mechanisms of LTP and LTD. A. During basal synaptic transmission at exctitatory synapses, glutamate is released from the presynaptic terminal and binds to both AMPARs and NMDARs. Na^+ flows through AMPARs but not NMDARs due to the existing Mg^{2+} block on NMDARs. During depolarisation of the postsynaptic cell, the Mg^{2+} block is lifted, allowing Na^+ and Ca^{2+} to enter the cell. The resultant dendritic increase of Ca^{2+} is required for driving synaptic plasticity. **B.** In the basal state (illustrated on top), receptors are constitutively cycled between synapses and the cellular cytosol. This is achieved as receptors possess lateral mobility. Once internalised, receptors are sorted for either degradation or endocytosis and reinsertion at synapses. During LTP, receptors undergo the endosomal pathway to enhance exocytosis and stabilisation at the synapse. This process involves CaMKII and Rab11a-mediated fusion of endosome fusion. This also leads to the phosphorylation of AMPARs, which enhances its mobility, recruitment to the synapses, and conductance. The induction of LTD activates the phosphatases, namely calcineurin and protein phosphatases 1 (PP1), and AMPAR endocytosis. This enhances the removal of AMPARs from the surface. Figure adapted from Citri and Malenka, 2008.

1.1.2 Structural plasticity

Structural plasticity, also known as anatomical plasticity, generally refers to the diverse range of anatomical remodelling of the neural circuit, occurring from the synaptic level to that of neuronal populations. These modulations include the structural alterations at synapses, the formation and elimination of synapses, of neuronal and dendritic processes, or of neurons and dendrites themselves.

One form of structural plasticity is the modulation of the number and degree of dendritic sprouting (Figure 2). Most excitatory synapses occur on these actin-rich protrusions; therefore, synapse pruning are inextricably linked to the structural remodelling of spine morphology (Hayashi and Majewska, 2005; Reza-Zaldivar *et al.*, 2020). Dendritic spines can be contacted by en passant presynaptic terminals, and are surrounded by astrocytic processes and glia. Alterations in spine morphology in response to changes in neural activity has long been documented. For instance, visual deprivation in rabbits caused a loss or deformity of the characteristic terminal enlargement of dendritic spines, a finding recorded as early as 1967 (Globus and Scheibel, 1967). Mice subjected to complete light deprivation possessed a decreased number of spines per dendritic segment (Valverde 1971). Similarly, spine density increases in response to an increase in sensory stimulation by means of continuous illumination (Parnavelas, 1978). Indeed, the study of spine plasticity has evolved tremendously since these early pivotal studies, especially with the development of advanced imaging techniques. 2-photon *in vivo* imaging revealed the formation and elimination of a small proportion of dendritic spines in CA1 neurons over a period of 16 days in adult mice (Gu *et al.*, 2014). Stimulated emission depletion (STED) microscopy has enabled the visualisation of dendritic structural changes in real time, such as changes in spine size and shape in organotypic hippocampal slices (Nägerl *et al.*, 2008), and *in vivo* (Berning *et al.*, 2012; Willig *et al.*, 2014).

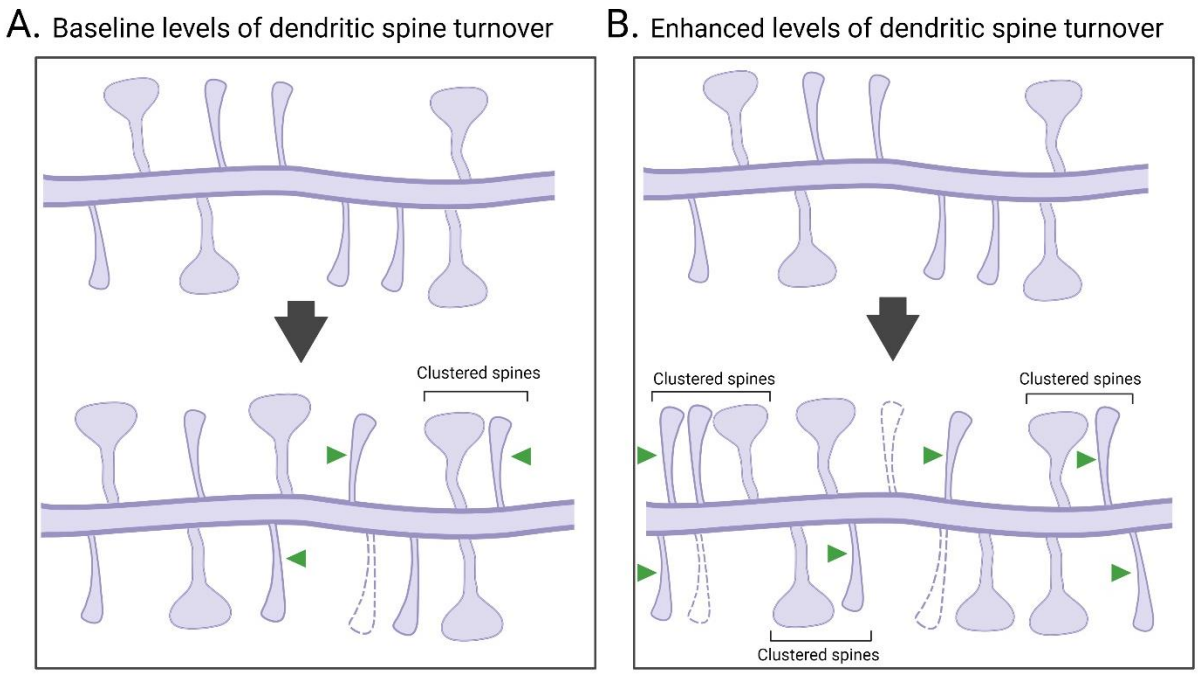

Figure 2. Schematic illustrating spine turnover under various conditions. Mature spines are depicted with a "mushroom" head, whereas immature spines are depicted as filopodial and thin spines. A. Under baseline conditions, there is continual turnover of spines, which includes both loss of spines (dashed spines) and gain of new ones (indicated by green arrows). B. Under conditions of enhanced plasticity, spine turnover is promoted, causing an increased formation and elimination of dendritic spines. Under both conditions, new spines formed can occur in clusters. Whilst connectivity dynamics are altered, the density of spines can remain unchanged.

Motor learning has been demonstrated to promote spine turnover (Xu *et al.*, 2009; Yang *et al.*, 2009), underscoring the importance of eliminating excessive and perhaps imprecise synaptic connections during learning. In a 2009 study, training in a forelimb reaching task resulted in the generation of postsynaptic dendritic spines on pyramidal neurons in the motor cortex in one-month old within an hour (Xu *et al.*, 2009). Novel skill learning also induced enhanced spine formation and elimination in adult mice, suggesting that dendritic pruning occurs during motor learning. Similarly, learning and novel sensory stimuli promoted spine pruning, and that this remodelling correlated with improvement in motor tasks (Yang *et al.*, 2009). Rotarod or treadmill training, new spines are formed on a subset of apical tuft branches of layer V pyramidal neurons (Yang *et al.*, 2014). This branch-specific dendritic plasticity during learning is also corroborated by the work of Cichon and Gan, wherein motor learning tasks induced dendritic calcium spikes on specific apical tuft branches on layer V in the motor cortex of awake, behaving mice (Cichon and Gan, 2015). Moreover, spine-

clustering appears to be an important facet of structural plasticity, especially in the context of learning and memory (Govindarajan *et al.,* 2006; DeBello *et al.,* 2014; Kastellakis *et al.,* 2015) (Figure 1). *In vivo* 2-photon microscopy of mice revealed that pre-learning the ratio of spine turnover (proportion of formed and lost spines) during prelearning correlated with levels of future contextual learning and memory as well as learning rate (Frank *et al.,* 2018), solidifying the notion that spine turnover is important in learning and memory. Importantly, this study showed that trained animals in contextual learning possessed an increase in the number of new spines that were clustered. Clustered spine formation occurred throughout training, but frequency increased with additional days of training, showing that acquisition of more information is concomitant with increase in spine clustering (Frank *et al.,* 2018). A combination of electrophysiology and calcium imaging showed that a pair of clustered synapses were more likely to be coactive than synapses that were further apart (Kleindienst *et al.,* 2011), reaffirming the importance of the spatiotemporal organisation of spines and synapses.

Importantly, evidence suggests that dendritic plasticity is reduced in models of disease or ageing. Indeed, elimination of spines in motor and sensory cortices were higher in old mice (> 20 months) than in mature adult (8-10 months) and young mice (3-5 months), indicating that the total spine number in old mice was low (Huang *et al.,* 2020). During motor learning, old mice had both fewer spines formed and lower Ca^{2+} activity in layer V of the motor cortex in comparison to younger mice. Such findings were demonstrated in non-humans primates as well; indeed, older rhesus monkeys had decreased number of spines on pyramidal cells and decreased density of axospinous spines in layer III of the dorsolateral prefrontal cortex (Dumitriu *et al.,* 2010). In tissues of aged humans, the presence of Alzheimer's pathology correlated with increased dendritic spine length, reduced thin spine head diameter, and enhanced filopodia density (Boros *et al.,* 2019). Intriguingly, increased thin spine head diameter correlated with better Mini-mental State Examination (MMSE) scores—a test commonly used to assess cognitive function in patients with memory impairment or dementia. Using human tissues with Alzheimer's pathology, Mijalkov and colleagues additionally discovered that the presence of tau pathology in CA1 pyramidal neurons determines the loss of dendritic spines in clusters, wherein spines were reorganised into shorter and smaller communities (Mijalkov *et al.,* 2021).

Studies of neurons from human epilepsy tissues revealed a decrease in spine density (Swann *et al.,* 2000; Bothwell *et al.,* 2001), and dendritic trees were found to be sparser (Bothwell *et*

al., 2001). In the context of autism spectrum disorder (ASD), spine densities of pyramidal cells within layers II of the frontal, temporal, and parietal lobe of the cortical location and layer V of the temporal lobe were increased in ASD subject tissues (Hutsler and Zhang, 2010). In agreement with this finding, mouse models of ASD displayed enhanced spine density and clustering (Ash *et al.*, 2021). The pathological detriment of excessive clustering and stabilization in ASD is not well-researched, but it may potentially explain the rigid and restricted behavioural repertoire that is commonly displayed in ASD (Ash *et al.*, 2021). What these studies highlight is that spine and synaptic turnover are intricate, well-orchestrated processes that form a synchronous and functioning neural circuit. Intuitively, the disruption of the balance of these processes underscores aberrant circuit function and numerous CNS disorders. Therefore, these neural circuits are not rigid and hard-wired, but malleable structures subject to continuous change and plasticity.

Astrocytes are emerging as vital regulatory elements contributing to structural plasticity. Astrocytes intimately interact with synapses, both structurally via the astrocytic processes that ensheathe dendritic spines and presynaptic terminals, and functionally through their ability to release signalling molecules and respond to neurotransmitters (Papouin *et al.*, 2017; Liu *et al.*, 2021; Lawal *et al.*, 2022). Astrocytes in the human CNS are remarkably intricate; intriguingly, as brain size and complexity increased, so did the overall size and degree of elaboration of astrocytes (Oberheim *et al.*, 2006; Oberheim *et al.*, 2009). Indeed, whilst a single mouse astrocyte can associate with 100,000 synapses, an individual human astrocyte can interact with over 1 million synapses (Bushong *et al.*, 2002; Oberheim *et al.*, 2009).

Stimuli that induce long-term potentiation and calcium signalling in astrocytes promoted peridendritic astrocytic process motility both *in vitro* and *in vivo* (Perez-Alvarez *et al.*, 2014) These events relied on the activation of Group I astrocytic metabotropic glutamate receptors (mGluRs). Retinal ganglion cells (RGCs) cultured in astrocyte-conditioned media possessed an increase in the number of synapses, which could be due to the release of thrombospondins (TSPs) (Christopherson *et al.*, 2005; Eroglu, 2009). Similarly, astrocytes induced an increase in GABAergic synapses in hippocampal neurons, whilst also increasing the neurite outgrowth of the neurons themselves (Hughes *et al.*, 2010). This observed promotion of GABAergic synaptogenesis is likely mediated by TSP release, *as* previously discussed.

1.1.3 Neurogenesis

In particular regions of the CNS, most notably the hippocampus, neuroplasticity also comprises neurogenesis (Kempermann *et al.,* 2004; Gage, 2019). Neurogenesis is the generation of neurons through the division of neural stem cells and subsequent maturation into neural progenitor cells, which then migrate and mature into neurons (Figure 3). These mature neurons are then integrated into established neural circuits. Once thought to be restricted to embryonic development, neurogenesis has now been established to occur throughout adulthood in the mammalian CNS in discrete brain regions. These regions with sustained adult neurogenesis are the dentate gyrus (DG) of the hippocampus and the subventricular zone of the lateral ventricles (Kempermann *et al.,* 2004; Abrous *et al.,* 2005; Gonçalves *et al.,* 2016; Toda *et al.,* 2019).

Research into adult neurogenesis and the factors that influence this dynamic process continues to flourish because of its therapeutic implications. External stimuli, for instance, has been shown to induce neurogenesis-dependent reorganisation of hippocampal neural circuity. An enriched environment (EE), including a spacious cage area, novel objects, and running wheels, has been shown to dramatically increase the number of adult-born within the granule cell layer (Kempermann *et al.,* 1997), increases the number of mature neurons in the DG (Komitova *et al.,* 2005; Olson *et al.,* 2006), and improves spatial learning in rodents (Kempermann *et al.,* 1997). EE has also been shown to increase dendritic number, length, and projections to the CA3 region of most mature adult newborn neurons in mice models of Alzheimer's disease (Valero *et al.,* 2011). Exercise leads to an increase in precursor cellular proliferation (Olson *et al.,* 2006; Fabel *et al.,* 2009), increased neurogenesis and attenuates apoptosis in the DG (Kim *et al.,* 2010).

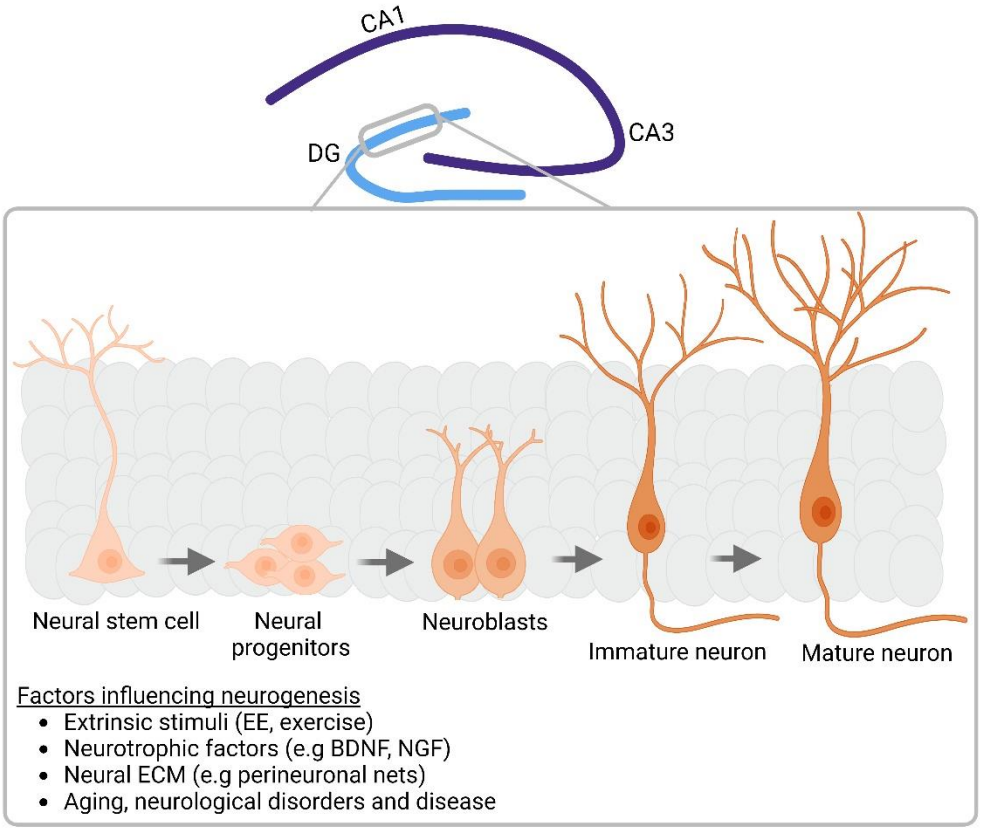

Figure 3. Schematic representation of adult neurogenesis in the hippocampal dentate gyrus. Adult neural stem cells in the hippocampus become activated and differentiate through intermediate neural progenitors to ultimately give rise to mature neurons. Neurogenesis is differentially influenced by a battery factors, some of which are listed and discussed in this review. *DG, dentate gyrus; EE, enriched environment; BDNF, brain-derived neurotrophic factor; NGF, nerve growth factor; ECM, extracellular matrix.*

Intrinsic neurotrophic factors, such as brain-derived neurotrophic factor (BDNF) and nerve growth factor (NGF), play integral roles in stimulating neural stem cell activation, proliferation, differentiation and overall CNS development (Auld *et al.*, 2001; Reichardt , 2006; Weissmiller *et al.*, 2012). In primates, BDNF and NGF are expressed by astrocytes within the subventricular zone (Tonchev *et al.*, 2011), although BDNF is also highly expressed in neurons in the DG (Li *et al.*, 2008). BDNF promotes neurogenesis by inducing cell survival (Lee at al., 2007) and proliferation (Katoh-Semba *et al.*, 2002; Lee *et al.*, 2008). Neurogenesis is abolished by BDNF knockdown in the DG using lentiviral-mediated RNAi (Taliaz *et al.*, 2010), but is increased in response to exogenous BDNF introduction (Scharfman *et al.*, 2005). BDNF has also been proven to influence late phases of neuronal differentiation in adults, in that dendritic development of adult-born granule cells is obstructed in BDNF conditional mutants (Chan *et al.*, 2008). Furthermore, BDNF deletion causes decreased dendrite growth in adult-born

hippocampal neurons (Wang *et al.*, 2015). The intraventricular administration of NGF in aged mice increased the number of neural progenitor cells (Fiore *et al.*, 2002), and intransal administration of NGF promoted the survival of newly generated cells in the subventricular zone of adult rat models of focal ischaemia (Zhu *et al.*, 2010). This corresponded to an improvement in functional recovery of injured rats.

1.1 Perineuronal nets

The ECM consists of a dense substrata, occupying the parenchyma of virtually all cells, and comprises a diverse spectrum of molecules (Table 1). Its functions extend beyond than being a supportive framework—it actively moulds the CNS by mediating cell migration (Hartman *et al*. 2017), axon regrowth and guidance, synaptogenesis (Lu *et al*. 2011, Burnside and Bradbury 2014, George & Geller 2018). In adulthood, it maintains synaptic stability and restricts aberrant reorganisation of the CNS (Burnside and Bradbury 2014, Ahuja and Fehlings 2016, Haggerty *et al*. 2017). Some of this CNS ECM is remodelled around a subset of neurons to yield unique and specialised structures known as perineuronal nets (PNNs) (Kwok *et al*. 2011, van 't Spijker and Kwok 2017).

Table 1. Types of Biomolecules in the neural ECM

Fibrous proteins	Collagen, elastin, fibronectin, vitronectin
Glycosaminoglycans (GAGs)	Hyaluronan (HA), chondroitin sulphate (CS), heparan sulphate (HS), dermatan sulphate (DS), keratin sulphate (KS)
Proteoglycans	Aggrecan, neurocan, brevican, and versican
Glycoproteins	Tenascin R, tenascin C, neural cell adhesion molecule (NCAM)

The neural ECM changes vastly during maturation and ageing; for instance, PNNs are formed during the postnatal period. Further alterations in the composition and condensation of the neural ECM occur, which substantially distinguishes the PNN from the diffuse ECM. First, PNNs are particularly saturated in chondroitin sulphate proteoglycans (CSPGs) and hyaluronan (HA). Approximately 2% of the CSPGs present in the general ECM of the mammalian CNS are present in the PNN. The remaining 98% of CNS CSPGs exist as part of the general, diffuse CNS ECM (Deepa *et al.*, 2006). The diffuse ECM contains multiple CSPGs together with extensive chains of HA, tenascin-C and tenascin-R. The condensed matrix of PNNs contains

these ECM molecules with the addition of one or more link proteins, known as hyaluronan and proteoglycan link protein 1 and 4 (Hapln1 and Hapln4) and greater amounts of tenascin-R. This ensemble forms a dense, honeycomb-like, pericellular structure (Carulli *et al.,* 2006, 2007; Deepa *et al.,* 2006; Galtrey *et al.,* 2008; Kwok *et al.,* 2010; Fawcett *et al.,* 2022).

Finally, PNNs possess a unique sulphation pattern that separates them from the general diffuse neural ECM. In particular, C6S comprises 2% of the diffuse ECM and 5% in the PNNs, C4S comprises 91% of the diffuse ECM and 81% in the PNNs, and C4, 6S (CS-E) is 1.4% in the difuse ECM, 2.1% in PNNs (Deepa *et al.,* 2006). The unique sulphation patterns of PNNs endow them with the capacity to have specific binding properties (Deepa *et al.,* 2006, Yabuno *et al.,* 2015). This enables PNNs to bind specifically to numerous effectors; for example, CS-E binds with high affinity to effectors such as semaphorin (sema) Sema3A, an axon guidance molecule, and orthodenticle homeobox 2 (Otx2), a transcription factor related to juvenile plasticity. These molecules are therefore concentrated in PNNs where they can affect synapse dynamics, PV cell maturity, and neural network plasticity (Vo *et al.,* 2013; Bernard and Prochiantz, 2016, Beurdeley *et al.,* 2012; de Winter *et al.,* 2016, van't Spijker *et al.,* 2017). There are also slight differences in the sulphation pattern of HSPGs between the diffuse matrix and PNNs: overall sulphation of HSPGs is 0.54 per disaccharide and 0.67 per disaccharide, respectively (Deepa *et al.,* 2006).

1.3 The structure of PNNs

Determining the structure of PNNs is tremendously vital to illuminate its biochemical and biophysical properties, which facilitates our understanding of their manipulation. PNNs were first described as a reticular structure that enveloped the cell bodies and extensions of neurons. Long believed to be a static ECM structure, the PNN is now understood to be a highly dynamic assembly of proteoglycans and a selection of proteins (Kwok *et al.* 2011, van 't Spijker and Kwok 2017, Wen *et al.* 2018) (Figure 4). Its formation begins with a HA backbone, synthesised by HA synthases expressed on the surface of neurons. The HA backbone enables the attachment of CSPGs; among the CSPGs, the lectican family members neurocan, aggrecan, brevican, and versican are principal components of PNNs. Aggrecan is likely an indispensable component of PNNs in the cortex—in dissociated cortical cultures derived from knockout mice lacking aggrecan, PNNs were not detected as demonstrated by the elimination of WFA staining (Giamanco *et al.* 2010). Moreover, it has recently been proposed that aggrecan sulfation patterns regulate its stability, and by extension, the formation of PNNs (Miyata and Kitagawa

2016). HAPLNs are recruited to stabilise the attachment of the CSPGs to the hyaluronan backbone. Tenascin-R, a member of the tenascin family of extracellular matrix glycoproteins, links the CSPGs together via their C-terminals (Morawski *et al.* 2014). The complex assembly of these molecules forms PNNs of great diversity. The heterogenic nature of PNNs is further amplified by other modifications—for instance, CS chains exist in varying sulfation patterns and CS and HA chain length (Sorg *et al.* 2016; Miyata *et al.* 2018). To further add to the complexity of PNNs, PNNs also bind to Sema3A and Otx2 (Figure 4). Sema3A is produced widely by neurons and surrounding tissue in the adult CNS but is highly localized to the PNNs, where it binds with great affinity to 4-sulphated, 6-sulphated (CS-E) motifs on the CS chains. This interaction brings it into association with the synaptic terminals on PNN-bearing PV^+ cells, where it can augment and fine-tune synapses and connectivity (Vo *et al.*, 2013; de Winter *et al.*, 2016). Otx2 is a cell-permeant diffusible transcription factor that modulates the development of PV^+ interneurons and maturation of PNNs. Otx2 also binds preferentially to the 4-sulphated, 6-sulphated CS motifs in CS glycosaminoglycans (GAG) chains (de Winter *et al.*, 2016). After binding to PNNs, Otx2 is then internalised by the cell to mediate its regulatory role in PNN maturation and plasticity (Beurdeley *et al.*, 2012) (Figure 4). Other signalling proteins, such as reelin (Berretta *et al.*, 2015; Lensjø *et al.*, 2017) and Narp (Chang *et al.*, 2010; Van't Spijker *et al.*, 2019), are also trapped within the PNN matrix.

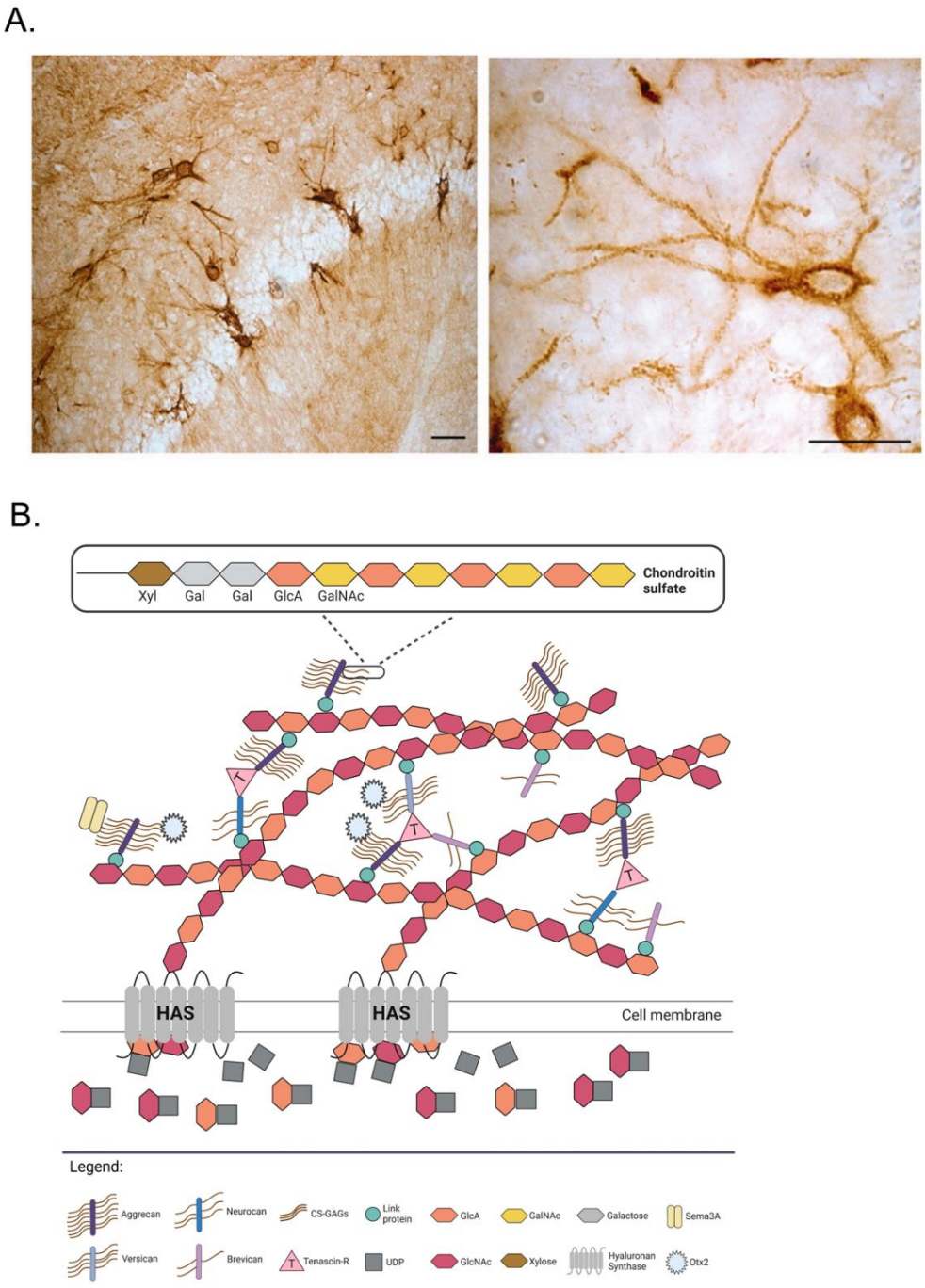

Figure 4. **The structure of the PNN. A.** PNNs stained with WFA in rat brains. **B.** Lecticans are tethered to a hyaluronan backbone via link proteins. HAS catalyses the synthesis of hyaluronan and anchors hyaluronan chains to the neuronal membrane. CSPGs are anchored to HA chains via link proteins. Tenascin-R enhances cross-linking of lecticans, contributing to the structural integrity of the PNN. Part A adapted Kwok *et al.*, 2011. Scale bar, 50 μm. *HAS, hyaluronan synthase; CS-GAGs, chondroitin sulphate glycosaminoglycans; UDP, uridine diphosophate; GlcA, glucuronic acid; GlcNAc, N-acetylglucosamine; GalNAc, N-acetylgalactosamine; Sema3A, semaphorin 3A; Otx2, orthodenticle homeobox 2.*

Identifying the neuronal populations that bear PNNs is crucial to the comprehension of their functional role in CNS plasticity. PNNs predominantly ensheathe fast-firing inhibitory interneurons expressing PV in the brain (Schüppel *et al.*, 2002; Dityatev *et al.*, 2007), which exert a crucial influence in the sculpting of neuronal circuit activity patterns by mediating inhibitory plasticity. PNNs are also found around glutamatergic neurons (Wegner *et al.*, 2003; Mészár *et al.*, 2012; Horii-Hayashi *et al.*, 2015; Vazquez-Sanroman *et al.*, 2015; Yamada *et al.*, 2015) and other fast-spiking neurons, such as those in the medial nucleus of the trapezoid body (MNTB) (Balmer, 2016) and the excitatory neurons in the deep cerebellar nucleus (Edamatsu *et al.*, 2018; Hirono *et al.*, 2018; Carulli *et al.*, 2020) and in the hippocampus (Lensjø *et al.*, 2017). Strikingly, ~80% of neurons in the CA2 of the hippocampus enwrapped by PNNs also expressed CamKII (Lensjø *et al.*, 2017). In the medial entorhinal cortex, PNNs colocalised to reelin-expressing stellate cells as well as PV^+ interneurons (Lensjø *et al.*, 2017). In the spinal cord, PNNs surround approximately 30% of the motoneurons in the ventral horn and 20% of neurons in the dorsal horn (Galtrey *et al.* 2008; Ritok *et al.*, 2022). Of these motoneurons, a significant proportion (approximately 72%) are alpha motoneurons (Irvine & Kwok 2018), which innervate force-generating extrafusal muscle fibres of the skeletal muscle.

1.4 PNNs regulate synaptic and structural plasticity

Among the PNN components, CSPGs and HA are some of the most studied constituents in mediating neural plasticity. Enzymatic removal of CS-GAGs and HA increased the lateral diffusion of AMPARs and prompted the exchange of desensitised receptors for naïve, functional ones on mature neurons (Frischknecht *et al*, 2009), and that the movement of AMPARs may be influenced by the interaction between brevican and the GluA1 subunit of the AMPARs (Favuzzi *et al.*, 2017). It is worth noting that this observation was absent on apsiny glutamatergic synapses on interneurons neurons and suggests that intracellular calcium levels are more important (Klueva *et al.*, 2014), reflecting intricately diverse roles of the PNN components for different neural populations. In a comprehensive study conducted in 2018, Yamada and colleagues highlighted that CSPGs were vital for the formation and differentiation of neurons in adulthood (Yamada *et al.*, 2018). Neural stem cells and progenitors were ensheathed by CSPGs; depletion of CSPGs using bacterial lyase chondroitinase ABC (chABC) reduced the number of neuronal progenitors and newborn granule cells, and inhibited maturation of newborn granule cells. In mice lacking *N*-acetylgalactosaminyltransferase 1 (GalNAcT1), an important enzyme for CSPG synthesis,

densities of newborn granule neurons were also reduced. Exposure to EE induced adult neurogenesis, and this was associated with an elevated synthesis of CSPGs (Yamada *et al.*, 2018). CSPGs also attach to neurotrophic factors, such as fibroblast growth factor-2 (FGF-2) and BDNF (Karumbaiah *et al.*, 2015), which may facilitate the regulatory roles of these factors on adult neurogenesis as discussed above. CSPG digestion additionally causes a recovery of dendritic spine density adult amblyopic rats (Pizzorusso *et al.*, 2006; de Vivo *et al.*, 2013). These studies highlight the immensely complex role in the balance of plasticity and consolidation in the neural circuitry, especially in adulthood.

HA has been found to be enriched in the subgranular zone (Su *et al.*, 2017); furthermore, neural stem cells express all three HAS (Su *et al.*, 2017). Disruption to HA signalling lead to an increase in neural stem cell proliferation yet delayed neuronal maturation (Su *et al.*, 2017). Removing the HA matrix results in defects in lamina-specific entorhinal projection to the hippocampus and aberrant sprouting in the hippocampus (Förster *et al.*, 2001). In hippocampal slices, HA facilitates induction of LTP by increasing the activity of L-type voltage-dependent calcium channels (L-VDCCs). Furthermore, ablating of HA before fear conditioning impairs contextual fear memory, and highlights the importance of HA-rich ECM in coordinating synaptic plasticity in the CNS (Kochlamazashvili *et al.*, 2010).

A pertinent component of PNNs, tenascin-R, has been shown to influence neuronal physiology. Tenascin-R modulates the subunits of sodium channels (Xiao *et al.*, 1999), causing a decrease in axonal conductance velocity in the CNS (Weber *et al.*, 1999). Aggrecan, which is particularly concentrated in PNNs, may already direct PNN-mediated neural plasticity. Deletion of tenascin-R additionally reduced the density and altered the spatial arrangement of synaptic vesicles at synaptic terminals and sequestering synaptic activity (Nikonenko *et al.*, 2003). The transgenic deletion of aggrecan, which affects PNNs to a greater degree than the general ECM, reinstates juvenile-like plasticity in the visual cortex of adults after MD (Rowlands *et al.*, 2018).

There are indeed many binding effectors of PNNs that are diffusely distributed throughout the extracellular milieu as well as concentrated within the PNN matrix, which contribute to the regulation of cell functioning (Plantman *et al.*, 2013; Gattazzo *et al.*, 2014). The reelin glycoprotein, a PNN binding partner, has been implicated in regulating the subunit composition of NMDARs and control their surface mobility (Groc *et al.*, 2007). Moreover, exogenous addition of reelin increases spine density in hippocampal neurons by a mechanism

involving CaMKIIβ expression, which is associated with actin cytoskeleton reorganisation (Kim *et al.,* 2015) and calcium entry into hippocampal neurons (Zernov *et al.,* 2022). Since PNNs are prevalent around CaMKII-expressing excitatory neurons in the hippocampus (Lensjø *et al.,* 2017), this could indeed be one mechanism of neural plasticity modulation mediated by PNNs that warrants further exploration. Furthermore, neuronal pentraxin 2 (NPTX2, also known as Narp), is an ECM scaffolding protein which accumulates at excitatory synapses of parvalbumin (PV)-expressing interneurons alongside PNNs (Chang *et al.,* 2010; Van't Spijker *et al.,* 2019), and has been suggested to recruit AMPARs onto PV^+ interneurons. In fact, PNNs were found to enhance NPTX2 expression, thus influencing homeostatic scaling of excitatory inputs onto PV^+ interneurons (Chang *et al.,* 2010).

As described, a pertinent function of CSPGs is to present semaphorins to synapses. The disruption of the Plexin-B2 and Sema4C suppresses dendritic complexity and spine density during fear conditioning in hippocampal neurons during fear learning; the treatment of recombinant soluble Sema4C reversed this effect (Simonetti *et al.,* 2021; Carulli *et al.,* 2021). Agrin, a heparan sulphate proteoglycan (HSPG), is also known to promote filopodia formation and increase spine density (Annies *et al.,* 2006; Ksiazek *et al.,* 2007; Lin *et al.,* 2010).

During the process of maturation, developing neural cells receive extensive synaptic input from neurons and interneurons (Dityatev and Rusakov, 2011; Song *et al.,* 2012). Indeed, adult mouse hippocampal neural precursors were found to receive GABAergic input from PV^+ interneurons. Intriguingly, optogenetic activation of PV^+ interneurons enhanced newborn progeny survival and development. This is a particularly important finding, as changes in synaptic activity have been posited to regulate the expression of PNNs (Dityatev *et al.,* 2007). PNN depletion via chondroitinase allowed for the formation of new inhibitory synapses by GABAergic vasoactive intestinal polypeptide (VIP)-positive neurons on PV^+ interneurons, described as a low PV nework configuration, and enhanced synaptic plasticity and memory retrieval in the CA3 region (Donato *et al.,* 2013). This shift additionally occurred when mice learned to navigate a Morris water maze, and this was also comparable to the shift seen during EE (Donato *et al.,* 2013).

Recently, it was reported that increasing neurogenesis led to a reduction in CA1 activity during context memory retrieval (Evans *et al.,* 2022). Increased neurogenesis decreases the density and contiguity of PNNs within this region as well. Pharmacological reduction of neurogenesis subsequently increased the expression of PNNs. This study provides evidence suggestive of

neurogenesis-induced forgetting in mice, potentially modulated in part by the degradation of PNNs, which may otherwise protect memories from elimination (Evans *et al.*, 2022). The optimisation of both learning and memory demands a finely-tuned balance between neural circuit plasticity and stability. PNNs may be the key in manipulating this multifaceted system, but additional work is required to uncover how this may be achieved.

The experimental manipulations of PNN molecules described above underscore these molecules as vital instruments in governing synaptic transmissition and structural plasticity, but do not point to a simple scenario. However, this review serves to discuss both the general principles and the complexities regarding the PNN-plasticity relationship.

1.5 PNNs orchestrate critical period plasticity

As we have discussed, neuroplasticity is a dynamic and intricate process enabling the remodelling of synaptic organisation in order to optimise the functioning of neural networks. Neuroplasticity is heightened during critical periods (CPs) of pre and postnatal brain development, when neuronal networks extensively develop and progressively consolidate and refine functional neuronal networks (Hensch 2004, Hensch 2005, Hübener and Bonhoeffer 2014; Mirzadeh *et al.*, 2019). Understanding of the neural circuitry changes that accompany CPs stems primarily from studies of the developing visual system. In animal models, amblyopia is usually induced by monocular deprivation (MD), wherein an eye is sutured shut to occlude visual input to the eye. This stimulates a cascade of functional and structural remodelling in the primary visual cortex that shifts ocular dominance (OD) of binocular neurons away from the occluded eye toward the open eye, causing loss of visual acuity in the deprived eye. (Wiesel, 1982; Wiesel and Hubel, 1963, 1970; Hensch *et al.*, 2004; Hensch and Quinlan, 2018; Hooks and Chen, 2020). If the occlusion is removed before CP terminates, this OD shift is reversed and visual acuity may be restored. However, if the occlusion is removed after CP termination, the shift is irreversible, indicating a "brake" of neural plasticity has occurred to favour neural network consolidation and stabilisation.

PNNs are thought to be one such molecular brake on neural plasticity as CP windows close (Figure 5). The maturation of PNNs is concomitant with the closure of CPs for plasticity in the visual cortex (Pizzorusso *et al.*, 2002), auditory cortex (Cisneros-Franco and de Villers-Sidani, 2019), and barrel cortex (Nowicka *et al.*, 2009). Similarly, PNNs mature in song control nuclei in parallel with the cessation of CP for sensorimotor vocal learning in birds (Balmer *et al.*, 2009; Cornez *et al.*, 2020).

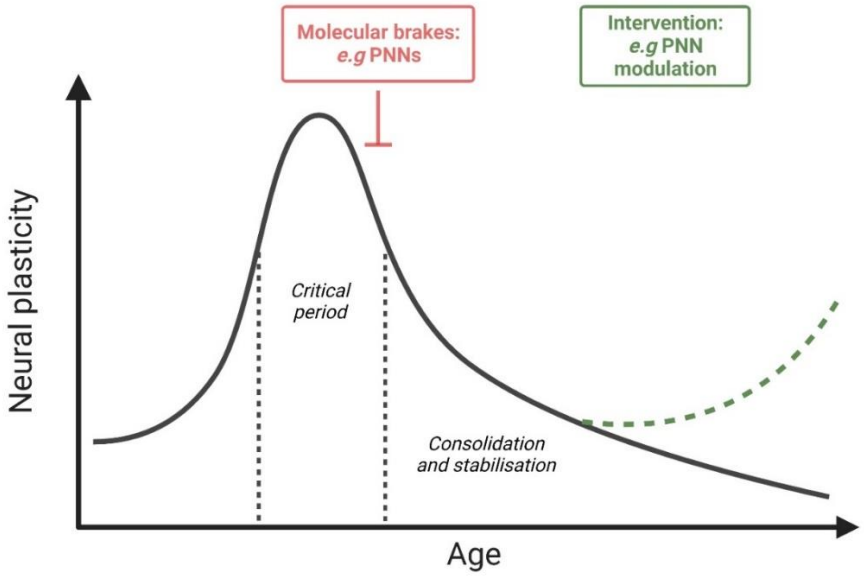

Figure 5. Neural plasticity as a function of age. Neural plasticity is dynamically regulated throughout life, peaking during a temporal window termed the critical period (CP). During this period, the neural network has the capacity to undergo extensive synaptic and structural remodelling. Once the critical period closes, neural plasticity declines in parallel with the consolidation and stabilisation of the neural circuity due to molecular brakes such as PNNs. Thus, modulating PNNs could be a method to reactive juvenile-like neural plasticity.

Rather than serving as merely a marker for CP closure, PNNs have been shown to be directly involved in CP plasticity. This notion emanates from studies demonstrating that digesting CS glycosaminoglycans (CS-GAGs) reinstated CP plasticity or prolonged it in adulthood. For instance, seminal studies have reported that chABC digestion of CS-GAGs allows the reactivation of OD plasticity (Pizzorusso *et al.*, 2002; Lesnikova *et al.*, 2021). Moreover, enhancement of OD plasticity may be due to alterations of the signalling pathways downstream of the protein tyrosine phosphatase-sigma (PTPσ)-CSPG complex, wherein tropomyosin receptor kinase B (TrkB) signaling in PV^{+} neurons was increased through inhibition of TrkB dephosphorylation after PNN removal (Lesnikova *et al.*, 2021).

Thus, the experimental manipulations of PNNs described in this chapter highlight that these molecules are instrumental in governing synaptic transmission and structural plasticity. Morevover, their CS-GAG chains may be the active component responsible for this regulation. PNN manipulation, potentially via their main constituents, is colossally important in neural plasticity, and represents as a viable method of intervention to extend CP duration and retain heightened levels of plasticity in adulthood (Figure 5).

Underpinning this malleability during CP are modulations of genetic, molecular, and cellular mechanisms that influence the dynamics of their connectivity, such as the formation of novel synapses and the decrement of others. These events culminate in changes to behaviour or function—especially important following trauma to neurons in brain and spinal cord.

1.6 PNNs are deterrents to neural repair

CNS injury induces a profound changes to the ECM composition and milieu, and CSPGs have been identified to be deterrents to neural repair. The first evidence of this stems from in vitro studies, where it was demonstrated using stripe assays that embryonic chick dorsal root ganglion (DRG) neurons preferentially grew on laminin-coated stripes while averting stripes rich in CSPGs and keratan sulphate proteoglycans (Snow *et al.* 1996). CSPGs constitute an integral part of the astrocytic glial scar, which serves as a physicochemical barrier to neural regeneration (Sharma *et al.* 2012). They are upregulated following CNS damage, the levels of which were shown to correlate extensively with abortive regeneration attempts in the spinal cord (Siebert *et al.* 2014, Keough *et al.* 2016). More recently, data suggest CSPGs initiate these inhibitory effects by their interaction with CSPG-specific signalling receptors. These are the adhesion-promoting, synaptogenesis-related leukocyte common antigen-related (LAR) and PTPσ receptors (Shen *et al.*, 2009; Xu *et al.*, 2015; Ohtake *et al.*, 2018). Blockade of these receptors attenuates cell death and oligodendrocyte demyelination observed in contusive spinal cord injury (SCI) (Dyck et al., 2019). PTPσ knockout mice exhibit greater regrowth of the injured corticospinal tract (CST) and elongation of sensory axons into an SCI lesion site (Shen *et al.* 2009). Similar regenerative capacity is observed in mice deficient in LAR: following SCI, enhanced regeneration with the CST and serotonergic sprouting is demonstrated, resulting in improved locomotor function (Xu *et al.* 2015). In 2022, a report described that the CSPGs/LAR/PTPσ signalling axis impedes neurogenesis and synaptic integration of transplanted neural precursors cells (NPCs) after SCI, possibly by suppressing Wnt/β-catenin pathway which is involved in expansion, proliferaton and differentiation of NPCs (Hosseini *et al.*, 2022). Indeed, the notion of CSPGs as neural regeneration attenuators has been firmly entrenched.

PNNs are thought to mediate their effects on plasticity through several ways (Figure 6). Firstly, we described that PNNs have been reported to restrict the lateral mobility of glutamate AMPARs at extrasynaptic sites (Frischknecht *et al.* 2009)—the primary mediators of transmission for PV^{+} interneurons (Hu *et al.* 2014). Whole-cell patch clamp recordings

revealed that the increased AMPAR diffusion triggered by PNN removal permitted the exchange of desensitised receptors for naïve functional ones, thereby promoting short-term plasticity. Secondly, the association of PNNs with several of their binding partners, including NPTX2, Otx2, and Sema3A, contribute to PNN-mediated plasticity. NPTX2 binds to both HA as well as 4,6 sulphated GAGs and HA of PNNs (van't Spijker *et al.*, 2019)

The specific binding and perpetual transfer of Otx2 is known to coordinate the maturation of PV interneurons (Beurdeley *et al.* 2012, Sugiyama *et al.* 2008, Lee *et al.* 2017). This arrest of maturation parallels the delay in the closure of critical periods (Lee *et al.* 2017), signifying the importance PNN-Otx2 interaction in critical period plasticity. The high-affinity binding of chemorepulsive molecule Sema3A to CS chains of PNNs is another critical factor in limiting plasticity (Dick *et al.* 2013, de Winter *et al.* 2016; Djerbal *et al.*, 2019). The removal of PNNs eliminates Sema3A from neuronal surface, thereby diminishing its chemorepulsive cues directed at approaching axons. Intriguingly, Sema3A binding induces the rigidification of GAG matrices, which may alter the physical properties of PNNs and affect neuroplasticity (Djerbal *et al.*, 2019), implicating a more complex role of the PNN-Sema3A relationship in mediating neuroplasticity.

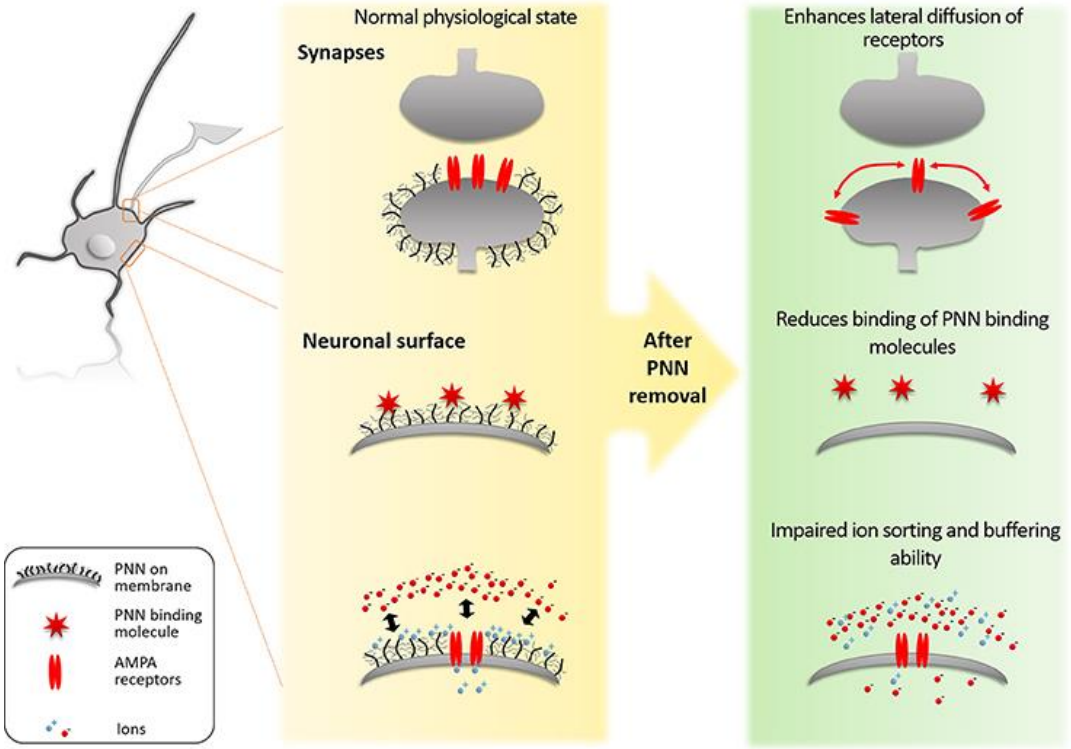

Figure 6. PNN-mediated mechanisms of restricting plasticity. 1) PNNs block the lateral diffusion of AMPA-type glutamate receptors to limit plasticity. **2)** PNNs associate with proteins such as Sema3A and Otx2, which are chemorepulsive molecules and coordinators of PV interneuron maturation respectively. **3)** Aside from serving as a physical barrier to prevent formation of synaptic contacts, PNNs mediate ion sorting and buffering on the neuronal surface, which facilitates high activity demanded by mature, fast-spiking interneurons. Adapted from (van 't Spijker & Kwok 2017).

Finally, the constituent components of PNNs, such as HA and CS chains, impart nets with an overall negative charge. This enables them to serve as a local buffer for cations within the vicinity of the synapse (Härtig *et al.* 1999), thereby affecting neurotransmission. Additionally, their anionic character enables them to reduce the oxidative potential in the neural microenvironment by scavenging and sequestering positively-charged toxic metal ions, such as redox-active iron (Morawski *et al.* 2004, Suttkus *et al.* 2012, Morawski *et al.* 2014). The PNN-mediated defence of PV interneurons against oxidative stress contributes to a favourable extracellular environment and facilitates the high activity of fast-spiking neurons (Suttkus *et al.* 2012). Indeed, Lensjø and team proved this PNN-evoked facilitation by showing that PNN degradation reduced putative inhibitory neuron activity both spontaneous and visually evoked activity, trends similar to an immature network state observed in juvenile rats (Lensjø *et al.* 2017b). Overall, it can be surmised that PNNs are important for restricting plasticity and instead supporting existing, preformed synapses.

1.7 Perineuronal nets as valid targets for plasticity enhancement

The relationship between neurons and PNNs is certainly drawing attention as a fundamental mechanism control CNS plasticity. Researchers worldwide have been attempting to disentangle a central question: if PNNs are to be modulators of neural plasticity, how can they be manipulated? Two general methods have been employed: removing PNNs and inhibiting their action (Figure 7).

1.7.1 Removing PNNs

The enzymatic digestion of PNNs using chondroitinase ABC (chABC) is the most popular means of removing PNNs (Figure 7). chABC is a bacterial lyase isolated from *Proteus* Vulgaris, which degrades CS (and partially HA) chains of PNNs (Snow *et al.* 1990; Prabhakar *et al.*, 2005), resulting in the liberation of soluble disaccharides and tetrasaccharides. Given that the structural integrity of PNNs depends critically on CS and HA chains, their digestion causes the collapse of PNNs, causing their components to disperse into the diffuse matrix. chABC has been extensively researched to clarify the effects of PNN removal on neural plasticity; some of this seminal work will be discussed in detail below.

In 2002, Pizzoruso and colleagues exploited the MD model—a classic example of experience-dependent cortical plasticity. Using *Wisteria floribunda* agglutinin (WFA) staining, one of the broadest markers of PNNs (Giamanco *et al.* 2010) and an antibody that recognises the CSPG neurocan, they discovered an increase in the number of PNNs in all cortical layers at P70—coincident with the end of the critical period. Following CSPG cleavage using chABC, MD caused an OD shift toward the non-occluded eye (Pizzorusso *et al.* 2002). Moreover, dendritic spines of the visual cortex in adult mice exhibited greater structural and functional plasticity following chABC exposure (de Vivo *et al.* 2013). chABC treatment can also restore object recognition (OR) memory following the diffuse neuronal loss and damage observed in two mouse models of tauopathy (Yang *et al.* 2015). Finally, PNNs have additionally been shown to densely localise on excitatory pyramidal neurons in CA2 of the hippocampal area, which normally fail to express LTP (Carstens *et al.* 2016). chABC treatment effectively reduced PNNs in area CA2 and induced synaptic potentiation of normally plasticity-resistant synapses (Carstens *et al.*, 2016). These findings strongly implicate PNNs as major suppressors of neuroplasticity, and that their degradation can effectively reinstate it.

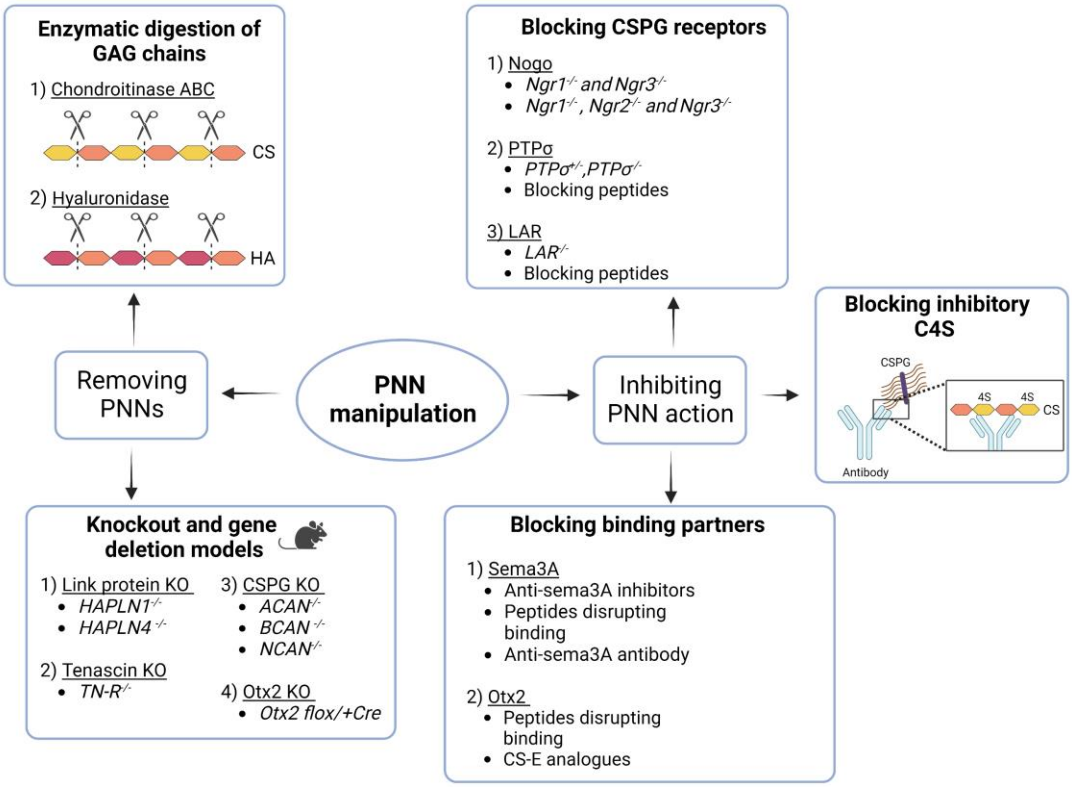

Figure 7. A summary of the common methods of PNN manipulation. *GAG, glycosaminoglycan; CSPG, chondroitin sulphate proteoglycan; Ngr, Nogo receptor; PTP, protein tyrosine phosphatase; LAR, leukocyte antigen receptor; PNN, perineuronal net; HAPLN, hyaluronan and proteoglycan link protein; TN-R, tenascin-R; ACAN, aggrecan; BCAN, brevican; NCAN, neurocan; Otx2, orthodenticle homeobox 2; Sema3A, semaphoring 3A; C4S, chondroitin 4 sulphate; CS, chondroitin sulphate*

The benefits of neuroplasticity is most evident in models of injury and disease. PNN digestion in the cuneate nucleus via chABC administration permitted substantial sprouting of forepaw afferents into its denervated areas, suggesting that the PNNs were curtailing plasticity and growth. The functional outcome of these observations was not determined. In earlier reports, PNN digestion via chABC was found to promote axonal regeneration and restore locomotor and proprioceptive function following CNS injury (Bradbury *et al.*, 2002; Huang *et al.*, 2006; Koh *et al.*, 2018).

Adult mice that underwent unilateral pyramidotomy—an injury that spares forepaw symmetry—displayed full recovery of function after chABC administration reduced PNN expression (Starkey *et al.* 2012). Another study reported that following complete transection of the spinal cord in rats, the intrathecal delivery of chABC resulted in a reduction in lesion size and extent and an increase in sprouting of regenerating axons, with some partially crossing

the lesion site. Notably, locomotor assessments revealed an improved recovery in chABC-treated rats (Cheng *et al.* 2015). In a key investigation led by Warren and group, adult rats received a C2 hemisection that severs glutamatergic and serotonergic projections from the brainstem to the phrenic motor pool, resulting in total and persistent ipsilateral hemidiaphragm paralysis. Astoundingly, 1.5 years after this injury, chABC treatment alone resulted in synchronised diaphragm electromyographic (EMG) activity in 100% of the injured rats (Warren *et al.* 2018). This restoration of respiratory function correlated with an increase in 5-HT sprouting and an increase in the expression of 5-HT and tropomyosin receptor kinase B (TrkB) receptors at the phrenic motor pool, indicating that PNN digestion and the consequential renewed supply of 5-HT fibres together promote the functional potential of the sprouting (Warren *et al.* 2018).

Another digestive enzyme used to degrade PNNs is hyaluronidase, which specifically digests HA chains (Figure 7). Digestion of the HA scaffold, upon which the assembly of the PNN occurs, by hyaluronidase rejuvenates synaptic plasticity by increasing AMPA receptor mobility (Frischknecht *et al.,* 2009) and cell surface expression of NMDA receptors (Schweitzer *et al.,* 2017). Another study utilised hyaluronidase to digest PNNs in the auditory cortex of adult Mongolian gerbils to assess cognitive flexibility during a reversal learning task. Their findings demonstrated an enhanced activity-dependent reorganization of neural circuits during this cognitively demanding task and led to an overall improvement in relearning performance (Happel *et al.,* 2014). Other studies have investigated the effects of a combination of chABC and hyaluronidase—this removal of PNNs in the hippocampus disrupted contextual and trace fear memory formation (Hylin *et al.* 2013). Endogenous hyaluronidase activity and expression increase following trauma and insults to the CNS; for instance, hyaluronidase 1 and 2 were elevated in neurons in both stroke and peri-infarct regions of ischaemic stroke patients (Al'Qteishat *et al.,* 2006). However, there are major constraints with the use of enzymes as therapeutic agents. For instance, chABC and exogenous hyaluronidase are predominantly administered via local injections or intrathecal infusion, which are invasive methods of administration. chABC's profile of thermal instability and short half-life mean that repeated dosing requirements are required to maintain therapeutically relevant suppression of PNNs. This is a significant disadvange especially in the context of CNS injury, wherein most patients would likely require long-term treatment regimens. In the case of hyaluronidase, the use of this enzyme is further complicated by the fact mammals express multiple hyaluronidase genes that regulate HA synthesis and catabolism.

Alternative methods of removing PNNs is through the modulation of other PNN components (Figure 7). Deletion and knockout of link proteins HAPLN1 and HAPLN4 caused an efficient degradation of PNNs (Carulli *et al.,* 2010; Bekku *et al.,* 2012; Romberg *et al.,* 2013; Suttkus *et al.,* 2014; Edamatsu *et al.,* 2018; Nojima *et al.,* 2021), indicating that HAPLNs are key players in the formation of PNNs. Indeed, the presence of HAPLNs is an important factor that distinguishes PNNs from the diffuse extracellular matrix (Carulli *et al.,* 2010). Furthermore, genetic suppression of these link proteins enhances neuroplasticity in the form of sustained juvenile-levels of ocular dominance plasticity in adult rodents (Carulli *et al.,* 2010) as well as improved recognition memory in adult rodents, possibly underscored by increased synaptic transmission and enhanced perirhinal LTD (Romberg *et al.,* 2013). Strikingly, these observations regarding neuroplasticity were found to be specifically due to the lack of PNNs, as this was the only difference between the ECM of wild type and knockout rodents (Carulli *et al.,* 2010). These methods of PNN modulation, however, usually lead to global attenuation of PNNs and are often irreversible (Romberg *et al.,* 2013).

Knockout of tenascin-R led to the alteration of PNNs (Haunsø *et al.,* 2000; Apostolova *et al.,* 2006; Suttkus *et al.,* 2014) and loss of CSPGs neurocan and phosphacan (Haunsø *et al.,* 2000). The ablation of tenascin-R promoted functional recovery mice after SCI (Apostolova *et al.,* 2006). The deletion of aggrecan, one of the key components of PNNs, also led to the substantial dissolution of PNNs (Suttkus *et al.,* 2014; Rowlands *et al.,* 2018), whereas brevican conferred negligible effects (Suttkus *et al.,* 2014). Indeed, the specific ablation of PNNs via aggrecan deletion reinstated juvenile plasticity in the visual cortex and improved object recognition memory (Rowlands *et al.,* 2018).

1.7.2 Inhibiting the action of PNNs

The constituents of PNNs underscore the action of PNNs, and their interactions with other ECM molecules can be targeted to manipulate PNN action (Figure 7). Notable work has revealed that key binding partners of PNNs are axon guidance proteins Sema3A and Sema3B, which are are immensely concentrated within PNNs of distinct neuronal populations in the maturing CNS, and are thus in a prime position to contribute to the orchestration of PNN-mediated plasticity (Carulli *et al.,* 2013; Vo *et al.,* 2013; de Winter *et al.,* 2016). The interaction of Sema3A with PNNs is sulphation specific; indeed, Sema3A binds preferentially to 4-sulphated and 6-sulphated positions of CS-GAGs (C4,6S, also known as CS-E) (Dick *et al.,* 2013), via specific peptidic sequences positioned in the Sema3A C-terminal region

(Carulli *et al.*, 2021). Blocking the binding of Sema3A to C4,6S relieves PNN-mediated inhibition of axon growth and plasticity of adult DRG neurons. Similar observations are also demonstrated in E13 cortical neuronal cultures—the repellent action of CSPGs was heightened in the presence of Sema3A (Zimmer *et al.*, 2010). Selective inhibitors of Sema3A have also proven to be beneficial in injury models. After spinal cord transection in adult rats, administration of a Sema3A inhibitor for 4 weeks caused the substantial regeneration and preservation of injured axons, all of which culminated in improved functional recovery (Kaneko *et al.*, 2006). Another peptide inhibitor of Sema3A, disrupts its binding to its receptor complex (neuropilin 1/plexin A1) and Sema3A-induced phosphorylation of GSK3 enhances neural regeneration of injured neurons (Montolio *et al.*, 2009). A highly specific monoclonal antibody that neutralises Sema3A has been developed and was found to be safe in mice, but as before, this antibody was administered via intraperitoneal and intravenous injections (Yamashita *et al.*, 2015), which are still invasive and introduces a risk of infection.

Another major binding partner of PNNs is the transcription factor Otx2. The transfer and internalisation of Otx2 into neurons, specifically into PV^+ interneurons within the visual cortex, plays a role in coordinating the onset and closure of the critical period window. It therefore represents as a target that can modulate PNNs and neuroplasticity. Otx2 contains an arginine-lysine doublet (RK peptide) and bears GAG-binding molecular characteristics that facilitate its interaction with PNNs. Otx2 binds to PNNs specifically to the C4,6S motif present on PNNs that enwrap PV^+ interneurons (Beurdeley *et al.*, 2012). Both gain-and loss-of-function reveal that Otx2 internalization elevate the expression of several markers of PV cell maturation as well as PNN formation itself, whilst concurrently regulating CP (Sugiyama *et al.*, 2008; Beurdeley *et al.*, 2012). An infusion of an RK peptide that disrupts localisation of Otx2 in PV^+ reduces PNN and PV expression. In this significant study, cortical acuity and the possibility of prolonging the critical period (CP) and rescue from amblyopia were examined. Using the well-established monocular deprivation, RK peptide infusion induced a substantial improvement of cortical acuity (Beurdeley *et al.*, 2012). A genetic point mutation of the GAG recognition motif of Otx2 markedly alters the accumulation of PNNs around PV^+ interneurons and delays their maturation in the visual cortex, ultimately altering CP timing (Lee *et al.*, 2017). The expression of PNNs and Otx2 is higher in a mouse model of behavioural deficits, and the reduction of PNNs ameliorates social memory deficiencies (Cope *et al.*, 2021). With the knowledge that Otx2 interacts with the CS-GAGs of PNNs via their C4,6S motifs, CS-E-like hexasaccharides were developed and screened, and were found

to effectively inhibit Otx2 *in vitro* binding to its gene promoters and its *in vivo* internalization into neurons (Depras *et al.*, 2013). In this study, biological function was assessed through protein binding, and no plasticity models were used as proof-of-concept that Otx2 targeting could enhance neuroplasticity. Additionally, the role of Otx2 has primarily been studied in visual cortex, despite being expressed in PV^+ neurons across structures governing more complex behaviours such as the amygdala, striatum, and limbic cortices (Spatazza *et al.*, 2013; Bernard and Prochiantz, 2016). The use of analogues disrupting the Otx2-PNN interaction in other regions of the CNS is sorely needed, and ideally, improvement of administration methods is required.

CSPGs are generally inhibitory to axonal sprouting and regeneration, and their effects are suppressed primarily by blocking the receptors Nogo, PTPσ, and LAR (Figure 7). Nogo receptor 1 and 3 were found to bind to GAG moieties of CSPGs with great affinity (Dickendesher *et al.*, 2012). Double and triple knockout of Nogo receptors 1, 2, and 3 induced axonal regeneration following optic nerve crush (Dickendesher *et al.*, 2012). PTPσ and LAR have been targeted in gene knockout studies and peptide mimetics to elucidate their role in CSPG-mediated inhibition of neural plasticity. For instance, DRGs harvested from double PTPσ and LAR knockout mice exhibited a greater degree of neurite outgrowth when grown on CSPG-coated surfaces than from wildtype mice (Ohtake *et al.*, 2016). Mice that were haploinsufficient for PTPσ promotes short-term memory performance, but long-term memory retention is disrupted (Lenisova *et al.*, 2021). Moreover, both PTPσ gene deletion and use of specific blocking peptides caused increase neurite outgrowth and neuroblast migration, which improved motor and cognitive function in stroke models (Luo *et al.*, 2022). CSPGs significantly decreased the ability of transplanted NPCs to sprout and differentiate into neurons, but these effects were reversed when both receptors were blocked using specific peptides of both PTPσ and LAR (Hosseini *et al.*, 2022). CSPGs decreased the density of newly-formed synapses of NPC-derived neurons, but PTPσ and LAR peptides recovered levels of synaptogenesis (Hosseini *et al.*, 2022). This verification is in accordance with other studies demonstrating the role of PTPσ and LAR in synaptogenesis in neurodevelopment (Takahashi and Craig, 2013). Peptide inhibition of PTPσ and LAR also induced the shift from a pro-inflammatory to a pro-regenerative state in SCI (Dyck *et al.*, 2018). Systemic delivery of a peptide mimetic of the PTPσ wedge domain that binds to PTPσ alleviates CSPG-induced inhibition and restored serotonergic innervation in an SCI model and facilitated functional

recovery (Lang *et al.*, 2015). However, *in vivo* use of these peptides can only be administered subcutaneously (Lang *et al.*, 2015)

Cat316 is an antibody that has been identified as a C4S binding antibody, with the ability of masking C4S on aggrecan, rendering PNNs less deterring to axon growth and sprouting (Yang *et al.*, 2017) (Figure 7). During embryonic development and on the onset CP, C6S predominates, however once CP has terminated only 4.9% of CS-GAGs are 6-sulphated, whereas 80.6% is 4-sulphated in the PNN fraction. This dramatic alteration of C4S/C6S ratio is indicative of its inhibitory profile (Deepa *et al.*, 2006; Carulli *et al.*, 2010) and raises the potential of Cat316 as a therapeutic agent in promoting juvenile-like plasticity. Indeed, Cat316 was found to specifically recognise C4S and even partially hinder the binding of Sema3A to PNNs (Yang *et al.*, 2017). In a mouse model of neurodegeneration and taupathy, injection of Cat316 into the perirhinal cortex attenuated PNN formation, restored memory loss and enhanced plasticity (Yang *et al.*, 2017). As promising as Cat316 is, it is an IgM antibody which cannot pass the blood brain barrier and has limited diffusion, necessitating repeated direct injections into the brain or target CNS region. These pose significant limitations due to invasiveness and overall increased risk of infection.

1.8 4-methylumbelliferone as a potent perineuronal net inhibitor (4-MU)

Contending with the complexities of PNN modulation as well as safe and efficient compound design, current methods of PNN manipulation are likely insufficient to serve as viable therapeutic agents. As discussed, chABC is currently the most prominent method of PNN manipulation, yet possesses numerous significant disadvantages. As mentioned, chABC is thermally sensitive, losing most of its enzymatic activity within a few days at 37°C (Lee *et al.*, 2010), warranting the use repeated injections or local infusions. Thermostabilised versions of chABC have been formulated for PNN removal and for the treatment of CNS injury in rats (Lee *at al.*, 2010) and canines (Hu *et al.*, 2018), but activity still wanes over time and these formulations still require injections. In 2018, Burnside and colleagues used an immune-evasive dual vector system, in which the expression of chondroitinase is regulated by the antibiotic doxycycline (dox) (Burnside *et al.*, 2018). However, this study reported low levels of "leaky" gene expression and enzyme activity without dox administration (Burnside *et al.*, 2018). This indicates that the activity of chABC, and by extension PNN removal, could not be tightly-controlled and that this system requires further optimisation (Burnside *et al.*, 2018). Another study created a Cre-dependent AAV vector that encodes for chABC, wherein the expression of

chABC controlled by tamoxifen, but this system still required infusion into the hippocampal target region (Carstens *et al.*, 2021). Overall, there is currently no evidence to indicate that chABC can be administered non-invasively, meaning that an abundance of research is still needed in order for chABC to gain therapeutic value. We thus arrive at the most cardinal question: is there a compound that could replace chABC?

A long-standing and established small molecule inhibitor of HA synthesis is 4-methylumbelliferone (4-MU) (Nagy *et al.,* 2015) (Figure 5). Derived from coumarin (7–hydroxy-4–methylcoumarin), it has been found to inhibit HA production in multiple cell lines, including melanoma and carcinoma (Kultti *et al.,* 2009; Edward *et al.,* 2010), fibroblast (Edward *et al.,* 2010), and endothelial cell lines (García-Vilas *et al.*, 2013). 4-MU is a competitive substrate for the enzyme uridine diphosphate (UDP)-glucuronyltransferase (UGT), which catalyses the conjugation of sugars using UDP-glucuronic acid (UDP-GlcA) as a sugar donors to appropriate substrates, in a process called glucuronidation (Tukey and Strassburg 2000; Nagy *et al.,* 2015). Glucuronidation is a vital phase II conjugative reaction which serves to eliminate endogenous substrates, dietary substances, toxins, and drugs (Sanchez *et al.,* 2010; Yang *et al.,* 2017). This process results in the formation of polarised, hydrophilic glucuronides that exit the cell via active transport to be eventually excreted in bile or urine. For instance, glucuronidation is key for the disposal of bilurbin, a toxic end product of heme catabolism (Zhou *et al.,* 2010). In prostrate epithelial cells, glucuronidation is key to coordinate the inactivation and elimination of androgens, thereby tightly-regulating their levels (Zimmer et al, 2021). In the presence of 4-MU, glucuronidation levels are increased from homeostatic levels, causing a depletion of UDP-GlcA and reducing HA synthesis (Kakizaki *et al.,* 2004; Kultti *et al.,* 2009; Vigetti *et al.,* 2009). 4-MU downregulates the mRNA levels of HA synthase 2 and 3 (Kultti *et al.,* 2009) and mRNA transcripts for UDP-glucose pyrophosphorylase and dehydrogenase, which are essential enzymes for HA synthesis (Vigetti *et al.,* 2009) (Figure 8). Its effects on other GAGs, however, remains to be definitively defined (Nagy *et al.,* 2015).

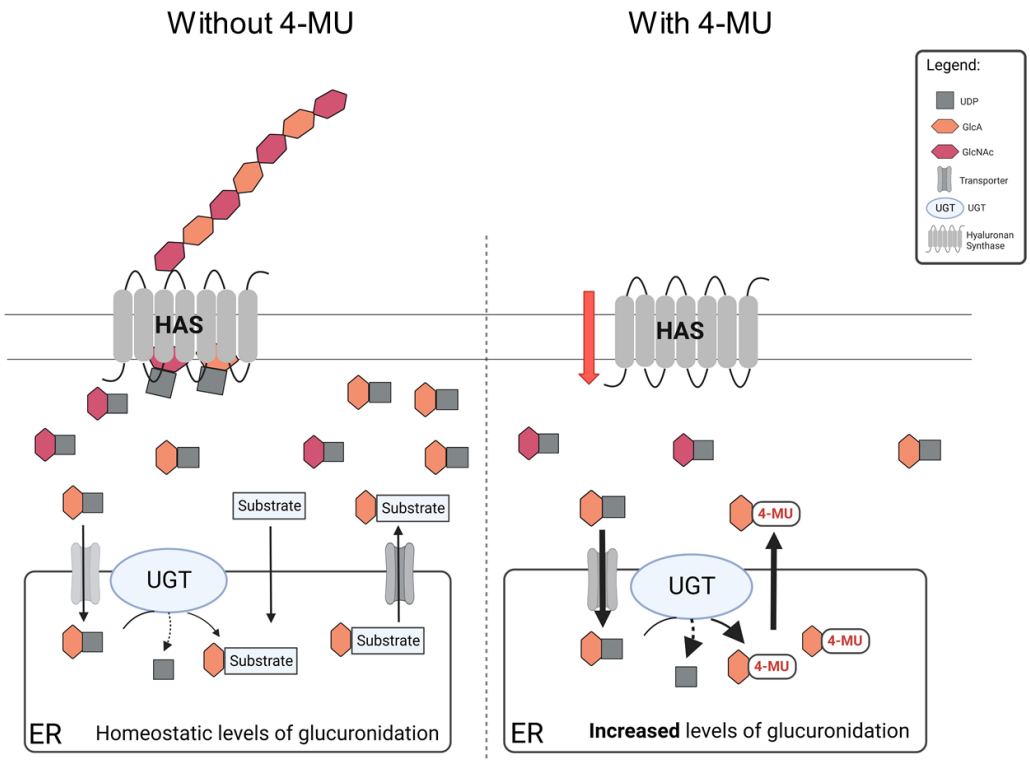

Figure 8. Known primary mechanisms of action of 4-MU. In the absence of 4-MU, a homeostatic level of glucuronidation takes place for the metabolism and clearance of endogenous substrates. This process takes place in the ER, catalysed by UGT, which utilises UDP-GlcA as a sugar donor to conjugate sugars to appropriate substrates. There is adequate supply of HA precursors UDP-GlcA and UDP-GlcNAc in the cytosol for the biosynthesis of HA chains by HAS. The presence of 4-MU markedly increases the levels of glucuronidation (illustrated by thicker arrows), as it acts as a favourable substrate for glucuronidation. This depletes the cytosolic levels of UDP-GlcA. Furthermore, HAS expression is also reduced, altogether causing a low amount of HA biosynthesis. *HAS, hyaluronan synthase; CS-GAGs, chondroitin sulphate glycosaminoglycans; UDP, uridine diphosophate; UGT, UDP-glucuronosyltransferase; GlcA, glucuronic acid; GlcNAc, N-acetylglucosamine; GalNAc, N-acetylgalactosamine; ER, endoplasmic reticulum.*

Other than serving as a scaffold for PNN assembly, as discussed, the roles of HA in regulating and maintaining the extracellular milieu is manifold. Importantly, its upregulation is a widespread occurrence in numerous pathologies (Nagy *et al.*, 2019). 4-MU has indeed been experimentally beneficial in studies concerning a myriad of cancers, inflammation, and autoimmunity (Nagy *et al.*, 2015; Nagy *et al.*, 2019). Its use in CNS plasticity and regeneration has only recently been achieved, and was found to improve memory retention in mice (Dubisova *et al.*, 2022).

The keystone feature of 4-MU is that it is already a commercially available compound approved in humans that can be administered orally, primarily to treat biliary spasm (Abate *et al.*, 2001; Nagy *et al.*, 2015). 4-MU is currently under investigation in numerous human clinical trials; for instance, it is the subject of a randomised, double-blind study to determine its safety, tolerability, and potential benefits in adults with pulmonary hypertension (ClinicalTrials.gov Identifier: NCT05128929), and has demonstrated high safety and tolerability data (Abate *et al.*, 2001; Nagy *et al.*, 2015). Despite these promising traits, 4-MU possesses low systemic bioavailability due to its extensive first pass glucuronidation within the liver and small intestine (Garrett *et al.*, 1993; Nagy *et al.*, 2015). Thus, in order to achieve and maintain effective compound activity, a much higher dose is needed. Indeed, the only study investigating the effects of 4-MU found that PNNs and plasticity were modulated at high doses of ~6.7mg/g/day in mice (Dubisova *et al.*, 2022), when the LD_{50} 2850 mg/kg in mice and 6200 mg/kg in rats (National Center for Biotechnology Information). While this study did not report any adverse behavioural sequelae, it is still worthwhile to explore how 4-MU can be improved.

Based on this vast amount of evidence, it is likely that 4-MU can effectively modulate PNNs, though this must be corroborated. Additionally, the effects of 4-MU on other GAGs remains elusive. In fact, a study proposes that CS-GAGs and HS are not affected by 4-MU, because CS and HS biosynthesis and polymerisation take place in the endoplasmic reticulum and Golgi apparatus, whereas HA biosynthesis occurs at the plasma membrane (Vigetti *et al.*, 2009). The assumption, therefore, is that the cytosolic depletion of UDP-GlcA would predominantly affect HA synthesis, and not CS or HS biosynthesis, due to the presence of the antiporter mechanisms required for substrate entry into the Golgi and ER lumen (Hirschberg *et al.*, 1998; Csala *et al.*, 2007). However, if we were to presume this theory to be true, this would indicate that HS- and CS-GAG synthesis would be less sensitive to fluctuations of substrates within the cytosol, not be completely unaffected, as has previously been reported (Rilla *et al.*, 2004; Vigetti *et al.*, 2009). Therefore, the ambiguity of the effects of substrate reduction in the cytosol—and by extension, the role of 4-MU—in CS and HS production is in desperate need of clarification.

1.9 Objectives of this thesis

In this chapter, we have explored the various forms of neural plasticity that can take place in the CNS. The involvement of PNNs in regulating plasticity is becoming increasingly entrenched, and research into the methods and compounds that can modulate these structures is accelerating. Therefore, removing PNNs, especially in conditions of injury, has been found

to promote neural plasticity and regeneration, culminating in improved functional recovery. The most popular method of modulating PNNs is chABC, commonly deemed as the first-generation PNN inhibitor. chABC has many disadvantageous characteristics that hinder its clinical translation. Circumventing these characteristics will plausibly require a large amount of time and funding. The overarching goal of this thesis is to establish a PNN-inhibiting role of 4-MU, and that PNN inhibition is achieved by influencing both HA and CS production.

We simultaneously assess novel derivatives of 4-MU for identical purposes. These 4-MU analogues, termed JD059 and JD060, were designed and synthesised in collaboration with Dr James Duncan and Dr Richard Foster, of the University of Leeds' School of Chemistry. It was envisaged that these analogues would possess improved aqueous solubility, and should theoretically have better bioavailability *in vivo* (Savjani *et al.*, 2012), yet retain functionality of 4-MU. Should these goals be successful, the data presented in this report would designate 4-MU, JD059, and JD060 as a new generation of PNN inhibitors to replace chABC.

To this end, the overarching objectives of this thesis are driven by the following hypotheses:

1. 4-MU, and its novel derivatives JD059 and JD060, are able to modulate PNNs effectively and safely. To address this, we will employ immunocytochemistry to determine if the compounds can efficiently attenuate the expression and morphology of PNNs using PNN markers. Furthermore, we will determine the toxicity of the compounds to cells by assessment of the morphology of cell nuclei and by the alamar blue metabolic viability assay.
2. 4-MU, JD059, and JD060 alter PNNs by influencing the expression of PNN components; specifically, HA and CS. We will first quantify total concentrations of GAGs by cetylpyridinium chloride (CPC) assay. Following which, we will assess the relative proportion of HA and CS, the two primary GAGs in PNNs, using fluorophore-assisted carbohydrate electrophoresis (FACE). Finally, we will explore the mechanisms of GAG reduction by measuring levels of molecular components involved in PNN formation using western blotting.
3. 4-MU, JD059, and JD060 promote neural plasticity. To interrogate this theory, we will harvest GAGs from PNN-HEK293 cells that had been either treated or untreated with our compounds to serve as growth substrates for dissociated DRG neurons extracted from adult rats.

Chapter 2 General Materials and Methods

2.1 Compound acquisition and preparation

4-methylumbelliferone was purchased from Sigma-Aldrich (Sigma-Aldrich, #M1381-100g). The novel analogues derived from 4-MU, termed JD059 and JD060, were designed and synthesised by Dr James Duncan. Once acquired or synthesised, all compounds were dissolved in dimethyl sulfoxide (DMSO) and stored at a stock concentration of 2 M.

2.2 HEK293 and PNN-HEK293 cell culture

Human embryonic kidney 293 (HEK293) cells expressing PNN components, termed PNN-HEK293 cells, were developed as described (Kwok *et al*, 2010). HEK293 and PNN-HEK293 cells were cultured in high glucose Dulbecco's modified Eagle's medium (DMEM) (Gibco, #11584486) supplemented with 10% fetal bovine serum (FBS) (Gibco, #26140079) and 1% antibiotic-antimycotic (Gibco, #15240062), maintained at 37°C, 5% CO_2. The cells were grown to 70% confluency before the addition of compounds.

2.3 Compound treatment

Stock concentrations of compounds were diluted in DMEM supplemented with 1% insulin transferrin selenium (ITS) (VWR, # 354352) and 1% antibiotic-antimycotic before addition to cells, to avoid excessive proliferation over the course of 3 days *in vitro* (DIV). Depending on the experiment, cells were treated to either: 1) varying concentrations of the compounds of 0.25 mM, 0.5 mM, and 1 mM for dose-dependent experiments or 2) 1 mM concentrations. At the highest concentration of 1 mM, the concentration of DMSO the cells are exposed did not exceed 0.05%.

2.4 Live-cell immunocytochemistry

For the immunofluorescent staining of HEK293 and PNN-HEK293 cells, 13 mm glass coverslips (SLS, #MIC3336) were prepared by alkaline-treating them with 0.1 M sodium hydroxide. They were then coated with 40 μg/ml Poly-D-Lysine (Sigma Aldrich, #P0899-50MG) for 1 hour at room temperature prior to the addition of cells. Cells were seeded at a density of 45, 000 cells/well in culture media.

After the cells were allowed to settle for 24 hours, cells treated with 0.25 mM, 0.5 mM, and 1 mM concentrations of the compounds as described in Section 2.3. After 3 DIV, cells were gently rinsed with cold 1 X phosphate buffered saline (PBS) before the addition of primary antibodies (see Table 2) diluted in blocking buffer composed of 1% Normal Donkey Serum (NDS) and 0.3% triton x-100 in 1x PBS. Cells were incubated with primary antibodies for 30 minutes at 4°C. Cells were rinsed with 1x PBS before fixation with 4% paraformaldehyde (PFA) for 20 minutes at room temperature. To block non-specific binding, cells were rinsed again before incubation in blocking buffer for 30 minutes at room temperature. The cells were then incubated in the appropriate secondary antibodies (see Table 2) in the dark for 1 hour at room temperature. Finally, cells were washed with 1x PBS and 1x tris-non saline (TNS) before being mounted onto SuperFrost Plus™ microscope slides (Fisher Scientific Ltd, #10149870) using Fluorsave (Merck #345789).

Table 2. List of antibodies used in project

Antibody	Species origin	Dilution	Supplier, catalog number
Primary antibodies			
Anti-β_3 Tubulin	Chicken	1:500	Abcam (Ab41489)
Anti-CS56[1]	Mouse	1:300	Merck Life Science Ltd (C8035)
Anti-HAS3[2]	Rabbit	1:1000	Thermo Fisher (PA530056)
Anti-HAPLN1[3]	Mouse	1:1000	R&D Systems (AF2608)
Biotinylated HABP[4]	-	1:1000	AMS Bio (AMS.HKD.B141)
Biotinylated WFA[5]	-	1:300	Sigma (L1516)
Secondary antibodies			
DAPI[6]	-	1:2000	New England BioLabs (4083S)
Alexa Fluor 488 anti-chicken	Goat	1:500	Invitrogen (A21449)
Alexa Fluor 568 anti-mouse	Donkey	1:500	Invitrogen (A10037)
Alexa Fluor Streptavidin 488	-	1:500	Invitrogen (S32354)
Alexa Fluor Streptavidin 568	-	1:500	Invitrogen (S11226)

[1] CS56: Chondroitin sulphate 56

[2] HAS3: Hyaluronan synthase 3

[3] HAPLN1: Hyaluronan and proteoglycan link protein 1

[4] HABP: Hyaluronan binding protein

[5] WFA: *Wisteria floribunda* agglutinin

[6] DAPI: 4′,6-diamidino-2-phenylindole

2.5 Imaging, quantification, and statistics

Imaging was done using either the LSM880 confocal microscope (Zeiss) with 20x or 40x objectives, or the AxioScan Z.1 Slidescanner (Zeiss) with a 20x objective. The visualisation of pericellular PNN structures was achieved using confocal microscopy under both 20x and 40x objectives. The imaging of DRG neurons was conducted using the Slidescanner at 20x objective, which was operated by the University of Leeds' Bioimaging Facility. Filters were set to ensure no intersection or overlap between channels. For fluorescence intensity measurements, five regions of interest were selected per coverslip across three independent experiments and measured using ImageJ software. Regions of interest were chosen by identifying regions of similar density of healthy cells with minimal background noise. Data was always obtained and averaged from at least 3 independent experiments; i.e, data were pooled from experiments utilising at least 3 separate cell cultures not exceeding Passage 40.

All data analyses and graph creation were achieved using OriginPro 2019b. Tests for significance ($p<0.05$) were performed using either: paired Student's *t-test* or one-way analysis of variance (ANOVA) with Tukey's post hoc test.

Chapter 3: The small molecule inhibitors 4-MU, JD059, and JD060 suppress synthesis of PNN components without affecting cell viability

3.1 Introduction

The manipulation or inhibition of perineuronal nets (PNNs) in adulthood has been shown to improve function and recovery after central nervous system (CNS) injury (Kwok *et al.*, 2011; Wang *et al.*, 2011) as well as enhance memory and learning associated with ageing and dementia (Duncan *et al.*, 2019; Dubisova *et al.*, 2022; Fawcett *et al.*, 2022). Evidence has also emerged showing that depletion of PNNs may be beneficial in certain neurodevelopmental conditions such as Rett syndrome (Carstens, 2021). This has spurred the field of glycosaminoglycans (GAGs) in neuroplasticity to identify, or develop, safe and effective modulators of PNNs.

This has proven to be a feat. Studying methods of PNN manipulation typically involves primary dissociated cultures or organotypic slice cultures. These models, while certainly beneficial, can be technically-challenging and time-consuming. Furthermore, their molecular complexities render drug screening difficult. Thus, the development of an immortal cell line expressing PNNs was needed in order to rapidly and easily examine PNN formation and disruption in response to compound treatment. Our lab has previously developed a human embryonic kidney 293 (HEK293) cell line that expresses PNN components to address this need (Kwok *et al.*, 2010). HEK293 cells do have the capacity to express PNN components such as aggrecan and tenascin-R, but they do not form a pericellular matrix (Kwok *et al.*, 2010). To this end, HEK293 cells were transfected with plasmids encoding a hyaluronan synthase 3 (HAS3) enzyme and hyaluronan and proteoglycan link protein 1 (HAPLN1). These modified cells, termed PNN-HEK293 cells, are able to produce pericellular matrix structures that bind to *Wisteria floribunda* agglutinin (WFA) lectin, a reliable pan-PNN marker, similar to those observed in primary neuronal cultures and *in vivo*. With the availability of a durable PNN cell line model, PNN formation and disruption can be explored efficiently.

In order to study neuroplasticity by PNN manipulation, a promising strategy would be to utilise small molecule modulators that could effectively halt the biosynthesis of PNN components, such as hyaluronan (HA). The HA chains serve as a scaffold for the binding of

proteoglycans (PGs) via HAPLN1, while tenascin-R further interconnects PGs (Kwok *et al.*, 2010; Carulli *et al.*, 2010; Wen *et al.*, 2018; Fawcett *et al.*, 2019; Fawcett *et al.*, 2022).

Despite the PNN serving as a physical and molecular barrier to plasticity, neural plasticity can still be manipulated. Digesting PNNs using bacterial enzyme chondroitinase ABC (chABC) has long been shown to induce ocular dominance plasticity in the adult visual cortex (Pizzorusso *et al.*, 2002). This increased plasticity has been shown to improve functional recovery after CNS injury (Bradbury *et al.*, 2002; Barritt *et al.*, 2006), stroke (Gherardini *et al.*, 2015; Hettiaratchi *et al.*, 2019), and neurological disorders (Yang *et al.*, 2015; Yang *et al.*, 2017). While chABC has been useful in modulating PNNs, its use is significantly limited by its innate instability at physiological temperatures (Lin *et al.*, 2007; Tester *et al.*, 2007; Hettiaratchi *et al.*, 2019). Additionally, administration of chABC is invasive, usually requiring repeated injections, intrathecal infusion, or secretion from an implanted biomaterial (Warren *et al.*, 2021). Therefore, there is burgeoning interest in identifying and developing a second-generation chABC compound that is equally or more effective in removing PNNs, yet can be administered non-invasively.

One compound have thus far proven to be promising candidate for PNN removal. As discussed in chapter 1.8, 4-MU is a safe, commercially available compound used to treat biliary spasms in humans (Abate *et al.*, 2001; Nagy *et al.*, 2015). Other than being used as a bile disease therapeutic, it is a known HA inhibitor both *in vitro* and *in vivo* (Nagy *et al.*, 2015; Nagy *et al.*, 2019), and has more recently been used to target PNNs (Dubisova *et al.*, 2022). Perhaps the most salient advantage of 4-MU is that it can be orally administered. Despite these promising traits, the rapid serum clearance and high dose required for therapeutic efficacy in the CNS limit its translation (Nagy *et al.*, 2015). Indeed, Dubisova and colleagues fed 4-MU (mixed in chow) to adult mice at a dose of ~6.7 mg/g a day. Although it is still well below the LD_{50} of 4-MU, it is still far higher than the approved dose to treat biliary spasm (Nagy *et al.*, 2015; Dubisova *et al.*, 2022). Therefore, even though 4-MU represents a promising replacement for chABC, there is a need for a second-generation class of compounds that have improved aqueous solubility whilst retaining the same PNN-inhibiting effects.

To this end, two analogues of 4-MU, termed JD059 and JD060, were designed and synthesised by Dr James Duncan to address the solubility and serum clearance issues that 4-MU possesses. Since 4-MU binds to glucuronic acid (GlcA) via its hydroxyl group, chemical

modifications to synthesise JD059 and JD060 were targeted away from this group. Therefore, the proposed mechanism of 4-MU-mediated HA inhibition would not be affected. Should these novel analogues possess improved solubility and efficacy in manipulating PNNs, they would be strong contenders for the replacement of chABC. This thesis thus comprehensively examines the use of 4-MU, JD059, and JD060 to serve as a first step in establishing their roles as potent PNN modulators.

3.2 Aims

The primary aims of this chapter were to:

i) establish the PNN-HEK293 cell model as a suitable *in vitro* model of PNNs for this study
ii) confirm the solubility profiles of 4-MU, JD059, and JD060
iii) establish the efficacy of all compounds in attenuating the formation of PNNs,
iv) assess whether these compounds were detrimental to cell viability by evaluating live cell number and metabolic function.

3.3 Materials and methods

3.3.1 HEK293 and PNN-HEK293 cell culture

For the protocol detailing the culture and maintenance of HEK293 and PNN-HEK293, please refer to chapter 2.2.

3.3.2 Compound treatment

For the protocol detailing compound preparation and treatment to PNN-HEK293 cells, please refer to chapter 2.3.

3.3.3 Solubility assay

All solubility assays were performed by Dr James Duncan. Calibration curves (500-3.13 μM) for each compound were made up in duplicate in 1.2 mL 96-well plates by adding appropriate volumes of a 25 mM stock in DMSO to a mixture of 80:20 TBS buffer (pH 7.4, 50 mM Tris-HCl, 150 mM NaCl):acetonitrile (ACN) to make a final total volume of 400 μL and keeping the final DMSO concentration at 2%. The plates were then covered and shaken at 300 rpm for 30 mins at room temperature. 200 μL of each well was added to a disposable UV analysis plate and the wells were scanned at 10 nm increments from 250-500 nm to obtain the absorbance at each wavelength. One or more wavelengths >270 nm were identified at which the maximum absorbance for the highest concentration was >0.1 absorbance units (A.U.). A single wavelength was selected for standard curve construction using one or more of the following criteria: the absorbance at 200 μM and 500 μM were less than 2.0 A.U.; the absorbance for the 50 μM standard was significantly greater than the absorbance for the 12.5 μM standard; the relationship between concentration and absorbance for three or more standards is linear. The R^2 had to be greater than 0.85 to use the calibration curve constructed.

196 μL of TBS buffer was dispensed into each well of a MultiScreenHTS – PCF 96-well filter plate (Millipore, # MSSLBPC50). 4 μL of DMSO or 25 mM compound stock solution was dispensed into each well; each compound was tested in triplicate. The plate was covered and incubated at room temperature with shaking at 300 rpm for 1.5 h. The MultiScreen plate was placed on a vacuum manifold andfiltered (10-12” Hg) into a clean polypropylene, 96-well V-bottom collection plate. 160 μL of filtrate from each well was transferred to a UV

analysis plate and 40 µL ACN was added to each well and mixed with a pipettor. The wells were scanned at 10 nm increments from 250-500 nm to obtain the absorbance at each wavelength. The selected wavelength used to generate the calibration curves was used in determining the aqueous solubility with the following formula:

Aqueous Solubility (µM) = (absorbance$_x$ - y intercept/slope) × 1.25

Where x = selected wavelength.

3.3.4 Alamar Blue metabolic viability assay

The metabolic activity assay was performed by seeding cells at 10,000 cells/well in triplicates into 24-well plates containing culture media. A volume of 25 µl/well of Alamar Blue stock solution was transferred into the assay plate for a final assay volume of 250 µl/well, yielding a final concentration of 10% Alamar Blue reagent exposed to cells. After a 4-hour incubation at 37°C and 5% CO_2, the plates were exposed to an excitation wavelength of 570 nm using a microplate reader. The cell metabolic function was expressed as a percentage of fluorescence counts of that in the vehicle.

3.3.5 Live-cell immunocytochemistry

For the immunofluorescent staining of HEK293 and PNN-HEK293 cells, 13 mm glass coverslips (SLS, #MIC3336) were prepared by alkaline-treating them with 0.1 M sodium hydroxide. They were then coated with 40 µg/ml Poly-D-Lysine (Sigma Aldrich, #P0899-50MG) for at least 1 hour at room temperature prior to the addition of cells. Cells were seeded at a density of 45, 000 cells/well in culture media.

After the cells were allowed to settle for 24 hours, cells treated with 0.25 mM, 0.5 mM, and 1 mM concentrations of the compounds as described in Section 2.3. After 3 DIV, cells were gently rinsed with cold 1 X phosphate buffered saline (PBS) before the addition of primary antibodies (see Table 2) diluted in blocking buffer composed of 1% Normal Donkey Serum (NDS) and 0.3% triton x-100 in 1x PBS. Cells were incubated with primary antibodies for 30 minutes at 4°C. Cells were rinsed with 1x PBS before fixation with 4% paraformaldehyde (PFA) for 20 minutes at room temperature. To block non-specific binding, cells were rinsed again before incubation in blocking buffer for 30 minutes at room temperature. The cells were then incubated in the appropriate secondary antibodies (see Table 1) in the dark for 1 hour at room temperature. Finally, cells were washed with 1x PBS and 1x tris-non saline

(TNS) before being mounted onto SuperFrost Plus™ microscope slides (Fisher Scientific Ltd, #10149870) using Fluorsave (Merck #345789).

3.3.6 Assessment of viable nuclei

PNN-HEK293 cells were treated to a range of concentrations (0.25 mM, 0.5 mM, and 1 mM) of 4-MU, JD059, and JD060 and stained as detailed in the previous section. Each treatment condition had a total of three coverslips across at least three independent experiments. Nuclei of cells were counterstained with 4′,6-diamidino-2-phenylindole (DAPI) and examined using ImageJ software. To quantify the number of viable cells, five regions of each coverslip were selected and healthy nuclei were manually counted (Figure 9).

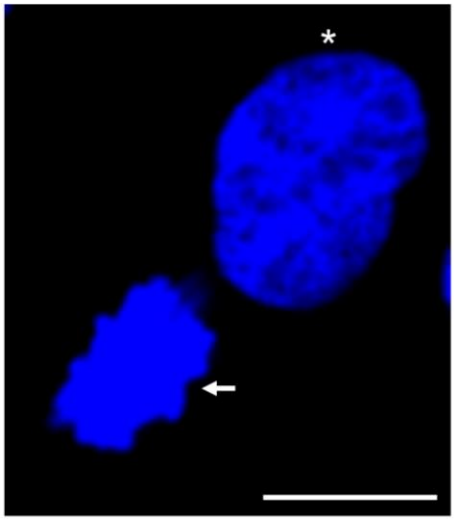

Figure 9. DAPI staining of healthy and unhealthy nuclei. Healthy nuclear morphology presents a round shape with a well-defined and regular edge, uniformly stained with other nuclei (white asterisk). Unhealthy nuclei that exhibits any nuclear irregularity, nuclear condensation, or nuclear fragmentation were categorised as unhealthy/non-viable, and were thus excluded from our manual cell count (white arrow). Scale bar is 20 µm. Image taken at 40x oil objective.

3.3.7 Western blotting

6-well plates were coated with 40 µg of Poly-D-Lysine for 1 hour at room temperature prior to the addition of cells. HEK293 and PNN-HEK293 were plated at a density of 1 x 10^6 cells per well and grown in culture media and maintained in an incubator at 37°C and 5% CO_2. After 24 hours, cells were removed from the incubator for protein extraction. Cells were rinsed with 1 x PBS and gently scraped from each well using cell scrapers (Fisher Scientific Ltd, #11597692). Cells were centrifuged at 2500g for 5 minutes at room temperature. The

resulting cell pellet was lysed thoroughly with radioimmunoprecipitation Assay (RIPA) buffer using a 26G needle until a homogenous solution was obtained. The cell solution was then centrifuged at 14,000g for 15 minutes at 4°C. The supernatant was transferred into fresh Eppendorf tubes and stored at -20°C until required.

To determine protein concentration, we ran a bicinchoninic acid (BCA) assay using the Pierce™ BCA Protein Assay Kit (Thermo Fisher Scientific Ltd, #23225). First, serial dilutions were made from a stock solution of 2 mg/ml bovine serum albumin (BSA) in milliQ-H_20. BSA standards were loaded in duplicates into a 96-well plate. 10 µl of samples were then loaded in duplicates, followed by 190 µl of the working reagent as instructed in the BCA assay kit. The samples in the 96-well plate were incubated in a bench top oven at 37°C for 30 min before absorbance at 562 nm was measured using spectroscopy. A BSA standard curve was generated in order to determine protein concentration within samples (Figure 10). The samples were stored at -20°C until required.

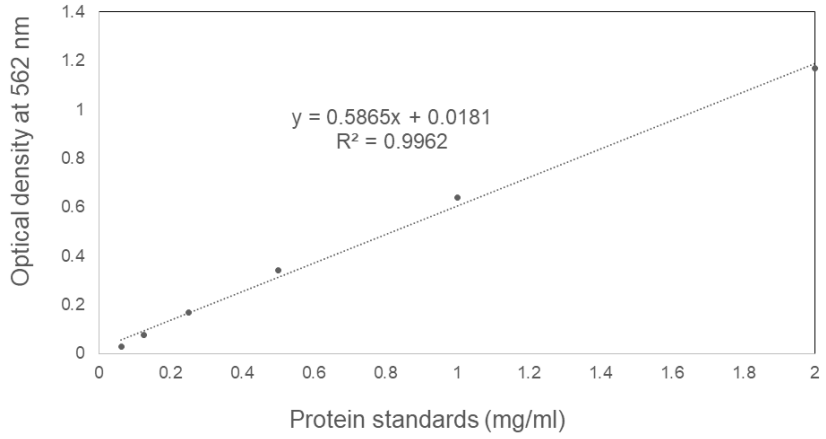

Figure 10. Standard curve for protein quantification using a BSA Assay. The R^2 values demonstrate the correlation between the two parameters.

To initiate sodium dodecyl sulfate (SDS)-polyacrylamide gel electrophoresis (PAGE), 4-12% precast polyacrylamide gels (Bio-Rad, #4561096) were prepared in an electrophoresis tank containing 1 x Tris-glycine SDS running buffer. The running buffer consisted of 25 mM Tris, 192 mM glycine, 0.1% SDS, pH 8.3. The samples were mixed with loading buffer. The loading buffer consisted of 2.5% (v/v) 2-mercaptoethanol and Laemmli buffer (69.45 mM Tris-HCl, pH 6.8, 11.1% (v/v) glycerol, 1.1% lithium dodecyl sulfate (LDS), 0.005% bromophenol blue). Samples were heated on a heating block at 100°C for 5 minutes to denature the proteins.

The first lane of each gel was loaded with 5 µl of dual colour protein standards ladder (Bio-Rad, #1610374), the molecular weights of which range from 250 kD to 10 kD. The subsequent lanes were loaded with 15 µg of protein of each sample. The samples were run at a constant amperage of 0.03 A, for 1 hour.

Once protein separation by SDS-PAGE was complete, the samples were electrotransferred onto a polyvinylidene fluoride (PVDF) membrane (0.4 µL pore size) in transfer buffer (25 mM Tris-HCL, 192 mM glycine, 10% methanol) for 75 minutes at a constant voltage of 130 V at 4 °C in Bio-Rad transfer tanks. The membranes were rinsed with Tris buffered saline with tween (TBS-T: 20 mM Tris base, 130 mM NaCl2, 0.1% tween, pH 7.4) at room temperature, then blocked in blocking buffer containing 5 % (w/v) skimmed milk (Fisher Scientific Ltd, # 10651135) diluted in TBS-T for 1 hour. The membranes were then incubated in primary antibodies (Table 2) diluted in blocking buffer overnight at 4°C. The next day, the membranes were rinsed thrice with TBS-T, for a duration of 10 minutes per rinse. They were then incubated with secondary antibodies (Table 2) diluted in blocking buffer for 1 hour at room temperature. The membranes were washed thrice with TBS-T, 10 minutes per wash. Finally, the membranes were exposed to the Pierce™ enhanced chemiluminescence (ECL) western blotting substrate (Thermo Scientific: 32106) then visualised using a Fujifilm chemiluminescent imager.

3.3.8 Microscopy, quantification, and statistics

Stained cells on coverslips were imaged using LSM880 confocal microscope (Zeiss) with a 20x or 40x oil objective. Filters were set to ensure no overlap between channels and therefore no overlap between fluorescent signals. Images of immunostained cells on coverslips were obtained by choosing regions that contained similar densities of cells between treatment conditions. Parameters measured for this chapter were total fluorescence intensity per cell and number of cells, which were achieved using the ImageJ software. Each experiment had three coverslips per treatment condition, and 5 regions per coverslip were imaged. Experiments were conducted at least three times (n=3). OriginPro 2019b software was used for graph creation and statistical analyses.

3.4 Results

3.4.1 Validation of *in vitro* model of PNNs for the study

The development of PNNs varies in brain regions, initiating between 1 month and 20 years of age in humans and coinciding with the closure of the critical period (Carulli *et al.,* 2006; Mauney *et al.,* 2013; Rogers *et al.,* 2018; Sigal *et al.,* 2019). As the PNN matures, its morphology transitions from that of a punctate appearance to a contiguous, reticular one (Ueno, *et al.,* 2017b; Lipachev, *et al.,* 2019; Sigal, *et al.,* 2019), yielded by molecular restructuring of CSPGs (Sigal *et al*, 2019).

To conveniently study the structure and formation of the mature, reticular PNN, we utilised the PNN-HEK293 cell line throughout this study. While neuronal cultures expressing PNNs would better resemble endogenous PNNs, they bear significant technical challenges for drug screening and characterisation purposes. These include low proliferation rates and long-term culture required; indeed, cortical neurons require 51 days in culture in order to form mature, reticular PNNs (Dickens *et al.,* 2022). The PNN-HEK293 cell line has previously been established as a reliable *in* vitro model of PNNs (Kwok *et al.,* 2010), developed by the transfection of HEK293 cells with HAS3 and HAPLN1 and the exogenous addition of aggrecan. These cells recapitulate the molecular composition of endogenous PNNs. Together with its robustness and high proliferation rate, they represent an ideal *in vitro* model for drug screening and to study molecular interactions and composition with ease.

We began by first characterising the molecular features of the PNN-HEK293 cells and used that as a baseline for compound screening. PNN-HEK293 and HEK293 cells were cultured up to a maximum of Passage 40 and the presence of PNN components were determined by both immunocytochemistry (Figure 11) and western blotting (Figure 12). Live-cell staining was performed using WFA and HA to avoid interference with cytoplasmic staining. Although WFA is widely-regarded as a pan-PNN marker, previous studies have shown it may not stain all PNNs (Irvine *et al.,* 2018; Ueno *et al.,* 2018b). We therefore included HA staining for the detection of PNNs, since the formation of the PNN relies heavily on the presence of a HA backbone and that 4-MU targets HA synthesis. High magnification of confocal microscopy was used to visualise the cells. The presence of a clear pericellular structure positive for both WFA (Figure 11A) and HA (Figure 11B) was observed. Magnified images illustrated the pericellular

structure that resembles a PNN distinctly, which is similar to mature PNNs observed *in vivo* (Miyata *et al.*, 2005; Dino *et al.*, 2006). In constrast, HEK cells do not possess a pericellular structure that resembles a PNN. Indeed, staining with WFA and HABP on HEK293 cells do not show a pericellular PNN-like structure. There are low, observable amounts of WFA and HA staining for HEK cells, but these do not form the archetypical pericellular structure as observed in PNN-HEK293 cells (Figure 11A and B, lower panels).

To further establish the PNN-HEK293 cell as a suitable model for the *in vitro* study of PNNs, protein levels of PNN-associated molecules were measured in both cell types via Western blotting. The molecules targeted for this analysis were HAS3 and HAPLN1, as these were the components found to be crucial for the formation of PNNs (Kwok *et al.*, 2010). Indeed, western blotting results revealed that PNN-HEK293 cells expressed HAPLN1, whereas HEK293 cells did not (Figure 12). PNN-HEK293 cells expressed high amounts of HAS3 in comparison to HEK293 cells, though it was an interesting observation that HEK293 cells possessed low amounts of endogenous HAS3 protein levels. This may explain the faint HA signals observed in Figure 11.

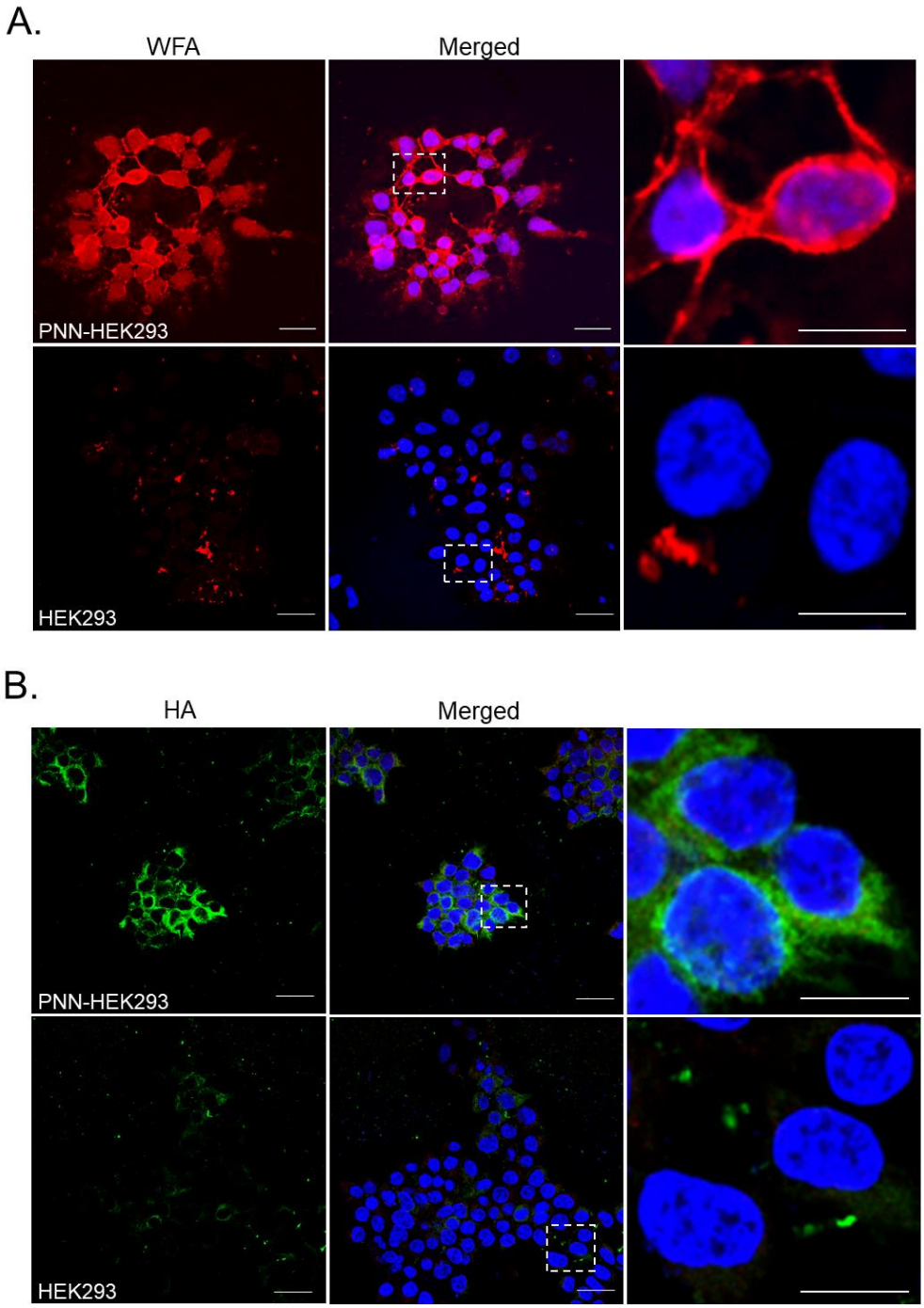

Figure 11. Comparison between HEK293 and PNN-HEK293 cells stained with WFA and HA. A. Representative images of WFA-positive PNNs in a PNN-HEK293 and HEK293 cell cultures. PNNs exhibit the typical reticular morphology as that of mature PNNs observed *in vivo*. HEK293 cells do not possess PNNs, although small amounts of WFA-positive CS staining can be observed. **B.** Representative images of HA-positive PNNs in PNN-HEK293 and HEK293 cells. There is a clear HA-positive matrix surrounding PNN-HEK293 cells, whereas this is absent in HEK293 cells. Scale bars: 10 µm.

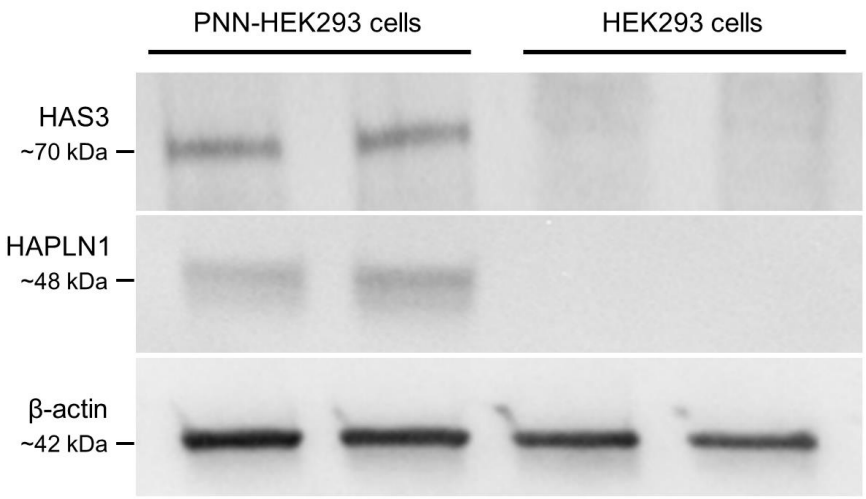

Figure 12. Protein levels of PNN components in HEK293 and PNN-HEK293. HEK293 cells do not possess any HAPLN1, and possess low amounts of HAS3 in comparison to transfected PNN-HEK293 cells. β-actin was used as a control for the amount of protein loaded.

3.4.2 The development of the 4-MU analogues JD059 and JD060

In order to facilitate the understanding of the 4-MU derivatives used in the following chapters, it is beneficial to describe the development and synthesis of the 4-MU analogues JD059 and JD060, which was achieved by a collaborator Dr Richard Foster and his student Dr James Duncan.

The design of JD059 and JD060 exploits the known characteristics of 4-MU. 4-MU is a potent HA inhibitor (Rilla *et al.*, 2004; Kultti et al, 2004; Vigetti *et al.*, 2009; Nagy *et al.*, 2015) that has only recently been exploited to modulate PNNs (Dubisova *et al.*, 2022). 4-MU has been purported to covalently bind to GlcA via its hydroxyl group (Nagy *et al.*, 2015), consequentially depleting the availability of GlcA for the conjugation to UDP. This reduces the cytosolic content of UDP-GlcA and suppressing HA synthesis (Rilla *et al.*, 2004; Kultti et al, 2004; Vigetti *et al.*, 2009; Nagy *et al.*, 2015). Whilst 4-MU exists as a commercially available oral drug used in humans, it possesses limitations, primarily its rapid serum clearance and poor solubility. Thus, JD059 and JD060 were designed with the aim of improving the solubility of 4-MU.

JD059 and JD060 were designed by incorporating polar and/or ionisable groups and increasing overall sp^3 character of each compound at 4-methyl substituent of 4-MU. These chemical modifications were incorporated away from the hydroxyl group of 4-MU in order to

avoid interfering with its HA-inhibiting function (Figure 13). The retention of the hydroxyl group was confirmed by nuclear magnetic resonance (NMR) and high resolution mass spectrometry (MS) (unpublished data). The two-step process of synthesising JD059 and JD060 culminated in purification by automated column chromatography, producing yields of 78% for J059 and 79% for JD060 (data produced by Dr James Duncan).

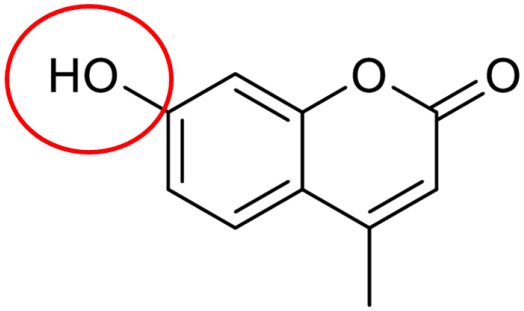

4-MU

Figure 13. The chemical structure of 4-MU. The functional hydroxyl group (circled in red) was retained during chemical modification to produce JD059 and JD060.

To determine the solubility of the newly-synthesised small molecules, the aqeuous solubility of JD059 and JD060 were tested in pH 7.4 buffer solutions and compared to 4-MU via spectrophotometry (Table 3). The solubility of 4-MU in physiological buffer pH 7.4 is 567 ± 75 µm, whereas the solubility of JD059 was increased by approximately 76%, reaching > 1000 ± 21 µm. A similar increase is observed for JD060, wherein approximately 74% increase was attained, reaching 987 ± 16 µm (Table 3) (data produced by Dr James Duncan).

Table 3. Aqueous solubility and cLogP of 4-MU, JD059, and JD060

Compound	Aqueous Solubility (µM)	cLogP
4-MU	567 ± 75	1.23
JD059	> 1000 ± 21	0.52
JD060	987 ± 16	0.49

3.4.3 4-MU, JD059, and JD060 reduce PNN expression by suppressing WFA in a dose-dependent manner, with JD060 conferring the greatest potency

As described in our literature review, 4-MU has been widely-regarded as a HA inhibitor. WFA is reported to mainly label the *N*-acetylgalactosamine residues associated with CS chains. Investigating its effects on WFA expression in addition to HA expression would therefore provide a reliable measurement into its role in PNN expression.

In this experiment, cells were cultured in increasing concentrations of 4-MU (0.25 mM, 0.5 mM, and 1 mM) for 3 DIV, as before. Cells were then live-stained with WFA (Figure 14) and HABP (Figure 15) to assess PNN formation and HA expression, respectively. The cells were imaged using confocal microscopy, and quantification of the fluorescence intensity per cell was derived in matched regions of interest. Overall fluorescence intensity was normalised to cell number (Figure 14B and 15B).

We confirmed that 4-MU treatment for 3 DIV reduced WFA expression, however, this reduction plateaued at approximately 40% (29.4 ± 2.36% at 0.5 mM and 36.6 ± 12.0% at 1 mM) (Figure 14A and 14B, red bars). Higher concentration of 4-MU does not lead to greater WFA reduction.

When cultured in 4-MU analogues for 3 DIV, JD059 and JD060 could suppress WFA expression in a dose-dependent manner. At 0.25 mM, neither JD059 nor JD060 caused a significant decrease in WFA expression, although levels appear lower. Although there is no change in fluorescence intensity measurements, a closer inspection of WFA patterns reveal disruption of the pericellular structure of PNNs after treatment with 1 mM of JD060 (Figure 14A). This suggests that JD060 is able to hinder PNN formation even at a low dose, but perhaps not CS expression. At 0.5 mM, JD059 and JD060 resulted in a 30.6 30.6 ± 2.16% and a 43.3 ± 7.30% decrease in WFA fluorescence intensity respectively. At 1 mM, JD059 and JD060 caused a 50.2 ± 15.9% and a 64.4 ± 8.91% decrease in WFA fluorescence intensity respectively. Importantly, JD060 was more effective at reducing WFA expression than 4-MU at 0.5 mM and 1 mM doses (Figure 14A and 14B).

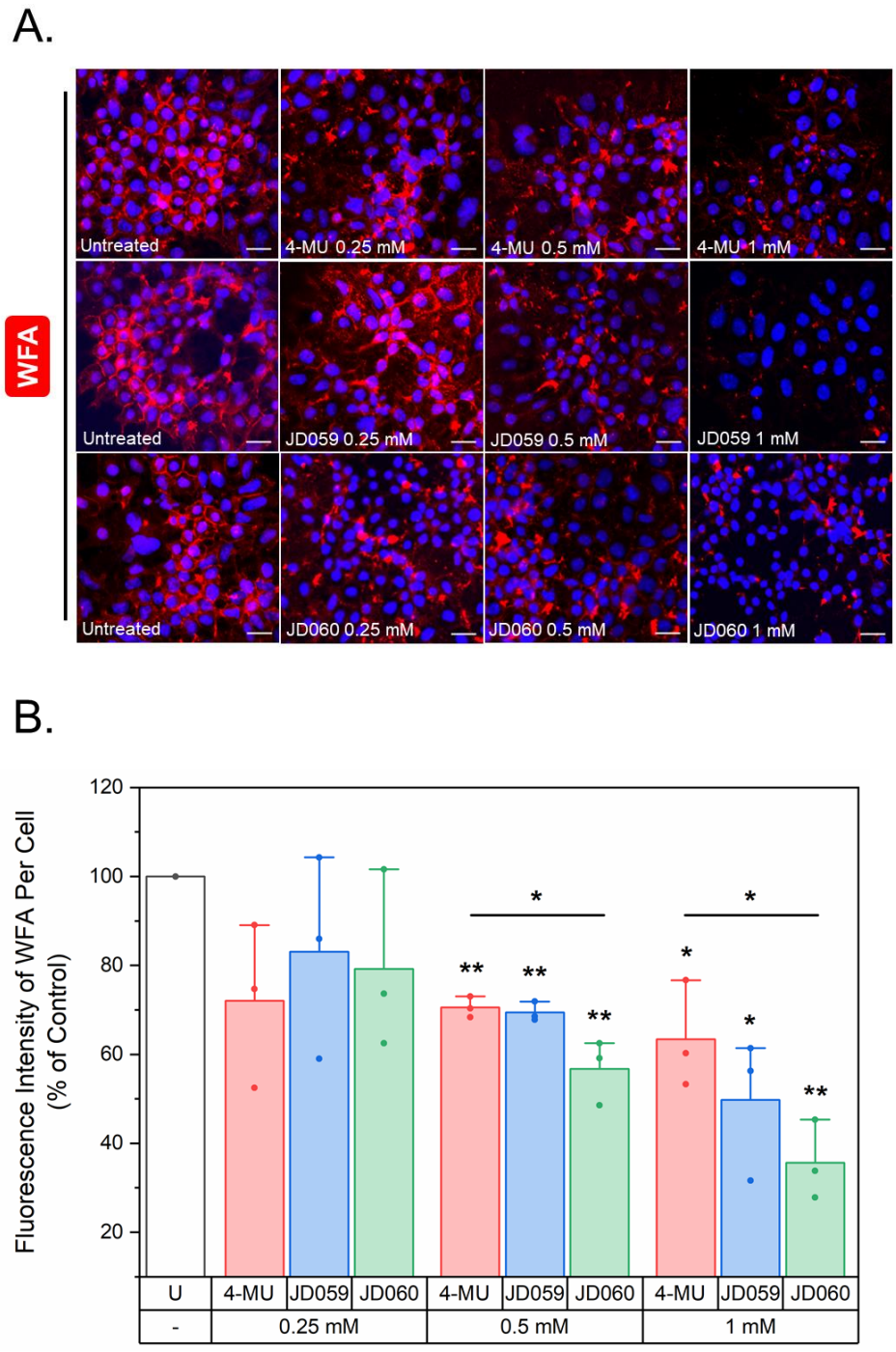

Figure 14. Imaging and quantification of PNN-HEK293 cells treated with 4-MU, JD059, JD060 and stained with WFA, a pan-PNN marker. A. WFA (red) and DAPI (blue) staining of PNN-HEK293 cells with or without treatment of compounds. **B**. Quantification of WFA staining of PNN-HEK293 cells with or without treatment of 4-MU, JD059, and JD060. Error bars on graphs represent mean ± S.D. of three independent experiments. n = 3; i.e, data were pooled from 3 independent experiments from 3 different cell cultures not exceeding Passage 40. Unpaired *t*-test statistical analysis and one-way ANOVA analyses; * (p=<0.05), ** (p=<0.01).

3.4.4 4-MU, JD059, and JD060 reduce HA expression of PNN-HEK293 cells

We continued to examine PNN formation following our treatment conditions by immunostaining PNN-HEK293 cells for HA using HABP. HABP is a biotinylated protein which binds to HA and allows for its visualisation when labelled by Streptavidin-Alexa Fluor. Following exposure to increasing concentrations of 4-MU, JD059, and JD060 for 3 DIV, HA expression was markedly reduced in a dose-dependent manner (Figure 15). At a low concentration of 0.25 mM, HA expression was significantly decreased by 61.1 ± 16.1 %, 52.2 ± 10.3%, and 75.5 ± 2.91% after 4-MU, JD059, and JD060 treatment exposure respectively. At 0.5 mM, HA expression was reduced by 74.0 ± 11.3%, 79.9 ± 8.34%, and 80.5 ± 2.16% after exposure to 4-MU, JD059, and JD060 respectively. Finally, 1 mM of 4-MU, JD059, and JD060 caused an 82.2 ± 1.84%, 90.9 ± 8.20%, and 96.9 ± 1.62% decrease in HA expression respectively. The marked reduction of HA expression even at the lowest dose of 0.25 mM suggests that HA expression on the cell surface is more sensitive to compound treatment than the CS chains labelled by WFA. Similar to what was observed with the WFA expression, we found that 1 mM of JD060 reduced the most HA expression, and that its effects were more potent than that of 4-MU at this dose (Figure 15).

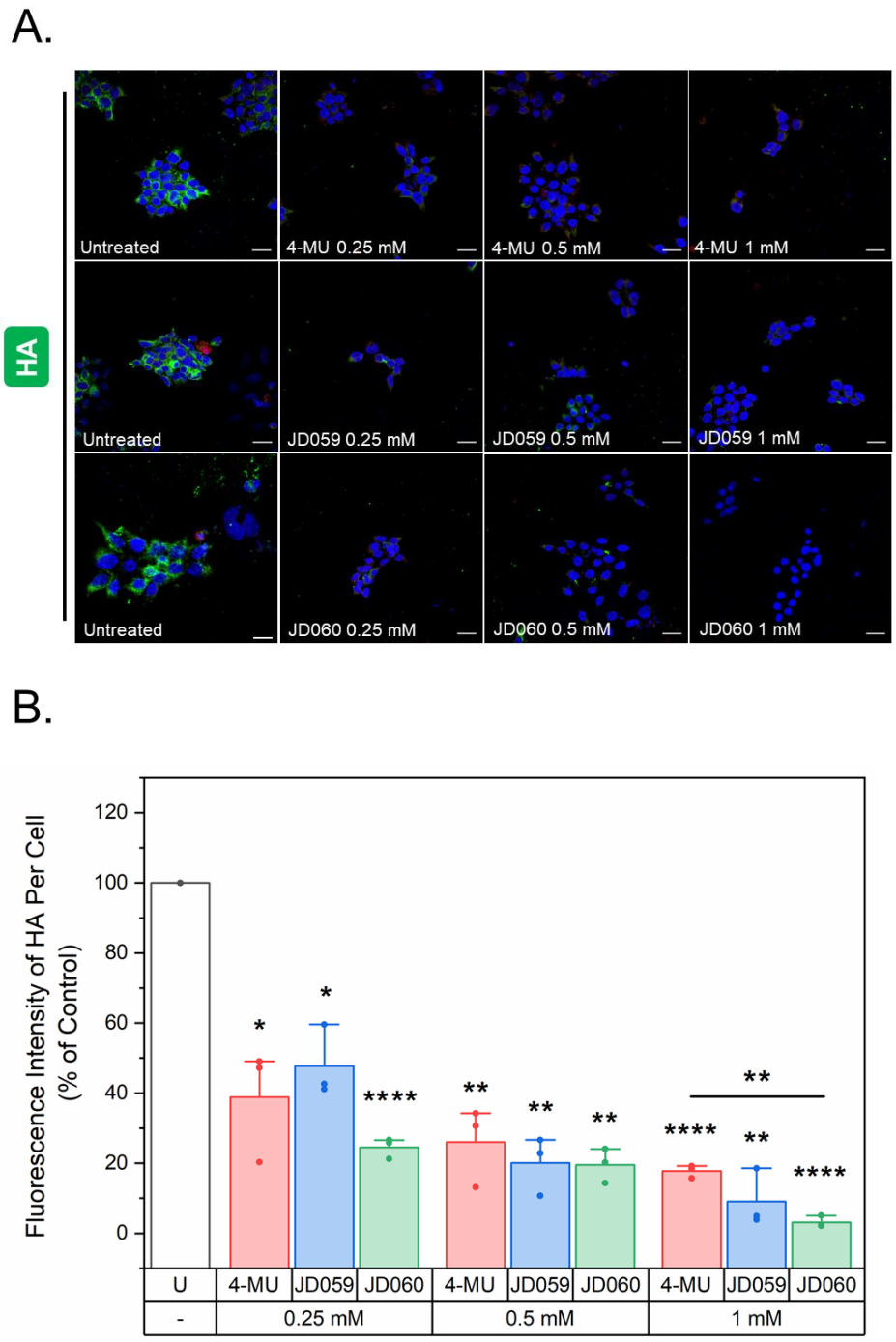

Figure 15. Imaging and quantification of PNN-HEK293 cells treated with 4-MU, JD059, JD060 and stained with HABP. A. HA (green) and DAPI (blue) staining of PNN-HEK293 cells with or without treatment of compounds. **B.** Quantification of HA staining of PNN-HEK cells with or without treatment of 4-MU, JD059, and JD060. Error bars on graphs represent mean ± S.D. of three independent experiments. n = 3; i.e, data were pooled from 3 independent experiments from 3 different cell cultures not exceeding Passage 40. Paired Student's *t*-test statistical analysis and one-way ANOVA analyses; *** (p=<0.001), **** (p=<0.0001).

3.4.5 4-MU, JD059, and JD060 do not affect cell viability

The effect of a high concentration of the small molecule inhibitors on cell viability was assessed by nuclei morphology and the cell metabolic rate.

First, quantification of PNN-HEK293 cell number was conducted with and without exposure to 1 mM of the compounds after 3 DIV (Figure 16A). This was conducted by the manual quantification of DAPI-stained nuclei, which is an easy and effective measure of the numbers of viable cells because nuclear morphology can be easily ascertained via microscopy. Cells that exhibit chromatin condensation or nuclear fragmentation are excluded. Figure 16A illustrates that small molecule modulator treatment does not lead to significant change in the number of healthy cells.

Cell viability was further assessed utilising the Alamar Blue assay after exposure to 1 mM of the compounds after 3 DIV. The Alamar Blue assay is a fast, convenient, and reliable method that relies on the metabolic activity of living cells. Metabolic respiration of NADH to NAD^+ in living cells will reduce resazurin to the red, highly-fluorescent resofurin. This process will be reduced in unhealthy cells, and be completely ablated in dead cells (Gould *et al.*, 2008). The changes in the red fluorescence will provide a proportional indication of the health status of a cell. When cells were treated with the small molecule modulators, there were no significant changes in metabolic function and cell viability after treatment when compared to the untreated controls (100% viability) (Figure 16B).

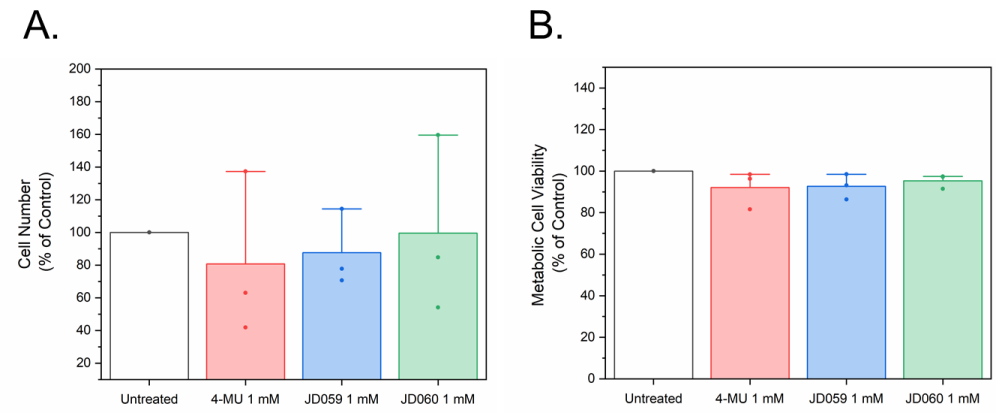

Figure 16. Cell viability assessments of PNN-HEK293 cells following treatment of 1 mM of 4-MU, JD059, and JD060 for 3 DIV. A. Cell number of each treatment condition was quantified from 60 fluorescence images per treatment condition. Untreated cells were used as controls. **B.** Alamar Blue viability assay of PNN-HEK293 cells following treatment of compounds. Untreated cells were used as controls. Error bars represent the mean ± S.D. of three independent experiments. n = 3; i.e, data were pooled from 3 independent experiments from 3 different cell cultures not exceeding Passage 40.

3.5 Discussion

3.5.1 Summary of results

It was first confirmed that the PNN-HEK293 cell line is a reliable model of PNNs and is suitable to use for this study. An important next step was to establish that the 4-MU derivatives JD059 and JD060 possessed improved solubility from 4-MU, as determined by Dr James Duncan. PNN-HEK293 cells express a pericellular PNN-like structure that is positive for WFA and HA, whereas HEK293 cells do not. Furthermore, it was verified that the PNN-HEK293 cells express HAS3 and HAPLN1 proteins, unlike HEK293 cells. The compounds 4-MU, JD059, and JD060 decreased WFA and HA fluorescence intensity in a dose-dependent manner. Finally, our compounds did not reduce cell number or alter metabolic function in comparison to untreated cells, and were therefore determined to be non-cytotoxic. This pilot study provides preliminary evidence for the effective and safe use of the compounds in manipulating PNNs in an *in vitro* model of PNNs.

3.5.2 The PNN-HEK293 cell line as an appropriate *in vitro* model for our PNN research

The PNN-HEK293 cell line was developed as previously reported (Kwok *et al.,* 2010), wherein HEK293 cells were transfected with PNN components HAS3 and HAPLN1. The live-cell staining of PNNs utilised WFA and HA. WFA is routinely used as a pan-PNN marker, but it has been revealed that WFA may not stain all PNNs (Yamada and Jinno, 2017; Irvine and Kwok, 2018; Ueno, *et al.,* 2018b), which is one reason we used HA staining to detect PNNs.

Our results show that PNN-HEK293 cells clearly produce a pericellular structure that was positive for WFA, a broad marker for PNNs and CS residues in particular. Furthermore, staining of PNN-HEK293 cells with HABP showed pericellular staining of HA around cells that appeared slightly more diffuse. These observations suggest that the PNN matrix formed is not only capable of capturing CS as part of its assembly, but WFA-positive CS assembles into a more condensed formation. This morphology exhibited by the PNNs around PNN-HEK293 cells replicates PNNs observed around neurons (Carulli *et al.,* 2010; Bozzelli *et al.,* 2018; Fawcett *et al.,* 2019).

Furthermore, we confirm that HEK293 cells do not possess HAS3 or HAPLN1, which are the PNN components indispensable for PNN synthesis (Kwok *et al.,* 2010). Without the expression of HAS3, HA cannot be synthesised to dock other PNN components; additionally, HAPLN1 is required for the attachment of CSPGs to HA. WFA^+ and HA^+ PNN expression was observed to be present on all PNN-HEK293 cells, which makes the cell line a model that exhibits a homogenous distribution and expression of PNNs. Evidently, this homogeneity is not present *in vivo.* For instance, when comparing all regions of the rat primary visual cortex (V1), medial entorhinal cortex (mEC), and the hippocampus, the expression WFA^+ PNNs was highest in V1 and mEC (Lensjø *et al.,* 2017). The hippocampus displays further heterogeneity of WFA+ PNNs, in that the dorsal hippocampus showed low levels of WFA^+ PNNs but there was dense expression in the CA2 region (Lensjø *et al.,* 2017). It is also well-established that WFA^+ PNNs preferentially ensheathe parvalbumin (PV) interneurons (Härtig *et al.,* 1992; Ueno *et al.,* 2017; Yamada and Jinno, 2017; Pletikos and Rockland, 2018; Lipachev *et al.,* 2019), and this was also observed in organotypic slice cultures obtained from the forebrains of three- to five-day-old rats (Brückner and Grosche, 2001). However, in some

regions of the brain, PNNs are primarily expressed around excitatory neurons in the lateral (LA) and basolateral (BA) nuclei of the amygdala (Morikawa *et al.*, 2017).

Recapitulating the heterogeneity and complexity as those of *in vivo* conditions has great utility in the research of PNN-modulating drugs. The obvious advantage of utilising models that closely, or accurately, replicate *in vivo* conditions is the ability to investigate the effects of compounds on physiological and biochemical reactions in living organisms. Such models would retain important cell-cell and cell-matrix interactions. For example, major PNN and ECM components, such as CSPGs, tenascin-R, and HA are synthesised and produced by CNS glia (Song and Dityatev). Furthermore, astrocytes release matrix-remodelling proteases to tightly regulate the integrity of PNNs (Fitch and Silver, 2008; Patel *et al.*, 2019). Recently, our lab developed a primary neuronal culture PNN model, supplemented with astrocyte-conditioned media, that accurately reproduces the maturity, molecular heterogeneity and morphology of cortical PNN populations observed *in vivo* (Dickens *et al.*, 2023).

These complexities, however, would render screening of compounds inappropriate, as it would be difficult to discern if any changes to PNNs were due to the effects of compounds or the variabilities of a neuronal culture or an *in vivo* model. Thus, an immortal and homogenous PNN cell line model allows the testing of our compounds relating to specific molecular components of the PNN in a controlled environment, without extraneous physiological influences. Furthermore, PNN-HEK293 cells can be grown indefinitely whilst still retaining its molecular characteristics, evidenced by their robust expression of PNN components more than a decade since the development of the cell line. This offers key advantages, including cost-effectiveness, ease of use, and bypasses ethical concerns regarding the use of animal and human tissue.

3.5.3 4-MU, JD059, and JD060 reduce WFA and HA expression in a dose-dependent manner

Quantitative analyses have shown that 4-MU, JD059, and JD060 are able to reduce the expression of both HA and CS on the surface of cells. The latter bears greater importance to PNN biology, as PNN-mediated regulation of neural plasticity is achieved primarily via their CS-GAGs (Rhodes and Fawcett, 2004; Dick *et al.*, 2013; Foscarin *et al.*, 2017; Yang *et al.*, 2021; Fawcett *et al.*, 2022).

While all small molecule modulators led to the reduction of HA and CS intensity, a dose-dependent reduction was only observed with JD059 and JD060 treatment. 4-MU only leads to a maximum of 36.6 ± 12.0% reduction of CS fluorescence intensity after a 1 mM dose. A direct comparison amongst the three molecules reveals that JD60 demonstrates the highest potency in CS and HA reduction (Figure 14 and 15). 1 mM of JD60 reduced WFA fluorescence intensity by 62.3%, in comparison to a reduction of 35.2% and 46.1% elicited by 4-MU and JD059 respectively. This indicates that JD060 is the most effective treatment, potentially due to its improved aqueous solubility in culture media.

Preliminary immunocytochemistry experiments conducted in the lab previously indicated that 0.5 - 1 mM of 4-MU may be effective in reducing WFA^+ PNNs (unpublished data). WFA is an *N*-acetylgalactosamine-specific lectin which preferentially binds to the CS chains of glycans in PNNs. Although we did not observe a clear reduction of WFA^+ fluorescence intensity at 0.25 mM, JD060 was still able to visibly disrupt the pericellular PNN-like structure at this dose (Figure 14). With the known HA-inhibiting properties in mind as discussed, this suggests that JD060 was able to reduce HA synthesis potently enough such that it disrupted the HA backbone for the condensed assembly of PNN molecules, including CS-GAGs. Our finding that 4-MU can reduce WFA fluorescence intensity concurs with that of recently published data (Dubisova *et al.*, 2022), and offers a glimpse into the potential CS-inhibiting properties. We also show for the first time that a novel, optimised derivative of 4-MU, confers greater potency in reducing WFA^+ PNNs. However, we cannot exclude the possibility that WFA has differential affinity for specific sulphated forms of CS-GAGs (Miyata *et al.*, 2018; Härtig *et al.*, 2022), and that this observed reduction in its fluorescence intensity could indicate a reduced expression of one form of CS-GAG and not the other. For example, primary cultured cortical neurons from aggrecan-deficient mice demonstrated a total loss of WFA staining, yet expression patterns of other PNN lecticans, such as brevican, remained unaltered (Giamanco *et al.*, 2010), indicating that WFA may preferentially recognise CS chains associated with aggrecan. It was therefore paramount to incorporate the staining of another key PNN marker, such as HA, within this study for a more comprehensive view on PNN expression.

To that end, we next demonstrated that all compounds were able to potently reduce HA expression based on the marked decrease in HA fluorescence signal intensity at all doses, even at the lowest dose of 0.25 mM. This suggest that the small molecule modulators are more efficient in inhibiting HA expression than CS. This potent inhibition of HA would

explain why we observed some degree of disruption to the pericellular morphology of PNNs after 0.25 mM of treatment when stained for WFA. At doses of 1 mM, we see an abolishment of HA across all treatments. This is unsurprising; in fact, many reports have demonstrated potent inhibition on HA production after 1 mM of 4-MU treatment in many cell lines: approximately 60% HA inhibition in keratinocytes (Rilla *et al.,* 2004), approximately 40% HA reduction in aortic smooth muscle cells (Vigetti *et al.,* 2009), 85.3% ± 2.9% reduction of HA in orbital fibroblasts (Galgoczi *et al.,* 2020). Kultti and coworkers screened the efficacy of HA inhibition on several cell lines, and 1 mM of 4-MU caused significant reductions of HA in all of them, with the highest being ~80% decrease of HA in human breast cancer cell lines (Kultti *et al.,* 2004). All these reports treated the respective cells between 6- 24 hours. Given the drastic complexities in cell types used, different methods of HA quantification, and limited duration of treatment, it is unsurprising that the degree of HA inhibition or amount of HA vary between these reports, and from our study.

3.5.4 4-MU, JD059, and JD060 do not negatively alter cell viability

At this point, our results indicate that our compounds have the capacity to substantially suppress the formation of both HA and WFA-stained CS components of PNNs. We then decided to determine the safety of these compounds by analysing two parameters of cell health: number of healthy nuclei and cellular metabolic function. The number of nuclei that displayed healthy morphology indicative of viable cells were manually counted, whereas unhealthy nuclei were excluded. To adopt a combinatorial approach to cell viability and cytoxicity screening, the alamar blue assay was also incorporated. Decreases in metabolic function has previously been shown to be proportional to the amount of cells viable, as cells rapidly lose the ability to reduce a reagent dye (as in the case of the alamar blue assay) to a product when under stress or undergoing death (Riss *et al.,* 2013). Analysing these two parameters of cell health provides an inexpensive, non-toxic, and convenient means of producing meaningful and representative predictions of safety profiles *in vivo.* Whilst 4-MU is already an established therapeutic used in humans and therefore has a good safety profile, it was important to test our novel analogues for their safety. There were no differences in healthy cell number or metabolic function when cells were treated to a high dose of 1 mM of all compounds for 3 DIV, indicating that these compounds are safe for cells even at high doses.

While there were distinct advantages to using a combination of these two methods of assessing cell viability, there are some disadvantages as well. Manual evaluation and counting of healthy nuclei is time consuming, and may be subjective to the viewer. Additionally, the alamar blue assay could arguably be viewed as an index for metabolic activity, and not a direct indicator of cytotoxicity. Other assays could be employed in the future for a more comprehensive view on cell health upon exposure to our compounds. Assays that measure the activity of cytosolic enzymes that have leaked into the culture media after damage to the plasma membrane are popular and reliable indicators of cytotoxicity. The most widely-studied enzyme for this purpose is lactate dehydrogenase (LDH), which is a crucial enzyme catalysing the conversion of pyruvate to lactate and in the process, converts NAD^+ to NADH (Riss *et al.,* 2013). LDH is present in all cells, and its leakage definitively indicates a disruption of cell membranes. Other useful assays that can be incorporated are those that measure esterase cleavage, wherein hydrophobic, non-fluorescent dyes such as calcein acetoxymethyl (AM) readily diffuse into cells and are cleaved by intracellular esterases in live cells. This produces fluorescent products (calcein in this example) which is retained in live cells and quantified.

Evidently, further testing will also be required to confirm if these analogues are safe in animals, and ultimately humans. This is especially important to consider, given that 4-MU, JD059, and JD060 hold potential in numerous CNS pathologies and injury, including spinal cord injury. Many of these pathologies will require long-term administration of our compounds, which could potentially effectuate adverse effects. It is therefore paramount to conduct a thorough, systemic investigation into the long-term effects of our compounds on major organs. However, for the purposes of this study, confirmation of safety on cells was first required, and is always an important initial facet when screening novel compounds.

3.6 Conclusion and future directions

The primary aims of this chapter were to: i) establish the PNN-HEK293 cell model as a suitable *in vitro* model of PNNs for this study ii) confirm the solubility profiles of 4-MU, JD059, and JD060, iii) establish the efficacy of all compounds in attenuating the formation of PNNs, and iv) assess whether these compounds were detrimental to cell viability by evaluating live cell number and metabolic function.

For our first aim, we demonstrated that PNN-HEK293 cells are able to produce a pericellular PNN-like structure that mimics what is observed in neuronal cultures and *in vivo*, and that

this structure contained HA and CS as determined by immunocytochemistry. These cells did not express HAS3 or HAPLN1, which are essential components of PNNs. Furthermore, the novel analogues JD059 and JD060 exhibited improved solubility than 4-MU, warranting their research into this study. The next aim was to evaluate the capacity of our compounds to diminish the expression of PNN components. This was illustrated by the attenuation of HA and WFA fluorescence intensity when PNN-HEK293 cells were treated with increasing doses of our compounds. Our results also imply that JD060 may confer greater efficacy in attenuating PNNs than 4-MU. Finally, 4-MU and our small molecule modulators JD059 and JD060 have been substantiated to be safe for cells when exposed at a high concentration of 1 mM. Based on these results, we expand our investigation further to investigate the effects of all compounds in suppressing PNN formation and sought to confirm our hypothesis that our compounds could influence CS production using biochemical assays.

Chapter 4: 4-MU, JD059, and JD060 reduce both chondroitin sulfate and hyaluronan production in PNN-HEK293 cells

4.1 Introduction

Perineuronal nets (PNNs) are glycosaminoglycan (GAG)-rich structures present throughout the central nervous system (CNS). PNNs are constructed by the hierarchical assembly of hyaluronan (HA) chains hyaluronan and proteoglycan link proteins (HAPLNs), chondroitin sulphate proteoglycans (CSPGs) tenascin R, and other associated molecules such as semaphorin 3A (Sema 3A). These honeycomb matrices predominantly ensheathe parvalbumin (PV)-expressing gamma-aminobutyric acid (GABA)ergic interneurons but are also associated with excitatory pyramidal cells and motoneurons, and are present in various regions in the CNS (Kwok *et al.,* 2010; Giamanco *et al.,* 2012; Vo *et al.,* 2013; Suttkus *et al.,* Dick *et al.,* 2013, 2014; Djerbal *et al.,* 2017; Yang *et al.,* 2021; Fawcett *et al.,* 2022).

Deposition of PNNs typically increases with neuronal activity and CNS maturation, and is associated with the closure of critical periods and diminished neuroplasticity (Hensch, 2003; Miyata *et al.,* 2015; Carulli and Verhaagen, 2021). The precise and effective remodelling of PNNs for the purposes of enhancing neuroplasticity is therefore an active area of research. To this end, 4-methylumbelliferone has been discovered to be a powerful inhibitor of HA biosynthesis and more recently of PNN formation (Dubisova *et al.,* 2022). Referred to as 4-MU in our study, the mechanisms that underlie its effects are of great interest. It has been established that one way 4-MU exerts its effects is by the downregulation of genes pertinent for HA synthesis, including hyaluronan synthase (HAS) (Kultti *et al.,* 2009; Vigetti *et al.,* 2009), UDP-glucose pyrophosphorylase, and UDP glucose dehydrogenase (Vigetti *et al.,* 2009). The second mechanism of 4-MU-mediated inhibition is by diminishing the cellular content of uridine diphosphate (UDP)-glucuronic acid (GlcA) due to 4-MU conjugating to GlcA (Kakizaki 2004; Kultti *et al.,* 2009; Jokela *et al.,* 2008 Vigetti *et al.,* 2009).

It is intriguing that while there is an abundance of data confirming the inhibitory effects of 4-MU on HA, there is a dearth of evidence on the potential CS-inhibiting effects of 4-MU. To date, few reports have directly studied the effects of 4-MU on CSPG production in cells. In 2004, the work of Rilla and colleagues reported no change in CS synthesis from cultured keratinocytes. In 2009, Vigetti and colleagues investigated the mechanisms of 4-MU in primary human aortic smooth muscle cells (AoSMCs). While their findings proved a strong

inhibition of HA mediated by 4-MU, these experiments were all performed with a short treatment time (between 6-24 hours). If 4-MU were to be used as a therapeutic for plasticity enhancement, the treatment duration would range from weeks to months. Indeed, the study conducted by Dubisova and colleagues fed mice with 4-MU for 6 months, leading to PNN attenuation, enhanced plasticity, and improved memory retention (Dubisova *et al.*, 2022). Given that UDP-GlcA is a vital building block of not only HA chains, but chondroitin sulphate (CS) and heparan sulphate (HS) chains as well, it is difficult to envisage that a chronic depletion of UDP-GlcA by 4-MU would not lead to other changes in GAGs.

This study focuses on investigating the changes in HA and CS production levels following treatment with 4-MU, JD059, and JD060 for two reasons. First, the function of PNNs is largely mediated through their CS-GAGs. Additionally, the ratio of CS to HS in the PNNs is 7:1 (Deepa *et al.*, 2006); thus, alongside HA, CS was chosen as the primary GAG of focus.

4.2 Aims

To address this gap in knowledge, we continued the endeavour of exploring the effects of 4-MU, as well as the 4-MU derivatives JD059 and JD060, on total GAG as well as CS production. To this end, the primary aims of this chapter were to:

i) biochemically assess the production levels of overall GAGs after treatment with 4-MU, JD059, and JD060, achieved by utilising a robust GAG extraction and isolation procedure
ii) characterise the GAGs that were altered, if any, with a focus on HA and CS levels after compound treatment by fluorophore-assisted carbohydrate electrophoresis
iii) explore protein levels of other vital PNN components by western blotting

4.3 Materials and methods

4.3.1 HEK293 and PNN-HEK293 cell culture

For the protocol detailing the culture and maintenance of HEK293 and PNN-HEK293, please refer to chapter 2.2.

4.3.2 Compound treatment

For the protocol detailing compound preparation and treatment to PNN-HEK293 cells, please refer to chapter 2.3.

4.3.3 Glycosaminoglycan (GAG) extraction and isolation

GAGs were extracted from PNN-HEK293 cells according to modified version of a protocol published previously (Kwok *et al.* and Dick *et al.*). The extraction procedure is summarised in Figure 17, and lasted three days:

Day One: homogenisation and pronase treatment

Extraction Buffer 1 (B1) was prepared fresh from 10x tris buffer saline (TBS) stock solution. B1 was composed of 1x TBS, 2 mM ethylenediaminetetraacetic acid (EDTA), and 150 mM sodium chloride (NaCl) in distilled H20 (dH20). PNN-HEK293 were grown in T80 and T175 flasks and either remained untreated or treated to 0.25 mM, 0.5 mM, and 1 mM of all compounds (see Section 2.3) prior to GAG extraction. After 3 DIV, cells were detached and mixed with B1. The cell suspension was gently homogenised with a 26G needle until a homogenous solution was obtained. Digestion was then conducted by adding pronase (Sigma, #P5147) at a working concentration of 10 mg/mL overnight at 37°C on an orbital shaking incubator.

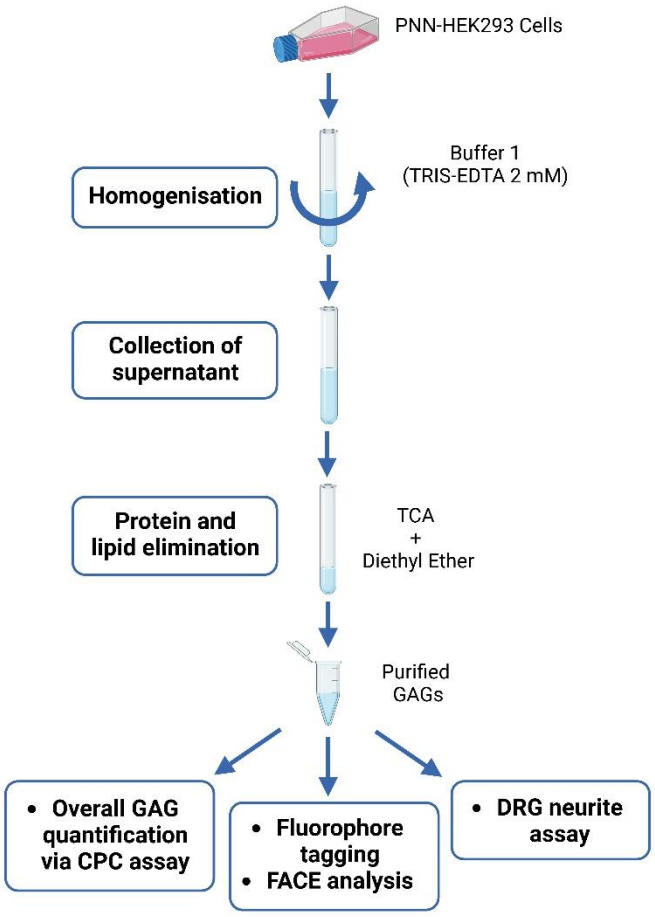

Figure 17. Schematic diagram summarising the protocol conducted for GAG extraction and isolation from PNN-HEK293 cells. GAGs are extracted from PNN-HEK293 cells and are isolated in a sequence of steps. Overall GAG quantity can be determined via the cetylpyridinium chloride (CPC) turbidity assay, analysed via fluorophore-assisted carbohydrate electrophoresis (FACE), or incorporated in a dorsal root ganglion (DRG) neurite outgrowth assay.

Day Two: protein precipitation

After pronase digestion, samples were centrifuged for 30 minutes at 20, 000g at 4°C, and supernatants were collected. Ice-cold 100% trichloroacetic acid (TCA) was added to the samples to a final concentration of 5% (v/v) for the precipitation of proteins. Samples were incubated on ice for 1 hour. Samples were then centrifuged for 20 minutes at 15,000g at 4°C. The supernatant of the samples was collected and placed on ice. The cell pellets were resuspended with 5 ml of 5% TCA and centrifuged again for 20 minutes 15,000 g at 4°C for further precipitation and removal of proteins. The supernatant from samples was pooled in preparation for the removal of lipids.

For the removal of lipids, diethyl ether was added to the samples to a final concentration of 50% (v/v), shaked vigorously, and the lipid layer was allowed to separate for 1 min (Figure 18). The upper phase containing lipids was discarded. This step was repeated until there were no more micelles forming in the upper layer, which took approximately 3-4 rinses. The remaining diethyl ether was allowed to evaporate in the fume hood for 4 hours at room temperature.

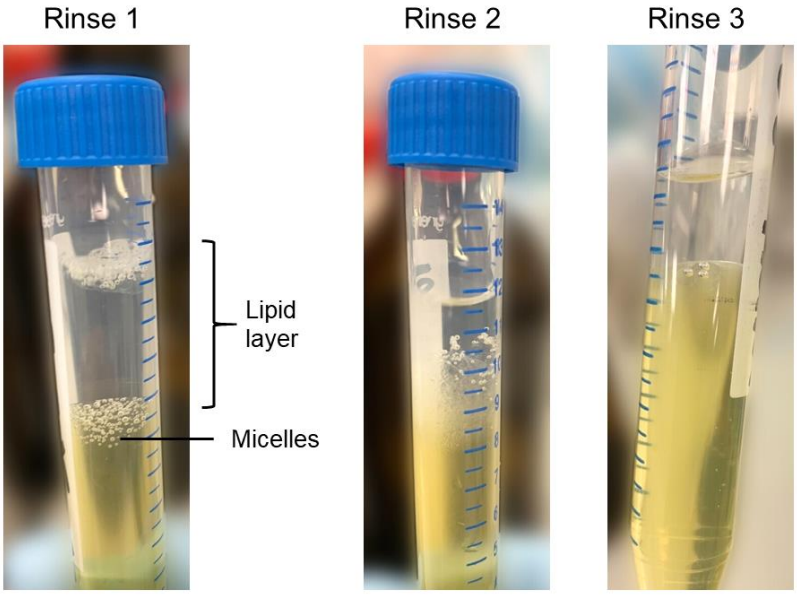

Figure 18. Elimination of lipids from samples using diethyl ether. Lipids can be rapidly separated from a sample using an organic solvent such as diethyl ether, and subsequently removed.

Once the remaining amount of diethyl ether had been evaporated, the acidity of the samples was neutralised with 1 M sodium carbonate until pH 7 was attained, as measured using pH strips. Finally, sodium acetate and ice-cold 100% ethanol were added to a final concentration

of 5% (w/v) and 75% (v/v), respectively. GAGs were allowed to precipitate from samples overnight at 4°C.

Day Three: GAG collection and quantification

Samples were centrifuged at 3000g for 15 minutes at 4°C. Supernatants were carefully discarded. GAG pellets were allowed to air-dry at room temperature for 30 minutes, to be resuspended in 400 µl of milliQ-H_20. Solubilised GAGs were stored at -20°C for further analysis via cetylpyridinium chloride (CPC) turbidity assay, fluorophore-assisted carbodyhydrate electrophoresis (FACE) analysis, or dorsal root ganglion (DRG) neurite outgrowth assay.

4.3.4 Cetylpyridinium chloride (CPC) turbidity assay

GAGs extracted were quantified using a rapid and efficient CPC turbidity assay, which has a sensitivity down to 0.15 µg of glycans (Kwok *et al.*, 2014), and can be completed in under 30 minutes. The CPC reagent used for this assay was prepared fresh by mixing 0.2% (w/v) and 133 mM magnesium chloride in an equal ratio. 25 µl of each extracted GAG sample was pipetted into a 96-well plate. CS-A concentrations ranging from 0 to 0.2 µg/ml diluted in milliQ-H_20 (8 concentrations) were also prepared in triplicates on the same 96-well plate t0 constitute the standard curve. 25 µl of CPC reagent was added to each well and mixed thoroughly. The absorbance of the samples was measured at 405 nm in a plate reader spectrophotometer. The quantity of isolated GAGs was calculated from the linear regression equation of CS-A standard (Figure 19).

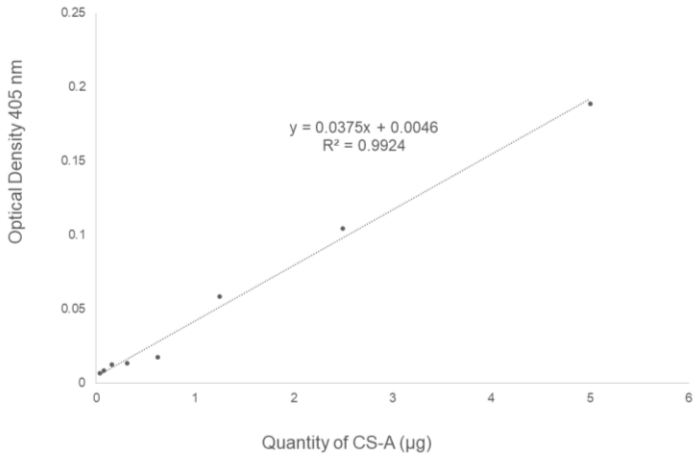

Figure 19. An example of the CS-A standard curve generated from the turbidity assay as measured by absorbance of 405 nm.

4.3.5 Fluorophore-assisted carbohydrate electrophoresis (FACE)

4.3.5.1 Sample preparation for FACE analysis

Fluorophore-assisted carbohydrate electrophoresis (FACE) is an efficient, high-resolution gel electrophoretic procedure that separates oligosaccharides by size (Jackson *et al.,* 1990 and Huang *et al.,* 2006). Isolated GAGs are prepared and tagged in a procedure that lasts for 4 days in a protocol modified slightly from Lin *et al.,* 2011, Kwok *et al.,* 2015, and Foscarin *et al.,* 2017.

Day One: digestion of GAGs into disaccharides

50 µg of GAG samples (extracted previously) as well as GAG standards HA (Rooster comb; Sigma, #H5388) chondroitin-4-sulphate (C4S) (Bovine trachea; Sigma, C9819), chondroitin-6-sulphate (C6S) (Shark cartilage; Sigma, 27043), were obtained and digested into disaccharides using 0.1 U/ml chondroitinase ABC (chABC) in 100 mM ammonium acetate at pH 8.0 for at least 16 hours on an orbital shaker set at 37°C.

Day Two: precipitation of GAGs

The digestion process was terminated by the addition of ice-cold 100% ethanol to a working concentration of 80% (v/v). Samples were incubated in 100% ethanol overnight at 4°C for the precipitation and recovery of GAGs and core proteins.

Day Three: lyophilisation and derivatisation

The precipitated GAGs were centrifuged at 14,000g for 15 minutes at 4°C. The samples were lyophilised by using a vacuum and heat to remove moisture. For the derivatisation of samples, the fluorphore 2-aminoacridone (2-AMAC) (Sigma-Aldrich, #06627) was used. This was prepared fresh prior to each experiment at 12.5 mM in 85% DMSO (v/v) and 15% acetic acid (v/v). 1.25 M sodium cyanoborohydride (Sigma-Aldrich, #156159) was also prepared fresh in milliQ-H_20. Dried disaccharide preparations were derivatised in 2-AMAC and sodium cyanoborohydride on an orbital shaker overnight at 37°C. The standard disaccharides were also tagged using the same method.

Day Four: Cessation of derivatisation

The tagging process was terminated by the addition of 30% glycerol in equal ratio. Samples were wrapped in aluminium foil and stored at -20°C until FACE gel analysis.

4.3.5.2 FACE

A gel-casting apparatus was cleaned and assembled. The gel solution was prepared, composed of: 30% polyacrylamide gel in 0.5 M tris-borate buffer, pH 8.3, and 10% (w/v) ammonium persulfate (APS) to a working concentration of 0.75% (v/v). Polymerisation was initiated by the addition of 0.625% (v/v) of tetramethylethylenediamine (TEMED). The 30% polyacrylamide gel solution was immediately poured into the gel-casting apparatus. A 1.5 mm comb was inserted, and the gel solution was allowed to solidify completely.

AMAC-conjugated samples were diluted in 87.5% (v/v) milliQ-H_20 and 12.5% FACE solvent (dimethyl sulfoxide (DMSO), glycerol, 0.1% phenol red (w/v) in milli Q-H_20), and 0.1 µg of samples were loaded into each well. 0.1 µg of standard disaccharides were also loaded. All samples were electrophoresed at a cool temperature at 300 V for 45 minutes, or until the phenol red exited the gel. Gels were imaged in a UV chamber using the Molecular Imager ChemiDoc XRS System (Biorad).

4.3.6 Imaging and quantification

Quantification of band intensity from our FACE experiment was conducted using ImageJ software. Once background was subtracted from individual band intensities, band intensity of treated samples were normalised to that of untreated sample and presented as a percentage. Data analysis and graph generation were achieved using the OriginPro 2019b software. . Tests for significance (p<0.05) were performed using either: paired Student's *T-test* or one-way analysis of variance (ANOVA) with Tukey's post hoc test.

4.4 Results

4.4.1 Establising the percentage loss of GAGs during the extraction and isolation procedure

Immunocytochemistry results revealed a trend of both WFA and HA intensity reduction following treatment of the inhibitors 4-MU, JD059, and JD060. To further affirm their effects on the PNN, we quantified the amount of overall GAG content following treatment with the compounds. This was done by the careful extraction and isolation of GAGs from the PNNs on the surface of the cells in Buffer 1 (physiological saline), which extracts GAGs from the ECM around cells (Deepa *et al.*, 2006; Kwok *et al.*, 2014). The resulting products are then quantified using cetylpyridinium chloride (CPC) turbidimetry and calculated from the linear regression equation of commercial CS-A standard (Figure 19) (Srimasorn *et al.*, 2022). This method of GAG harvesting and isolation has been exploited in previous reports (Dick *et al.*, 2013).

In order to establish the percentage loss of GAGs from the GAG extraction and isolation protocol, 5 mg of CS-A was included and subjected to the same isolation procedure as PNN-HEK293 GAGs to ascertain the average amount of GAGs lost during the procedure. Quantification of GAGs using CPC turbidity assay showed that an average of 17.2 ± 5.01% of CS-A was lost during the isolation procedure, as summarised in Table 4. We can therefore estimate the amount of GAGs extracted from PNN-HEK293 cells lost during the isolation process.

Table 4. Mean amount of CS-A extracted

Experiment number	Starting quantity (µg)	Final quantity of GAGs (µg)	GAGs lost (%)
1	5000	3808.8	23.8
2	5000	4429.2	11.4
3	5000	4182.3	16.4
		Average %	17.2

4.4.2 4-MU, JD059, and JD060 cause a decrease in GAG content at all concentrations

The amount (µg) of total GAG content extracted from cells in all treatment conditions is illustrated in Figure 20. Results were normalised against the untrated condition for comparison. In comparison to the untreated control cells, 4-MU, JD059, and JD060 led to a dose-dependent decrease in GAGs produced (Figure 20). 0.25 mM of 4-MU, JD059, and JD060 treatment led to a 22.2 ± 9.12%, 34.0 ± 15.0%, and a 36.0 ± 5.29% decrease in GAGs respectively. 0.5 mM of 4-MU, JD059, and JD060 led to a greater 55.9 ± 20.3%, 46.7 ± 13.2%, and a 51.5 ± 9.57% reduction in GAGs respectively. Finally, 1 mM of 4-MU, JD059, and JD060 caused a 53.9 ± 17.3%, 52.6 ± 10.5%, and a 59.3 ± 12.9% reduction in GAGs produced.

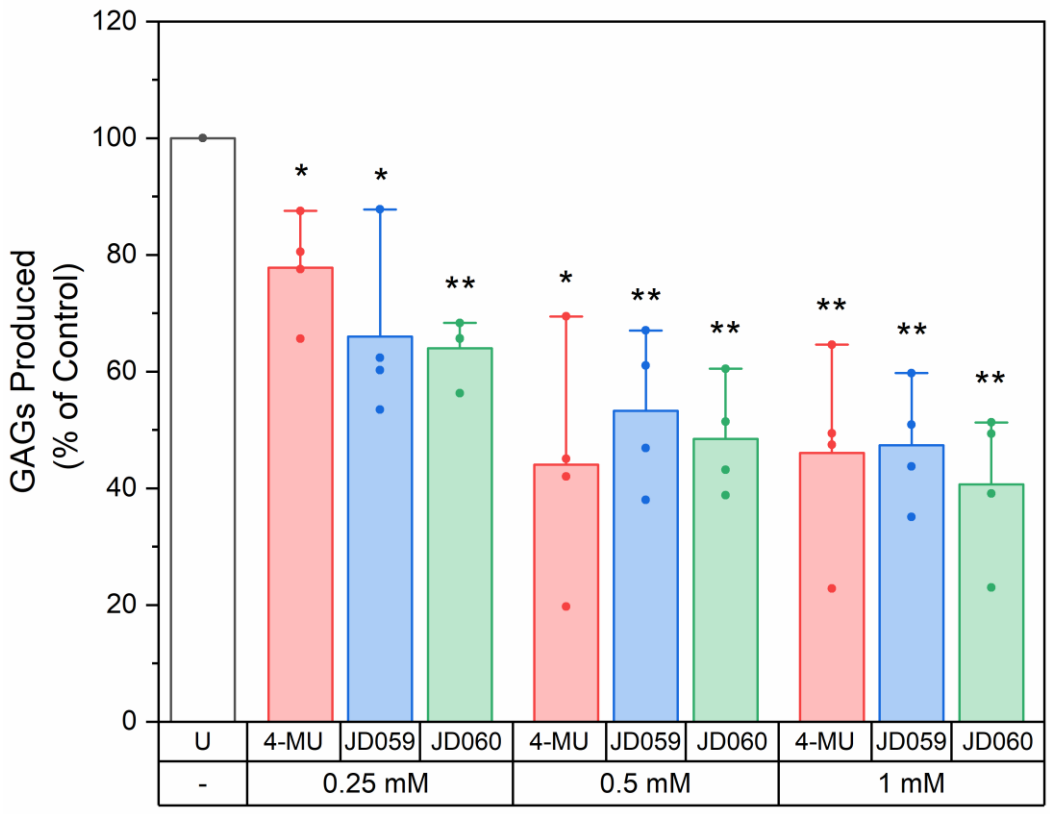

Figure 20. The effect of 4-MU, JD059, and JD060 on overall GAG production. Extracted GAG concentration in cell lysates was quantified using CPC turbidity assay. Error bars represent the mean ± S.D. of four independent experiments. n = 4; i.e, data were pooled from 4 independent experiments from 4 different cell cultures not exceeding Passage 40. One-way ANOVA statistical analysis; * (p<0.05), ** (p<0.01) *** (p<0.001).

4.4.3 4-MU not only reduces HA but CS disaccharides as well

Thus far, we have ascertained that all compounds are able to reduce overall GAG content effectively. To investigate if this was due only to the inhibition of HA, or whether this was due to the inhibition of both HA and CS, FACE was utilised to determine the levels of HA and CS disaccharides following treatment of 1 mM of 4-MU. As previously described, FACE is a rapid and sensitive method of measuring the levels of saccharides based on the coupling of a fluorophore to a reducing end carbohydrate via reductive amination (Starr *et al.*, 1996). FACE gels provide a high resolution separation of oligosaccharides by size in an electric field (Jackson *et al.*, 1990 and Huang *et al.*, 2006). Long chains of GAGs, such as CS and HA in this case, can be digested into disaccharides (ΔDi) using GAG-specific enzymes, such as chondroitinase ABC (chABC).

This creates a reducing end for fluorophore labelling. The fluorescence intensity of the disaccharide bands produced would be proportional to the amount of fluorophore (Starr *et al.*, 1996; Calabro *et al*, 2000), facilitating the quantification of HA and CS disaccharides coupled to the fluorophore. In addition, the selection of the enzyme used will allow for a specific characterisation of the disaccharides of interest.

With the use of FACE, it was observed for the first time that 4-MU indeed has the capacity to reduce CS levels (Figure 21; for image of entire gel, please refer to image 31 of the Appendix), and not only HA as currently reported. Three days treatment of PNN-HEK293 cells with 4-MU led to a dose-dependent decrease of ΔDi-HA (Figure 21B; 26.1 ± 7.04% at 0.25 mM, 31.1 ± 7.74% at 0.5 mM, and 47.6 ± 8.02% at 1 mM) and ΔDi-CS (Figure 21C; the combined band ΔDi-4S and ΔDi-6S: 13.4 ± 2.97% at 0.25 mM, 24.7 ± 6.67% at 0.5 mM, and 28.0 ± 4.33% at 1 mM). These results illustrate two key findings: 1) 4-MU is indeed a highly-effective HA inhibitor and 2) 4-MU possesses CS-inhibiting properties, which has previously not been firmly established.

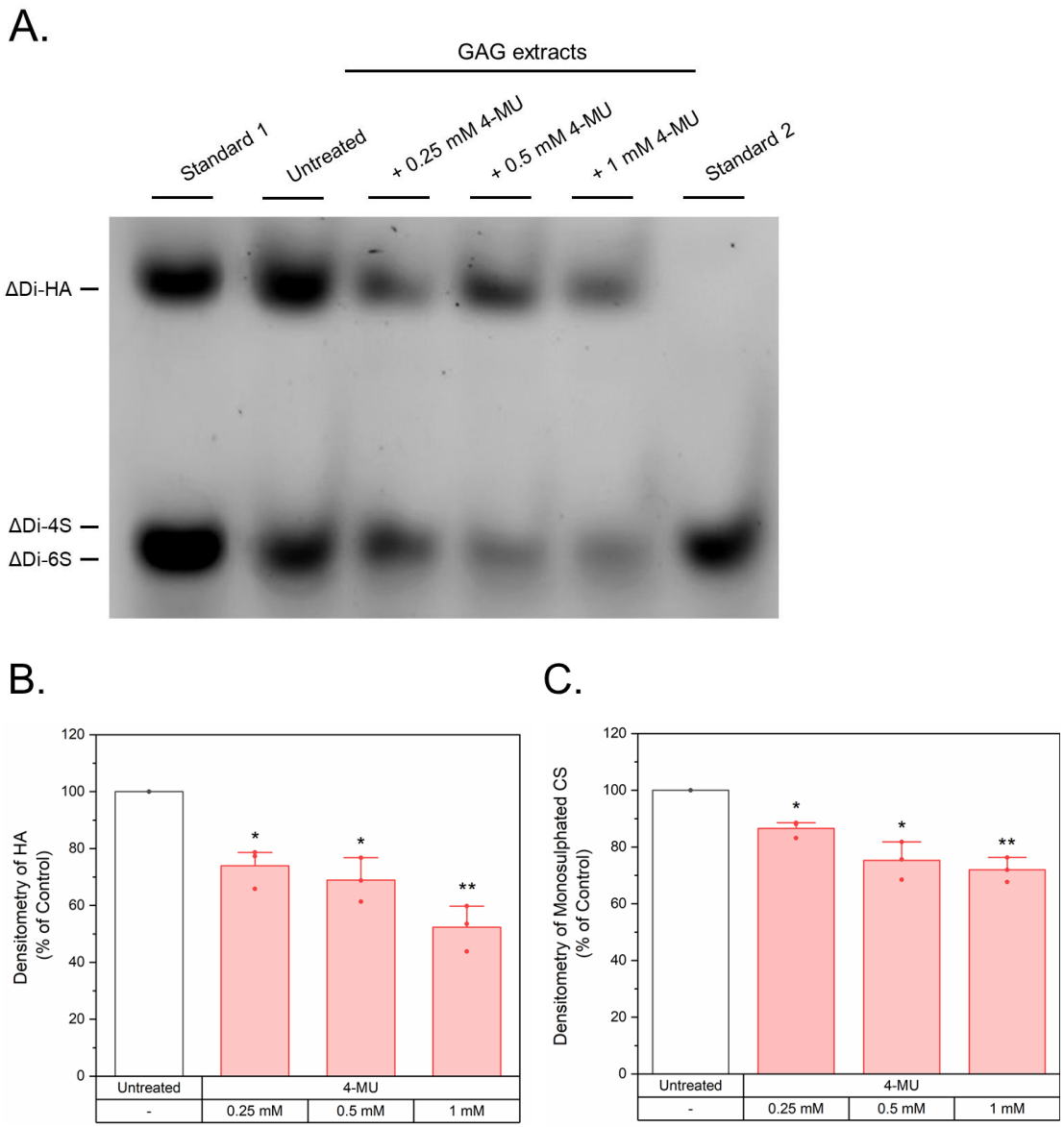

Figure 21. Biochemical analysis of HA and CS-GAGs extracted from PNN-HEK293 cells following treatment with 0.25 mM, 0.5 mM, and 1 mM 4-MU. The GAGs were digested into disaccharides using chABC and the resulting disaccharides were labelled with a fluorophore and electrophoresed in the FACE gel. ΔDi-HA combined with ΔDi-4S (standard 1) and ΔDi-6S (standard 2) were identified by comparing the migration of the band to standard disaccharides in the first two lanes. **A.** Treatment with increasing doses of 4-MU resulted in a significant decrease of ΔDi-HA band intensity and of ΔDi-4S or ΔDi-6S band intensities. Densitometric analysis of **B.** HA and C. Combined C4S and C6S band intensities showed that the observed reduction in band intensities were significant, with 1 mM being the most potent dose. Error bars on graphs represent mean ± SD of three independent experiments. n = 3; i.e, data were pooled from 3 independent experiments from 3 different cell cultures not exceeding Passage 40. Paired Student's *t*-test statistical analysis. * (p<0.05), ** (p<0.01).

4.4.4 The 4-MU analogues JD059 and JD060 also reduce CS and HA disaccharides

Chapter 3 has shown that JD059 and JD060 exhibit greater potency in HA and CS expression than 4-MU. It was pertinent to determine if the 4-MU-derived analogues JD059 and JD060 also elicited similar effects on HA and CS disaccharide levels as 4-MU. FACE experiment was conducted on GAGs isolated from PNN-HEK293 cells treated to 1 mM of JD059 and JD060 for 3 DIV.

FACE results demonstrated that JD059 and JD060 reduced both HA and CS disaccharides, as observed with 4-MU (Figure 22, for image of entire gel, please refer to Figure 32 of the Appendix). Three days of JD059 treatment resulted in a 55.1 ± 10.3% decrease of ΔDi-HA and a 52.6 ± 9.17 % decrease in the combined band for ΔDi-4S and ΔDi-6S. Treatment with JD060 led to a 54.4 ± 3.02% decrease of ΔDi-HA and a 62.9 ± 5.80% decrease in the overall size of the combined band for ΔDi-4S and ΔDi-6S (Figure 22B and 22C). These findings confirm that JD059 and JD060 bear the same HA- and CS-inhibiting characteristics as 4-MU. Importantly, 1 mM of JD060 was more effective than 1 mM of 4-MU in reducing CS-GAGs.

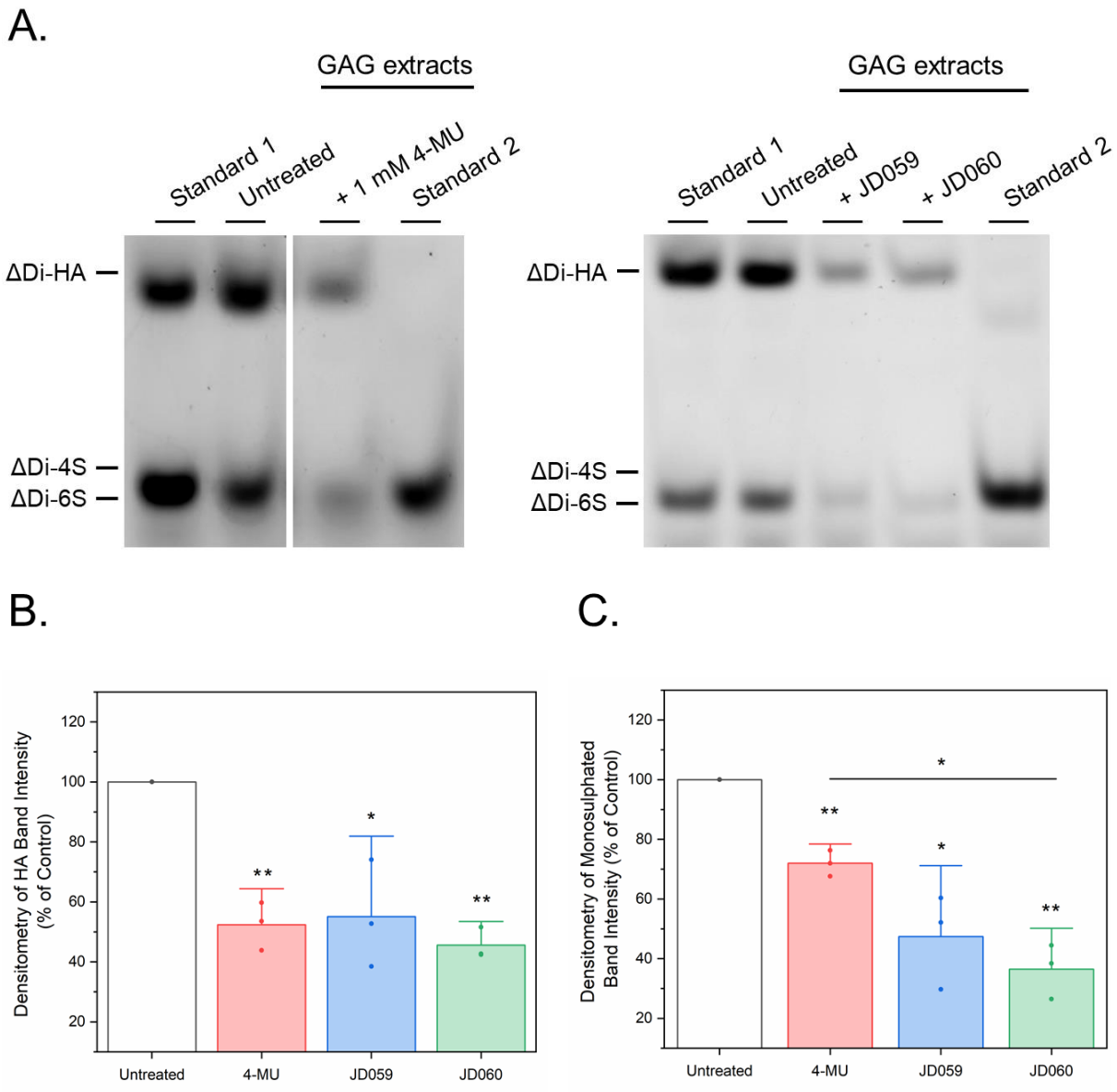

Figure 22. Biochemical analysis of HA and CS-GAGs extracted from PNN-HEK293 cells, compared between 1 mM of 4-MU, JD059, and JD060 treatments. The GAGs were digested into disaccharides using chABC and the resulting disaccharides were electrophoresed in the FACE gel ΔDi-HA (standard 1) and a combination of ΔDi-4S and ΔDi-6S (standard 2) were identified by comparing the band location to the standard disaccharides in the far left lanes. **A.** ΔDi-HA (standard 1) and a combination of ΔDi-4S and ΔDi-6S (standard 2). Treatments of all compounds caused a marked decrease in band intensities of ΔDi-HA and in the combined band intensity of ΔDi-4S and ΔDi-6S. Densitometric analysis of **B.** HA and **C.** Combined C4S and C6S band intensities illustrate that the observed reduction in band intensities were significant. Error bars on graphs represent mean ± SD of three independent experiments. n = 3; i.e, data were pooled from 3 independent experiments using 3 different cell cultures not exceeding Passage 40. Paired Student's *t*-test statistical analysis. * ($p<0.05$), ** ($p<0.01$).

4.4.5 4-MU, JD059, and JD060 decrease HAS3 expression

Finally, we sought to explore the influence our compounds had on HAS3 and HAPLN1 protein expression as a possible mechanism for PNN inhibition. While the effect of 4-MU on HA and GAG synthesis was mediated by blocking UDP-GlcA synthesis, there are reports showing that 4-MU is also able to reduce HAS (Kakizaki *et al.,* 2004; Kultti *et al.,* 2009; Vigetti *et al.* 2009). HAS3 and HAPLN1 have been established to be crucial for producing a pericellular PNN structure around HEK cells, as discussed. In the CNS, HAS2 and HAS3 are prevalently expressed by neurons, whereas HAS1 is confined to the endothelium (Carulli *et al.,* 2006; 2007). HAS3 likely precedes HAS1 during PNN formation (Zimmerman *et al.,* 2008; Kwok *et al.,* 2010).

Total cell lysate was prepared from PNN-HEK293 cells treated with 0.25 mM, 0.5 mM, and 1 mM of 4-M, JD059, and JD060 for 3 DIV. The changes of HAS3 and HAPLN1 were assayed by western blotting. With the use of an anti-HAS3 antibody, it was observed that all three small molecule modulators led to a reduction of HAS3 expression, and that this was demonstrated at all doses (Figure 23A and 23B). With 4-MU, the reduction at 0.25 mM, 0.5 mM, and 1 mM was 8.82 ± 5.27%, 15.5 ± 4.62%, and 23.8 ± 4.61%, respectively. Similarly, for JD059, there was a reduction of 8.42 ± 4.66%, 19.7 ± 9.12%, and 18.8 ± 6.05% levels, and JD060 caused a 18.3 ± 7.36%, 31.6 ± 15.8%, and 28.4 ± 6.87% decrease in HAS3 protein levels at the respective doses. This concurs with known data relating to the effect of 4-MU on HAS3 expression. 4-MU has been shown to reduce HAS2 transcripts in rat fibroblasts (Kakizaki *et al.,* 2004). Both HAS2 and HAS3 mRNA levels were reduced in numerous cancer cell lines (Kultti *et al.,* 2009). In smooth muscle cells, transcripts coding for HAS1 and HAS3 were reduced after 1 mM of 4-MU treatment (Vigetti *et al.,* 2009). Our findings therefore corroborate with known literature that 4-MU may exert its effects by regulating expression of HAS3. We did not observe a significant difference in HAPLN1 protein expression levels under any treatment condition (Figure 23C).

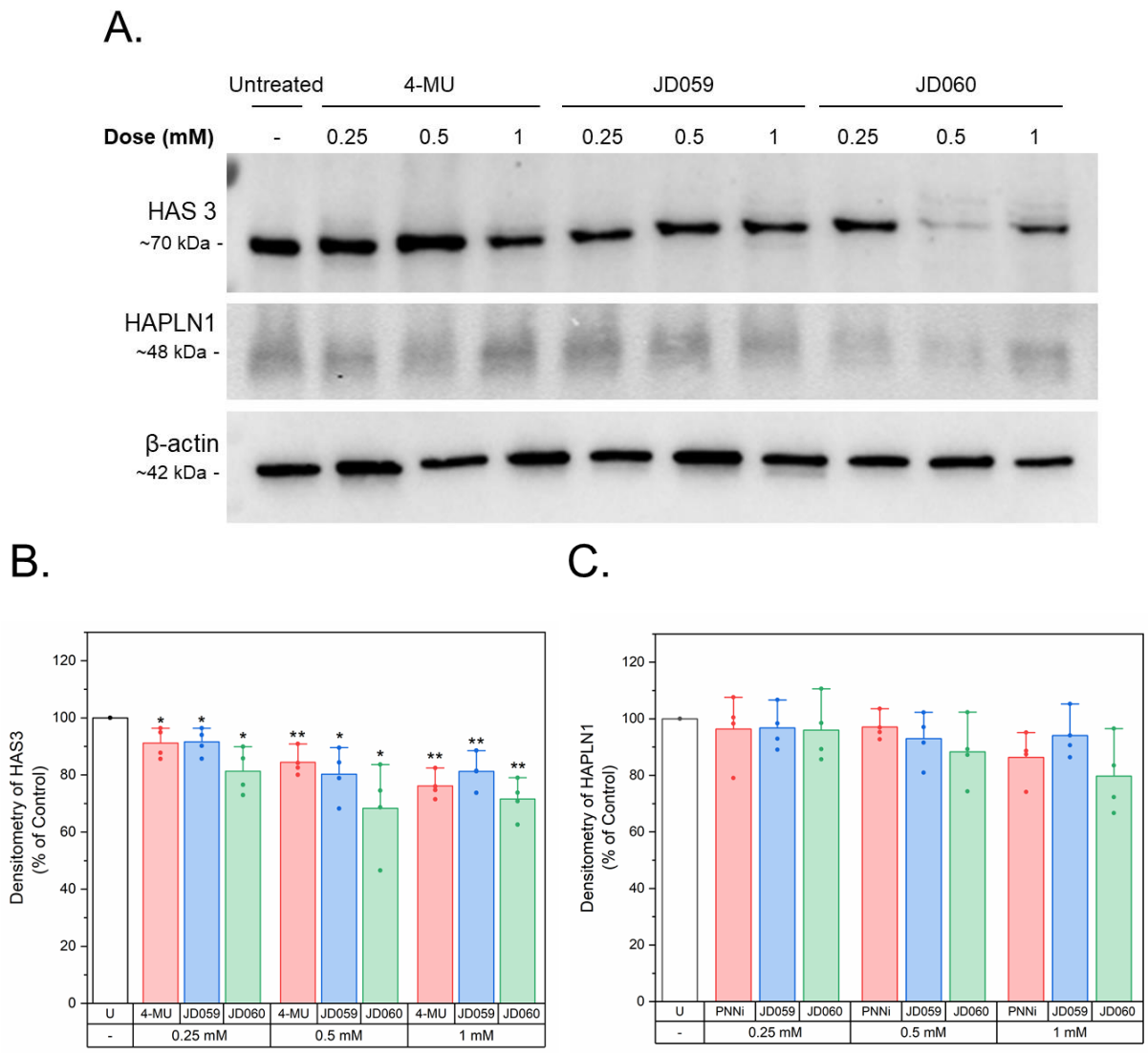

Figure 23. HAPLN1 protein levels in PNN-HEK293 cells following treatment with 4-MU, JD059, and JD060. β-actin protein levels were used as the control. Densitometric analysis of **B.** HAS3 **C.** HAPLN1 protein levels in PNN-HEK cells following treatment with 4-MU, JD059, or JD060. Error bars on graphs represent mean ± SD of three independent experiments. n = 3; i.e, data were pooled from 3 independent experiments using 3 different cell cultures not exceeding Passage 40. Paired *t*-test statistical analysis; * (p<0.05), ** (p<0.01).

4.5 Discussion

4.5.1 Summary of results

We have successfully extracted and isolated GAGs, and assessed GAG content produced by PNN-HEK293 cells. Semi-quantitative CPC turbidity assay on GAGs recovered from cells treated with 0.25 mM, 0.5 mM, and 1 mM of 4-MU, JD059, and JD060 showed a dose-dependent decrease in GAG production across all treatment conditions. To establish the components of GAGs that were decreased by the treatment, the isolated GAG fractions were analysed using FACE. It was shown that 4-MU has the capacity to attenuate not just HA, but monosulphated CS. The degree of attenuation increased with higher doses of 4-MU. Finally, we were able to illustrate that JD059 and JD060 were able to elicit similar CS- and HA-inhibiting effects, highlighting the efficacy of these compounds and their potential as replacements of 4-MU.

4.5.2 4-MU, JD059, and JD060 reduce overall GAG production of PNN-HEK293 cells

We have successfully demonstrated the efficacies of our compounds to reduce overall GAG production in an *in vitro* model of PNNs. HA is a major GAG in the ECM as well as in the PNN across the CNS. As discussed, the HA-inhibiting properties of 4-MU have been widely-reported (Kakizaki *et al.,* 2004; Kultti *et al.,* 2009, Vigetti *et al.,* 2009; Vigetti *et al.,* 2011; Cheng *et al.,* 2018; Sukowati *et al.,* 2019), but its potential CS-inhibiting characteristics is still a matter of contention. We first executed the careful extraction and isolation of GAGs from an *in vitro* model of cells, done using a modified protocol published previously (Deepa *et al.,* 2006; Dick *et al.,* 2013; Kwok *et al.,* 2015). To determine if we were losing a substantial amount of GAGs during the isolation process, we included a known amount of CS-A and subjected it to the same protocol as our extracted GAGs. We found that we lost 17.2 ± 5.01% across three independent experiments, which was determined to be within an acceptable range based on prior observations made by senior scientists in the lab who had conducted the same procedure (Foscarin *et al.,* 2017). We could then use this result to estimate the amount of GAGs lost from our PNN-HEK293 samples. Across four independent experiments, we found that 1 mM of our compounds to be the most potent in reducing GAG content, ranging from 52.6 to 59.3% decrease in GAGs.

4.5.3 4-MU has the capacity to reduce CS and HA

We demonstrated in our previous chapter the potential of our compounds in impeding expression of WFA^+-CS residues, assessed morphologically via immunostaining. In this chapter, we found that our compounds could reduce overall GAG production; however, it was fundamental to characterise the GAGs that were affected. In order to achieve this, we subjected the isolated GAG fractions to FACE.

Our CPC turbidity results show that 4-MU reduces the overall levels of GAGs, and of these GAGs, our FACE analyses demonstrate that HA and monosulphated CS levels were decreased. For this experiment, GAGs were harvested from the surface of PNN-HEK293 cells. Given this method of GAG isolation, we can draw an important conclusion from our FACE results: the production of HA and monosulphated CS were each directly impeded by 4-MU. Importantly, the direct inhibition of 4-MU on CS production has not been reported before to our knowledge, establishing our result as a novel finding. This result additionally supports the observed reduction of WFA labelling in our PNN-HEK293 culture (chapter 3.4.2), which has been reported to predominantly bind to *N*-acetylgalactosamine (GalNAc) of CS-GAG sugars.

Our findings contradict the few reports to have directly investigated the effects of 4-MU on CS production. Since both studies measured CS released into the culture media (Rilla *et al.,* 2004; Vigetti *et al.,* 2009), there is one major reason that could account for this discrepancy, which is the duration of 4-MU treatment.

Our study had a longer duration of 4-MU treatment, amounting to 3 DIV for cultured PNN-HEK293 cells, in comparison to the reports published by Rilla's and Vigetti's teams. The limited incubation time of 4-MU used in cultured keratinocytes (6 hours) (Rilla *et al.,* 2004) and in AoSMCs (24 hours) (Vigetti *et al.,* 2009) could account for the lack of 4-MU-mediated suppression of CS synthesis. A longer treatment time would lead to a cumulative effect, thus causing observable changes in our assay. We cultured our HEK cells in the presence of 4-MU for a total of 3 days, which may reflect an optimum time point at which 4-MU functions. Our treatment duration of 3 DIV was chosen based on preliminary data conducted in the lab previously (unpublished data). Additionally, it has been reported that 4-MU elicits considerable HA-reducing effects for 3 DIV with no alterations in cell viability

(Cheng *et al.*, 2018), which supports our assumption of great efficacy at this time period. However, there is a need to comprehensively study cellular uptake and internalisation of 4-MU, which would aid in determining the optimum duration that causes the greatest reduction of HA and CS, without affecting cell viability. The process of CS biosynthesis is highly complicated, involving the participation of a battery of enzymes (Silbert and Sugumaran, 2002; Afratis *et al.*, 2012; Kwok *et al.*, 2012). It is therefore plausible that a longer treatment of 4-MU is required in order for CS biosynthesis to be affected.

4.5.4 The rationale behind using FACE for our study

As described, there are some limitations to the common methods of GAG analysis and quantification. Techniques involving radioactivity may not affect the quality of results obtained, but it is generally not ideal due to concerns regarding health hazards and complications with waste disposal. Column chromatographic techniques are highly sensitive technique to assay specific GAGs but it generally require large amounts of starting material and is time-consuming, and would thus be infeasible for the application of mass screening (Kubaski *et al.*, 2017). Thus, a sensitive technique for profiling GAGs from a small amount of starting material that is ready available and economically viable was sorely needed for the purposes of this study.

To that end, FACE was selected for our analysis of GAGs. Because of the high percentage of acrylamide (30%) used for our FACE protocol, only carbohydrates are able to migrate through the gel, whereas high molecular weight molecules such as proteins are not. We also utilised the fluorophore 2-aminoacridone (2-AMAC) to label our GAGs through a derivatisation step to the reducing termini of saccharides to form a Schiff base, the reaction of which is then stabilised by sodium cyanoborohydride (Bigge *et al.*, 1995; Calabro *et al.*, 2000; Ruhaak *et al.*, 2010; Barnes *et al.*, 2016). 2-AMAC has been used to derivatise the reducing ends of numerous monosaccharides and oligosaccharides since the 1990s (Jackson, 1991; Jackson, 1996; Barnes *et al.*, 2016), and these labelled saccharides can subsequently be separated with high resolution by PAGE. The fluorotagging process with 2-AMAC introduces a highly fluorescent label that provides an identical signal for every free reducing group of the saccharides in our samples, thus allowing molar quantities to be determined.

We selected standards for ΔDi-HA, ΔDi-4S, and ΔDi-6S due to the fact that these GAGs comprise the majority of GAGs with the diffuse ECM in the adult rat brain (Deepa *et al.*, 2006) In fact, the proportion of ΔDi-4S within the diffuse ECM is 91.2%, making it the major

CS-GAG in the adult rat brain (Deepa *et al.*, 2006). Because the molecular weights of ΔDi-4S and ΔDi-6S are the same (Osago *et al.*, 2014), we are unable to ascertain if ΔDi-4S, ΔDi-6S, or both disaccharides were reduced in the presence of our compound. It will be necessary and highly informative to characterise this in future research (discussed further in chapter 6). We are also unable to ascertain if other CS-GAG disaccharides, such as ΔDi-4,6S (disaccharide of CS-E, sulphated at C-4 and C-6 of *N*-acetylgalactosamine) were affected by our compounds via this method, as we did not see the presence of any other disacharride bands other than the ones corresponding to our standards (Appendix). CS-E and CS-D comprise 1.4% and 0.7% respectively of total CS-GAGs in the brain (Deepa *et al.*, 2006), and it is thus highly likely that amounts synthesised by our cells were too low to be detected, which represents a minor limitation of this method. However, for the purposes of this study, the focus on C4S and C6S was necessary, due to their high proportions as well as their effects on neuroplasticity (Yang *et al.*, 2014; Foscarin *et al.*, 2017; Yang *et al.*, 2021).

4.5.5 JD059 and JD060 possess similar CS- and HA-inhibiting traits, with JD060 eliciting greater potency as a CS inhibitor

We found that the PNN-derived analogues JD059 and JD060 were able to reduce HA and CS disaccharide quantity. Given that the functionality of the analogues was unchanged from that of 4-MU, this result was reassuring. Our results indicate that our analogues JD059 and JD060 reduce HA levels to similar levels as 4-MU; however, they do exhibit a trend of greater potency in reducing CS levels, which may be attributed to its increase in solubility. Indeed, 1 mM of JD060 led to significantly lower CS GAG levels of PNNs than 1 mM of 4-MU, which could be attributed to its increased solubility. These analogues therefore possess superior aqueous solubility to 4-MU and retained their PNN-inhibitory activity.

It is intriguing that the effects of the small molecule modulators on CS reduction appear stronger in the FACE analysis than in the *Wisteria floribunda* agglutinin $(WFA)^+$ expression in chapter 3, though there are several possible explanations for this disparity. First, WFA could be less specific than expected, possibly binding to other GAGs other than CS. In fact, WFA has been reported to bind strongly to heparin (Nadanaka *et al.*, 2020). Second, it is conceivable that WFA preferentially binds to certain sulphation patterns exhibited by CS chains, although this has not been clarified. For instance, a study utilising WFA and the antibody Cat316 reported that Cat316 strongly associated with C4S specifically (Yang *et al.*, 2017); however, there is little to no overlap between WFA and Cat316 (Ueno *et al.*, 2018;

Nadanaka *et al.*, 2020). This implies that WFA could bind to subsets of CS chains, which could lead to the presence of a WFA signal even after treatment with a compound, as observed in our immunocytochemistry results in chapter 3 following 0.25 mM doses. In contrast, the FACE analysis employed here shows that treatment with the small molecule modulators induce a direct decrease in the combined levels of C4S and C6S, which are the two major forms of CS chains.

4.5.6 HAS3 protein expression levels were altered upon treatment with all compounds

The mechanisms by which 4-MU, and by extension our novel compounds, inhibits PNN synthesis remains to be elucidated. We studied their effects on a potential regulatory step: HAS3 protein expression. We found a significant reduction of protein levels of HAS3, suggesting that the observed attenuation of HA and overall GAG levels may be ascribed to a decrease in HAS-mediated HA synthesis. 4-MU has been reported to downregulate HAS2 and HAS3 mRNA (Rilla *et al.*, 2004; Kultti *et al.*, 2009), indicating that 4-MU regulates HAS gene expression, and is in accordance with our observed reduction of HAS3 protein levels. These effects are likely mediated by the proposed mechanism of 4-MU: 4-MU reduces the levels of HAS substrate UDP-GlcA, which is consumed when 4-MU becomes glucuronidated (Kakizaki 2004; Kultti *et al.*, 2009; Vigetti *et al.*, 2009). HAS activity and expression are heavily reliant on the cytosolic concentration of its substrates UDP-GlcA and UDP-GlcNAc (Nakamura *et al.*, 1995; Jokela *et al.*, 2008; Rilla *et al.*, 2013; Deen *et al.*, 2016), it is plausible that this is one way 4-MU regulates HAS expression.

The relationship between availability of HAS substrates and HAS3 expression and activity has been under some scrutiny. One theory of burgeoning interest is that the availability of HAS substrate may influence vesicular trafficking and plasma membrane abundance of HAS3. However, this may prove technically difficult to achieve. Trafficking of HAS from the Golgi to the membrane is complex, and additionally HAS may be recycled within the Golgi, much like numerous glycosyltransferases (Shestakova *et al.*, 2005; Liu *et al.*, 2018).

Another possible mechanism is that endocytosis of HAS3 is modulated in the presence of 4-MU. In 2016, trafficking kinetics of HAS3 were analysed in MV3 cells, a melanoma cell line by Deen's group (Deen *et al.*, 2016). These cells were transfected with human HAS3 (termed Dendra2-HAS3) plasmids. Deep Mask Red was used as a plasma membrane marker, allowing the tracing of HAS3 retrograde trafficking (endocytosis) between the plasma

membrane. The study found that the treatment of 4-MU increased the outflow of HAS3 from the Golgi, and reduce its appearance towards the cell membrane (Deen *et al.,* 2016). Additionally, depletion of UDP-GlcA by 4-MU caused an increase in HAS3 endocytosis, significantly decreasing the amount of HAS3 localised to the plasma membrane (Deen *et al.,* 2016, Figure 3b). Furthermore, they found that lowering levels of UDP-GlcA decreased vesicles containing HAS3 and significantly increased the fraction of HAS3 co-localised with early endosomes. Overall, these findings highlight that UDP-sugars play a more complex role in HA synthesis besides serving as substrates of HAS3. This seminal work provides evidence of a relationship between 4-MU and expression of HAS3, but unfortunately does little in providing a potential mechanism for our observed reduction of total cellular HAS3 protein levels, though it may explain why we showed attenuated HA on the surface of PNN-HEK293 cells (chapter 3). It would be greatly insightful if we could corroborate this with our compounds to elucidate their mechanisms in regulating HAS3. Nevertheless, our observation of reduced total HAS3 protein levels leads us to propose that transcription and biosynthesis of HA was affected by our compounds, and we this notion in chapter 6.6.

HAPLN1 is a key element of PNNs, linking CSPGs to HA chains. It is necessary for the formation of a compact, pericellular PNN structure around HEK cells (Kwok *et al.,* 2010; Kwok *et al.,* 2011). In fact, HAPLN1 is the only PNN component present exclusively around neurons bearing PNNs (Carulli *et al.,* 2007), and HAPLN1 knockout animals displayed abrogated PNN production (Carulli *et al.,* 2010). We did not find any alteration in HAPLN1 protein expression, suggesting that the mechanism of action of our compounds targets does not alter the relative abundance of HAPLN1 protein within cells. This may be attributed to the fact that the attenuation of HA chains and CS caused by our compounds meant less HAPLN1 was secreted out of the cells once it had been synthesised. It should be noted however that gene expression analyses of HAPLN1 will be needed to verify this and concretely determine whether HAPLN1 is altered in the presence of compound treatment.

4.6 Conclusion and future directions

In this section we investigated the capacity of 4-MU and its more soluble derivatives JD059 and JD060 in inhibiting the production of major constituents of PNNs: HA and CS. We have first shown that all compounds were able to reduce overall GAG content on the surface of PNN-HEK293 cells. We then confirmed that these compounds reduced not just HA, but CS components as well, which has not been established in current literature. Finally, we

demonstrated that our compounds altered turnover of HAS3 protein expression levels, implying that while a diminished supply of UDP-GlcA has a substantial impact on HA and overall GAG synthesis, it is not solely due to a direct effect as a substrate in an enzymatic reaction. Our results offer a glimpse into the biological and biochemical mechanisms of 4-MU-mediated PNN inhibition. Moreover, JD059 and JD060 possess similar PNN inhibiting qualities, with JD060 potentially eliciting greater potency in reducing CS production than 4-MU. Given the novelty of 4-MU mediating PNN inhibition by modulating both HA and CS, it is imperative that this study is advanced further by examining how CS components are regulated by 4-MU. These proposals are explored in detail in chapter 6.

Chapter 5: GAGs treated with 4-MU, JD059, and JD060 are more permissive for neurite outgrowth of adult dissociated dorsal root ganglion (DRG) neurons

5.1 Introduction

Neural plasticity of the central nervous system (CNS) describes the capacity of the CNS to modulate the formation, strength, organisation of its neural network in response to stimuli. Neural plasticity is prominent in the developing nervous system, peaking during discrete time windows of postnatal life termed critical periods (Wiesel *et al.*, 1982). As the CNS matures and the critical period closes, neural plasticity persists but at severely diminished levels (Hensch, 2005; Hübener and Bonhoeffer, 2014). The onset and closure of critical periods is tightly-regulated by cellular and molecular mechanisms, the most significant of them being the maturation of GABAergic neurons, mainly fast-spiking parvalbumin-bearing (PV^+) basket cells (Hensch, 2005; Carulli and Verhaagen, 2021). Indeed, the termination of the critical period coincides with the maturation of PV^+ interneurons and formation of perineuronal nets (PNNs) around them (Wang and Fawcett, 2012; Umemori *et al.*, 2018; Fawcett *et al.*, 2019; Carulli and Verhaagen, 2021). PNNs are specialised extracellular matrix (ECM) structures saturated with hyaluronan (HA) and chondroitin sulphate proteoglycans (CSPGs). Among regulating the functional maturity of PV+ interneurons, they stabilise established synaptic connections, but are thought to restrict plasticity by doing so (Kwok *et al.*, 2011; Sorg *et al.*, 2016; Carulli and Verhaagen, 2021; Fawcett *et al.*, 2022). Thus, the centralizing concept is that the establishment of PNNs coincides with a decline in neural plasticity. However, these structures can be disrupted to reinstate juvenile-like plasticity to encourage neurite sprouting, as well as regeneration of neurons and recovery of function in diseased or injured states (Kwok *et al.*, 2011; Sorg *et al.*, 2016; Fawcett *et al.*, 2022).

The role of GAG-enriched PNNs in modulating neural plasticity and sprouting has been explored, typically using *in vitro* neurite outgrowth assays. The growth of dorsal root ganglion (DRG) neurons was greatly hindered when grown on substrates saturated with PNN glycosaminoglycans (GAGs) as opposed to GAGs from the diffuse matrix, which confirm that PNNs are a specialised inhibitory structures of the extracellular matrix (ECM) (Dick *et al.*, 2013; Foscarin *et al.*, 2017). *In vitro* treatment of chondroitinase ABC (chABC), the most commonly-employed method of PNN removal, on organotypic hippocampus cultures

enhanced dendritic spine motility (Orlando *et al.,* 2012). chABC treatment to cortical neuronal cultures induced an immature molecular phenotype, wherein expression of developmentally regulated genes Ascl1, Dlx2, and Kcnc were altered to mimic that of neurons in early development (Willis *et al.,* 2022). After *in vivo* ChABC treatment, cortical spines become more motile and exhibit increased structural and functional plasticity, leading to increased spine turnover (de Vivo *et al.,* 2013; Donato *et al.,* 2013).

The results in chapter 3 and 4 have demonstrated the suppression of CS and HA expression in PNN-HEK293 cells. Whether these PNN-inhibiting effects of our compounds govern neural plasticity, however, remains to be elucidated. To address this, a model of neurite outgrowth and regeneration was used within this study as a proof-of-concept model for neuroplasticity, as previously published (Dick *et al.,* 2013; Foscarn *et al.,* 2017). We used an *in vitro* dorsal root ganglion (DRG) cultures and assessed how neurite outgrowth is affected when grown on GAG-coated substrates that had been treated with our compounds. A vital benefit to utilising DRG neuronal culture is that DRGs can be harvested from the rat's vertebral column with relative ease, and DRGs settle and project their neurites in culture at a much higher rate than other CNS neurons, which dramatically shortens an experiment's duration (Al-Ali *et al.,* 2013). Furthermore, adult DRG neurons have been shown to be responsive to environmental stimuli, including the molecular composition of PNNs (Dick *et al.,* 2013; Foscarin *et al.,* 2017). Overall, establishing the effects of the isolated GAGs after small molecule inhibitor treatment in a model of neurite outgrowth will glean insight into their modulation of neural plasticity, and is an important facet of this pilot study.

5.2 Aims

The aim of this chapter were to:

i) determine whether GAGs treated by our compounds would serve as a permissive or inhibitory substrates to dissociated DRG neurons, assessed by staining neurons with the neurite marker β3-tubulin and measuring neurite outgrowth.

5.3 Materials and methods

5.3.1 HEK293 and PNN-HEK293 cell culture

For the protocol detailing the culture and maintenance of HEK293 and PNN-HEK293, please refer to chapter 2.2.

5.3.2 Compound treatment

For the protocol detailing compound preparation and treatment to PNN-HEK293 cells, please refer to chapter 2.3.

5.3.3 Glycosaminoglycan (GAG) extraction and isolation

For the protocol detailing compound preparation and treatment to PNN-HEK293 cells, please refer to chapter 4.3.3.

5.3.4 Dorsal root ganglion (DRG) neurite outgrowth assay

5.3.4.1 DRG extraction

Prior to GAG harvesting and extraction, alkaline-washed coverslips were placed in 24-well plates and coated with 40 µg/ml Poly-D-Lysine in an incubator 37°C overnight. On the day of the DRG harvest, coverslips were rinsed with milliQ-H_20 twice. All coverslips were then coated with 1 µg/ml of laminin (Sigma-Aldrich, #L2020), diluted in 1x Hanks' Balanced Salt Solution (HBSS) without Ca^{2+} and Mg^{2+}, for 1 hour at room temperature in a sterile fume hood. To serve as growth substrates, GAG preparations (described in chapter 4.3.3) were used. Briefly, GAGs were extracted from PNN-HEK293 cells that had been either been untreated or treated with 1 mM of 4-MU, JD059, and JD060. Once isolated, they were stored in milliQ-H_20 water as stock solutions. In a sterile fume hood, GAGs from the various extractions were diluted at 25 µg/ml in 1x HBSS. Diluted GAGs were then applied to the relevant coverslips to serve as growth substrate conditions (Table 5) for 2 hours at room temperature under sterile conditions. During this incubation time, DRG bulbs were extracted from adult rats.

Table 5. Growth substrate conditions for the culture of dissociated DRG neurons

Source of GAG Fractions	Laminin (1 µg/ml)	GAG Fractions (25 µg/ml)	chABC (0.1 U/ml)
Control	+	-	-
Untreated PNN-HEK293 cells	+	+	-
4-MU-treated PNN-HEK293 cels	+	+	-
JD059-treated PNN-HEK293	+	+	-
JD060-treated PNN-HEK293	+	+	-
Control	+	-	+
Untreated PNN-HEK293 cells	+	+	+
4-MU-treated PNN-HEK293 cels	+	+	+
JD059-treated PNN-HEK293	+	+	+
JD060-treated PNN-HEK293	+	+	+

For DRG bulb extraction, 2-3 month-old adult Wistar rats were euthanised via overdose of pentobarbitone (Henry Schein, #VDPEN01). The spinal cord was quickly isolated, cleaned of flesh and muscle tissue, cut in 3 pieces and placed in cold DMEM. Sagittal cuts of each piece was made. Under a dissection microscope, each DRG was isolated and removed individually by their nerves to avoid directly damaging the DRG bulbs using a pair of microscissors and fine point forceps (Fine Science Tools). DRGs were kept in DMEM on ice until all DRG bulbs were removed. DRG bulbs were further cleaned to remove nerves, arachnoid matter, and blood vessels, and transferred to another petri dish containing fresh DMEM on ice.

5.3.4.2 DRG dissociation and culture

DRG bulbs were incubated in 2 ml of 0.2% (w/v) collagenase (Sigma, #C907) and 1 ml of DMEM in an incubator at 37°C for 90 minutes. The petri dish of DRG bulbs was gently rocked every 20 minutes to ensure thorough submersion in the collagenase solution. 30 minutes before the end of collagenase treatment, the relevant coverslips in the 24-well plate were treated with 0.1 U/ml of chABC (Sigma-Aldrich, #C2905) for 30 minutes in a 37°C, 5% CO_2 incubator, while the other coverslips were replaced with 1x HBSS. After 30 minutes, the chABC solution was also replaced with 1x HBSS to end the enzymatic digestion.

Following 90 minutes of collagenase treatment, 2 ml of 0.1% trypsin (Sigma, #T0303) was added to the DRG bulbs and incubated for 10 minutes at 37°C. During this incubation, trituration solution was prepared containing 1% (w/v) bovine serum albumin (BSA), 0.002%

(w/v) DNase I (Sigma, #DN25). DRG bulbs were then triturated gently in the trituration solution using Pasteur pipettes with decreasing diameter until a homogenous solution was obtained. Following centrifugation at 2000g for 2 minutes, the DRG pellet was resuspended in trituration solution and gently layered on 15% BSA in DMEM to separate debris from cells. The cell solution was centrifuged for 1000g for 15 minutes. The supernatant was discarded and the cell pellet was resuspended in culture media (DMEM + 10% FBS + 1% antibiotic-antimycotic. 500 µl final plating media, composed of DMEM, 1% ITS, 1% antibiotic-antimycotic, and 0.1% nerve growth factor-β (NGF- β) (Sigma-Aldrich, # N2513), was added to each well of the plate. 10 µl of dissociated DRG neuron solution was added to each well. DRGs were allowed to settle and cultivate in an incubator at 37°C for 24 hours before staining.

5.3.4.3 DRG immunocytochemistry

DRG neurons were washed with 1x PBS and fixed with warm 4% PFA for 15 minutes at room temperature. The cells were rinsed thrice before blocking of non-specific epitopes in blocking buffer (0.1% Triton x-100 and 3% NDS in 1x PBS) for 1 hour at room temperature on an orbital shaker. They were subsequently incubated in primary antibodies diluted in blocking buffer for 2 hours at room temperature on a shaker (see Table 2). For the staining of DRG neurites, we utilised the β-III tubulin antibody (Sigma, T8660), which recognises and binds to an epitope of βIII tubulin specific to the microtubules of neurons. To label the GAG-enriched substrates coated on the coverslips, the primary antibody chondroitin sulfate (CS)-56 was used, which binds to 4-sulphated (C4S) and 6-sulphated (C6S) CS GAG chains. Excess antibody solution was removed by rinsing the cells thrice with 1x PBS. Cells were then incubated in secondary antibodies diluted in blocking buffer for 1 hour at room temperature. Again, excess antibody solution was discarded by rinsing the cells thrice with 1x PBS and again with 1x TNS. Finally, the coverslips were mounted onto glass slides with Fluorsave and allowed to dry at room temperature overnight in the dark.

5.3.5 Imaging, quantification, and statistics

Imaging was done using either the LSM880 confocal microscope (Zeiss) with 20x or 40x objectives, or the AxioScan Z.1 Slidescanner (Zeiss) with a 20x objective. The filters were set and standardised to ensure no overlap occurred between channels. The Slidescanner was operated by the Bioimaging facility. Solitary neurons were identified, and neurite number and

length were measured using the software ImageJ (Figure 24). Only neurons which possessed neurite length of at least 2 times longer than cell body were taken into account. Data were obtained from cultures of 3 adult rats and for each treatment condition, 150 neurons were counted. To measure the intensity of substrates coated with CS-GAGs, overall fluorescence intensity of 5 selected regions per coverslip was quantified using ImageJ. Paired Student's *T-test* and One-way ANOVA were used to test for statistical significance between treatment conditions.

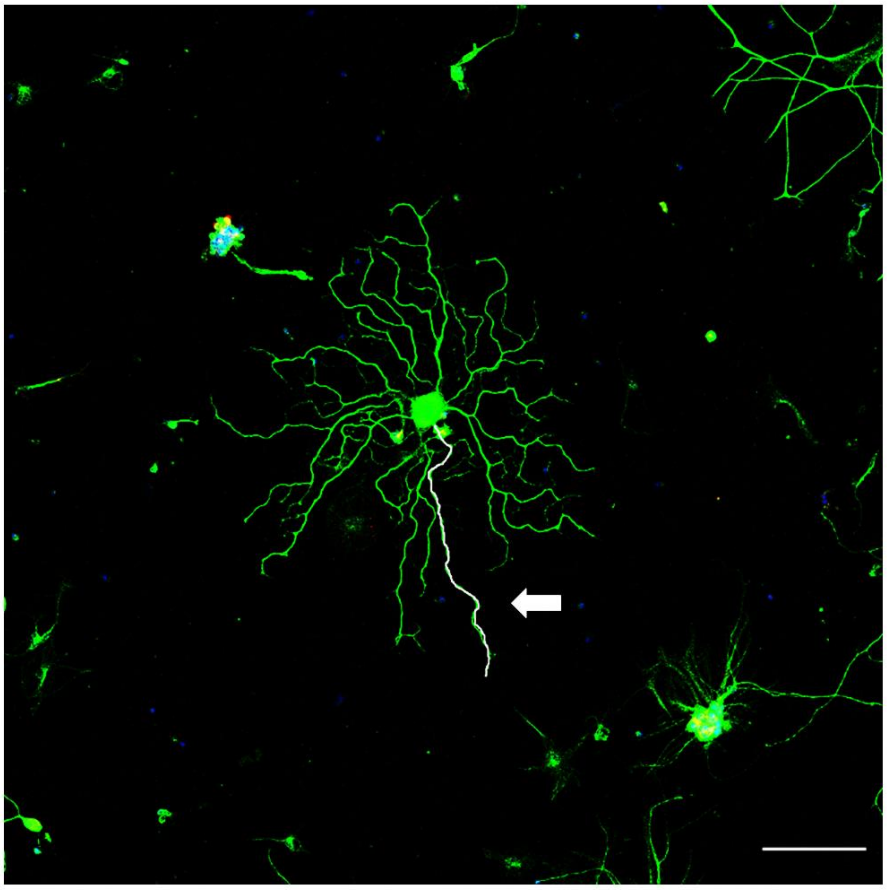

Figure 24. Example image of DRG neurons analysed using ImageJ. The longest neurite on each neuron was identified and manually traced, shown in white (white arrow). The length of the trace is then measured on ImageJ software. Scale bar: 100 µm.

5.4 Results

5.4.1 GAGs from untreated cells inhibit neurite outgrowth, which is partially rescued by chABC

The DRG neurite outgrowth assay is a robust and reliable technique to evaluate neuroplasticity. In this study, adult rat DRGs were cultured on various substrates to assess whether these substrates were inhibitory or permissive to neurite outgrowth.

We first examined the effects of using the GAGs extracted from PNN-HEK293 cells on DRG neurite inhibition. DRGs from adult rats were cultured on coverslips coated with GAG extracts from PNN-HEK293 cells at a concentration of 25 µg/ml, with coverslips coated with 1 µg/ml of laminin only to serve a permissive substrate control. After 24 hours, DRGs were fixed and stained. To affirm the presence of GAGs on the growth substrates, we stained for CS-GAGs using the antibody CS56 and quantified overall fluorescence intensity. CS56 recognises chondroitin 4 sulphate (C4S) and chondroitin 6 sulphate (C6S), which are major CS types expressed in the CNS and PNNs. We then quantified the average longest neurite from 150 neurons across three repeats as a measure of neurite outgrowth.

We verified the presence of CS-GAGs in our coated growth substrates (Figure 25). In comparison to laminin only surfaces, CS56 fluorescence intensity was increased by 293% on GAG surfaces isolated from untreated PNN-HEK293 cells (4.28 ± 0.33 a.u vs 16.8 ± 3.10 a.u, $p<0.0001$). Removal of CS chains using chABC, a widely-applied compound for CS digestion, reduced CS-GAG expression (16.8 ± 3.10 a.u vs 8.34 ± 1.72 a.u after chABC digestion, $p<0.0001$).

When assessing length of neurite outgrowth, we found that DRGs cultured on laminin alone displayed extensive neurite projections, with an average longest neurite length of 518.8 ± 40.0 µm after 24 hours in culture (Figure 25A and 25C). In contrast, DRG neurons cultured on GAGs isolated from untreated PNN-HEK293 exhibited shorter neurite length, with the longest axon per neuron averaging at 200.3 ± 34.3 µm ($p<0.0001$). These findings demonstrate the overall inhibitory nature of the GAG surface extracted from PNN-HEK293 cells on DRG neurite outgrowth and neuroplasticity. To evaluate if this GAG-mediated inhibition could be abolished, GAG-coated coverslips were treated with 0.1 U/ml of the enzyme chABC before DRG neurons were plated on. DRGs cultured on these coverslips displayed longer projections, with the longest neurite averaging at 339.0 ± 50.2 µm, which is

a significant reversal of the GAG-mediated inhibition, amounting to a 69% increase ($p<0.01$) (Figure 25C).

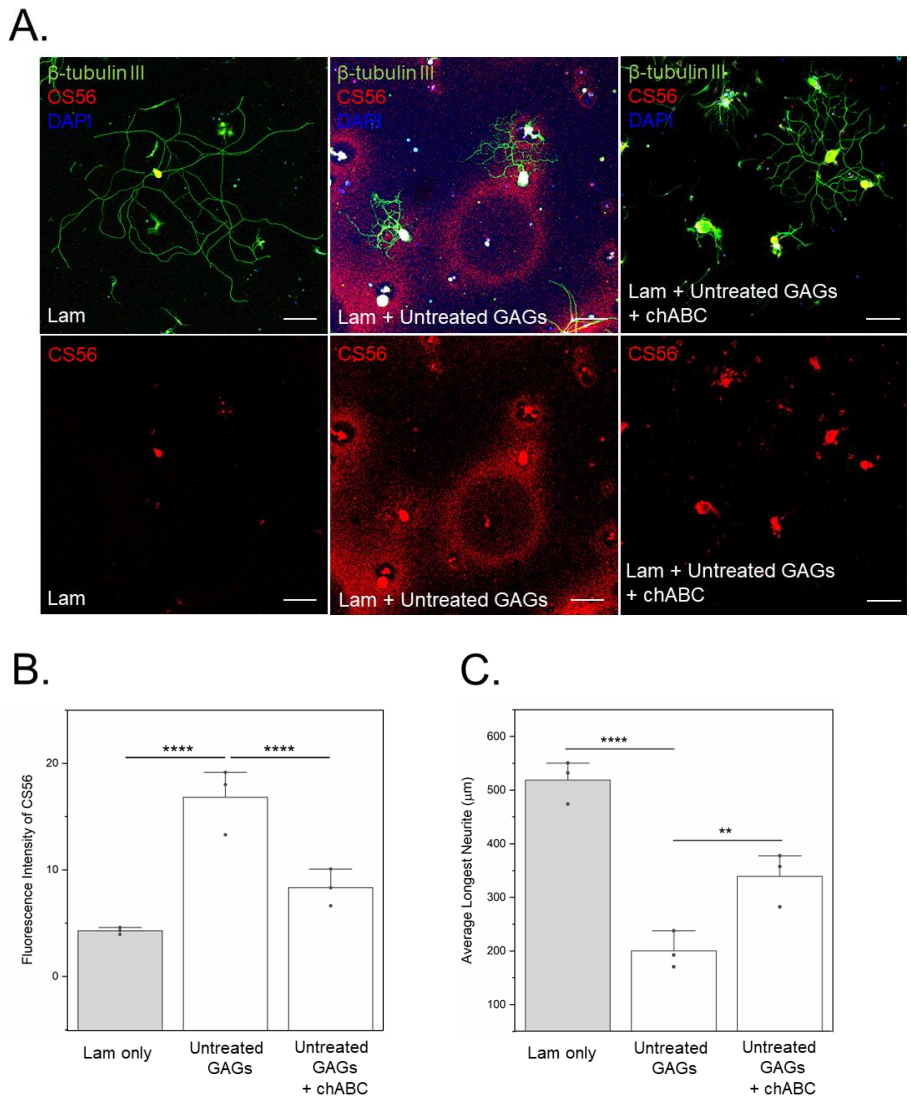

Figure 25. chABC overcomes the inhibition of DRG neurite outgrowth mediated by extracted GAGs. A. DRG neurons were grown on various substrates for 24 hours before being fixed and stained β-III tubulin, CS56, and DAPI. DRG neurons grown on laminin-only substrates had extensive sprouting. Neurons grown on laminin-only with untreated GAGs extracted from PNN-HEK293 cells had stunted growth, which was ameliorated when chABC was added. **B.** Fluorescence intensity of CS56 was markedly increased in substrates containing GAGs from untreated cultures in comparison to laminin-only surfaces, but this CS56 was abolished with chABC. **C.** Measurement of average longest neurite of DRG neurons on different plating conditions show that GAGs from untreated cells inhibited growth when compared to laminin alone, but this effect is partially rescued by the addition of chABC. Representative confocal images were taken using Zeiss LSM 880 microscope at 20x objective. Scale bars: 100 µm. Graphs show mean ±SD. n = 3; i.e, data were pooled from 3 independent DRG cultures harvested from 3 different adult rats. Significance was determined by one-way ANOVA: ** $p<0.01$, **** $p<0.0001$. *DAPI, 4',6-diamidino-2-phenylindole; lam, laminin; GAGs, glycosaminoglycans; chABC, chondroitinase ABC.*

5.4.2 GAG extracts treated with all small molecule modulators served as permissive substrates for neurite outgrowth

We then assessed the growth properties of DRG neurons on substrates coated with GAG extracts from compound-treated PNN-HEK293 cells to determine if this had any effect neurite outgrowth. The content of CS-GAGs present on the substrates after coating was confirmed by immunostaining.

DRG neurons cultured on GAG surfaces treated with 4-MU, JD059, and JD060 all exhibited extensive neurite arborisation in comparison to surfaces containing GAGs from untreated cells (Figure 26 and Figure 27). GAGs from untreated PNN-HEK293 cells were demonstrated to be significantly inhibitory to neurite outgrowth, with the average longest neurite measured was 200.3 ± 34.3 μm (Figure 27A). In contrast, neurons grown on GAG substrates recovered from 1 mM of 4-MU-, JD059-, and JD060-treated cells were more permissive to neurite outgrowth, as neurite extensions were long and complex similar to those seen in laminin control conditions. For 1 mM 4-MU-treated GAGs, the average longest neurite was 367.7 ± 28.6 μm. For 1 mM JD059-treated GAG substrates, the average longest neurite was 358.4 ± 34.9 μm. Finally, for 1 mM JD060-treated GAGs, the longest neurite measured at 412.2 ± 41.5 μm (Figure 23A). These represented an 83.6%, 78.9%, and 105.8% increase in length, respectively, with JD060 inducing the greatest increase in length.

ChABC addition to untreated GAG substrates increased average longest neurite length by approximately 69%. The presence of chABC to GAGs recovered from small molecule treatment did not significantly potentiate any neurite extension (Figure 27A), suggesting that the observed effect in neurite extension was due to the presence of CSs. Importantly, these measurements were not statistically significant from laminin only controls, which had average longest neurite length of 518.8 ± 40.0 μm (Figure 27A). The number of neurites extending from each DRG cell body was also counted as another parameter of neurite plasticity. Whilst we observed a decreasing trend of neurite number when grown on GAGs harvested from untreated cells, this was not significant. However, data from average longest neurite length measurements demonstrate that GAGs that had been treated with all our compounds served as permissive substrates for DRG arborisation.Taken together, it is inferred that despite a high content of CS-GAGs harvested from treated PNN-HEK293 cells, neurite projection length was elongated in comparison to substrates containing GAG fractions

from untreated cells. These observations support our hypothesis that our small molecule modulators 4-MU, JD059, and JD060 possess plasticity-enhancing properties.

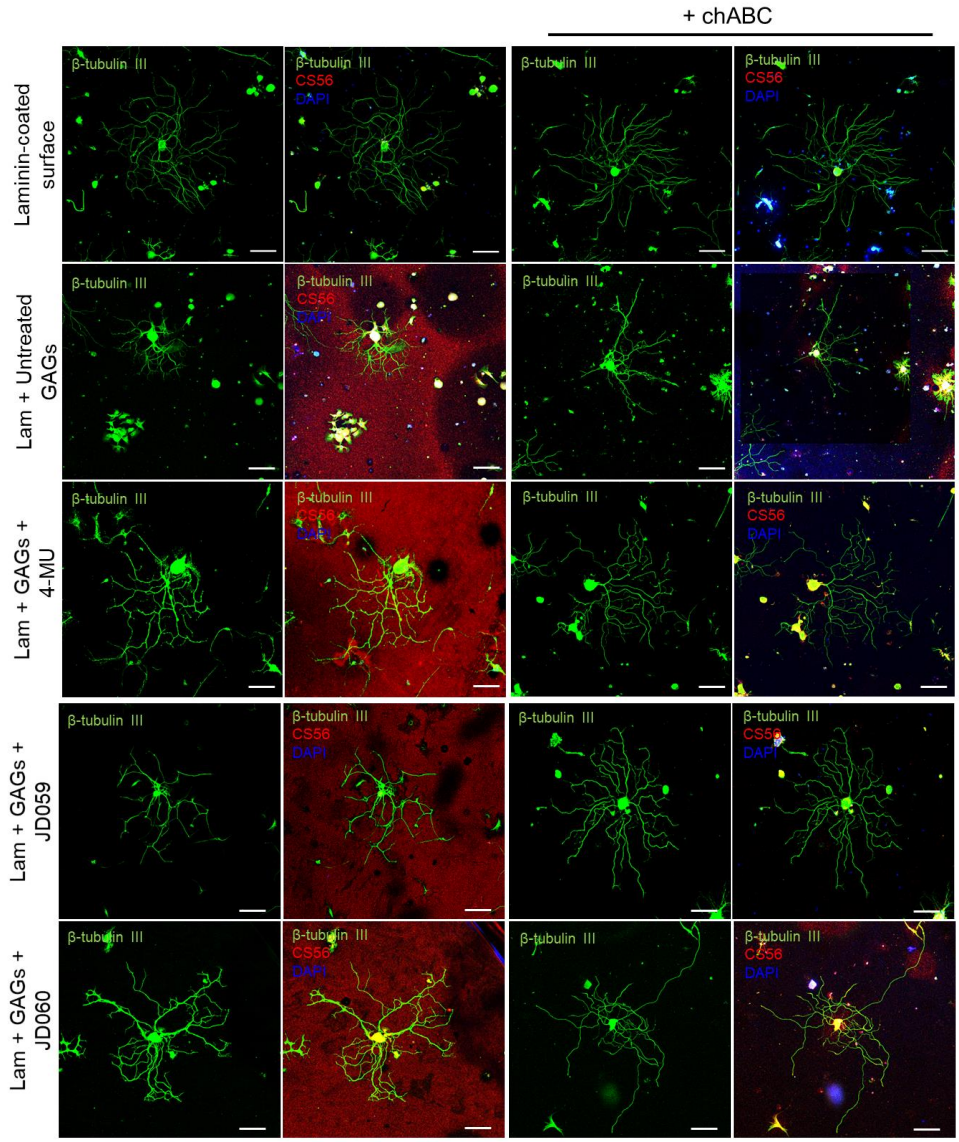

Figure 26. Effect of GAGs harvested from 4-MU-, JD059-, and JD060-treated PNN-HEK293 cells on DRG neurite outgrowth. DRG neurons were cultured on different substrates: laminin only, laminin with GAGs from untreated cells, and laminin with GAGs from cells treated with either 4-MU, JD059, or JD060; all of which were either in the absence or presence of chABC. Neurons were then fixed and stained with β-III tubulin, CS56, and DAPI. Neurons on laminin-only surfaces had long neurite projections, whereas this is stunted when neurons are grown on GAG extracts from untreated cells. This inhibition is reversed with the addition of chABC. Compound-treated GAG extracts allowed for greater neurite sprouting to a similar degree as that of laminin only conditions. Representative confocal images were taken using Zeiss LSM 880 microscope at 20x objective. Scale bars: 100 µm. *DAPI, 4',6-diamidino-2-phenylindole; lam, laminin; GAGs, glycosaminoglycans; chABC, chondroitinase ABC.*

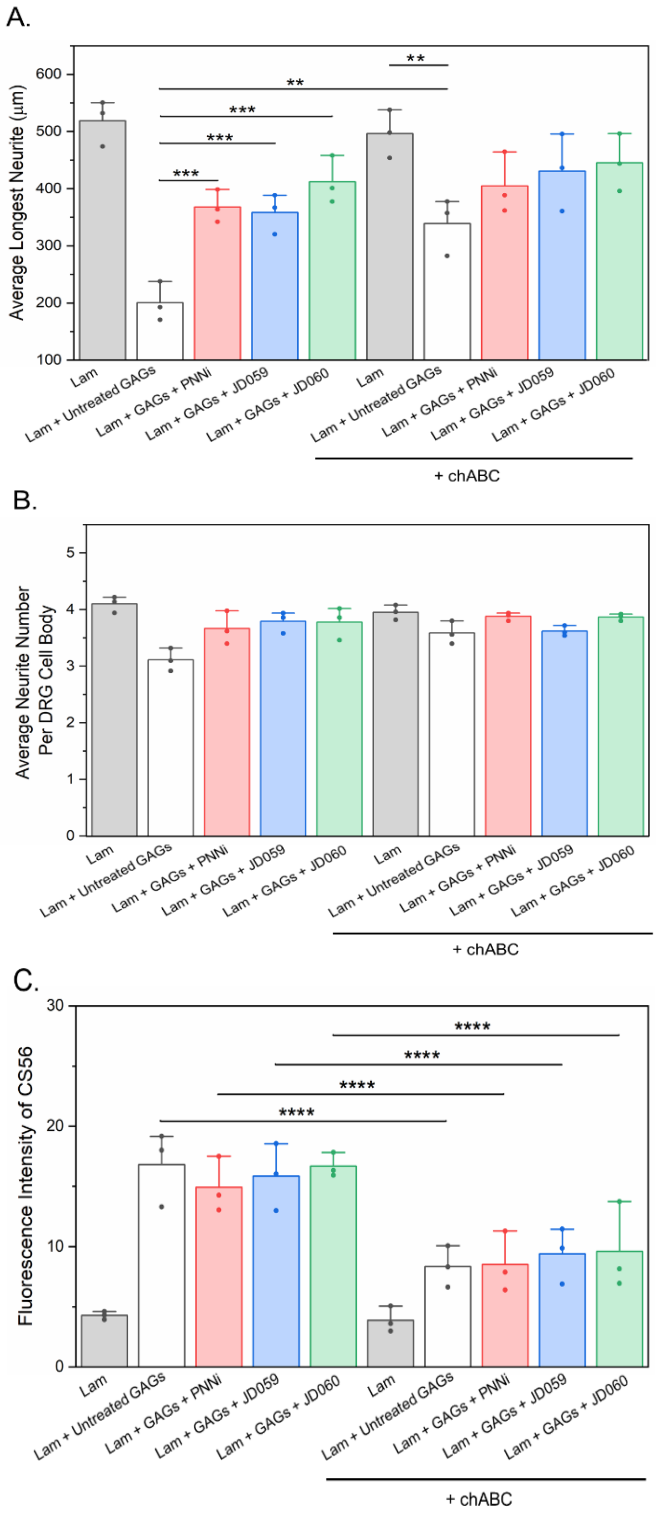

Figure 27. Effect of GAGs harvested from 4-MU-, JD059-, and JD060-treated PNN-HEK293 cells on DRG neurite length. **A.** The graph shows the average longest neurite of DRGs grown over 24 hours on each substrate treatment condition. All substrates containing GAGs inhibited neurite outgrowth when compared to laminin alone, and untreated GAGs was the most inhibitory substrate condition. Neurite growth in increased on GAG substrates from 4-MU-, JD059-, and JD060-treated cells, and was further promoted when substrates were treated with chABC. **B.** GAG fractions untreated and cells caused a minute decrease in average neurite number per cell body, but this was not significant. **C.** Fluorescence intensity of CS-binding antibody CS56 was measured of all substrates under all treatment conditions. Error bars shown are ±SD. n = 3; i.e, data were pooled from 3 independent DRG cultures harvested from 3 individual adult rats. Significance was determined by paired Student's *t-test* and one-way ANOVA: * $p<0.05$, ** $p<0.01$, *** $p<0.001$, **** $p<0.0001$.

5.5 Discussion

5.5.1 Summary of results

In this chapter, we have shown that GAGs extracted from the surface of PNN-HEK293 cells were inhibitory growth substrates for DRG neurons, whereas GAGs extracted from cells that had been treated to all compounds were more permissive for neurite outgrowth, and that JD060 potentially confers the greatest potency.

5.5.2 GAGs extracted from PNN-HEK293 cells are inhibitory to neurite outgrowth

We have thus far been able to demonstrate the successful extraction and isolation of GAGs from PNN-HEK293 cells, our *in vitro* model of PNNs. Our hypothesis was that the isolated GAGs, composed of hyaluronan (HA) and chondroitin sulphate (CS) as highlighted by our biochemical results in chapter 4, could affect neurite outgrowth when acting as a growth substrate. We found that adult DRG neurite growth was significantly hindered when grown on this substrate. A crucial benefit of utilising the PNN-HEK293 model of PNNs is that we can exclude the possibility that these effects were elicited by the diffuse extracellular matrix (ECM), as only GAGs tethered to the surfaces of PNN-HEK293 cells were harvested for GAG extraction. This finding addresses a central question in PNN-mediated plasticity research: is the control of neural plasticity due to the components of PNNs, or due to the diffuse ECM? Afterall, only approximately 2% of CS-GAGs in the mammalian CNS are contained within the PNN (Deepa *et al.*, 2006)—arguably a small amount for the significant influence of neural plasticity. A critical paper that provides insight into this fundamental discussion was published in 2010, wherein a brain knockout of the PNN component HAPLN1 led to depleted PNNs without any significant change in overall quantitiy of CS-GAGs within the brain—yet, these animals exhibited continued critical period plasticity (Carulli *et al.*, 2010). Our findings focus attention on the GAGs within PNNs rather than in the diffuse matrix, and demonstrate that these PNN-associated GAGs are responsible for the changes in DRG arborisation. The observed PNN-mediated inhibition of neurite outgrowth is in accordance with other published work—PNNs extracted from rat brains are established to be more inhibitory to neurite sprouting than GAGs isolated from the diffuse matrix (Foscarin *et al.*, 2017).

The role of PNNs in plasticity and its inhibition has been explored in chapter 1. PNNs are immensely heterogeneous in its molecular composition and in the glycan structures of their CSPGs. Out of all the CS types, it is established that C4S and C6S are the major CS types expressed in the PNN (Deepa *et al.*, 2006). Indeed, we were able to verify that our growth substrates contained C4S and C6S by the increased positive staining of CS56. Furthermore, the enzyme chABC was able to digest these chains, markedly reducing the signal intensity of CS56. We then established that neurite outgrowth was dramatically restricted when grown on substrates coated with untreated GAGs, that is, substrates coated with intact PNNs undisrupted by any compound. This inhibition was dramatic in comparison to neurites sprouting on laminin only surfaces, which is known to be highly permissive to neurite outgrowth. We found that this inhibition was removed when chABC was added to the substrate, implying that the CS moieties of PNNs were at least partially, if not primarily, responsible for the observed inhibition. CSPGs have two primary structural features: a single protein core and one or more unbranched polysaccharide GAG chains tethered to the protein core. CSPGs have long been the subject of intense research in the context of neural plasticity and regeneration. They are strongly implicated in inhibiting neurite projections, path-finding, axonal regeneration, and plasticity (Bradbury *et al.*, 2002; Wang *et al.*, 2008). These inhibitory properties are largely attributed to their GAG chains, as GAG chains are thought to confer inhibition in a myriad of ways, such as by binding to specific receptors, such as transmembrane protein tyrosine phosphatase, (PTPσ) and leukocyte antigen receptor (LAR).

In DRG cultures, the CS chains of PNNs interact with PTPσ with high affinity (Shen *et al.*, 2009). DRG neurons express high levels of PTPσ throughout life (Haworth *et al.*, 1998). DRG neurons harvested from mice with targeted gene disruption of PTPσ (*PTPσ−/−)* and from wild type controls were cultured with a mixture of CSPGs. The CSPG-rich substrate reduced wild type neurite branching significantly, but had substantially less of an effect on neurons from *PTPσ−/−* mice (Shen *et al.*, 2009), indicating that CSPG-mediated neurite stunting was at least partially via *PTPσ* signalling. The *in vivo* significance of *PTPσ* signalling was assessed: lesioned ascending sensory axons in the fasciculus gracilis following a dorsal column crush injury were extracted from *PTPσ−/−* mice. They concluded that there was increased regeneration of tracer-labeled axons into the CSPG-rich lesion area in PTPσ −/− mice, although regeneration beyond the core of the injury site did not occur. This is consistent with the notion that other growth impediments are at play. Similarly, damaged

CNS corticospinal tract fibres in *PTPσ−/−* regenerate and extend for long distances after injury, in contrast to wild type mice (Fry *et al.,* 2010).

Similar effects were seen with LAR-deficient mice. DRGs from *LAR−/−* mice enhanced neurite length in the presence of CSPGs (Fisher *et al.,* 2011). This was further confirmed by introducing LAR blocking peptides to wild type DRG neurons, which led to increased neurite sprouting as well. In order to establish relevancy to the CNS, cerebellar granular neurons (CGNs) were subjected to blockade of LAR by peptides. Similarly, LAR blocking overcame CSPG-mediated inhibition of growth. This identifies another receptor by which CSPGs of PNNs can induce potent inhibition on growth and regeneration in both the PNS and CNS.

CSPGs are dramatically upregulated at sites of nervous system injury, forming a potent physical and chemical barrier for axon sprouting and regeneration (Kwok *et al.,* 2011; Bradbury *et al.,* 2019). Removal of CS-GAGs, such as by chABC, surmounts neural outgrowth inhibition, encourages plasticity, and promotes anatomical and functional recovery in injured states (Bradbury *et al.,* 2002; Kwok *et al.,* 2011; Bradbury and Burnside, 2019). Our findings of increased DRG sprouting following chABC treatment are hence in accordance with current literature.

There are different types of CSPGs present in the PNN, including aggrecan, brevican, versican, and neurocan (Zimmermann and Dours-Zimmermann, 2008; Kwok *et al.,* 2011; Fawcett *et al.,* 2022). These core proteins themselves have inhibitory domains with the ability to restrict plasticity (Cua *et al.,* 2013). Aggrecan is found almost exclusively within the PNN (Bruckner *et al.,* 1993; Morawski *et al.,* 2012; Rowlands *et al.,* 2018; Ueno *et al.,* 2018), and is also present within PNNs located around PNN-HEK293 cells (Kwok *et al.,* 2010). It is therefore conceivable that aggrecan contributed to the attenuation neural plasticity observed in our DRG experiment. This assumption would be in line with published literature; for instance, deletion of aggrecan in the visual cortex of adult mice ablated PNNs and reinstated juvenile-like ocular dominance plasticity (Rowlands *et al.,* 2018). Versican v2 was found to be directly inhibitory to neurite outgrowth, and this was only abolished upon core protein degradation using proteinase k (Schmalfeldt *et al.,* 2000). Neurite outgrowth has also shown to be stunted when grown on neurocan substrata (Cua *et al.,* 2013; Wright *et al.,* 2014). With that in mind, could our compounds have influenced the expression of aggrecan, the core protein present in our PNN-HEK293 cells? It is certainly plausible, given that the loss of the hyaluronan (HA) backbone results in the destabilisation of the PNN architecture. Thus, less

aggrecan would be able to be tethered to cell surfaces. However, we cannot rule out that there could be low amounts of HA chains retained on cell surfaces even after compound treatment, and because the protein levels of link protein hyaluronan and proteoglycan link protein 1 (HAPLN1) remained unchanged, it is possible that there were low levels of aggrecan bound to the HA chains on cells. These residual amounts of aggrecan and CS chains extracted from the compound-treated PNN matrix could be why we do not see a complete recovery of neurite branching in the absence of chABC.

The role of hyaluronan (HA)—the other major constituent of PNNs—has been investigated in neurite outgrowth assays and neuroplasticity. Degradation of HA using hyaluronidase promoted local sprouting of transected CNS neurons within the nigrostriatal tract, presumably because digestion of HA caused the release of CSPG inhibitory molecules (Moon *et al.*, 2001). Other than acting as an anchor for CSPGs, HA has been studied in plasticity in other ways. Downregulation of CD44, a major HA receptor, using short-hairpin RNA (shRNA) constructs in cultured neuronal cells increased dendritic sprouting and complexity—these effects are reliant on Src tyrosine kinase activity (Skupien *et al.*, 2014). Given that the HA-CD44 interaction promotes c-Src activity (Bourguignon *et al.*, 2010), it could be surmised that signalling pathways mediated by HA-CD44 could be involved in the observed increase of dendritic arborisation observed in Skupien *et al.*'s work. It is also plausible our untreated GAG extracts contained the PNN component tenascin-R, and that this elicited some inhibitory effects on neurite sprouting. Tenascin-R is glycoprotein expressed primarily in the central nervous system (CNS) but is particularly enriched in the PNNs and is in fact critical for their assembly (Bruckner *et al.*, 2000; Galtrey *et al.*, 2008; Carulli *et al.*, 2010). Untransfected HEK293 cells were shown to express tenascin-R at detectable levels (Kwok *et al.*, 2010). Tenascin-R has been shown to obstruct adult retinal ganglion cell regeneration (Becker *et al.*, 2004) even after optic nerve crush (Becker *et al.*, 2000). We did not confirm the levels of tenascin-R in our PNN-HEK293 cell samples, and we therefore did not assess how our compounds regulate these levels, but it may be worthwhile to do this in the future.

5.5.3 GAG extracts after treatment with 4-MU, JD059, and JD060 were permissive for neurite outgrowth in adult DRG neurons

The crux of this pilot study was to examine the effects of not only 4-MU, which is already an established therapeutic, but of our 4-MU derivatives JD059 and JD060, on PNN modulation and neuroplasticity. We treated PNNs to 1 mM of our compounds and these compound-

treated GAGs were applied to coverslips to serve as substrates for neuronal attachment and growth. In the previous section, we discovered that untreated GAGs as a growth substrate were restrictive to neurite sprouting and extension. In contrast, we found that compound treated-GAGs were a permissive growth substrate, enabling long, healthy neurite projections. This was a 78% to 104% increase of average longest neurite length grown on GAGs recovered from untreated cells. An observation we made was that JD060-treated GAG surfaces enabled the longest average neurite length compared to 4-MU-treated and JD059-treated surfaces, although this was not found to be statistically significant. Nevertheless, it is an intriguing observation, as it hints at JD060 possessing greater efficacy in promoting neurite outgrowth. This may be attributable to its increased solubility.

Another observation made was that chABC slightly increased the neurite enhancing effects of GAGs from treated cells. The proposed mechanism of our compounds is related to suppressing the biosynthesis of PNNs, whereas chABC is an enzyme that acts by cleaving GAG chains from their core proteins (Prabhakar *et al.,* 2005). It therefore stands to reason that these two different methods of PNN attenuation would have a positive synergistic effect on neurite sprouting. Notably, even though chABC application increased neurite sprouting for neurons grown on GAGs from untreated cells, this was not to the same degree as when these GAGs had been from as compound-treated cells. This finding implies that chABC treatment alone is insufficient to recover neurite outgrowth to near that of control levels.

Early studies have reported similar findings that growth inhibition activity persists after CS chain removal (Schmalfeldt *et al.,* 2000; Lemons *et al.,* 2003). A convincing explanation for this is that the core proteins and carbohydrate stubs that remain following chABC digestion exert inhibitory effects on neuroplasticity, as briefly discussed in the previous section. Candidate proteases for degrading CSPGs, including their core proteins, include the matrix metalloproteinases (MMPs) and the ADAMTSs (a disintegrin-like and metalloproteinase with thrombospondin type 1 motifs) (Howell and Gottschall, 2012; Cua *et al.,* 2013). Treatment of ADAMTS-4 overcame CSPG-mediated neurite outgrowth inhibition, and an additive effect with chABC was observed (Cua at el., 2013). These large proteolytic enzyme families are considered as the primary proteases that coordinate ECM remodelling in pathophysiological environments. These proteases share similar functional domains, and have diverse substrate specificities for proteoglycans, elastin, native type IV, V, VII, and X collagen and denaturated collagen but are also able to cleave non-ECM molecules such as growth factors and cytokines (Shiomi *et al.,* 2010). Targetting their proteolytic activity as a

therapeutic strategy remains an impractical endeavour, mainly due to the lack of selectivity for MMPs and ADAMSTs.

5.5.4 GAG-mediated inhibition of neurite arborisation could be due to its composition

Untreated GAGs and compound treated-GAGs were applied to DRG growth surfaces at equal concentration (25 µg/ml), and this was confirmed by the fact that there were no significant differences in CS56 fluorescence intensity between these groups. This verification is pertinent because this indicates that the potent inhibition of neurite outgrowth observed was not due to the overall amount of CS-GAGs present, but possibly their composition. The varying sulphation patterns of CS-GAGs strongly govern CSPG function (Kitagawa *et al.*, 1997; Kwok *et al.*, 2012; Djerbal *et al.*, 2016; Pearson *et al.*, 2018), which also contributes to the molecular heterogeneity of PNNs. PNNs are enriched with C4S and C6S, which was reaffirmed by our CS56 signal intensity measurements. C6S is associated with heightened neural plasticity, whereas C4S is involved in the restriction of plasticity (Lin *et al.*, 2011; Miyata *et al.*, 2012; Yang *et al.*, 2021). This C4S/C6S ratio changes throughout development, with an increase in the ratio of C4S/C6S during maturation and aging. Fascinatingly, this change is only observed in the PNN, as C4S and C6S proportions remain stable in the diffuse ECM throughout maturation (Foscarin *et al.*, 2017; Carulli and Verhaagen, 2021). Hence, it is exclusively within the PNN matrix where the C4S/C6S ratio is modulated during maturation, rendering it more inhibitory to neural plasticity (Yu *et al.*, 2018; Carulli and Verhaagen, 2021; Fawcett *et al.*, 2022).

With this in mind, it is conceivable that 4-MU, JD059, and JD060 altered CS-GAG composition by decreasing the synthesis of inhibitory C4S ratio on the surfaces of PNN-HEK293 cells, which could underscore the observed circumvention of inhibition of DRG growth. We did not characterise this ratio in our PNN extracts from PNN-HEK293 cells, as this was not the primary aim of this study. However, determining the C4S and C6S proportions after compound treatment would point to a potential mechanism conferred by our compounds in their mediation of neural plasticity.

5.6 Conclusions and future directions

In this study, we aimed to resolve the biochemical mechanisms of 4-MU—a commercially available compound—and its novel derivatives JD059 and JD060 on PNN modulation. We

have shown that these series of compounds attenuated the expression of PNNs, and that this was likely mediated by suppressing HA and CS synthesis. The influence of 4-MU on CS synthesis is a novel finding, as current literature has established the effects of 4-MU to be specific to HA. The goal of this final chapter was to explore if the PNN-inhibiting effects conferred by our compounds translated into the alteration of neurite outgrowth, which could indicate an enhancement of neural plasticity. We have shown that GAGs recovered from untreated cells, that is, intact PNNs, served as an unfavourable environment for DRG neural arborisation. This inhibition was partially reversed by the treatment of chABC, an enzyme that digests CS-GAGs. We were then able to prove that GAGs that had been treated to our series of compounds were permissive growth substrates for neurons, provoking extensive neurite sprouting. We have thus demonstrated that our compounds are endowed with plasticity-enhancing capabilities, warranting further research into our compounds.

Chapter 6: General discussion and future perspectives

6.1 Introduction

In this study, we sought to answer an overarching question: could our compounds represent as promising new generation of potent perineuronal net (PNN) inhibitors for the manipulation of plasticity? The conventional and popular approach to modulating PNNs is through the use of a bacterial enzyme chondroitinase ABC (chABC), which cleaves the glycosaminoglycan (GAG) side chains of chondroitin sulphate proteoglycans (CSPGs) and leads to the dissolution of PNNs. However, it bears many disadvantageous traits: first, its large size obstructs its diffusion from the site of injection, meaning that administration of chABC must be localised. Second, it is inherently unstable at body temperature, thus requiring frequent high dose administrations. Finally, methods of administration are invasive, as the compound is usually delivered via injection or intrathecal infusion. In order for chABC to be clinically relevant, much innovation into its long-term activity, stability, and administration is sorely needed. A small molecule compound that does not bear the same limitations would hence be invaluable.

To this end, 4-MU represents as a promising candidate to replace chABC. It is a commercially-available compound with excellent safety data. It is well-established to repress HA biosynthesis, and has only very recently been shown to confer efficacy in modulating PNN expression (Dubisova *et al.*, 2022). 4-MU is thus favoured to be a new, superior generation of compounds for the manipulation of PNNs. Despite these positive traits, it has poor aqueous solubility, meaning high doses are required for efficacy. Effective, more soluble compounds, could represent as improved third-generation PNN inhibitors.

We therefore endeavoured to subject 4-MU and our novel PNN inhibitors JD059 and JD060 to scrutiny through biological and biochemical assessments, in order to evaluate their effects on PNNs and neural plasticity. JD059 and JD060 were designed and synthesised to possess improved aqueous solubility whilst still retaining the same functionality as 4-MU. Given the known hyaluronan (HA)-inhibiting properties of 4-MU, we expected that all compounds should efficiently suppress the expression of PNNs, since HA forms the backbone upon which the assembly of PNNs occur.

Our study additionally aimed to explore the mechanisms by which 4-MU, and by extension, JD059 and JD060, attenuated PNN expression and formation. Notably, 4-MU is regarded as

an exclusive HA inhibitor, but its other potential influences on other glycosaminoglycans (GAGs) have not been thoroughly explored to date. In fact, a small number of studies reported an absence of effect on other GAGs. We theorized that if 4-MU depletes the cellular content of UDP-glucuronic acid (UDP-GlcA) as is widely-reported, then its effects should extend to chondroitin sulphates (CS) as well and not be exclusive to HA. Finally, there is an abundance of literature that chronicles the benefits of PNN attenuation on enhancing neural plasticity. Indeed, chABC-mediated degradation of PNNs has been reported to induce neural plasticity and promotes structural and functional recovery in a plethora of central nervous system injury and disease models. Our final objective was thus to assess whether PNN attenuation mediated by our compounds could promote neurite arborisation in dissociated dorsal root ganglion (DRG) cultures as a marker of stimulated neural plasticity.

6.2 Establishment of PNN-HEK293 cells as a robust model of PNNs

In chapter 3, we first highlighted the suitability of an *in vitro* model of PNNs (termed PNN-HEK293), developed previously in the lab (Kwok *et al.,* 2010). HEK293 cells were incapable of producing a PNN-like structure enmeshing cells; in stark contrast, PNN-HEK293 cells produce a distinct PNN structure that was positive for the expression of hyaluronan (HA), the backbone of PNNs, and *Wisteria floribunda* agglutinin (WFA), a pan-PNN marker. This report is the first to utilise PNN-HEK293 as a model for scrutinising PNN formation and the molecules that may impede it. PNN-HEK293 cells proved to be an extremely robust model, and allowed us to study the biological and biochemical characteristics of PNNs in the absence and presence of our compounds with ease. This is highly significant, as popular *in vitro* models to study PNNs utilise primary neuronal cultures, such as primary mouse hippocampal neurons and rat cortical neurons (Miyata *et al.,* 2005; Dityatev *et al.,* 2007; Giamanco *et al.,* 2010; Geissler *et al.,* 2013; Dickens *et al.,* 2023). As such, these cultures bear the same general disadvantages of primary cell cultures. One major disadvantage of primary neuronal culture is that cells do not divide in culture, and cells thus need to be harvested from animals routinely. Successful dissection and preparation of cell cultures also require expertise, time, and expense. Moreover, analysing the molecular changes when screening our compounds would be difficult on these cells, as there may be interference from other neuronal cell types if the culture is not pure. There is evidently more relevancy using primary neuronal cultures, as PNN expression and subsequent modulation by our compounds would more closely recapitulate that of *in vivo* settings. Furthermore, PNNs ensheathing neurons are expected to

be denser than the PNN-HEK293 counterpart as it contains additional cross-linkers such as Sema3a (Dick, *et al.*, 2013; Morawski, *et al.*, 2014). However, our PNN-HEK293 cell model serves as an invaluable and accessible tool for thorough research into the molecular composition of the PNNs.

6.3 4-MU, JD059, and JD060 reduce both CS and HA moieties of PNNs

In chapters 3 and 4, we demonstrated that 4-MU, JD059, and JD060 had the capacity to reduce the expression of PNNs. This initial result was confirmed by the reduced expression of hyaluronan (HA), the backbone of PNNs, and *Wisteria floribunda* agglutinin (WFA), a pan-PNN marker. At low doses, HA and WFA fluorescence intensity was unchanged, but immunostaining allowed us to observe that the morphology of PNNs were already disrupted at this dose. Morphological assessments revealed the disruption of the PNN-like pericellular structure upon exposure to our compounds, with a complete abolishment of the PNN-like pericellular structures at high doses.

Biochemical analyses employed in chapter 4 aimed built on these findings, and we confirmed our hypothesis that both HA and CS moieties of PNNs were targeted by our compounds. Indeed, we found a significant decrease in the combined content of 4-sulphated (C4S) and 6-sulphated (C6S), across all compound treatments. Importantly, HA and the combined content for C4S and C6S was reduced even at low doses of 4-MU. This would support our inference that the disruption of WFA-positive PNN structures at these doses was caused by a slight reduction in HA and CS production. This would therefore hinder PNN assembly.

As our results regarding 4-MU-mediated CS inhibition contradict suggestions in previous literature, we propose several conceivable mechanisms underlying regulation of CS production. As discussed, only a few studies have directly scrutinised the relationship between 4-MU and CS-(GAGs), and no significant effect was reported (Rilla *et al.*, 2004; Vigetti *et al.*, 2009). It has been speculated that although CS synthesis requires the precursor UDP-GlcA as well, CS production is not altered because its synthesis occurs in the Golgi apparatus and UDP-GlcA must be transported into the Golgi, making the Golgi a privileged compartment. However, we postulate that the content of UDP-GlcA should still theoretically influence CS biosynthesis, albeit to a lower degree. A lower amount of UDP-GlcA would be available to be transported into the Golgi for CS synthesis. Our results have supported our hypothesis.

CS biosynthesis is a complex and multi-stepped process involving a battery of enzymes, and they are depicted in Figure 27. If 4-MU alters CS expression, it is possible that this compound could affect one or more of the regulatory steps of CS biosynthesis. The point of attachment is a serine residue of core proteins to which GAG chains are tethered via a tetrasaccharide linkage region (Protein-Xyl-Gal-Gal-GlcA-chondroitin sulphate) (Kwok *et al.*, 2012). Given that 4-MU is known to be a ubiquitous substrate of UDP-glucuronosyltransferase (UGT) (Nagy *et al.*, 2015), we could potentially explore its effects on other regulatory glucuronysyltransferases. The enzyme of β1,3-glucuronyltransferase I (GlcAT-I), which is an enzyme responsible for transferring the GlcA moieties from UDP-GlcA to the tetrasaccharide linkage region, could be modulated in the presence of our compounds. Moreover, if we were to assume that CS formation is differentially regulated from HA biosynthesis by 4-MU because CS biosynthesis takes place in the Golgi, it stands to reason that the transporters responsible for the shuttling of activated sugars from the cytosol to the Golgi could be involved. These transporters are known as nucleotide sugar transporters (NSTs). Indeed, inactivation of SLC35, a member of an NST family, resulted in a decrease in UDP-GlcA and UDP-GlcNAc uptake from the cytosol. Interestingly, SLC35C1 gene silencing in cells caused a mild increase in CSPG levels (Sosicka *et al.*, 2019), implying that there are compensatory mechanisms at play in CSPG production. Indeed, the cellular biochemical mechanisms regulating the production of glycosaminoglycans are intricate and highly-complex, and unpicking the steps that are affected by the presence of our compounds would be a vast undertaking. Nevertheless, it is worthwhile to pursue further research into how 4-MU and our compounds are involved in these processes, in order to elucidate how they may be refined for therapeutic interventions or even applied to other research fields that focus on GAG biosynthesis and production.

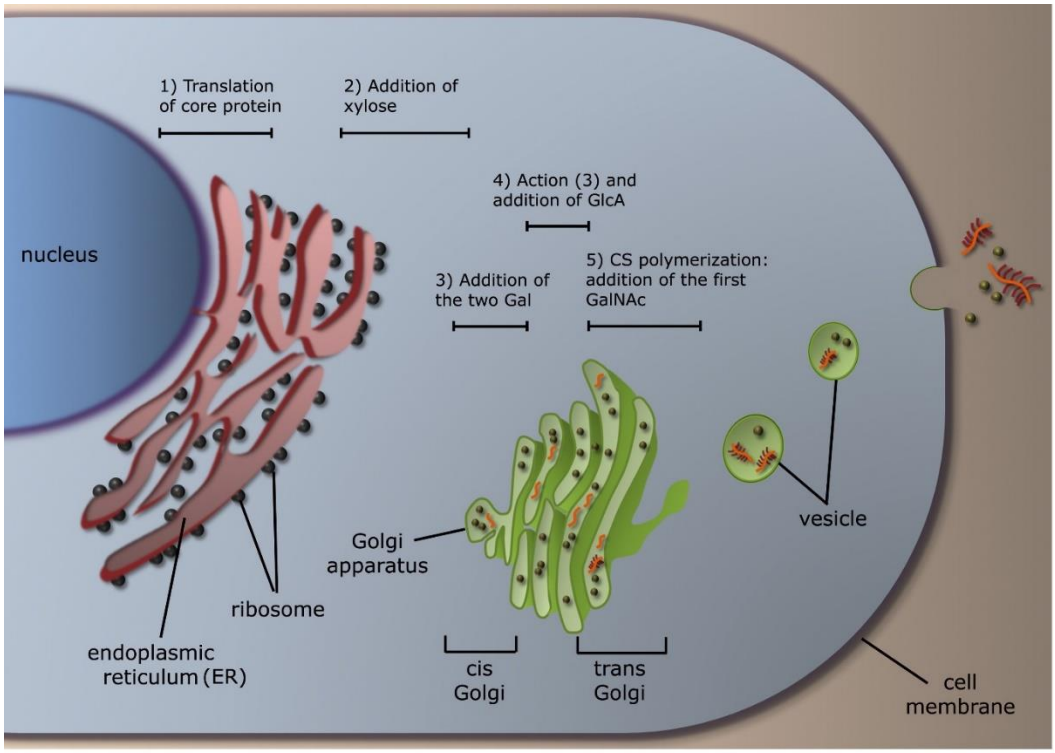

Action	Location	Enzyme
1) Translation of core protein	Cytosol	
2) Addition of xylose	ER membrane	xylosyltransferase
3) Addition of Gal	cis Golgi membrane	Gal I and Gal II transferases
4) Addition of Gal and GlcA	medial Golgi membrane	Gal I, Gal II and GlcA I transferases
5) **CS polymerization**: - Addition of the first GalNAc	trans Golgi membrane	GalNAc transferase
Polymer modification: - Phosphorylation of xylose in the linkage region - Sulfation of xylose and CS chains - Epimerization		

Figure 28. Biosynthesis of chondroitin sulphate proteoglycans within the cell. The core proteins of CSPGs are synthesised in the endoplasmic reticular lumen, and the polymerisation of CS chains occurs in the Golgi apparatus (Kwok *et al.,* 2012).

An intriguing prospect is that our compounds alter the sulphation patterns of CS chains within the PNN matrix. As detailed throughout this manuscript, sulphation patterns significantly dictate the functionality of CSPGs, and specific sulphation patterns can even confer enhanced or reduced plasticity. Indeed, C4S has been proven to be restrictive to neural plasticity, whereas C6S is reported to be permissive (Foscarin *et al.,* 2017; Yang *et al.,* 2021). Overall, changes in CS-GAG sulphation patterns can dysregulate PNNs and predispose to their loss over time (Miyata *et al.,* 2012). Our study was unable to define the composition CS-GAGs that are affected by our compounds, but future work achieving this would be immensely informative. This can be achieved in future work by repeating our fluorophore-assisted carbohydrate electrophoresis (FACE) experiments with the incorporation of chondro-

6-sulphatase, which catalyses the cleavage of 6-sulphate chains. Thus, the combined band intensity for C4S and C6S can be distinguished from each other after digestion. Additional methods such as anion-exchange high performance liquid chromatography (HPLC) produce elution profiles of GAG chains which provide information on both extent of sulphation and sulphation pattern (Garud *et al.,* 2008).

A noteworthy finding was that 1 mM of JD060 bestowed greater inhibition of combined C4S and C6S expression than 1 mM of 4-MU, presumably through the increased solubility in culture media. The strategies employed to improve aqueous solubility of our novel analogues were concealed for this study to prevent bias, but this result showed a biochemical effect as a result of this modification.

6.4 HAS3 protein regulation may underscore compound-mediated PNN inhibition

In chapter 4, we briefly explored the mechanisms by which our compounds suppressed PNN formation. HA synthesis by HAS3 is a critical regulatory step of PNN expression, as HA forms the backbone upon which the assembly of PNNs occur. A mild reduction of total HAS3 protein levels was observed at low doses of our compounds, but this effect was greater at higher concentrations. This is in line with published literature (Kakizaki *et al.,* 2004; Rilla *et al.,* 2005; Jokela *et al.,* 2008; Kultti *et al.,* 2009; Vigetti *et al.,* 2009; Galgoczi *et al.,* 2020), wherein HAS gene and protein levels were all reduced by 4-MU treatment. Our study did not scrutinise the mechanisms by which HAS3 protein expression was altered, but further research most certainly should. 4-MU has been reported to deplete the cellular pool of UDP-GlcA, as well as enzymes required for the synthesis of HA precursors, UDP glucose pyrophosphorylase (UGPP) and UDP glucose dehydrogenase (UGDH) (Vigetti *et al.,* 2006; Vigetti *et al.,* 2009). However, how this occurs has not been fully elucidated, although it has been speculated that a reduction of a HAS substrate may influence HAS protein modification, packaging, and trafficking to the plasma membrane (Shestakova *et al.,* 2005; Deen *et al.,* 2016; Liu *et al.,* 2018). Our understanding of the trafficking and localisation dynamics has been facilitated by the use of fluorescent HAS proteins together with live cell imaging As described in chapter 4, the availability of a HAS3 substrate could influence vesicular trafficking, endocytosis, and plasma membrane abundance of HAS3 (Deen *et al.,* 2016). This is an intriguing prospect that warrants further study, and provides an important piece of the puzzle regarding the mechanisms of 4-MU and our compounds. However, because our

compounds caused a decrease in total HAS3 protein levels within cells, alterations in HAS3 trafficking may not be sufficient to explain our findings, and it is more likely that transcription of HAS3 was involved. We explore the conceivable mechanisms of PNN inhibition elicited by our compounds at the end of the chapter.

6.5 PNN inhibition conferred by 4-MU, JD059, and JD060 enhanced neurite outgrowth

Our final chapter delved into whether PNN attenuation coordinated by our compounds translated into alterations in neurite growth and branching. GAGs that had been harvested from the surface of PNN-HEK293 cells, i.e, intact PNNs, served as inhibitory substrates for explanted DRG neurons. GAGs that had been treated to our compounds, however, proved to be significantly more favourable for the growth of DRGs. Suppression of PNNs, exerted by our small molecule inhibitors, may be driving the induction of neurite outgrowth. These benefits of PNN removal on neural plasticity are in line with a wealth of research (Shen *et al.*, 2009; Fry *et al.*, 2010; Dick *et al.*, 2013; van 't Spijker and Kwok, 2016; Fawcett *et al.*, 2022), and justifies the notion that our compounds are promising candidates for the promotion of neuroplasticity through PNN manipulation.

6.6 Proposed mechanisms for PNN removal mediated by 4-MU, JD059, and JD060

During this project, we have demonstrated that 4-MU and our novel 4-MU derivatives JD059, and JD060, were able to diminish the formation of PNN-like structures in our *in vitro* model of PNNs. Importantly, this was achieved by the reduced production of both integral PNN GAGs HA and CS, the latter of which has not been proven before. Furthermore, we also show that HAS3 protein regulation is altered by our compounds. Functionally, this proved to promote DRG neurite extension in comparison to DRGs grown on GAG-enriched surfaces. In this section, we will tie these results together with current research to postulate a mechanism for PNN reduction, illustrated in Figure 29.

Under basal conditions, homeostatic levels of glucuronidation take place within cells (Figure 28, left). UGTs are primarily located within the endoplasmic reticulum (ER) and are partially associated with the ER membrane (Liu and Coughtrie, 2017). These enzymes are responsible for the transfer of GlcA from the donor co-factor UDP-GlcA onto various acceptor substrates. While these acceptor substrates diffuse into the ER, UDP-GlcA is transported into the ER via

NSTs from the cytosol (Song, 2013, Parker and Newstead, 2019). The reaction causes the release of UDP and the formation of a β-D-glucuronide, which is polar and hydrophillic, and is subsequently actively transported out of the ER (Ouzzine *et al.*, 2014; Liu and Coughtrie, 2017). UDP-GlcA is additionally transported into the Golgi from the cytosol via transporters (Ashikov *et al.*, 2005) for the polymerisation of CS chains (Figure 29) (Kwok *et al.*, 2012; Silbert and Sugumaran, 2002). Once the synthesis of CSPGs has been terminated, they are packaged into secretory vesicles (SV) and utilised accordingly (Kwok *et al.*, 2012).

With homeostatic levels of glucuronidation taking place, an abundance of nucleotide sugars within the cytoplasm is ensured. This facilitates HAS enzymes, located on the plasma membrane of cells, to utilise UDP-GlcA and UDP-GlcNAc for the synthesis of HA polymers, and for the synthesis of other GAGs within the Golgi apparatus. The HA chains consist of alternating β-1,3- and β-1,4-linked *N*-GlcNAc and GlcA units that can typically reach megadaltons in size (Cyphert *et al.*, 2015; Cowman *et al.*, 2015). Link proteins, such as HAPLN1, stabilise the interaction between HA and the N-terminal G1 domain of CSPGs (Richter *et al.*, 2018). Finally, trimeric proteins tenascin-R interlinks up to 3 CSPGs together via their C-terminal G3 domains (Richter *et al.*, 2018; Fawcett *et al.*, 2022). Overall, the availability of an important nucleotide sugar precursor, UDP-GlcA, effectuates the formation of HA and CSPGs and initiates PNN assembly (Figure 29, left).

In the presence of 4-MU, JD059, or JD060, the levels of glucuronidation are increased (Figure 29, right). A greater amount of UDP-GlcA is transported into the ER to facilitate the glucuronidation of these compounds (termed “perineuronal net inhibitor” (PNNi) for brevity). With a depletion of the cellular content of UDP-GlcA, less is available for the synthesis of HA at the plasma membrane, and we postulate that less can be transported into the Golgi for CSPG synthesis. Consequentially, less HA and CSPG are synthesised which disrupts the formation of PNNs (Figure 29, right).

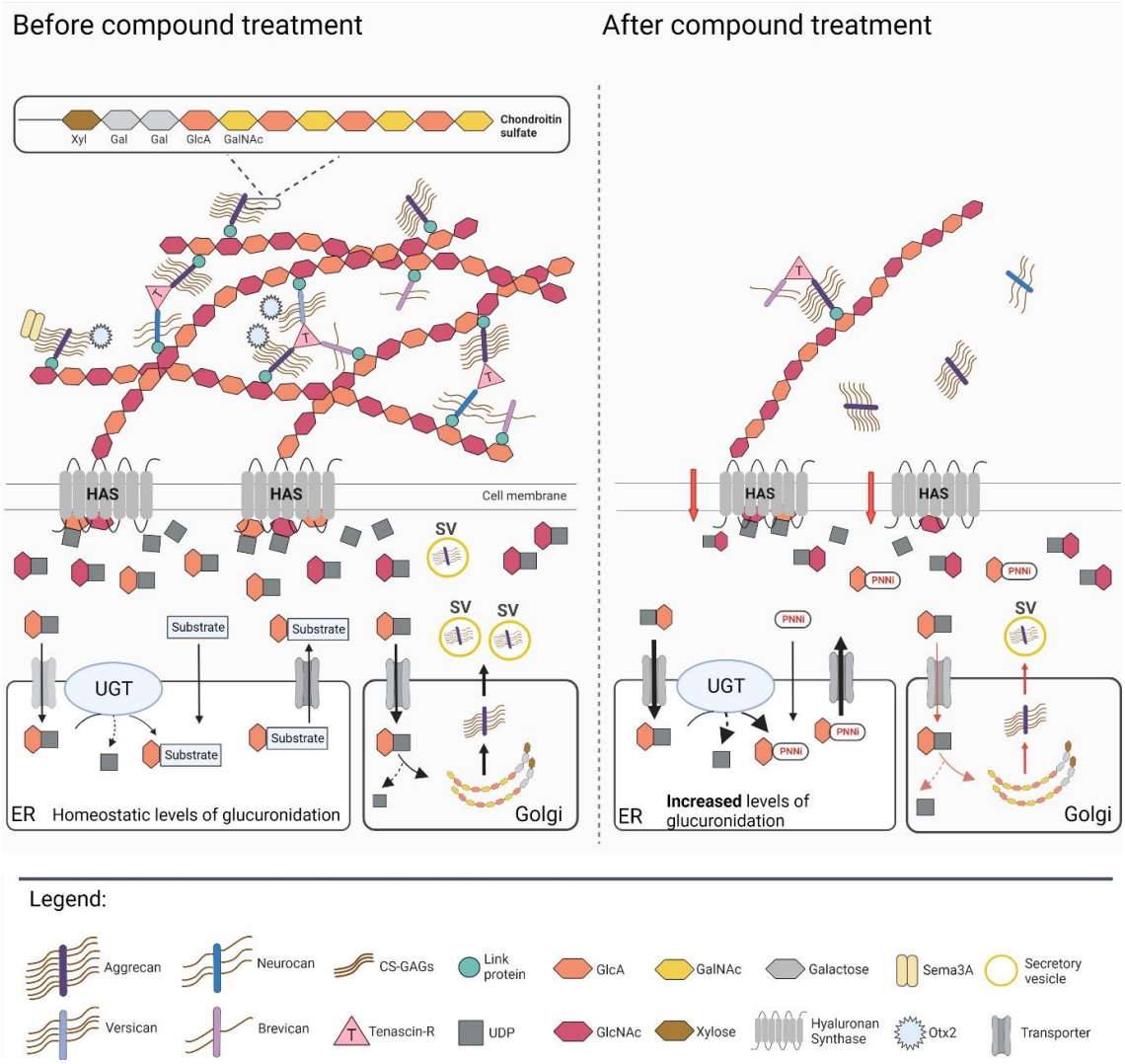

Figure 29. Comparison of PNN structure and expression before and after treatment with compounds. For brevity, perienuronal net inhibitor (PNNi) is used to refer to 4-MU, JD059, and JD060, as all compounds would theoretically possess the same functionality. Combined, our data suggest that PNNi effectively blocks PNN formation by interfering with the synthesis of HA and CS which are vital components of the PNN. PNNi undergo glucuronidation in the ER, increasing levels of glucuronidation from homeostatic levels, which requires an increased uptake of UDP-GlcA from the cytosol. Thus, there is a lower availability of UDP-GlcA for HAS to synthesise HA chains. Furthermore, HAS protein expression is reduced in the presence of our compounds. Finally, we propose the reduced pool of cytosolic UDP-GlcA resulted in less of this precursor being transported into the Golgi for CS synthesis (illustrated by red arrows). Thus, lower amounts of CSPGs could be synthesised and transported out of the Golgi for extracellular expression. *HAS, hyaluronan synthase; UDP, uridine diphosphate; UGT, UDP-glucuronosyltransferase; 4-MU, perineuronal net inhibitor; ER, endoplasmic reticulum; GlcA, glucuronic acid; GlcNAc, N-acetylglucosamine; GalNAc, N-acetylegalactosamineSV, secretory vesicle; Sema3A, semaphorin 3A; Otx2; orthodenticle homeobox 2.*

4-MU has indeed been confirmed to suppress HA production by reducing the pool of UDP-GlcA present in the cell cytosol (Kakizaki 2004; Kultti *et al.,* 2009; Vigetti *et al.,* 2009). Furthermore, the activity of HAS hinges on the supply of UDP-sugars (Jokela *et al.,* 2008; Rilla *et al.,* 2013; Deen *et al.,* 2016). There is a theory that a reduction of UDP-GlcA coordinates the trafficking kinetics of HAS3 between the endosomes and the cell membrane (Deen *et al*, 2016). Interestingly, this 2016 study uncovered that an exhaustion of the availability of UDP-GlcA pivoted the balance towards HAS3 endocytosis, which influenced HA synthesis (Deen *et al*, 2016). While this is still plausible, our results illustrate a reduction in overall protein levels within cells. We therefore propose that HAS3 transcription and expression were strongly impacted by our compounds, which rasies an intriguing question: could nucleotide sugars act as cellular sensors in the tranhscriptional regulation or activity of genes encoding for biosynthetic enzymes?

Multiple signalling pathways have been implicated to be responsible for the onset and maintenance of HAS3 expression. Phosphatidylinositol 3-kinase (PI3K) inhibition has been shown to potentiate the expression of HAS3 in cultured keratinocytes in a scratch wound model (Fitsialos *et al.,* 2007). The HAS3 gene promoter contains putative binding sites for key transcription factors such as CCAAT/enhancer binding protein (C/EBP) and nuclear factor kappa B (NFκB) (Wang *et al.,* 2015), with TNF-alpha playing an inducing role on canonical NFκB activation (Karin and Delhase, 2000; Kuo *et al.,* 2017). The involvement of NFκB in HAS3 transcription was validated by treating cells with TNF-α, whilst concurrently pharmacologically inhibiting NFκB. This led to the substantial reduction of HAS3 mRNA, indicating an important role of NFκB activation in regulating HAS3 transcription (Kuo *et al.,* 2017). There is a dearth of information regarding how the supply of UDP-GlcA/UDP-sugars modify the transcription of HAS3, and it would be pertinent to identify the signalling pathways that are involved in HAS3 regulation mediated by our compounds. We considered the possibility that HAS3 expression is reduced by mechanisms independent of UDP-GlcA supply, however, this is unlikely to be the case. Previous research has shown that excess UDP-GlcA supplied to cells transfected with HAS and UDP-glucuronyltransferases (UGT) resulted in the diminishing of 4-MU-mediated inhibition of HAS activity (Kakizaki *et al.,* 2004). This indicates that the depletion of UDP-GlcA content is the primary factor in the inhibitory action of 4-MU.

We postulate that CS synthesis was suppressed due to the direct reduction of UDP-GlcA, which is an essential precursor for CS biosynthesis, despite UDP-GlcA requiring transporters

to pump UDP-GlcA into the Golgi from the cytosol (Figure 29). As with any hypothesis, further questions emerge that are in dire need of addressing. Alterations in adequate supply of UDP-GlcA on CS biosynthesis has not been thoroughly studied to the same degree as UDP-GlcNAc; indeed, an increase in UDP-GlcNAc (a precursor for UDP-GalNAc) availability caused an increase in CS synthesis (Vigetti *et al.,* 2012). UDP-GlcA is used to form UDP-xylose by UDP-xylose synthase. Xylose is transferred to a polypeptide acceptor by xylotransferases, which initiates the chain synthesis (Silbert and Sugumaran, 2002). In order to confirm if the reduction of UDP-GlcA supply affects CS biosynthesis, it would be immensely important to assess the expression and activity of of these enzymes that utilise UDP-GlcA as a precursor.

6.7 Future perspectives

We have established that 4-MU and our compounds block the formation of PNNs by the reduction of HA and CS synthesis. We have posited that this is due to the direct reduction of UDP-GlcA, which is a precursor required for the synthesis of both of these GAGs. There is a fervent need to further characterise the mechanisms by which 4-MU, and our compounds, reduce HA and CS synthesis. Uncovering these mechanisms would assist in divulging the complex biological roles of HA and CS in PNNs at much higher molecular resolution. In this section, we will explore potential advancements of this work.

6.7.1 In vitro assessments

Futher biochemical insights into how 4-MU, JD059, and JD060 influence GAG synthesis and PNN expression is desperately needed. Whilst our results show convincing evidence that all our compounds reduce both HA and CS expression, the experimental method of FACE is considered to be semi-quantitative. A panel of separation techniques, such as capillary electrophoresis or high-performance liquid chromatography (HPLC) are frequently used in conjunction with mass spectrophotometry for simultaneous separation and identification of GAG composition and structure, and has successfully been applied to cell, tissue, and biological fluid samples (Yang *et al.,* 2012). It would be tremendously informative to implement these techniques in order to definitively demonstrate the reduction of both HA and CS expression upon exposure to our compounds, and to characterise the specific types of sulphated CS that are reduced.

The advent of a state of the art technique known as time of flight secondary ion mass spectrometry (ToF-SIMS) is a promising approach for GAG analysis. ToF-SIMS focuses a

beams of primary ions on the surface of samples, producing secondary ions, the flight times of which are accurately measured for the identification of molecules (Welker, 2012; Hook *et al.*, 2021). Immense sensivity and resolution was achieved when used to analyse a microarray containing all six GAG types: HA, CS, HS, KS, dermatan sulphate, porcine mucosal heparin, and clinical grade heparin from different animal sources (Hook *et al.*, 2021). This technique facilitated the chemical discernment between the GAG classes with great accuracy, whilst notably being able to distinguish between heparin samples procured from the various animal sources and manufacturer batches (Hook *et al.*, 2021). The approach hence has broad applicability, and can be readily adapted to analytically characterise GAGs produced by cells following treatment with our compounds in a quantitative manner.

The completion of the tetrasaccharide linkage region (xylose-galactose-galactose-GlcA-) on the core protein is a prerequisite for the biosynthesis of CS and HS (Figure 30) (Kwok *et al.*, 2012; Fawcett and Kwok, 2022). The biosynthesis of these chains is initiated by the xylosation of the proteoglycan (PG) by xylotransferase (XT). The xylosylated protein is then galactosylated sequentially by the galactosyltransferases galactosyltransferase-1 (Gal-TI) and Gal-TII; finally, glucuronyltransferase-I (GlcAT-I) mediates the transfer of GlcA residue to the linkage tetrasaccharide (Uyama *et al.*, 2007, Kwok *et al.*, 2012). A comprehensive anaylsis on the expression and activity of core enzymes involved in CS/HS synthesis, as well as HA synthesis (i.e HAS, UGDH, UGPP) would provide a molecular description on the mechanisms underlying 4-MU, JD059, and JD060.

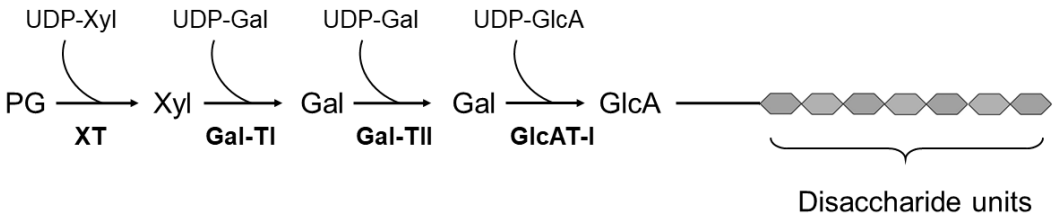

Figure 30. Biosynthesis of the tetrasaccharide linkage.

Finally, we discussed the benefits of our PNN-HEK293 model over primary neuronal culture models of PNNs in chapter 3.5.2 as well as chapter 6.2. For the purposes of an initial investigation into the efficacy of novel analogues, an immortal *in vitro* PNN model provides a rapid means for studying the genetic and cellular mechanisms underlying PNN attenuation elicited by our compounds. However, the CNS comprises a plethora of neurons of many distinct subtypes, which are arranged in interconnected assemblies that give rise to intricate and complex neuronal circuits. The next step from this research would be to decipher the

effects of our compounds on PNNs expressed by neurons. As briefly described in chapter 3.5.2, our lab has recently developed a neuronal model that accurately replicates the PNN heterogeneity and complexity observed in the cortex (Dickens *et al.*, 2023). Indeed, by DIV56, the mature reticular PNN morphology is the predominant population, accounting for 90% of PNNs within the culture (Dickens *et al.*, 2023). The PNNs additionally express PNN components present in the cortex: aggrecan, neurocan, brevican, HAPLN1, and tenascin-R. Because a neuronal PNN cell model possesses a molecular profile somewhat faithful to *in vivo* conditions, it would closely mimic the pharmacokinetics, pharmacodynamics, and toxicity profiles of our PNN inhibitors.

6.7.2 In vivo evaluation of novel 4-MU derivatives

This study has demonstrated for the first time that novel 4-MU derivatives JD059 and JD060 efficiently reduces PNN expression *in vitro*, likely via the attenuation of HA and CS synthesis. Moreover, analogue JD060 holds promise as a more effective PNN inhibitor than 4-MU and JD059. Finally, these compounds did not exhibit any cytotoxicity. These results provide a strong basis for further *in vivo* studies not only to validate their biological relevance in neuroplasticity, but to establish the most effective dosing regimen.

Our study has provided convincing evidence that our newly-synthesised 4-MU derivatives JD059 and JD060 not only possess the ability to inhibit PNNs *in vitro*, but may do so with greater efficacy. An important question is thus posed: how long is it necessary for compound treatment to inhibit PNN formation, and how long does this last following the cessation of their treatment? We can extrapolate theories from current literature regarding the pharmacokinetics of 4-MU in animals. In rodents, a significant decrease in serum HA levels was not observed until day 7 of 4-MU feeding (Kuipers *et al.*, 2016). In rats, the attenuation of PNNs persisted 1 month after the termination of 4-MU treatment (Dubisova *et al.*, 2022). Both these studies used the same dosage of 4-MU (5% 4-MU chow formulation).

A paper has recently been published in collaboration with our lab wherein a thorough toxicology assessment was conducted in rats (Štěpánková *et al.*, 2023). Healthy rats were examined after they were orally administered 1.2 g/kg/day of 4-MU for 10 weeks, and after a wash-out period. In agreement with the known 4-MU-mediated choleretic activity, there was a significant increase in bile acids, blood sugars and proteins, as well as interleukins IL10 IL12p70 and IFN-γ following 4-MU treatment, but no significant differences were found

between control- and 4-MU-treated groups following a 9-week wash-out period (Štěpánková *et al.*, 2023). Notably, biomechanical properties of tendons were unchanged following this treatment regimen (Štěpánková *et al.*, 2023), which is of particular interest given the importance of HA in tendon growth and integrity (Papakonstantinou *et al.*, 2012; Sikes *et al.*, 2018). The results imply that this dosing regimen is well-tolerated and does not cause any adverse effects on normal physiology.

To this end, JD059 and JD060 could be tested according to this dosing regimen, alongside 4-MU and a control without any compound, and a comprehensive toxicology report could be executed. We can additionally employ HPLC-mass spectrometry to measure plasma concentrations of our compounds at varying time points, and concomitantly assess PNN expression in the central nervous system by immunohistochemistry. This would allow us to ascertain the improved bioavailability of JD059 and JD060, which would hopefully correlate with the efficient suppression of PNNs. Identifying the full spectrum of targets within an organism is crucial not only to elucidate the mechanisms of our compounds, but exploit multivalency to circumvent potential problems of drug resistance. These analyses would be key in order to resolve any limitations of 4-MU, JD059, and JD060 and would facilitate clinical progression.

A particularly intriguing avenue to pursue would be to measure alterations in the patterns of activity of neurons in response to treatment with 4-MU and its analogues. Population recordings—which capture the intrinsic activity of neuronal populations simultaneously—are achieved mainly via extracellular electrophysiology and two-photon Ca^{2+} imaging. These foundational methods enable researchers to interrogate how these changes in neural activity relate to function and behaviour.

In testament to the functionality of these powerful techniques, much has been revealed regarding PNN-mediated plasticity using these methods. Degradation or transgenic suppression of PNNs has shown to enhance plasticity by means of *in vivo* electrophysiology (Massey *et al.*, 2006; Cafferty *et al.*, 2008; de Vivo *et al.*, 2013;) and *in vitro* electrophysiology (Bukalo *et al.*, 2001; Saghatelyan *et al.*, 2001; Yang *et al.*, 2015; Hayani *et al.*, 2018; Shi *et al.*, 2019). The effects of PNN attenuation on synaptic plasticity has also been confirmed using Ca^{2+} two-photon imaging (de Vivo *et al.*, 2013). Most recently, a study exploited *in vivo* two-photon Ca^{2+} imaging to determine that excitability of inhibitory interneurons in a mouse model of tauopathy was augmented following disruption of PNNs

(Kudo *et al.*, 2023). These two modalities provide related but different perspectives on underlying neural activity: extracellular electrophysiology offers information on a neuron's spiking output, whereas Ca^{2+} imaging measures neuronal spikes indirectly, reporting it instead through a transformation from intracellular Ca^{2+} (Wei *et al.*, 2020; Siegle *et al.*, 2021). These experiments remain essential to neuroscientific progress and will be critical for the advancement of this work.

Chapter 7: Conclusions

The overall aims of this study was two-fold: 1) investigate the potential of novel 4-MU-derived analogues in reducing PNN formation and 2) concomitantly explore the molecular mechanisms by which 4-MU and our novel analogues JD059 and JD60 could achieve this. Towards this endeavour, we first validated the suitability of an immortal *in vitro* model of PNNs (PNN-HEK293 cells). This model was able to produce a PNN-like matrix that was immunocytochemically positive for hyaluronan (HA) and *Wisteria floribunda* agglutinin (WFA), a pan-PNN marker. Exploiting this model, we were able to confirm that our compounds were non-toxic to cultured cells, which was essential due to the use of newly-synthesised analogues. The series of compounds were then tested for their ability to reduce PNNs by employing immunocytochemistry and biochemical techniques. Indeed, our compounds reduced HA^+ and WFA^+ PNNs in a dose-dependent manner. Given that WFA has been suggested to stain β-*N*-acetylgalactosamine residues of chondroitin sulphate (CS) chains, the reduction of WFA^+ PNNs brought to light the possibility of CS being a target of our compounds. 4-MU has been consistently proven to reduce the cellular content of the precursor uridine diphosphate-glucuronic acid (UDP-GlcA), and we hypothesised that this would lead to the reduction of both HA and CS formation.

This steered our research into exploring the overall glycosaminoglycan (GAG) production in the presence of our compounds. We extracted GAGs from the surface our PNN-HEK293 cells and quantified them. Our compounds elicited a potent ability to reduce overall GAGs in a dose-dependent manner in PNN-HEK293 cells. We then sought to characterise the specific PNN components that were attenuated, and we demonstrated that 1 mM of our compounds reduced both HA and CS, the latter of which has not been definitively shown before and which confirmed our hypothesis that CS production would additionally be affected.

In a proof-of-principle experiment, we isolated GAGs from the surface of PNN-HEK293 cells following treatment with our compounds, and coated them on coverslips to serve as growth substrates for dorsal root ganglion (DRG) neurons. GAGs recovered from untreated cells stunted DRG neurite arborisation and outgrowth, whereas GAGs extracted from cells treated with our compounds were a favourable growth substrate that promoted neurite outgrowth. These findings highlight the potential of our compounds in enhancing neuroplasticity, and that our novel 4-MU derivatives represent as potentially superior small molecule inhibitors of PNNs in existence to date.

Chapter 8: Bibliography

Abate, A., Dimartino, V., Spina, P., Costa, P. L., Lombardo, C., Santini, A., del Piano, M., & Alimonti, P. (2001). Hymecromone in the treatment of motor disorders of the bile ducts: a multicenter, double-blind, placebo-controlled clinical study. *Compounds under Experimental and Clinical Research*, *27*(5–6), 223–231.

Abraham, W. C., Jones, O. D., & Glanzman, D. L. (2019). Is plasticity of synapses the mechanism of long-term memory storage? *NPJ Science of Learning*, *4*, 9. https://doi.org/10.1038/s41539-019-0048-y

Abrous, D. N., Koehl, M., & le Moal, M. (2005). Adult neurogenesis: from precursors to network and physiology. *Physiological Reviews*, *85*(2), 523–569. https://doi.org/10.1152/physrev.00055.2003

Adusumalli, R., Åsheim, H., Lupashin, V., Blackburn, J. B., & Prydz, K. (2021). Proteoglycan synthesis in conserved oligomeric Golgi subunit deficient HEK293Tcells is affected differently, depending on the lacking subunit. Traffic, 22(7), 230–239. https://doi.org/10.1111/tra.12804

Afratis, N., Gialeli, C., Nikitovic, D., Tsegenidis, T., Karousou, E., Theocharis, A. D., Pavão, M. S., Tzanakakis, G. N., & Karamanos, N. K. (2012). Glycosaminoglycans: key players in cancer cell biology and treatment. *FEBS Journal*, *279*(7), 1177–1197. https://doi.org/10.1111/j.1742-4658.2012.08529.x

Ahuja, C. S., Wilson, J. R., Nori, S., Kotter, M. R. N., Druschel, C., Curt, A., & Fehlings, M. G. (2017). Traumatic spinal cord injury. *Nature Reviews Disease Primers*, *3*(1), 17018. https://doi.org/10.1038/nrdp.2017.18

Al-Ali, H., Beckerman, S. R., Bixby, J. L., & Lemmon, V. P. (2017). In vitro models of axon regeneration. *Experimental Neurology*, *287*(Pt 3), 423–434. https://doi.org/10.1016/j.expneurol.2016.01.020

Al'Qteishat, A., Gaffney, J., Krupinski, J., Rubio, F., West, D., Kumar, S., Kumar, P., Mitsios, N., & Slevin, M. (2006). Changes in hyaluronan production and metabolism following ischaemic stroke in man. *Brain : A Journal of Neurology*, *129*(Pt 8), 2158–2176. https://doi.org/10.1093/brain/awl139

Annies, M., Bittcher, G., Ramseger, R., Löschinger, J., Wöll, S., Porten, E., Abraham, C., Rüegg, M. A., & Kröger, S. (2006). Clustering transmembrane-agrin induces filopodia-like processes on axons and dendrites. *Molecular and Cellular Neurosciences*, *31*(3), 515–524. https://doi.org/10.1016/j.mcn.2005.11.005

Apostolova, I., Irintchev, A., & Schachner, M. (2006). Tenascin-R restricts posttraumatic remodeling of motoneuron innervation and functional recovery after spinal cord injury in adult mice. *Journal of Neuroscience*, *26*(30), 7849–7859. https://doi.org/10.1523/jneurosci.1526-06.2006

Appelbaum, L. G., Shenasa, M. A., Stolz, L., & Daskalakis, Z. (2023). Synaptic plasticity and mental health: methods, challenges and opportunities. *Neuropsychopharmacology : Official Publication of the American College of Neuropsychopharmacology*, *48*(1), 113–120. https://doi.org/10.1038/s41386-022-01370-w

Arai, E., Nishida, Y., Wasa, J., Urakawa, H., Zhuo, L., Kimata, K., Kozawa, E., Futamura, N., & Ishiguro, N. (2011). Inhibition of hyaluronan retention by 4-methylumbelliferone suppresses osteosarcoma cells in vitro and lung metastasis in vivo. *British Journal of Cancer*, *105*(12), 1839–1849. https://doi.org/10.1038/bjc.2011.459

Ashikov, A., Routier, F., Fuhlrott, J., Helmus, Y., Wild, M., Gerardy-Schahn, R., & Bakker, H. (2005). The Human Solute Carrier Gene SLC35B4 Encodes a Bifunctional Nucleotide Sugar Transporter with

Specificity for UDP-Xylose and UDP-N-Acetylglucosamine. Journal of Biological Chemistry, 280(29), 27230–27235. https://doi.org/10.1074/jbc.M504783200

Ash, R. T., Park, J., Suter, B., Zoghbi, H. Y., & Smirnakis, S. M. (2021). Excessive Formation and Stabilization of dendritic spine clusters in the MECP2-duplication syndrome mouse model of autism. *ENeuro*, *8*(1). https://doi.org/10.1523/ENEURO.0282-20.2020

Auld, D. S., Mennicken, F., & Quirion, R. (2001). Nerve growth factor rapidly induces prolonged acetylcholine release from cultured basal forebrain neurons: differentiation between neuromodulatory and neurotrophic influences. *Journal of Neuroscience*, *21*(10), 3375–3382. https://doi.org/10.1523/JNEUROSCI.21-10-03375.2001

Baerwald-de la Torre, K., Winzen, U., Halfter, W., & Bixby, J. L. (2004). Glycosaminoglycan-dependent and -independent inhibition of neurite outgrowth by agrin. *Journal of Neurochemistry*, *90*(1), 50–61. https://doi.org/10.1111/j.1471-4159.2004.02454.x

Balmer, T. S., Carels, V. M., Frisch, J. L., & Nick, T. A. (2009). Modulation of perineuronal nets and parvalbumin with developmental song learning. *Journal of Neuroscience*, *29*(41), 12878–12885. https://doi.org/10.1523/JNEUROSCI.2974-09.2009

Barnes, J., Tian, L., Loftis, J., Hiznay, J., Comhair, S., Lauer, M., & Dweik, R. (2016). Isolation and analysis of sugar nucleotides using solid phase extraction and fluorophore assisted carbohydrate electrophoresis. *MethodsX*, *3*, 251–260. https://doi.org/10.1016/j.mex.2016.03.010

Bekku, Y., Saito, M., Moser, M., Fuchigami, M., Maehara, A., Nakayama, M., Kusachi, S., Ninomiya, Y., & Oohashi, T. (2012). Bral2 is indispensable for the proper localization of brevican and the structural integrity of the perineuronal net in the brainstem and cerebellum. *The Journal of Comparative Neurology*, *520*(8), 1721–1736. https://doi.org/10.1002/cne.23009

Berdugo-Vega, G., Arias-Gil, G., López-Fernández, A., Artegiani, B., Wasielewska, J. M., Lee, C.-C., Lippert, M. T., Kempermann, G., Takagaki, K., & Calegari, F. (2020). Increasing neurogenesis refines hippocampal activity rejuvenating navigational learning strategies and contextual memory throughout life. *Nature Communications*, *11*(1), 135. https://doi.org/10.1038/s41467-019-14026-z

Bernard, C., & Prochiantz, A. (2016). Otx2-PNN Interaction to regulate cortical plasticity. *Neural Plasticity*, *2016*, 1–7. https://doi.org/10.1155/2016/7931693

Berning, S., Willig, K. I., Steffens, H., Dibaj, P., & Hell, S. W. (2012). Nanoscopy in a living mouse brain. *Science (New York, N.Y.)*, *335*(6068), 551. https://doi.org/10.1126/science.1215369

Beurdeley, M., Spatazza, J., Lee, H. H. C., Sugiyama, S., Bernard, C., di Nardo, A. A., Hensch, T. K., & Prochiantz, A. (2012). Otx2 binding to perineuronal nets persistently regulates plasticity in the mature visual cortex. *Journal of Neuroscience*, *32*(27), 9429–9437. https://doi.org/10.1523/JNEUROSCI.0394-12.2012

Bickford, M. E., Slusarczyk, A., Dilger, E. K., Krahe, T. E., Kucuk, C., & Guido, W. (2010). Synaptic development of the mouse dorsal lateral geniculate nucleus. *The Journal of Comparative Neurology*, *518*(5), 622–635. https://doi.org/10.1002/cne.22223

Bigge, J. C., Patel, T. P., Bruce, J. A., Goulding, P. N., Charles, S. M., & Parekh, R. B. (1995). Nonselective and efficient fluorescent labeling of glycans using 2-amino benzamide and anthranilic acid. *Analytical Biochemistry*, *230*(2), 229–238. https://doi.org/10.1006/abio.1995.1468

Boros, B. D., Greathouse, K. M., Gearing, M., & Herskowitz, J. H. (2019). Dendritic spine remodeling accompanies Alzheimer's disease pathology and genetic susceptibility in cognitively normal aging. *Neurobiology of Aging*, *73*, 92–103. https://doi.org/10.1016/j.neurobiolaging.2018.09.003

Bothwell, S., Meredith, G. E., Phillips, J., Staunton, H., Doherty, C., Grigorenko, E., Glazier, S., Deadwyler, S. A., O'Donovan, C. A., & Farrell, M. (2001). Neuronal hypertrophy in the neocortex of patients with temporal lobe epilepsy. *The Journal of Neuroscience*, *21*(13), 4789–4800. https://doi.org/10.1523/JNEUROSCI.21-13-04789.2001

Bradbury, E. J., Moon, L. D. F., Popat, R. J., King, V. R., Bennett, G. S., Patel, P. N., Fawcett, J. W., & McMahon, S. B. (2002). Chondroitinase ABC promotes functional recovery after spinal cord injury. *Nature*, *416*(6881), 636–640. https://doi.org/10.1038/416636a

Brückner, G., Brauer, K., Härtig, W., Wolff, J. R., Rickmann, M. J., Derouiche, A., Delpech, B., Girard, N., Oertel, W. H., & Reichenbach, A. (1993). Perineuronal nets provide a polyanionic, glia-associated form of microenvironment around certain neurons in many parts of the rat brain. *Glia*, *8*(3), 183–200. https://doi.org/10.1002/glia.440080306

Burket, J. A., Webb, J. D., & Deutsch, S. I. (2021). Perineuronal nets and metal cation concentrations in the microenvironments of fast-Spiking, parvalbumin-expressing GABAergic interneurons: relevance to neurodevelopment and neurodevelopmental disorders. *Biomolecules*, *11*(8). https://doi.org/10.3390/biom11081235

Burnside, E. R., & Bradbury, E. J. (2014). Manipulating the extracellular matrix and its role in brain and spinal cord plasticity and repair. *Neuropathology and Applied Neurobiology*, *40*(1), 26–59. https://doi.org/10.1111/nan.12114

Bushong, E. A., Martone, M. E., Jones, Y. Z., & Ellisman, M. H. (2002). Protoplasmic astrocytes in CA1 stratum radiatum occupy separate anatomical domains. *The Journal of Neuroscience : The Official Journal of the Society for Neuroscience*, *22*(1), 183–192. https://doi.org/10.1523/JNEUROSCI.22-01-00183.2002

Cafferty, W. B. J., Bradbury, E. J., Lidierth, M., Jones, M., Duffy, P. J., Pezet, S., & McMahon, S. B. (2008). Chondroitinase ABC-Mediated Plasticity of Spinal Sensory Function. The Journal of Neuroscience, 28(46), 11998–12009. https://doi.org/10.1523/jneurosci.3877-08.2008

Calabro, A., Benavides, M., Tammi, M., Hascall, V. C., & Midura, R. J. (2000). Microanalysis of enzyme digests of hyaluronan and chondroitin/dermatan sulfate by fluorophore-assisted carbohydrate electrophoresis (FACE). *Glycobiology*, *10*(3), 273–281. https://doi.org/10.1093/glycob/10.3.273

Campanac, E., Gasselin, C., Baude, A., Rama, S., Ankri, N., & Debanne, D. (2013). Enhanced intrinsic excitability in basket cells maintains excitatory-inhibitory balance in hippocampal circuits. *Neuron*, *77*(4), 712–722. https://doi.org/10.1016/j.neuron.2012.12.020

Carceller, H., Gramuntell, Y., Klimczak, P., & Nacher, J. (2022). Perineuronal nets: subtle structures with large implications. *The Neuroscientist*, 107385842211063. https://doi.org/10.1177/10738584221106346

Carstens, K. E., Phillips, M. L., Pozzo-Miller, L., Weinberg, R. J., & Dudek, S. M. (2016). Perineuronal nets suppress plasticity of excitatory synapses on CA2 pyramidal neurons. *The Journal of Neuroscience : The Official Journal of the Society for Neuroscience*, *36*(23), 6312–6320. https://doi.org/10.1523/JNEUROSCI.0245-16.2016

Carulli, D., de Winter, F., & Verhaagen, J. (2021). Semaphorins in adult nervous system plasticity and disease. *Frontiers in Synaptic Neuroscience*, *13*. https://doi.org/10.3389/fnsyn.2021.672891

Carulli, D., Kwok, J. C. F., & Pizzorusso, T. (2016). Perineuronal nets and CNS plasticity and rpair. *Neural Plasticity*, *2016*, 1–2. https://doi.org/10.1155/2016/4327082

Carulli, D., Pizzorusso, T., Kwok, J. C. F., Putignano, E., Poli, A., Forostyak, S., Andrews, M. R., Deepa, S. S., Glant, T. T., & Fawcett, J. W. (2010). Animals lacking link protein have attenuated perineuronal nets and persistent plasticity. *Brain*, *133*(8), 2331–2347. https://doi.org/10.1093/brain/awq145

Carulli, D., Rhodes, K. E., Brown, D. J., Bonnert, T. P., Pollack, S. J., Oliver, K., Strata, P., & Fawcett, J. W. (2006). Composition of perineuronal nets in the adult rat cerebellum and the cellular origin of their components. *The Journal of Comparative Neurology*, *494*(4), 559–577. https://doi.org/10.1002/cne.20822

Carulli, D., Rhodes, K. E., & Fawcett, J. W. (2007). Upregulation of aggrecan, link protein 1, and hyaluronan synthases during formation of perineuronal nets in the rat cerebellum. *The Journal of Comparative Neurology*, *501*(1), 83–94. https://doi.org/10.1002/cne.21231

Carulli, D., & Verhaagen, J. (2021). An extracellular perspective on CNS maturation: perineuronal nets and the control of plasticity. *International Journal of Molecular Sciences*, *22*(5). https://doi.org/10.3390/ijms22052434

Chan, C.-S., Levenson, J. M., Mukhopadhyay, P. S., Zong, L., Bradley, A., Sweatt, J. D., & Davis, R. L. (2007). Alpha3-integrins are required for hippocampal long-term potentiation and working memory. *Learning & Memory (Cold Spring Harbor, N.Y.)*, *14*(9), 606–615. https://doi.org/10.1101/lm.648607

Chan, C.-S., Weeber, E. J., Zong, L., Fuchs, E., Sweatt, J. D., & Davis, R. L. (2006). Beta 1-integrins are required for hippocampal AMPA receptor-dependent synaptic transmission, synaptic plasticity, and working memory. *The Journal of Neuroscience : The Official Journal of the Society for Neuroscience*, *26*(1), 223–232. https://doi.org/10.1523/JNEUROSCI.4110-05.2006

Chang, M. C., Park, J. M., Pelkey, K. A., Grabenstatter, H. L., Xu, D., Linden, D. J., Sutula, T. P., McBain, C. J., & Worley, P. F. (2010). Narp regulates homeostatic scaling of excitatory synapses on parvalbumin-expressing interneurons. *Nature Neuroscience*, *13*(9), 1090–1097. https://doi.org/10.1038/nn.2621

Chan, J. P., Cordeira, J., Calderon, G. A., Iyer, L. K., & Rios, M. (2008). Depletion of central BDNF in mice impedes terminal differentiation of new granule neurons in the adult hippocampus. *Molecular and Cellular Neurosciences*, *39*(3), 372–383. https://doi.org/10.1016/j.mcn.2008.07.017

Cheng, C.-H., Lin, C.-T., Lee, M.-J., Tsai, M.-J., Huang, W.-H., Huang, M.-C., Lin, Y.-L., Chen, C.-J., Huang, W.-C., & Cheng, H. (2015). Local delivery of high-dose chondroitinase ABC in the sub-Acute stage promotes axonal outgrowth and functional recovery after complete spinal cord transection. *PloS One*, *10*(9), e0138705. https://doi.org/10.1371/journal.pone.0138705

Cheng, X.-B., Sato, N., Kohi, S., Koga, A., & Hirata, K. (2018). 4-Methylumbelliferone inhibits enhanced hyaluronan synthesis and cell migration in pancreatic cancer cells in response to tumor-stromal interactions. *Oncology Letters*, *15*(5), 6297–6301. https://doi.org/10.3892/ol.2018.8147

Chklovskii, D. B., Mel, B. W., & Svoboda, K. (2004). Cortical rewiring and information storage. *Nature*, *431*(7010), 782–788. https://doi.org/10.1038/nature03012

Christensen, A. C., Lensjø, K. K., Lepperød, M. E., Dragly, S.-A., Sutterud, H., Blackstad, J. S., Fyhn, M., & Hafting, T. (2021). Perineuronal nets stabilize the grid cell network. *Nature Communications*, *12*(1), 253. https://doi.org/10.1038/s41467-020-20241-w

Christopherson, K. S., Ullian, E. M., Stokes, C. C. A., Mullowney, C. E., Hell, J. W., Agah, A., Lawler, J., Mosher, D. F., Bornstein, P., & Barres, B. A. (2005). Thrombospondins are astrocyte-Secreted proteins that promote CNS synaptogenesis. *Cell*, *120*(3), 421–433. https://doi.org/10.1016/j.cell.2004.12.020

Cichon, J., & Gan, W.-B. (2015). Branch-specific dendritic Ca2+ spikes cause persistent synaptic plasticity. *Nature*, *520*(7546), 180–185. https://doi.org/10.1038/nature14251

Cisneros-Franco, J. M., & de Villers-Sidani, É. (2019). Reactivation of critical period plasticity in adult auditory cortex through chemogenetic silencing of parvalbumin-positive interneurons. *Proceedings of the National Academy of Sciences*, *116*(52), 26329–26331. https://doi.org/10.1073/pnas.1913227117

Citri, A., & Malenka, R. C. (2008). Synaptic plasticity: multiple forms, functions, and mechanisms. *Neuropsychopharmacology : Official Publication of the American College of Neuropsychopharmacology*, *33*(1), 18–41. https://doi.org/10.1038/sj.npp.1301559

Cope, E. C., Zych, A. D., Katchur, N. J., Waters, R. C., Laham, B. J., Diethorn, E. J., Park, C. Y., Meara, W. R., & Gould, E. (2022). Atypical perineuronal nets in the CA2 region interfere with social memory in a mouse model of social dysfunction. *Molecular Psychiatry*, *27*(8), 3520–3531. https://doi.org/10.1038/s41380-021-01174-2

Cornez, G., Collignon, C., Müller, W., Ball, G. F., Cornil, C. A., & Balthazart, J. (2020). Seasonal changes of perineuronal nets and song learning in adult canaries (Serinus canaria). *Behavioural Brain Research*, *380*, 112437. https://doi.org/10.1016/j.bbr.2019.112437

Cornez, G., Collignon, C., Müller, W., Cornil, C. A., Ball, G. F., & Balthazart, J. (2020). Development of perineuronal nets during ontogeny correlates with sensorimotor vocal learning in canaries. *ENeuro*, *7*(2). https://doi.org/10.1523/ENEURO.0361-19.2020

Cowman, M. K., Lee, H.-G., Schwertfeger, K. L., McCarthy, J. B., & Turley, E. A. (2015). The Content and Size of Hyaluronan in Biological Fluids and Tissues. Frontiers in Immunology, 6, 261. https://doi.org/10.3389/fimmu.2015.00261

Csala, M., Marcolongo, P., Lizák, B., Senesi, S., Margittai, É., Fulceri, R., Magyar, J. É., Benedetti, A., & Bánhegyi, G. (2007). Transport and transporters in the endoplasmic reticulum. Biochimica et Biophysica Acta (BBA) - Biomembranes, 1768(6), 1325–1341. https://doi.org/10.1016/j.bbamem.2007.03.009

Cua, R. C., Lau, L. W., Keough, M. B., Midha, R., Apte, S. S., & Yong, V. W. (2013). Overcoming neurite-inhibitory chondroitin sulfate proteoglycans in the astrocyte matrix. *Glia*, *61*(6), 972–984. https://doi.org/10.1002/glia.22489

Curinga, G. M., Snow, D. M., Mashburn, C., Kohler, K., Thobaben, R., Caggiano, A. O., & Smith, G. M. (2007). Mammalian-produced chondroitinase AC mitigates axon inhibition by chondroitin sulfate proteoglycans. *Journal of Neurochemistry*, *102*(1), 275–288. https://doi.org/10.1111/j.1471-4159.2007.04530.x

Cyphert, J. M., Trempus, C. S., & Garantziotis, S. (2015). Size Matters: Molecular Weight Specificity of Hyaluronan Effects in Cell Biology. International Journal of Cell Biology, 2015, 563818. https://doi.org/10.1155/2015/563818

Dankovich, T. M., Kaushik, R., Olsthoorn, L. H. M., Petersen, G. C., Giro, P. E., Kluever, V., Agüi-Gonzalez, P., Grewe, K., Bao, G., Beuermann, S., Hadi, H. A., Doeren, J., Klöppner, S., Cooper, B. H., Dityatev, A., & Rizzoli, S. O. (2021). Extracellular matrix remodeling through endocytosis and resurfacing of Tenascin-R. *Nature Communications*, *12*(1), 7129. https://doi.org/10.1038/s41467-021-27462-7

Deakin, J. A., & Lyon, M. (2008). A simplified and sensitive fluorescent method for disaccharide analysis of both heparan sulfate and chondroitin/dermatan sulfates from biological samples. *Glycobiology*, *18*(6), 483–491. https://doi.org/10.1093/glycob/cwn028

DeBello, W. M., McBride, T. J., Nichols, G. S., Pannoni, K. E., Sanculi, D., & Totten, D. J. (2014). Input clustering and the microscale structure of local circuits. *Frontiers in Neural Circuits*, *8*. https://doi.org/10.3389/fncir.2014.00112

Deen, A. J., Arasu, U. T., Pasonen-Seppänen, S., Hassinen, A., Takabe, P., Wojciechowski, S., Kärnä, R., Rilla, K., Kellokumpu, S., Tammi, R., Tammi, M., & Oikari, S. (2016). UDP-sugar substrates of HAS3 regulate its O-GlcNAcylation, intracellular traffic, extracellular shedding and correlate with melanoma progression. *Cellular and Molecular Life Sciences*, *73*(16), 3183–3204. https://doi.org/10.1007/s00018-016-2158-5

Deepa, S. S., Carulli, D., Galtrey, C., Rhodes, K., Fukuda, J., Mikami, T., Sugahara, K., & Fawcett, J. W. (2006). Composition of perineuronal net extracellular matrix in rat brain: a different disaccharide composition for the net-associated proteoglycans. *The Journal of Biological Chemistry*, *281*(26), 17789–17800. https://doi.org/10.1074/jbc.M600544200

Despras, G., Bernard, C., Perrot, A., Cattiaux, L., Prochiantz, A., Lortat-Jacob, H., & Mallet, J.-M. (2013). Toward libraries of biotinylated chondroitin sulfate analogues: from synthesis to in vivo studies. *Chemistry - A European Journal*, *19*(2), 531–540. https://doi.org/10.1002/chem.201202173

de Vivo, L., Landi, S., Panniello, M., Baroncelli, L., Chierzi, S., Mariotti, L., Spolidoro, M., Pizzorusso, T., Maffei, L., & Ratto, G. M. (2013). Extracellular matrix inhibits structural and functional plasticity of dendritic spines in the adult visual cortex. *Nature Communications*, *4*(1), 1484. https://doi.org/10.1038/ncomms2491

de Winter, F., Kwok, J. C. F., Fawcett, J. W., Vo, T. T., Carulli, D., & Verhaagen, J. (2016). The chemorepulsive protein semaphorin 3A and perineuronal net-mediated plasticity. *Neural Plasticity*, *2016*, 3679545. https://doi.org/10.1155/2016/3679545

Dickendesher, T. L., Baldwin, K. T., Mironova, Y. A., Koriyama, Y., Raiker, S. J., Askew, K. L., Wood, A., Geoffroy, C. G., Zheng, B., Liepmann, C. D., Katagiri, Y., Benowitz, L. I., Geller, H. M., & Giger, R. J. (2012). NgR1 and NgR3 are receptors for chondroitin sulfate proteoglycans. *Nature Neuroscience*, *15*(5), 703–712. https://doi.org/10.1038/nn.3070

Dick, G., Tan, C. L., Alves, J. N., Ehlert, E. M. E., Miller, G. M., Hsieh-Wilson, L. C., Sugahara, K., Oosterhof, A., van Kuppevelt, T. H., Verhaagen, J., Fawcett, J. W., & Kwok, J. C. F. (2013). Semaphorin 3A binds to the perineuronal nets via chondroitin sulfate type E motifs in rodent brains. *The Journal of Biological Chemistry*, *288*(38), 27384–27395. https://doi.org/10.1074/jbc.M111.310029

Dityatev, A., Brückner, G., Dityateva, G., Grosche, J., Kleene, R., & Schachner, M. (2007). Activity-dependent formation and functions of chondroitin sulfate-rich extracellular matrix of perineuronal nets. *Developmental Neurobiology*, *67*(5), 570–588. https://doi.org/10.1002/dneu.20361

Dityatev, A., & Rusakov, D. A. (2011). Molecular signals of plasticity at the tetrapartite synapse. *Current Opinion in Neurobiology*, *21*(2), 353–359. https://doi.org/10.1016/j.conb.2010.12.006

Djerbal, L., Lortat-Jacob, H., & Kwok, J. (2017). Chondroitin sulfates and their binding molecules in the central nervous system. *Glycoconjugate Journal*, *34*(3), 363–376. https://doi.org/10.1007/s10719-017-9761-z

Donato, F., Rompani, S. B., & Caroni, P. (2013). Parvalbumin-expressing basket-cell network plasticity induced by experience regulates adult learning. *Nature*, *504*(7479), 272–276. https://doi.org/10.1038/nature12866

Dubisova, J., Burianova, J. S., Svobodova, L., Makovicky, P., Martinez-Varea, N., Cimpean, A., Fawcett, J. W., Kwok, J. C. F., & Kubinova, S. (2022). Oral treatment of 4-methylumbelliferone reduced

perineuronal nets and improved recognition memory in mice. *Brain Research Bulletin*, *181*, 144–156. https://doi.org/10.1016/j.brainresbull.2022.01.011

Dumitriu, D., Hao, J., Hara, Y., Kaufmann, J., Janssen, W. G. M., Lou, W., Rapp, P. R., & Morrison, J. H. (2010). Selective changes in thin spine density and morphology in monkey prefrontal cortex correlate with aging-related cognitive impairment. *The Journal of Neuroscience : The Official Journal of the Society for Neuroscience*, *30*(22), 7507–7515. https://doi.org/10.1523/JNEUROSCI.6410-09.2010

Dyck, S., Kataria, H., Alizadeh, A., Santhosh, K. T., Lang, B., Silver, J., & Karimi-Abdolrezaee, S. (2018). Perturbing chondroitin sulfate proteoglycan signaling through LAR and PTPσ receptors promotes a beneficial inflammatory response following spinal cord injury. *Journal of Neuroinflammation*, *15*(1), 90. https://doi.org/10.1186/s12974-018-1128-2

Dyck, S., Kataria, H., Akbari-Kelachayeh, K., Silver, J., & Karimi-Abdolrezaee, S. (2019). LAR and PTPσ receptors are negative regulators of oligodendrogenesis and oligodendrocyte integrity in spinal cord injury. *Glia*, *67*(1), 125–145. https://doi.org/10.1002/glia.23533

Edamatsu, M., Miyano, R., Fujikawa, A., Fujii, F., Hori, T., Sakaba, T., & Oohashi, T. (2018). Hapln4/Bral2 is a selective regulator for formation and transmission of GABAergic synapses between Purkinje and deep cerebellar nuclei neurons. *Journal of Neurochemistry*, *147*(6), 748–763. https://doi.org/10.1111/jnc.14571

Edward, M., Quinn, J. A., Pasonen-Seppänen, S. M., McCann, B. A., & Tammi, R. H. (2010). 4-Methylumbelliferone inhibits tumour cell growth and the activation of stromal hyaluronan synthesis by melanoma cell-derived factors. *British Journal of Dermatology*, *162*(6), 1224–1232. https://doi.org/10.1111/j.1365-2133.2010.09699.x

Eroglu, C. (2009). The role of astrocyte-secreted matricellular proteins in central nervous system development and function. *Journal of Cell Communication and Signaling*, *3*(3–4), 167–176. https://doi.org/10.1007/s12079-009-0078-y

Evans, A., Terstege, D. J., Scott, G. A., Tsutsui, M., & Epp, J. R. (2022). Neurogenesis mediated plasticity is associated with reduced neuronal activity in CA1 during context fear memory retrieval. *Scientific Reports*, *12*(1), 7016. https://doi.org/10.1038/s41598-022-10947-w

Fabel, K., Wolf, S. A., Ehninger, D., Babu, H., Leal-Galicia, P., & Kempermann, G. (2009). Additive effects of physical exercise and environmental enrichment on adult hippocampal neurogenesis in mice. *Frontiers in Neuroscience*, *3*, 50. https://doi.org/10.3389/neuro.22.002.2009

Faust, T. E., Gunner, G., & Schafer, D. P. (2021). Mechanisms governing activity-dependent synaptic pruning in the developing mammalian CNS. *Nature Reviews Neuroscience*, *22*(11), 657–673. https://doi.org/10.1038/s41583-021-00507-y

Fauth, M., & Tetzlaff, C. (2016). Opposing Effects of Neuronal Activity on Structural Plasticity. *Frontiers in Neuroanatomy*, *10*, 75. https://doi.org/10.3389/fnana.2016.00075

Favuzzi, E., Marques-Smith, A., Deogracias, R., Winterflood, C. M., Sánchez-Aguilera, A., Mantoan, L., Maeso, P., Fernandes, C., Ewers, H., & Rico, B. (2017). Activity-dependent gating of parvalbumin interneuron function by the perineuronal net protein brevican. *Neuron*, *95*(3), 639-655.e10. https://doi.org/10.1016/j.neuron.2017.06.028

Fawcett, J. W., Fyhn, M., Jendelova, P., Kwok, J. C. F., Ruzicka, J., & Sorg, B. A. (2022). The extracellular matrix and perineuronal nets in memory. *Molecular Psychiatry*, *27*(8), 3192–3203. https://doi.org/10.1038/s41380-022-01634-3

Fawcett, J. W., Oohashi, T., & Pizzorusso, T. (2019). The roles of perineuronal nets and the perinodal extracellular matrix in neuronal function. *Nature Reviews Neuroscience*, *20*(8), 451–465. https://doi.org/10.1038/s41583-019-0196-3

Ferrer-Ferrer, M., & Dityatev, A. (2018). Shaping Synapses by the Neural Extracellular Matrix. *Frontiers in Neuroanatomy*, *12*, 40. https://doi.org/10.3389/fnana.2018.00040

Fiore, M., Triaca, V., Amendola, T., Tirassa, P., & Aloe, L. (2002). Brain NGF and EGF administration improves passive avoidance response and stimulates brain precursor cells in aged male mice. *Physiology & Behavior*, *77*(2–3), 437–443. https://doi.org/10.1016/S0031-9384(02)00875-2

Fisher, D., Xing, B., Dill, J., Li, H., Hoang, H. H., Zhao, Z., Yang, X.-L., Bachoo, R., Cannon, S., Longo, F. M., Sheng, M., Silver, J., & Li, S. (2011). Leukocyte Common Antigen-Related Phosphatase Is a Functional Receptor for Chondroitin Sulfate Proteoglycan Axon Growth Inhibitors. *Journal of Neuroscience*, *31*(40), 14051–14066. https://doi.org/10.1523/JNEUROSCI.1737-11.2011

Fitch, M. T., & Silver, J. (2008). CNS injury, glial scars, and inflammation: Inhibitory extracellular matrices and regeneration failure. Experimental Neurology, 209(2), 294–301. https://doi.org/10.1016/j.expneurol.2007.05.014

Fitsialos, G., Chassot, A.-A., Turchi, L., Dayem, M. A., LeBrigand, K., Moreilhon, C., Meneguzzi, G., Buscà, R., Mari, B., Barbry, P., & Ponzio, G. (2007). Transcriptional signature of epidermal keratinocytes subjected to in vitro scratch wounding reveals selective roles for ERK1/2, p38, and phosphatidylinositol 3-kinase signaling pathways. *Journal of Biological Chemistry*, *282*(20), 15090–15102. https://doi.org/10.1074/jbc.M606094200

Forrest, M. P., Parnell, E., & Penzes, P. (2018). Dendritic structural plasticity and neuropsychiatric disease. *Nature Reviews. Neuroscience*, *19*(4), 215–234. https://doi.org/10.1038/nrn.2018.16

Förster, E., Zhao, S., & Frotscher, M. (2006). Laminating the hippocampus. *Nature Reviews Neuroscience*, *7*(4), 259–268. https://doi.org/10.1038/nrn1882

Foscarin, S., Raha-Chowdhury, R., Fawcett, J. W., & Kwok, J. C. F. (2017). Brain ageing changes proteoglycan sulfation, rendering perineuronal nets more inhibitory. *Aging*, *9*(6), 1607–1622. https://doi.org/10.18632/aging.101256

Frank, A. C., Huang, S., Zhou, M., Gdalyahu, A., Kastellakis, G., Silva, T. K., Lu, E., Wen, X., Poirazi, P., Trachtenberg, J. T., & Silva, A. J. (2018). Hotspots of dendritic spine turnover facilitate clustered spine addition and learning and memory. *Nature Communications*, *9*(1), 422. https://doi.org/10.1038/s41467-017-02751-2

Frischknecht, R., Heine, M., Perrais, D., Seidenbecher, C. I., Choquet, D., & Gundelfinger, E. D. (2009). Brain extracellular matrix affects AMPA receptor lateral mobility and short-term synaptic plasticity. *Nature Neuroscience*, *12*(7), 897–904. https://doi.org/10.1038/nn.2338

Fry, E. J., Chagnon, M. J., López-Vales, R., Tremblay, M. L., & David, S. (2009). Corticospinal tract regeneration after spinal cord injury in receptor protein tyrosine phosphatase sigma deficient mice. *Glia*, NA-NA. https://doi.org/10.1002/glia.20934

Gage, F. H. (2019). Adult neurogenesis in mammals. *Science*, *364*(6443), 827–828. https://doi.org/10.1126/science.aav6885

Galgoczi, E., Jeney, F., Katko, M., Erdei, A., Gazdag, A., Sira, L., Bodor, M., Berta, E., Ujhelyi, B., Steiber, Z., Gyory, F., & Nagy, E. v. (2020). Characteristics of hyaluronan synthesis inhibition by 4-methylumbelliferone in orbital fibroblasts. *Investigative Opthalmology & Visual Science*, *61*(2), 27. https://doi.org/10.1167/iovs.61.2.27

Galtrey, C. M., Kwok, J. C. F., Carulli, D., Rhodes, K. E., & Fawcett, J. W. (2008). Distribution and synthesis of extracellular matrix proteoglycans, hyaluronan, link proteins and tenascin-R in the rat spinal cord. *The European Journal of Neuroscience*, *27*(6), 1373–1390. https://doi.org/10.1111/j.1460-9568.2008.06108.x

García-Vilas, J. A., Quesada, A. R., & Medina, M. Á. (2013). 4-Methylumbelliferone inhibits angiogenesis in vitro and in vivo. *Journal of Agricultural and Food Chemistry*, *61*(17), 4063–4071. https://doi.org/10.1021/jf303062h

Garrett, E. R., Venitz, J., Eberst, K., & Cerda, J. J. (1993). Pharmacokinetics and bioavailabilities of hymecromone in human volunteers. *Biopharmaceutics & Compound Disposition*, *14*(1), 13–39. https://doi.org/10.1002/bdd.2510140103

Garud, D. R., Tran, V. M., Victor, X. v., Koketsu, M., & Kuberan, B. (2008). Inhibition of heparan sulfate and chondroitin sulfate proteoglycan biosynthesis. *Journal of Biological Chemistry*, *283*(43), 28881–28887. https://doi.org/10.1074/jbc.M805939200

Gattazzo, F., Urciuolo, A., & Bonaldo, P. (2014). Extracellular matrix: a dynamic microenvironment for stem cell niche. *Biochimica et Biophysica Acta*, *1840*(8), 2506–2519. https://doi.org/10.1016/j.bbagen.2014.01.010

Geissler, M., Gottschling, C., Aguado, A., Rauch, U., Wetzel, C. H., Hatt, H., & Faissner, A. (2013). Primary hippocampal neurons, which lack four crucial extracellular matrix molecules, display abnormalities of synaptic structure and function and severe deficits in perineuronal net formation. *The Journal of Neuroscience : The Official Journal of the Society for Neuroscience*, *33*(18), 7742–7755. https://doi.org/10.1523/JNEUROSCI.3275-12.2013

George, N., & Geller, H. M. (2018). Extracellular matrix and traumatic brain injury. *Journal of Neuroscience Research*, *96*(4), 573–588. https://doi.org/10.1002/jnr.24151

Giamanco, K. A., Morawski, M., & Matthews, R. T. (2010). Perineuronal net formation and structure in aggrecan knockout mice. *Neuroscience*, *170*(4), 1314–1327. https://doi.org/10.1016/j.neuroscience.2010.08.032

Globus, A., & Scheibel, A. B. (1967). The effect of visual deprivation on cortical neurons: A golgi study. *Experimental Neurology*, *19*(3), 331–345. https://doi.org/10.1016/0014-4886(67)90029-5

Gonçalves, J. T., Schafer, S. T., & Gage, F. H. (2016). Adult neurogenesis in the hippocampus: from stem cells to behavior. *Cell*, *167*(4), 897–914. https://doi.org/10.1016/j.cell.2016.10.021

Govindarajan, A., Kelleher, R. J., & Tonegawa, S. (2006). A clustered plasticity model of long-term memory engrams. *Nature Reviews Neuroscience*, *7*(7), 575–583. https://doi.org/10.1038/nrn1937

Groc, L., Choquet, D., Stephenson, F. A., Verrier, D., Manzoni, O. J., & Chavis, P. (2007). NMDA Receptor surface trafficking and synaptic subunit composition are developmentally regulated by the extracellular matrix protein reelin. *Journal of Neuroscience*, *27*(38), 10165–10175. https://doi.org/10.1523/JNEUROSCI.1772-07.2007

Grosche, J., & Bruckner, G. (2001). Perineuronal nets show intrinsic patterns of extracellular matrix differentiation in organotypic slice cultures. *Experimental Brain Research*, *137*(1), 83–93. https://doi.org/10.1007/s002210000617

Gu, L., Kleiber, S., Schmid, L., Nebeling, F., Chamoun, M., Steffen, J., Wagner, J., & Fuhrmann, M. (2014). Long-term in vivo imaging of dendritic spines in the hippocampus reveals structural plasticity. *The Journal of Neuroscience : The Official Journal of the Society for Neuroscience*, *34*(42), 13948–13953. https://doi.org/10.1523/JNEUROSCI.1464-14.2014

Happel, M. F. K., Niekisch, H., Castiblanco Rivera, L. L., Ohl, F. W., Deliano, M., & Frischknecht, R. (2014). Enhanced cognitive flexibility in reversal learning induced by removal of the extracellular matrix in auditory cortex. *Proceedings of the National Academy of Sciences of the United States of America*, *111*(7), 2800–2805. https://doi.org/10.1073/pnas.1310272111

Härtig, W., Derouiche, A., Welt, K., Brauer, K., Grosche, J., Mäder, M., Reichenbach, A., & Brückner, G. (1999). Cortical neurons immunoreactive for the potassium channel Kv3.1b subunit are predominantly surrounded by perineuronal nets presumed as a buffering system for cations. *Brain Research*, *842*(1), 15–29. https://doi.org/10.1016/s0006-8993(99)01784-9

Härtig, W., Meinicke, A., Michalski, D., Schob, S., & Jäger, C. (2022). Update on Perineuronal Net Staining With Wisteria floribunda Agglutinin (WFA). Frontiers in Integrative Neuroscience, 16. https://doi.org/10.3389/fnint.2022.851988

Hartman, C. D., Isenberg, B. C., Chua, S. G., & Wong, J. Y. (2017). Extracellular matrix type modulates cell migration on mechanical gradients. *Experimental Cell Research*, *359*(2), 361–366. https://doi.org/10.1016/j.yexcr.2017.08.018

Haunsø, A., Ibrahim, M., Bartsch, U., Letiembre, M., Celio, M. R., & Menoud, P. (2000). Morphology of perineuronal nets in tenascin-R and parvalbumin single and double knockout mice. *Brain Research*, *864*(1), 142–145. https://doi.org/10.1016/s0006-8993(00)02173-9

Haworth, K., Shu, K. K., Stokes, A., Morris, R., & Stoker, A. (1998). The expression of receptor tyrosine phosphatases is responsive to sciatic nerve crush. *Molecular and Cellular Neuroscience*, *12*(3), 93–104. https://doi.org/10.1006/mcne.1998.0707

Hayashi, Y., & Majewska, A. K. (2005). Dendritic spine geometry: functional implication and regulation. *Neuron*, *46*(4), 529–532. https://doi.org/10.1016/j.neuron.2005.05.006

Hensch, T. K. (2004). Critical period regulation. *Annual Review of Neuroscience*, *27*, 549–579. https://doi.org/10.1146/annurev.neuro.27.070203.144327

Hensch, T. K. (2005). Critical period mechanisms in developing visual cortex. *Current Topics in Developmental Biology*, *69*, 215–237. https://doi.org/10.1016/S0070-2153(05)69008-4

Hensch, T. K., & Quinlan, E. M. (2018). Critical periods in amblyopia. *Visual Neuroscience*, *35*, E014. https://doi.org/10.1017/S0952523817000219

Higashi, K., Takeuchi, Y., Mukuno, A., Tomitori, H., Miya, M., Linhardt, R. J., & Toida, T. (2015). Composition of glycosaminoglycans in elasmobranchs including several deep-sea sharks: identification of chondroitin/dermatan sulfate from the dried fins of Isurus oxyrinchus and Prionace glauca. *PloS One*, *10*(3), e0120860. https://doi.org/10.1371/journal.pone.0120860

Hirschberg, C. B., Robbins, P. W., & Abeijon, C. (1998). Transporters of Nucleotide Sugars, ATP, And Nucleotide Sulfate In The Endoplasmic Reticulum And Golgi Apparatus. Annual Review of Biochemistry, 67(1), 49–69. https://doi.org/10.1146/annurev.biochem.67.1.49

Hook, A. L., Hogwood, J., Gray, E., Mulloy, B., & Merry, C. L. R. (2021). High sensitivity analysis of nanogram quantities of glycosaminoglycans using ToF-SIMS. Communications Chemistry, 4(1), 67. https://doi.org/10.1038/s42004-021-00506-1

Hooks, B. M., & Chen, C. (2020). Circuitry underlying experience-dependent plasticity in the mouse visual system. *Neuron*, *106*(1), 21–36. https://doi.org/10.1016/j.neuron.2020.01.031

Hosseini, S. M., Alizadeh, A., Shahsavani, N., Chopek, J., Ahlfors, J.-E., & Karimi-Abdolrezaee, S. (2022). Suppressing CSPG/LAR/PTPσ axis facilitates neuronal replacement and synaptogenesis by human

neural precursor grafts and improves recovery after spinal cord injury. *The Journal of Neuroscience*, *42*(15), 3096–3121.

Huang, L., Zhou, H., Chen, K., Chen, X., & Yang, G. (2020). Learning-Dependent Dendritic Spine Plasticity Is Reduced in the Aged Mouse Cortex. *Frontiers in Neural Circuits*, *14*. https://doi.org/10.3389/fncir.2020.581435

Huang, W.-C., Kuo, W.-C., Cherng, J.-H., Hsu, S.-H., Chen, P.-R., Huang, S.-H., Huang, M.-C., Liu, J.-C., & Cheng, H. (2006). Chondroitinase ABC promotes axonal re-growth and behavior recovery in spinal cord injury. *Biochemical and Biophysical Research Communications*, *349*(3), 963–968. https://doi.org/10.1016/j.bbrc.2006.08.136

Hübener, M., & Bonhoeffer, T. (2014). Neuronal plasticity: beyond the critical period. *Cell*, *159*(4), 727–737. https://doi.org/10.1016/j.cell.2014.10.035

Hughes, E. G., Elmariah, S. B., & Balice-Gordon, R. J. (2010). Astrocyte secreted proteins selectively increase hippocampal GABAergic axon length, branching, and synaptogenesis. *Molecular and Cellular Neuroscience*, *43*(1), 136–145. https://doi.org/10.1016/j.mcn.2009.10.004

Hughes, H., Morgan, C., Brunyak, E., Barranco, K., Cohen, E., Edmunds, T., & Lee, K. (2009). A multi-tiered analytical approach for the analysis and quantitation of high-molecular-weight aggregates in a recombinant therapeutic glycoprotein. *The AAPS Journal*, *11*(2), 335–341. https://doi.org/10.1208/s12248-009-9108-1

Hu, H., Gan, J., & Jonas, P. (2014). Interneurons. fast-spiking, parvalbumin^{+} GABAergic interneurons: from cellular design to microcircuit function. *Science (New York, N.Y.)*, *345*(6196), 1255263. https://doi.org/10.1126/science.1255263

Hussein, R. K., Mencio, C. P., Katagiri, Y., Brake, A. M., & Geller, H. M. (2020). Role of chondroitin sulfation following spinal cord injury. *Frontiers in Cellular Neuroscience*, *14*, 208. https://doi.org/10.3389/fncel.2020.00208

Hutsler, J. J., & Zhang, H. (2010). Increased dendritic spine densities on cortical projection neurons in autism spectrum disorders. *Brain Research*, *1309*, 83–94. https://doi.org/10.1016/j.brainres.2009.09.120

Hylin, M. J., Orsi, S. A., Moore, A. N., & Dash, P. K. (2013). Disruption of the perineuronal net in the hippocampus or medial prefrontal cortex impairs fear conditioning. *Learning & Memory (Cold Spring Harbor, N.Y.)*, *20*(5), 267–273. https://doi.org/10.1101/lm.030197.112

Irvine, S. F., & Kwok, J. C. F. (2018). Perineuronal Nets in Spinal Motoneurones: Chondroitin Sulphate Proteoglycan around Alpha Motoneurones. *International Journal of Molecular Sciences*, *19*(4). https://doi.org/10.3390/ijms19041172

Itoh, H., Tokumoto, K., Kaji, T., Paudel, A., Panthee, S., Hamamoto, H., Sekimizu, K., & Inoue, M. (2019). Development of a high-throughput strategy for discovery of potent analogues of antibiotic lysocin E. *Nature Communications*, *10*(1), 2992. https://doi.org/10.1038/s41467-019-10754-4

Jackson, P. (1991). Polyacrylamide gel electrophoresis of reducing saccharides labeled with the fluorophore 2-aminoacridone: subpicomolar detection using an imaging system based on a cooled charge-coupled device. *Analytical Biochemistry*, *196*(2), 238–244. https://doi.org/10.1016/0003-2697(91)90460-b

Jackson, P. (1996). The analysis of fluorophore-labeled carbohydrates by polyacrylamide gel electrophoresis. *Molecular Biotechnology*, *5*(2), 101–123. https://doi.org/10.1007/BF02789060

Jokela, T. A., Jauhiainen, M., Auriola, S., Kauhanen, M., Tiihonen, R., Tammi, M. I., & Tammi, R. H. (2008). Mannose inhibits hyaluronan synthesis by down-regulation of the cellular pool of UDP-N-acetylhexosamines. *Journal of Biological Chemistry*, *283*(12), 7666–7673. https://doi.org/10.1074/jbc.M706001200

Kakizaki, I., Kojima, K., Takagaki, K., Endo, M., Kannagi, R., Ito, M., Maruo, Y., Sato, H., Yasuda, T., Mita, S., Kimata, K., & Itano, N. (2004). A novel mechanism for the inhibition of hyaluronan biosynthesis by 4-methylumbelliferone. *Journal of Biological Chemistry*, *279*(32), 33281–33289. https://doi.org/10.1074/jbc.M405918200

Kaneko, S., Iwanami, A., Nakamura, M., Kishino, A., Kikuchi, K., Shibata, S., Okano, H. J., Ikegami, T., Moriya, A., Konishi, O., Nakayama, C., Kumagai, K., Kimura, T., Sato, Y., Goshima, Y., Taniguchi, M., Ito, M., He, Z., Toyama, Y., & Okano, H. (2006). A selective Sema3A inhibitor enhances regenerative responses and functional recovery of the injured spinal cord. *Nature Medicine*, *12*(12), 1380–1389. https://doi.org/10.1038/nm1505

Karin, M., & Delhase, M. (2000). The I kappa B kinase (IKK) and NF-kappa B: key elements of proinflammatory signalling. *Seminars in Immunology*, *12*(1), 85–98. https://doi.org/10.1006/smim.2000.0210

Karumbaiah, L., Enam, S. F., Brown, A. C., Saxena, T., Betancur, M. I., Barker, T. H., & Bellamkonda, R. v. (2015). Chondroitin sulfate glycosaminoglycan hydrogels create endogenous niches for neural stem cells. *Bioconjugate Chemistry*, *26*(12), 2336–2349. https://doi.org/10.1021/acs.bioconjchem.5b00397

Kastellakis, G., Cai, D. J., Mednick, S. C., Silva, A. J., & Poirazi, P. (2015). Synaptic clustering within dendrites: an emerging theory of memory formation. *Progress in Neurobiology*, *126*, 19–35. https://doi.org/10.1016/j.pneurobio.2014.12.002

Katoh-Semba, R., Asano, T., Ueda, H., Morishita, R., Takeuchi, I. K., Inaguma, Y., & Kato, K. (2002). Riluzole enhances expression of brain-derived neurotrophic factor with consequent proliferation of granule precursor cells in the rat hippocampus. *FASEB Journal : Official Publication of the Federation of American Societies for Experimental Biology*, *16*(10), 1328–1330. https://doi.org/10.1096/fj.02-0143fje

Kempermann, G., Kuhn, H. G., & Gage, F. H. (1997). More hippocampal neurons in adult mice living in an enriched environment. *Nature*, *386*(6624), 493–495. https://doi.org/10.1038/386493a0

Kempermann, G., Song, H., & Gage, F. H. (2015). Neurogenesis in the Adult Hippocampus. *Cold Spring Harbor Perspectives in Biology*, *7*(9), a018812. https://doi.org/10.1101/cshperspect.a018812

Keough, M. B., Rogers, J. A., Zhang, P., Jensen, S. K., Stephenson, E. L., Chen, T., Hurlbert, M. G., Lau, L. W., Rawji, K. S., Plemel, J. R., Koch, M., Ling, C.-C., & Yong, V. W. (2016). An inhibitor of chondroitin sulfate proteoglycan synthesis promotes central nervous system remyelination. *Nature Communications*, *7*(1), 11312. https://doi.org/10.1038/ncomms11312

Kim, M., Jeong, Y., & Chang, Y.-C. (2015). Extracellular matrix protein reelin regulate dendritic spine density through CaMKIIβ. *Neuroscience Letters*, *599*, 97–101. https://doi.org/10.1016/j.neulet.2015.05.033

Kim, S.-E., Ko, I.-G., Kim, B.-K., Shin, M.-S., Cho, S., Kim, C.-J., Kim, S.-H., Baek, S.-S., Lee, E.-K., & Jee, Y.-S. (2010). Treadmill exercise prevents aging-induced failure of memory through an increase in neurogenesis and suppression of apoptosis in rat hippocampus. *Experimental Gerontology*, *45*(5), 357–365. https://doi.org/10.1016/j.exger.2010.02.005

Kitagawa, H., Tsutsumi, K., Tone, Y., & Sugahara, K. (1997). Developmental regulation of the sulfation profile of chondroitin sulfate chains in the chicken embryo brain. *The Journal of Biological Chemistry*, *272*(50), 31377–31381. https://doi.org/10.1074/jbc.272.50.31377

Kleindienst, T., Winnubst, J., Roth-Alpermann, C., Bonhoeffer, T., & Lohmann, C. (2011). Activity-dependent clustering of functional synaptic inputs on developing hippocampal dendrites. *Neuron*, *72*(6), 1012–1024. https://doi.org/10.1016/j.neuron.2011.10.015

Klueva, J., Gundelfinger, E. D., Frischknecht, R. R., & Heine, M. (2014). Intracellular Ca^{2+} and not the extracellular matrix determines surface dynamics of AMPA-type glutamate receptors on aspiny neurons. *Philosophical Transactions of the Royal Society of London. Series B, Biological Sciences*, *369*(1654), 20130605. https://doi.org/10.1098/rstb.2013.0605

Kochlamazashvili, G., Henneberger, C., Bukalo, O., Dvoretskova, E., Senkov, O., Lievens, P. M.-J., Westenbroek, R., Engel, A. K., Catterall, W. A., Rusakov, D. A., Schachner, M., & Dityatev, A. (2010). The extracellular matrix molecule hyaluronic acid regulates hippocampal synaptic plasticity by modulating postsynaptic L-type Ca(2+) channels. *Neuron*, *67*(1), 116–128. https://doi.org/10.1016/j.neuron.2010.05.030

Koh, C. H., Pronin, S., & Hughes, M. (2018). Chondroitinase ABC for neurological recovery after acute brain injury: systematic review and meta-analyses of preclinical studies. *Brain Injury*, *32*(6), 715–729. https://doi.org/10.1080/02699052.2018.1438665

Komitova, M., Mattsson, B., Johansson, B. B., & Eriksson, P. S. (2005). Enriched environment increases neural stem/progenitor cell proliferation and neurogenesis in the subventricular zone of stroke-lesioned adult rats. *Stroke*, *36*(6), 1278–1282. https://doi.org/10.1161/01.STR.0000166197.94147.59

Ksiazek, I., Burkhardt, C., Lin, S., Seddik, R., Maj, M., Bezakova, G., Jucker, M., Arber, S., Caroni, P., Sanes, J. R., Bettler, B., & Ruegg, M. A. (2007). Synapse loss in cortex of agrin-deficient mice after genetic rescue of perinatal death. *Journal of Neuroscience*, *27*(27), 7183–7195. https://doi.org/10.1523/JNEUROSCI.1609-07.2007

Kubaski, F., Osago, H., Mason, R. W., Yamaguchi, S., Kobayashi, H., Tsuchiya, M., Orii, T., & Tomatsu, S. (2017). Glycosaminoglycans detection methods: applications of mass spectrometry. *Molecular Genetics and Metabolism*, *120*(1–2), 67–77. https://doi.org/10.1016/j.ymgme.2016.09.005

Kudo, T., Takuwa, H., Takahashi, M., Urushihata, T., Shimojo, M., Sampei, K., Yamanaka, M., Tomita, Y., Sahara, N., Suhara, T., & Higuchi, M. (2023). Selective dysfunction of fast-spiking inhibitory interneurons and disruption of perineuronal nets in a tauopathy mouse model. IScience, 26(4), 106342. https://doi.org/10.1016/j.isci.2023.106342

Kuipers, H. F., Nagy, N., Ruppert, S. M., Sunkari, V. G., Marshall, P. L., Gebe, J. A., Ishak, H. D., Keswani, S. G., Bollyky, J., Frymoyer, A. R., Wight, T. N., Steinman, L., & Bollyky, P. L. (2016). The pharmacokinetics and dosing of oral 4-methylumbelliferone for inhibition of hyaluronan synthesis in mice. *Clinical and Experimental Immunology*, *185*(3), 372–381. https://doi.org/10.1111/cei.12815

Kultti, A., Pasonen-Seppänen, S., Jauhiainen, M., Rilla, K. J., Kärnä, R., Pyöriä, E., Tammi, R. H., & Tammi, M. I. (2009). 4-Methylumbelliferone inhibits hyaluronan synthesis by depletion of cellular UDP-glucuronic acid and downregulation of hyaluronan synthase 2 and 3. *Experimental Cell Research*, *315*(11), 1914–1923. https://doi.org/10.1016/j.yexcr.2009.03.002

Kuo, Y.-Z., Fang, W.-Y., Huang, C.-C., Tsai, S.-T., Wang, Y.-C., Yang, C.-L., & Wu, L.-W. (2017). Hyaluronan synthase 3 mediated oncogenic action through forming inter-regulation loop with tumor

necrosis factor alpha in oral cancer. *Oncotarget*, *8*(9), 15563–15583. https://doi.org/10.18632/oncotarget.14697

Kwok, J. C. F., Carulli, D., & Fawcett, J. W. (2010). In vitro modeling of perineuronal nets: hyaluronan synthase and link protein are necessary for their formation and integrity. *Journal of Neurochemistry*, no-no. https://doi.org/10.1111/j.1471-4159.2010.06878.x

Kwok, J. C. F., Dick, G., Wang, D., & Fawcett, J. W. (2011). Extracellular matrix and perineuronal nets in CNS repair. *Developmental Neurobiology*, *71*(11), 1073–1089. https://doi.org/10.1002/dneu.20974

Kwok, J. C. F., Foscarin, S., & Fawcett, J. W. (2015). *Perineuronal nets: a special structure in the central nervous system extracellular matrix* (pp. 23–32). https://doi.org/10.1007/978-1-4939-2083-9_3

Kwok, J. C. F., Warren, P., & Fawcett, J. W. (2012). Chondroitin sulfate: A key molecule in the brain matrix. *The International Journal of Biochemistry & Cell Biology*, *44*(4), 582–586. https://doi.org/10.1016/j.biocel.2012.01.004

Lamprecht, R., & LeDoux, J. (2004). Structural plasticity and memory. *Nature Reviews. Neuroscience*, *5*(1), 45–54. https://doi.org/10.1038/nrn1301

Lang, B. T., Cregg, J. M., DePaul, M. A., Tran, A. P., Xu, K., Dyck, S. M., Madalena, K. M., Brown, B. P., Weng, Y.-L., Li, S., Karimi-Abdolrezaee, S., Busch, S. A., Shen, Y., & Silver, J. (2015). Modulation of the proteoglycan receptor PTPσ promotes recovery after spinal cord injury. *Nature*, *518*(7539), 404–408. https://doi.org/10.1038/nature13974

Lawal, O., Ulloa Severino, F. P., & Eroglu, C. (2022). The role of astrocyte structural plasticity in regulating neural circuit function and behavior. *Glia*, *70*(8), 1467–1483. https://doi.org/10.1002/glia.24191

Leach, J. B., & Powell, E. M. (n.d.). *Extracellular Matrix*. http://www.springer.com/series/7657

Lee, H. H. C., Bernard, C., Ye, Z., Acampora, D., Simeone, A., Prochiantz, A., di Nardo, A. A., & Hensch, T. K. (2017). Genetic Otx2 mis-localization delays critical period plasticity across brain regions. *Molecular Psychiatry*, *22*(5), 680–688. https://doi.org/10.1038/mp.2017.1

Lee, S.-H., Kim, Y.-J., Lee, K.-M., Ryu, S., & Yoon, B.-W. (2007). Ischemic preconditioning enhances neurogenesis in the subventricular zone. *Neuroscience*, *146*(3), 1020–1031. https://doi.org/10.1016/j.neuroscience.2007.02.058

Lensjø, K. K., Lepperød, M. E., Dick, G., Hafting, T., & Fyhn, M. (2017). Removal of perineuronal nets unlocks juvenile plasticity through network mechanisms of decreased inhibition and increased gamma activity. *The Journal of Neuroscience*, *37*(5), 1269–1283. https://doi.org/10.1523/JNEUROSCI.2504-16.2016

Lesnikova, A., Casarotto, P. C., Fred, S. M., Voipio, M., Winkel, F., Steinzeig, A., Antila, H., Umemori, J., Biojone, C., & Castrén, E. (2021). Chondroitinase and antidepressants promote plasticity by releasing TRKB from dephosphorylating control of PTPσ in parvalbumin neurons. *The Journal of Neuroscience*, *41*(5), 972–980.

Lesnikova, A., Casarotto, P., Moliner, R., Fred, S. M., Biojone, C., & Castrén, E. (2021). Perineuronal net receptor PTPσ regulates retention of memories. *Frontiers in Synaptic Neuroscience*, *13*. https://doi.org/10.3389/fnsyn.2021.672475

Levelt, C. N., & Hübener, M. (2012). Critical-period plasticity in the visual cortex. *Annual Review of Neuroscience*, *35*, 309–330. https://doi.org/10.1146/annurev-neuro-061010-113813

Levy, A. D., Omar, M. H., & Koleske, A. J. (2014). Extracellular matrix control of dendritic spine and synapse structure and plasticity in adulthood. *Frontiers in Neuroanatomy*, *8*, 116. https://doi.org/10.3389/fnana.2014.00116

Lewis, D. A. (2009). Neuroplasticity of excitatory and inhibitory cortical circuits in schizophrenia. *Dialogues in Clinical Neuroscience*, *11*(3), 269–280. https://doi.org/10.31887/DCNS.2009.11.3/dalewis

Lewis, D. A., & González-Burgos, G. (2008). Neuroplasticity of neocortical circuits in schizophrenia. *Neuropsychopharmacology : Official Publication of the American College of Neuropsychopharmacology*, *33*(1), 141–165. https://doi.org/10.1038/sj.npp.1301563

Libovner, Y., Fariborzi, M., Tabba, D., Ozgur, A., Jafar, T., & Lur, G. (2020). Repeated exposure to multiple concurrent stresses induce circuit specific loss of inputs to the posterior parietal cortex. *The Journal of Neuroscience : The Official Journal of the Society for Neuroscience*, *40*(9), 1849–1861. https://doi.org/10.1523/JNEUROSCI.1838-19.2020

Li, M., Cui, Z., Niu, Y., Liu, B., Fan, W., Yu, D., & Deng, J. (2010). Synaptogenesis in the developing mouse visual cortex. *Brain Research Bulletin*, *81*(1), 107–113. https://doi.org/10.1016/j.brainresbull.2009.08.028

Lin, L., McCroskery, S., Ross, J. M., Chak, Y., Neuhuber, B., & Daniels, M. P. (2010). Induction of filopodia-like protrusions by transmembrane agrin: Role of agrin glycosaminoglycan chains and Rho-family GTPases. *Experimental Cell Research*, *316*(14), 2260–2277. https://doi.org/10.1016/j.yexcr.2010.05.006

Lin, R., Kwok, J. C. F., Crespo, D., & Fawcett, J. W. (2008). Chondroitinase ABC has a long-lasting effect on chondroitin sulphate glycosaminoglycan content in the injured rat brain. *Journal of Neurochemistry*, *104*(2), 400–408. https://doi.org/10.1111/j.1471-4159.2007.05066.x

Lin, R., Rosahl, T. W., Whiting, P. J., Fawcett, J. W., & Kwok, J. C. F. (2011). 6-Sulphated chondroitins have a positive influence on axonal regeneration. *PloS One*, *6*(7), e21499. https://doi.org/10.1371/journal.pone.0021499

Li, S., Wang, C., Wang, W., Dong, H., Hou, P., & Tang, Y. (2008). Chronic mild stress impairs cognition in mice: from brain homeostasis to behavior. *Life Sciences*, *82*(17–18), 934–942. https://doi.org/10.1016/j.lfs.2008.02.010

Liu, J., Andya, J. D., & Shire, S. J. (2006). A critical review of analytical ultracentrifugation and field flow fractionation methods for measuring protein aggregation. *The AAPS Journal*, *8*(3), E580-9. https://doi.org/10.1208/aapsj080367

Liu, L., Doray, B., & Kornfeld, S. (2018). Recycling of Golgi glycosyltransferases requires direct binding to coatomer. *Proceedings of the National Academy of Sciences of the United States of America*, *115*(36), 8984–8989. https://doi.org/10.1073/pnas.1810291115

Liu, Y., & Coughtrie, M. (2017). Revisiting the Latency of Uridine Diphosphate-Glucuronosyltransferases (UGTs)—How Does the Endoplasmic Reticulum Membrane Influence Their Function? Pharmaceutics, 9(3), 32.

Loers, G., Liao, Y., Hu, C., Xue, W., Shen, H., Zhao, W., & Schachner, M. (2019). Identification and characterization of synthetic chondroitin-4-sulfate binding peptides in neuronal functions. *Scientific Reports*, *9*(1), 1064. https://doi.org/10.1038/s41598-018-37685-2

Loh, S. H. Y., Francescut, L., Lingor, P., Bähr, M., & Nicotera, P. (2008). Identification of new kinase clusters required for neurite outgrowth and retraction by a loss-of-function RNA interference screen. *Cell Death and Differentiation*, *15*(2), 283–298. https://doi.org/10.1038/sj.cdd.4402258

Luo, F., Wang, J., Zhang, Z., You, Z., Bedolla, A., Okwubido-Williams, F., Huang, L. F., Silver, J., & Luo, Y. (2022). Inhibition of CSPG receptor PTPσ promotes migration of newly born neuroblasts, axonal sprouting, and recovery from stroke. *Cell Reports*, *40*(4), 111137. https://doi.org/10.1016/j.celrep.2022.111137

Lu, P., Takai, K., Weaver, V. M., & Werb, Z. (2011). Extracellular matrix degradation and remodeling in development and disease. *Cold Spring Harbor Perspectives in Biology*, *3*(12), a005058–a005058. https://doi.org/10.1101/cshperspect.a005058

Magee, J. C., & Grienberger, C. (2020). Synaptic Plasticity forms and functions. *Annual Review of Neuroscience*, *43*, 95–117. https://doi.org/10.1146/annurev-neuro-090919-022842

Massey, J. M., Hubscher, C. H., Wagoner, M. R., Decker, J. A., Amps, J., Silver, J., & Onifer, S. M. (2006). Chondroitinase ABC Digestion of the Perineuronal Net Promotes Functional Collateral Sprouting in the Cuneate Nucleus after Cervical Spinal Cord Injury. The Journal of Neuroscience, 26(16), 4406–4414. https://doi.org/10.1523/JNEUROSCI.5467-05.2006

McCroskery, S., Bailey, A., Lin, L., & Daniels, M. P. (2009). Transmembrane agrin regulates dendritic filopodia and synapse formation in mature hippocampal neuron cultures. *Neuroscience*, *163*(1), 168–179. https://doi.org/10.1016/j.neuroscience.2009.06.012

Mijalkov, M., Volpe, G., Fernaud-Espinosa, I., DeFelipe, J., Pereira, J. B., & Merino-Serrais, P. (2021). Dendritic spines are lost in clusters in Alzheimer's disease. *Scientific Reports*, *11*(1), 12350. https://doi.org/10.1038/s41598-021-91726-x

Mirzadeh, Z., Alonge, K. M., Cabrales, E., Herranz-Pérez, V., Scarlett, J. M., Brown, J. M., Hassouna, R., Matsen, M. E., Nguyen, H. T., Garcia-Verdugo, J. M., Zeltser, L. M., & Schwartz, M. W. (2019). Perineuronal net formation during the critical period for neuronal maturation in the hypothalamic arcuate nucleus. *Nature Metabolism*, *1*(2), 212–221. https://doi.org/10.1038/s42255-018-0029-0

Miyata, S., & Kitagawa, H. (2016). Chondroitin 6-sulfation regulates perineuronal net formation by controlling the stability of aggrecan. *Neural Plasticity*, *2016*, 1305801. https://doi.org/10.1155/2016/1305801

Miyata, S., Nadanaka, S., Igarashi, M., & Kitagawa, H. (2018). Structural Variation of Chondroitin Sulfate Chains Contributes to the Molecular Heterogeneity of Perineuronal Nets. Frontiers in Integrative Neuroscience, 12. https://doi.org/10.3389/fnint.2018.00003

Miyata, S., Nishimura, Y., Hayashi, N., & Oohira, A. (2005). Construction of perineuronal net-like structure by cortical neurons in culture. *Neuroscience*, *136*(1), 95–104. https://doi.org/10.1016/j.neuroscience.2005.07.031

Montolio, M., Messeguer, J., Masip, I., Guijarro, P., Gavin, R., Antonio del Río, J., Messeguer, A., & Soriano, E. (2009). A semaphorin 3a inhibitor blocks axonal chemorepulsion and enhances axon regeneration. *Chemistry & Biology*, *16*(7), 691–701. https://doi.org/10.1016/j.chembiol.2009.05.006

Moon, L. D., Asher, R. A., Rhodes, K. E., & Fawcett, J. W. (2001). Regeneration of CNS axons back to their target following treatment of adult rat brain with chondroitinase ABC. *Nature Neuroscience*, *4*(5), 465–466. https://doi.org/10.1038/87415

Morawski, M., Brückner, G., Arendt, T., & Matthews, R. T. (2012). Aggrecan: beyond cartilage and into the brain. *The International Journal of Biochemistry & Cell Biology*, *44*(5), 690–693. https://doi.org/10.1016/j.biocel.2012.01.010

Morawski, M., Brückner, M. K., Riederer, P., Brückner, G., & Arendt, T. (2004). Perineuronal nets potentially protect against oxidative stress. *Experimental Neurology*, *188*(2), 309–315. https://doi.org/10.1016/j.expneurol.2004.04.017

Morawski, M., Dityatev, A., Hartlage-Rübsamen, M., Blosa, M., Holzer, M., Flach, K., Pavlica, S., Dityateva, G., Grosche, J., Brückner, G., & Schachner, M. (2014). Tenascin-R promotes assembly of the extracellular matrix of perineuronal nets via clustering of aggrecan. *Philosophical Transactions of the Royal Society of London. Series B, Biological Sciences*, *369*(1654), 20140046. https://doi.org/10.1098/rstb.2014.0046

Nagai-Okatani, C., Nishigori, M., Sato, T., Minamino, N., Kaji, H., & Kuno, A. (2019). Wisteria floribunda agglutinin staining for the quantitative assessment of cardiac fibrogenic activity in a mouse model of dilated cardiomyopathy. *Laboratory Investigation; a Journal of Technical Methods and Pathology*, *99*(11), 1749–1765. https://doi.org/10.1038/s41374-019-0279-9

Nagase, H., Kudo, D., Suto, A., Yoshida, E., Suto, S., Negishi, M., Kakizaki, I., & Hakamada, K. (2017). 4-Methylumbelliferone suppresses hyaluronan synthesis and tumor progression in scid mice intra-abdominally inoculated with pancreatic cancer cells. *Pancreas*, *46*(2), 190–197. https://doi.org/10.1097/MPA.0000000000000741

Nägerl, U. V., Willig, K. I., Hein, B., Hell, S. W., & Bonhoeffer, T. (2008). Live-cell imaging of dendritic spines by STED microscopy. *Proceedings of the National Academy of Sciences*, *105*(48), 18982–18987. https://doi.org/10.1073/pnas.0810028105

Nagy, N., Gurevich, I., Kuipers, H. F., Ruppert, S. M., Marshall, P. L., Xie, B. J., Sun, W., Malkovskiy, A. v., Rajadas, J., Grandoch, M., Fischer, J. W., Frymoyer, A. R., Kaber, G., & Bollyky, P. L. (2019). 4-methylumbelliferyl glucuronide contributes to hyaluronan synthesis inhibition. *Journal of Biological Chemistry*, *294*(19), 7864–7877. https://doi.org/10.1074/jbc.RA118.006166

Nagy, N., Kuipers, H. F., Frymoyer, A. R., Ishak, H. D., Bollyky, J. B., Wight, T. N., & Bollyky, P. L. (2015). 4-methylumbelliferone treatment and hyaluronan inhibition as a therapeutic strategy in inflammation, autoimmunity, and cancer. *Frontiers in Immunology*, *6*, 123. https://doi.org/10.3389/fimmu.2015.00123

Nakamura, T., Takagaki, K., Shibata, S., Tanaka, K., Higuchi, T., & Endo, M. (1995). Hyaluronic-acid-deficient extracellular matrix induced by addition of 4-methylumbelliferone to the medium of cultured human skin fibroblasts. *Biochemical and Biophysical Research Communications*, *208*(2), 470–475. https://doi.org/10.1006/bbrc.1995.1362

National Center for Biotechnology Information. PubChem Compound Summary for CID 5280567, Hymecromone. https://pubchem.ncbi.nlm.nih.gov/compound/Hymecromone. Accessed Jan. 27, 2023.

Nikonenko, A., Schmidt, S., Skibo, G., Brückner, G., & Schachner, M. (2003). Tenascin-R-deficient mice show structural alterations of symmetric perisomatic synapses in the CA1 region of the hippocampus. *Journal of Comparative Neurology*, *456*(4), 338–349. https://doi.org/10.1002/cne.10537

Nojima, K., Miyazaki, H., Hori, T., Vargova, L., & Oohashi, T. (2021). Assessment of possible contributions of hyaluronan and proteoglycan binding link protein 4 to differential perineuronal net formation at the calyx of held. *Frontiers in Cell and Developmental Biology*, *9*, 730550. https://doi.org/10.3389/fcell.2021.730550

Nowicka, D., Soulsby, S., Skangiel-Kramska, J., & Glazewski, S. (2009). Parvalbumin-containing neurons, perineuronal nets and experience-dependent plasticity in murine barrel cortex. *European Journal of Neuroscience*, *30*(11), 2053–2063. https://doi.org/10.1111/j.1460-9568.2009.06996.x

Oberheim, N. A., Takano, T., Han, X., He, W., Lin, J. H. C., Wang, F., Xu, Q., Wyatt, J. D., Pilcher, W., Ojemann, J. G., Ransom, B. R., Goldman, S. A., & Nedergaard, M. (2009). Uniquely hominid features of adult human astrocytes. *Journal of Neuroscience*, *29*(10), 3276–3287. https://doi.org/10.1523/JNEUROSCI.4707-08.2009

Oberheim, N. A., Wang, X., Goldman, S., & Nedergaard, M. (2006). Astrocytic complexity distinguishes the human brain. *Trends in Neurosciences*, *29*(10), 547–553. https://doi.org/10.1016/j.tins.2006.08.004

Ohtake, Y., Saito, A., & Li, S. (2018). Diverse functions of protein tyrosine phosphatase σ in the nervous and immune systems. *Experimental Neurology*, *302*, 196–204. https://doi.org/10.1016/j.expneurol.2018.01.014

Ohtake, Y., Wong, D., Abdul-Muneer, P. M., Selzer, M. E., & Li, S. (2016). Two PTP receptors mediate CSPG inhibition by convergent and divergent signaling pathways in neurons. *Scientific Reports*, *6*(1), 37152. https://doi.org/10.1038/srep37152

Olson, A. K., Eadie, B. D., Ernst, C., & Christie, B. R. (2006). Environmental enrichment and voluntary exercise massively increase neurogenesis in the adult hippocampus via dissociable pathways. *Hippocampus*, *16*(3), 250–260. https://doi.org/10.1002/hipo.20157

Orlando, C., Ster, J., Gerber, U., Fawcett, J. W., & Raineteau, O. (2012). Perisynaptic chondroitin sulfate proteoglycans restrict structural plasticity in an integrin-dependent manner. *The Journal of Neuroscience : The Official Journal of the Society for Neuroscience*, *32*(50), 18009–18017, 18017a. https://doi.org/10.1523/JNEUROSCI.2406-12.2012

Osago, H., Shibata, T., Hara, N., Kuwata, S., Kono, M., Uchio, Y., & Tsuchiya, M. (2014). Quantitative analysis of glycosaminoglycans, chondroitin/dermatan sulfate, hyaluronic acid, heparan sulfate, and keratan sulfate by liquid chromatography–electrospray

Ouzzine, M., Gulberti, S., Ramalanjaona, N., Magdalou, J., & Fournel-Gigleux, S. (2014). The UDP-glucuronosyltransferases of the blood-brain barrier: their role in drug metabolism and detoxication. Frontiers in Cellular Neuroscience, 8, 349. https://doi.org/10.3389/fncel.2014.00349

Papakonstantinou, M. K., Pan, W.-R., le Roux, C. M., & Richardson, M. D. (2012). New approach to the study of intraosseous vasculature. ANZ Journal of Surgery, 82(10), 704–707. https://doi.org/10.1111/j.1445-2197.2012.06142.x

Papouin, T., Dunphy, J., Tolman, M., Foley, J. C., & Haydon, P. G. (2017). Astrocytic control of synaptic function. *Philosophical Transactions of the Royal Society B: Biological Sciences*, *372*(1715), 20160154. https://doi.org/10.1098/rstb.2016.0154

Parnavelas, J. G. (1978). *Influence of Stimulation on Cortical Development* (pp. 247–260). https://doi.org/10.1016/S0079-6123(08)61027-4

Patel, D. C., Tewari, B. P., Chaunsali, L., & Sontheimer, H. (2019). Neuron-glia interactions in the pathophysiology of epilepsy. Nature Reviews. Neuroscience, 20(5), 282–297. https://doi.org/10.1038/s41583-019-0126-4

Pearson, C. S., Mencio, C. P., Barber, A. C., Martin, K. R., & Geller, H. M. (2018). Identification of a critical sulfation in chondroitin that inhibits axonal regeneration. *ELife*, *7*. https://doi.org/10.7554/eLife.37139

Perez-Alvarez, A., Navarrete, M., Covelo, A., Martin, E. D., & Araque, A. (2014). structural and functional plasticity of astrocyte processes and dendritic spine interactions. *Journal of Neuroscience*, *34*(38), 12738–12744. https://doi.org/10.1523/JNEUROSCI.2401-14.2014

Pizzorusso, T., Medini, P., Berardi, N., Chierzi, S., Fawcett, J. W., & Maffei, L. (2002). Reactivation of ocular dominance plasticity in the adult visual cortex. *Science (New York, N.Y.)*, *298*(5596), 1248–1251. https://doi.org/10.1126/science.1072699

Pizzorusso, T., Medini, P., Landi, S., Baldini, S., Berardi, N., & Maffei, L. (2006). Structural and functional recovery from early monocular deprivation in adult rats. *Proceedings of the National Academy of Sciences of the United States of America*, *103*(22), 8517–8522. https://doi.org/10.1073/pnas.0602657103

Plantman, S. (2013). Proregenerative properties of ECM molecules. *BioMed Research International*, *2013*, 1–11. https://doi.org/10.1155/2013/981695

Prabhakar, V., Capila, I., Bosques, C. J., Pojasek, K., & Sasisekharan, R. (2005). Chondroitinase ABC I from Proteus vulgaris: cloning, recombinant expression and active site identification. *The Biochemical Journal*, *386*(Pt 1), 103–112. https://doi.org/10.1042/BJ20041222

Prabhakar, V., Raman, R., Capila, I., Bosques, C. J., Pojasek, K., & Sasisekharan, R. (2005). Biochemical characterization of the chondroitinase ABC I active site. *The Biochemical Journal*, *390*(Pt 2), 395–405. https://doi.org/10.1042/BJ20050532

Ramirez, A., & Arbuckle, M. R. (2016). Synaptic Plasticity: The role of learning and unlearning in addiction and beyond. *Biological Psychiatry*, *80*(9), e73–e75. https://doi.org/10.1016/j.biopsych.2016.09.002

Reichardt, L. F. (2006). Neurotrophin-regulated signalling pathways. *Philosophical Transactions of the Royal Society of London. Series B, Biological Sciences*, *361*(1473), 1545–1564. https://doi.org/10.1098/rstb.2006.1894

Reza-Zaldivar, E. E., Hernández-Sápiens, M. A., Minjarez, B., Gómez-Pinedo, U., Sánchez-González, V. J., Márquez-Aguirre, A. L., & Canales-Aguirre, A. A. (2020). Dendritic spine and synaptic plasticity in Alzheimer's disease: a focus on microRNA. *Frontiers in Cell and Developmental Biology*, *8*, 255. https://doi.org/10.3389/fcell.2020.00255

Rhodes, K. E., & Fawcett, J. W. (2004). Chondroitin sulphate proteoglycans: preventing plasticity or protecting the CNS? Journal of Anatomy, 204(1), 33–48. https://doi.org/10.1111/j.1469-7580.2004.00261.x

Richter, R. P., Baranova, N. S., Day, A. J., & Kwok, J. C. (2018). Glycosaminoglycans in extracellular matrix organisation: are concepts from soft matter physics key to understanding the formation of perineuronal nets? *Current Opinion in Structural Biology*, *50*, 65–74. https://doi.org/10.1016/j.sbi.2017.12.002

Rilla, K., Pasonen-Seppänen, S., Rieppo, J., Tammi, M., & Tammi, R. (2004). The hyaluronan synthesis inhibitor 4-methylumbelliferone prevents keratinocyte activation and epidermal hyperproliferation induced by epidermal growth factor. *Journal of Investigative Dermatology*, *123*(4), 708–714. https://doi.org/10.1111/j.0022-202X.2004.23409.x

Riss, T. L., Moravec, R. A., Niles, A. L., Duellman, S., Benink, H. A., Worzella, T. J., & Minor, L. (2004). *Cell Viability Assays*.

Ritok, A., Kiss, P., Zaher, A., Wolf, E., Ducza, L., Bacskai, T., Matesz, C., & Gaal, B. (2022). Distribution and postnatal development of chondroitin sulfate proteoglycans in the perineuronal nets of cholinergic

motoneurons innervating extraocular muscles. *Scientific Reports*, *12*(1), 21606. https://doi.org/10.1038/s41598-022-25692-3

Romberg, C., Yang, S., Melani, R., Andrews, M. R., Horner, A. E., Spillantini, M. G., Bussey, T. J., Fawcett, J. W., Pizzorusso, T., & Saksida, L. M. (2013). Depletion of perineuronal nets enhances recognition memory and long-term depression in the perirhinal cortex. *The Journal of Neuroscience : The Official Journal of the Society for Neuroscience*, *33*(16), 7057–7065. https://doi.org/10.1523/JNEUROSCI.6267-11.2013

Rowlands, D., Lensjø, K. K., Dinh, T., Yang, S., Andrews, M. R., Hafting, T., Fyhn, M., Fawcett, J. W., & Dick, G. (2018). Aggrecan directs extracellular matrix-mediated neuronal plasticity. *The Journal of Neuroscience : The Official Journal of the Society for Neuroscience*, *38*(47), 10102–10113. https://doi.org/10.1523/JNEUROSCI.1122-18.2018

Ruhaak, L. R., Zauner, G., Huhn, C., Bruggink, C., Deelder, A. M., & Wuhrer, M. (2010). Glycan labeling strategies and their use in identification and quantification. *Analytical and Bioanalytical Chemistry*, *397*(8), 3457–3481. https://doi.org/10.1007/s00216-010-3532-z

Scharfman, H., Goodman, J., Macleod, A., Phani, S., Antonelli, C., & Croll, S. (2005). Increased neurogenesis and the ectopic granule cells after intrahippocampal BDNF infusion in adult rats. *Experimental Neurology*, *192*(2), 348–356. https://doi.org/10.1016/j.expneurol.2004.11.016

Schmalfeldt, M., Bandtlow, C. E., Dours-Zimmermann, M. T., Winterhalter, K. H., & Zimmermann, D. R. (2000). Brain derived versican V2 is a potent inhibitor of axonal growth. *Journal of Cell Science*, *113 (Pt 5)*, 807–816. https://doi.org/10.1242/jcs.113.5.807

Schweitzer, B., Singh, J., Fejtova, A., Groc, L., Heine, M., & Frischknecht, R. (2017). Hyaluronic acid based extracellular matrix regulates surface expression of GluN2B containing NMDA receptors. *Scientific Reports*, *7*(1), 10991. https://doi.org/10.1038/s41598-017-07003-3

Sharma, K., Selzer, M. E., & Li, S. (2012). Scar-mediated inhibition and CSPG receptors in the CNS. *Experimental Neurology*, *237*(2), 370–378. https://doi.org/10.1016/j.expneurol.2012.07.009

Shen, Y., Tenney, A. P., Busch, S. A., Horn, K. P., Cuascut, F. X., Liu, K., He, Z., Silver, J., & Flanagan, J. G. (2009). PTPsigma is a receptor for chondroitin sulfate proteoglycan, an inhibitor of neural regeneration. *Science (New York, N.Y.)*, *326*(5952), 592–596. https://doi.org/10.1126/science.1178310

Shestakova, A., Zolov, S., & Lupashin, V. (2006). COG complex-mediated recycling of golgi glycosyltransferases is essential for normal protein glycosylation. *Traffic*, *7*(2), 191–204. https://doi.org/10.1111/j.1600-0854.2005.00376.x

Shiomi, T., Lemaître, V., D'Armiento, J., & Okada, Y. (2010). Matrix metalloproteinases, a disintegrin and metalloproteinases, and a disintegrin and metalloproteinases with thrombospondin motifs in non-neoplastic diseases. *Pathology International*, *60*(7), 477–496. https://doi.org/10.1111/j.1440-1827.2010.02547.x

Siebert, J. R., Conta Steencken, A., & Osterhout, D. J. (2014). Chondroitin sulfate proteoglycans in the nervous system: inhibitors to repair. *BioMed Research International*, *2014*, 845323. https://doi.org/10.1155/2014/845323

Siegle, J. H., Ledochowitsch, P., Jia, X., Millman, D. J., Ocker, G. K., Caldejon, S., Casal, L., Cho, A., Denman, D. J., Durand, S., Groblewski, P. A., Heller, G., Kato, I., Kivikas, S., Lecoq, J., Nayan, C., Ngo, K., Nicovich, P. R., North, K., … de Vries, S. E. (2021). Reconciling functional differences in populations of neurons recorded with two-photon imaging and electrophysiology. ELife, 10. https://doi.org/10.7554/eLife.69068

Sikes, K. J., Renner, K., Li, J., Grande-Allen, K. J., Connell, J. P., Cali, V., Midura, R. J., Sandy, J. D., Plaas, A., & Wang, V. M. (2018). Knockout of hyaluronan synthase 1, but not 3, impairs formation of the retrocalcaneal bursa. Journal of Orthopaedic Research®, 36(10), 2622–2632. https://doi.org/10.1002/jor.24027

Silbert, J. E., & Sugumaran, G. (2002). Biosynthesis of chondroitin/dermatan Sulfate. *IUBMB Life (International Union of Biochemistry and Molecular Biology: Life)*, *54*(4), 177–186. https://doi.org/10.1080/15216540214923

Simonetti, M., Paldy, E., Njoo, C., Bali, K. K., Worzfeld, T., Pitzer, C., Kuner, T., Offermanns, S., Mauceri, D., & Kuner, R. (2021). The impact of Semaphorin 4C/Plexin-B2 signaling on fear memory via remodeling of neuronal and synaptic morphology. *Molecular Psychiatry*, *26*(4), 1376–1398. https://doi.org/10.1038/s41380-019-0491-4

Skupien, A., Konopka, A., Trzaskoma, P., Labus, J., Gorlewicz, A., Swiech, L., Babraj, M., Dolezyczek, H., Figiel, I., Ponimaskin, E., Wlodarczyk, J., Jaworski, J., Wilczynski, G. M., & Dzwonek, J. (2014). CD44 regulates dendrite morphogenesis through Src tyrosine kinase-dependent positioning of the Golgi. *Journal of Cell Science*, *127*(Pt 23), 5038–5051. https://doi.org/10.1242/jcs.154542

Snow, D. M., Brown, E. M., & Letourneau, P. C. (1996). Growth cone behavior in the presence of soluble chondroitin sulfate proteoglycan (CSPG), compared to behavior on CSPG bound to laminin or fibronectin. *International Journal of Developmental Neuroscience : The Official Journal of the International Society for Developmental Neuroscience*, *14*(3), 331–349. https://doi.org/10.1016/0736-5748(96)00017-2

Song, I., & Dityatev, A. (2018). Crosstalk between glia, extracellular matrix and neurons. Brain Research Bulletin, 136, 101–108. https://doi.org/10.1016/j.brainresbull.2017.03.003

Song, J., M. Christian, K., Ming, G., & Song, H. (2012). Modification of hippocampal circuitry by adult neurogenesis. *Developmental Neurobiology*, *72*(7), 1032–1043. https://doi.org/10.1002/dneu.22014

Sorg, B. A., Berretta, S., Blacktop, J. M., Fawcett, J. W., Kitagawa, H., Kwok, J. C. F., & Miquel, M. (2016). Casting a wide net: role of perineuronal nets in neural plasticity. *The Journal of Neuroscience : The Official Journal of the Society for Neuroscience*, *36*(45), 11459–11468. https://doi.org/10.1523/JNEUROSCI.2351-16.2016

Sosicka, P., Bazan, B., Maszczak-Seneczko, D., Shauchuk, Y., Olczak, T., & Olczak, M. (2019). SLC35A5 Protein—A golgi complex member with putative nucleotide sugar transport activity. *International Journal of Molecular Sciences*, *20*(2), 276. https://doi.org/10.3390/ijms20020276

Spatazza, J., Lee, H. H. C., Di Nardo, A. A., Tibaldi, L., Joliot, A., Hensch, T. K., & Prochiantz, A. (2013). Choroid-plexus-derived Otx2 homeoprotein constrains adult cortical plasticity. *Cell Reports*, *3*(6), 1815–1823. https://doi.org/10.1016/j.celrep.2013.05.014

Srimasorn, S., Souter, L., Green, D. E., Djerbal, L., Goodenough, A., Duncan, J. A., Roberts, A. R. E., Zhang, X., Débarre, D., DeAngelis, P. L., Kwok, J. C. F., & Richter, R. P. (2022). A quartz crystal microbalance method to quantify the size of hyaluronan and other glycosaminoglycans on surfaces. *Scientific Reports*, *12*(1), 10980.

Starkey, M. L., Bartus, K., Barritt, A. W., & Bradbury, E. J. (2012). Chondroitinase ABC promotes compensatory sprouting of the intact corticospinal tract and recovery of forelimb function following unilateral pyramidotomy in adult mice. *The European Journal of Neuroscience*, *36*(12), 3665–3678. https://doi.org/10.1111/ejn.12017

Štěpánková, K., Mareková, D., Kubášová, K., Sedláček, R., Turnovcová, K., Vacková, I., Kubinová, Š., Makovický, P., Petrovičová, M., Kwok, J. C. F., Jendelová, P., & Machová Urdzíková, L. (2023). 4-

Methylumbeliferone Treatment at a Dose of 1.2 g/kg/Day Is Safe for Long-Term Usage in Rats. International Journal of Molecular Sciences, 24(4), 3799. https://doi.org/10.3390/ijms24043799

Südhof, T. C. (2021). The cell biology of synapse formation. *The Journal of Cell Biology*, *220*(7). https://doi.org/10.1083/jcb.202103052

Sugiyama, S., di Nardo, A. A., Aizawa, S., Matsuo, I., Volovitch, M., Prochiantz, A., & Hensch, T. K. (2008). Experience-dependent transfer of Otx2 homeoprotein into the visual cortex activates postnatal plasticity. *Cell*, *134*(3), 508–520. https://doi.org/10.1016/j.cell.2008.05.054

Sukowati, C. H. C., Anfuso, B., Fiore, E., Ie, S. I., Raseni, A., Vascotto, F., Avellini, C., Mazzolini, G., & Tiribelli, C. (2019). Hyaluronic acid inhibition by 4-methylumbelliferone reduces the expression of cancer stem cells markers during hepatocarcinogenesis. *Scientific Reports*, *9*(1), 4026. https://doi.org/10.1038/s41598-019-40436-6

Suttkus, A., Rohn, S., Jäger, C., Arendt, T., & Morawski, M. (2012). Neuroprotection against iron-induced cell death by perineuronal nets - an in vivo analysis of oxidative stress. *American Journal of Neurodegenerative Disease*, *1*(2), 122–129.

Suttkus, A., Rohn, S., Weigel, S., Glöckner, P., Arendt, T., & Morawski, M. (2014). Aggrecan, link protein and tenascin-R are essential components of the perineuronal net to protect neurons against iron-induced oxidative stress. *Cell Death & Disease*, *5*(3), e1119. https://doi.org/10.1038/cddis.2014.25

Su, W., Foster, S. C., Xing, R., Feistel, K., Olsen, R. H. J., Acevedo, S. F., Raber, J., & Sherman, L. S. (2017). CD44 transmembrane receptor and hyaluronan regulate adult hippocampal neural stem cell quiescence and differentiation. *Journal of Biological Chemistry*, *292*(11), 4434–4445. https://doi.org/10.1074/jbc.M116.774109

Swann, J. W., Al-Noori, S., Jiang, M., & Lee, C. L. (2000). Spine loss and other dendritic abnormalities in epilepsy. *Hippocampus*, *10*(5), 617–625. https://doi.org/10.1002/1098-1063(2000)10:5<617::aid-hipo13>3.0.co;2-r

Takahashi, H., & Craig, A. M. (2013). Protein tyrosine phosphatases PTPδ, PTPσ, and LAR: presynaptic hubs for synapse organization. *Trends in Neurosciences*, *36*(9), 522–534. https://doi.org/10.1016/j.tins.2013.06.002

Taliaz, D., Stall, N., Dar, D. E., & Zangen, A. (2010). Knockdown of brain-derived neurotrophic factor in specific brain sites precipitates behaviors associated with depression and reduces neurogenesis. *Molecular Psychiatry*, *15*(1), 80–92. https://doi.org/10.1038/mp.2009.67

Toda, T., Parylak, S. L., Linker, S. B., & Gage, F. H. (2019). The role of adult hippocampal neurogenesis in brain health and disease. *Molecular Psychiatry*, *24*(1), 67–87. https://doi.org/10.1038/s41380-018-0036-2

Tonchev, A. B. (2011). Brain ischemia, neurogenesis, and neurotrophic receptor expression in primates. *Archives Italiennes de Biologie*, *149*(2), 225–231. https://doi.org/10.4449/aib.v149i2.1368

Tukey, R. H., & Strassburg, C. P. (2000). Human UDP-Glucuronosyltransferases: metabolism, expression, and disease. *Annual Review of Pharmacology and Toxicology*, *40*(1), 581–616. https://doi.org/10.1146/annurev.pharmtox.40.1.581

Ueno, H., Fujii, K., Suemitsu, S., Murakami, S., Kitamura, N., Wani, K., Aoki, S., Okamoto, M., Ishihara, T., & Takao, K. (2018). Expression of aggrecan components in perineuronal nets in the mouse cerebral cortex. *IBRO Reports*, *4*, 22–37. https://doi.org/10.1016/j.ibror.2018.01.002

Umemori, J., Winkel, F., Didio, G., Llach Pou, M., & Castrén, E. (2018). Induced juvenile-like plasticity in the adult brain as a mechanism of antidepressants. *Psychiatry and Clinical Neurosciences*, *72*(9), 633–653. https://doi.org/10.1111/pcn.12683

Uyama, T., Kitagawa, H., & Sugahara, K. (2007). Biosynthesis of Glycosaminoglycans and Proteoglycans. In Comprehensive Glycoscience (pp. 79–104). Elsevier. https://doi.org/10.1016/B978-044451967-2/00036-2

Valero, J., España, J., Parra-Damas, A., Martín, E., Rodríguez-Álvarez, J., & Saura, C. A. (2011). Short-term environmental enrichment rescues adult neurogenesis and memory deficits in APP(Sw,Ind) transgenic mice. *PloS One*, *6*(2), e16832. https://doi.org/10.1371/journal.pone.0016832

Valverde, F. (1971). Rate and extent of recovery from dark rearing in the visual cortex of the mouse. *Brain Research*, *33*(1), 1–11. https://doi.org/10.1016/0006-8993(71)90302-7

Van't Spijker, H. M., & Kwok, J. C. F. (2017). A sweet talk: the molecular systems of perineuronal nets in controlling neuronal communication. *Frontiers in Integrative Neuroscience*, *11*, 33. https://doi.org/10.3389/fnint.2017.00033

Van't Spijker, H. M., Rowlands, D., Rossier, J., Haenzi, B., Fawcett, J. W., & Kwok, J. C. F. (2019). Neuronal pentraxin 2 binds pnns and enhances PNN formation. *Neural Plasticity*, *2019*, 1–13. https://doi.org/10.1155/2019/6804575

Vigetti, D., Deleonibus, S., Moretto, P., Karousou, E., Viola, M., Bartolini, B., Hascall, V. C., Tammi, M., de Luca, G., & Passi, A. (2012). Role of UDP-N-acetylglucosamine (GlcNAc) and O-GlcNAcylation of hyaluronan synthase 2 in the control of chondroitin sulfate and hyaluronan synthesis. *The Journal of Biological Chemistry*, *287*(42), 35544–35555. https://doi.org/10.1074/jbc.M112.402347

Vigetti, D., Rizzi, M., Viola, M., Karousou, E., Genasetti, A., Clerici, M., Bartolini, B., Hascall, V. C., de Luca, G., & Passi, A. (2009). The effects of 4-methylumbelliferone on hyaluronan synthesis, MMP2 activity, proliferation, and motility of human aortic smooth muscle cells. *Glycobiology*, *19*(5), 537–546. https://doi.org/10.1093/glycob/cwp022

Vo, T., Carulli, D., Ehlert, E. M. E., Kwok, J. C. F., Dick, G., Mecollari, V., Moloney, E. B., Neufeld, G., de Winter, F., Fawcett, J. W., & Verhaagen, J. (2013). The chemorepulsive axon guidance protein semaphorin3A is a constituent of perineuronal nets in the adult rodent brain. *Molecular and Cellular Neuroscience*, *56*, 186–200. https://doi.org/10.1016/j.mcn.2013.04.009

Wang, D., & Fawcett, J. (2012). The perineuronal net and the control of CNS plasticity. *Cell and Tissue Research*, *349*(1), 147–160. https://doi.org/10.1007/s00441-012-1375-y

Wang, H., Katagiri, Y., McCann, T. E., Unsworth, E., Goldsmith, P., Yu, Z.-X., Tan, F., Santiago, L., Mills, E. M., Wang, Y., Symes, A. J., & Geller, H. M. (2008). Chondroitin-4-sulfation negatively regulates axonal guidance and growth. *Journal of Cell Science*, *121*(Pt 18), 3083–3091. https://doi.org/10.1242/jcs.032649

Wang, L., Chang, X., She, L., Xu, D., Huang, W., & Poo, M. (2015). Autocrine action of bdnf on dendrite development of adult-born hippocampal neurons. *The Journal of Neuroscience*, *35*(22), 8384–8393. https://doi.org/10.1523/JNEUROSCI.4682-14.2015

Wang, S., Zhen, L., Liu, Z., Ai, Q., Ji, Y., Du, G., Wang, Y., & Bu, Y. (2015). Identification and analysis of the promoter region of the human HAS3 gene. *Biochemical and Biophysical Research Communications*, *460*(4), 1008–1014. https://doi.org/10.1016/j.bbrc.2015.03.142

Wang, X., Balaji, S., Steen, E. H., Blum, A. J., Li, H., Chan, C. K., Manson, S. R., Lu, T. C., Rae, M. M., Austin, P. F., Wight, T. N., Bollyky, P. L., Cheng, J., & Keswani, S. G. (2020). High-molecular

weight hyaluronan attenuates tubulointerstitial scarring in kidney injury. *JCI Insight*, *5*(12). https://doi.org/10.1172/jci.insight.136345

Warren, P. M., Steiger, S. C., Dick, T. E., MacFarlane, P. M., Alilain, W. J., & Silver, J. (2018). Rapid and robust restoration of breathing long after spinal cord injury. *Nature Communications*, *9*(1), 4843. https://doi.org/10.1038/s41467-018-06937-0

Weber, P., Bartsch, U., Rasband, M. N., Czaniera, R., Lang, Y., Bluethmann, H., Margolis, R. U., Levinson, S. R., Shrager, P., Montag, D., & Schachner, M. (1999). Mice deficient for tenascin-R display alterations of the extracellular matrix and decreased axonal conduction velocities in the CNS. *The Journal of Neuroscience*, *19*(11), 4245–4262. https://doi.org/10.1523/JNEUROSCI.19-11-04245.1999

Weissmiller, A. M., & Wu, C. (2012). Current advances in using neurotrophic factors to treat neurodegenerative disorders. *Translational Neurodegeneration*, *1*(1), 14. https://doi.org/10.1186/2047-9158-1-14

Wei, Z., Lin, B.-J., Chen, T.-W., Daie, K., Svoboda, K., & Druckmann, S. (2020). A comparison of neuronal population dynamics measured with calcium imaging and electrophysiology. PLOS Computational Biology, 16(9), e1008198. https://doi.org/10.1371/journal.pcbi.1008198

Welker, R. W. (2012). Size Analysis and Identification of Particles. In Developments in Surface Contamination and Cleaning (pp. 179–213). Elsevier. https://doi.org/10.1016/B978-1-4377-7883-0.00004-3

Wen, T. H., Binder, D. K., Ethell, I. M., & Razak, K. A. (2018). The Perineuronal "Safety" Net? Perineuronal net abnormalities in neurological disorders. *Frontiers in Molecular Neuroscience*, *11*, 270. https://doi.org/10.3389/fnmol.2018.00270

Wiesel, T. N. (1982). Postnatal development of the visual cortex and the influence of environment. *Nature*, *299*(5884), 583–591. https://doi.org/10.1038/299583a0

Wiesel, T. N., & Hubel, D. H. (1970). The period of susceptibility to the physiological effects of unilateral eye closure in kittens. *The Journal of Physiology*, *206*(2), 419–436. https://doi.org/10.1113/jphysiol.1970.sp009022

Wiesel, T. N., & Hubel, D. H. (1963). Single-cell responses in striate cortex of kittens deprived of vision in one eye. *Journal of Neurophysiology*, *26*(6), 1003–1017. https://doi.org/10.1152/jn.1963.26.6.1003

Willig, K. I., Steffens, H., Gregor, C., Herholt, A., Rossner, M. J., & Hell, S. W. (2014). Nanoscopy of Filamentous actin in cortical dendrites of a living mouse. *Biophysical Journal*, *106*(1), L01–L03. https://doi.org/10.1016/j.bpj.2013.11.1119

Willis, A., Pratt, J. A., & Morris, B. J. (2022). Enzymatic degradation of cortical perineuronal nets reverses GABAergic interneuron maturation. *Molecular Neurobiology*, *59*(5), 2874–2893. https://doi.org/10.1007/s12035-022-02772-z

Wright, K. T., Uchida, K., Bara, J. J., Roberts, S., el Masri, W., & Johnson, W. E. B. (2014). Spinal motor neurite outgrowth over glial scar inhibitors is enhanced by coculture with bone marrow stromal cells. *The Spine Journal*, *14*(8), 1722–1733. https://doi.org/10.1016/j.spinee.2014.01.021

Xiao, Z.-C., Ragsdale, D. S., Malhotra, J. D., Mattei, L. N., Braun, P. E., Schachner, M., & Isom, L. L. (1999). Tenascin-R is a functional modulator of sodium channel β subunits. *Journal of Biological Chemistry*, *274*(37), 26511–26517. https://doi.org/10.1074/jbc.274.37.26511

Xu, B., Park, D., Ohtake, Y., Li, H., Hayat, U., Liu, J., Selzer, M. E., Longo, F. M., & Li, S. (2015). Role of CSPG receptor LAR phosphatase in restricting axon regeneration after CNS injury. *Neurobiology of Disease*, *73*, 36–48. https://doi.org/10.1016/j.nbd.2014.08.030

Xu, T., Yu, X., Perlik, A. J., Tobin, W. F., Zweig, J. A., Tennant, K., Jones, T., & Zuo, Y. (2009). Rapid formation and selective stabilization of synapses for enduring motor memories. *Nature*, *462*(7275), 915–919. https://doi.org/10.1038/nature08389

Yabuno, K., Morise, J., Kizuka, Y., Hashii, N., Kawasaki, N., Takahashi, S., Miyata, S., Izumikawa, T., Kitagawa, H., Takematsu, H., & Oka, S. (2015). A sulfated glycosaminoglycan linkage region is a novel type of human natural killer-1 (HNK-1) epitope expressed on aggrecan in perineuronal nets. *PLOS ONE*, *10*(12), e0144560. https://doi.org/10.1371/journal.pone.0144560

Yamada, J., Nadanaka, S., Kitagawa, H., Takeuchi, K., & Jinno, S. (2018). Increased synthesis of chondroitin sulfate proteoglycan promotes adult hippocampal neurogenesis in response to enriched environment. *The Journal of Neuroscience*, *38*(39), 8496–8513. https://doi.org/10.1523/JNEUROSCI.0632-18.2018

Yamashita, N., Jitsuki-Takahashi, A., Ogawara, M., Ohkubo, W., Araki, T., Hotta, C., Tamura, T., Hashimoto, S., Yabuki, T., Tsuji, T., Sasakura, Y., Okumura, H., Takaiwa, A., Koyama, C., Murakami, K., & Goshima, Y. (2015). Anti-Semaphorin 3A neutralization monoclonal antibody prevents sepsis development in lipopolysaccharide-treated mice. *International Immunology*, *27*(9), 459–466. https://doi.org/10.1093/intimm/dxv014

Yang, B., Chang, Y., Weyers, A. M., Sterner, E., & Linhardt, R. J. (2012). Disaccharide analysis of glycosaminoglycan mixtures by ultra-high-performance liquid chromatography-mass spectrometry. Journal of Chromatography. A, 1225, 91–98. https://doi.org/10.1016/j.chroma.2011.12.063

Yang, G., Lai, C. S. W., Cichon, J., Ma, L., Li, W., & Gan, W.-B. (2014). Sleep promotes branch-specific formation of dendritic spines after learning. *Science (New York, N.Y.)*, *344*(6188), 1173–1178. https://doi.org/10.1126/science.1249098

Yang, G., Pan, F., & Gan, W.-B. (2009). Stably maintained dendritic spines are associated with lifelong memories. *Nature*, *462*(7275), 920–924. https://doi.org/10.1038/nature08577

Yang, S., Cacquevel, M., Saksida, L. M., Bussey, T. J., Schneider, B. L., Aebischer, P., Melani, R., Pizzorusso, T., Fawcett, J. W., & Spillantini, M. G. (2015). Perineuronal net digestion with chondroitinase restores memory in mice with tau pathology. *Experimental Neurology*, *265*, 48–58. https://doi.org/10.1016/j.expneurol.2014.11.013

Yang, S., Gigout, S., Molinaro, A., Naito-Matsui, Y., Hilton, S., Foscarin, S., Nieuwenhuis, B., Tan, C. L., Verhaagen, J., Pizzorusso, T., Saksida, L. M., Bussey, T. M., Kitagawa, H., Kwok, J. C. F., & Fawcett, J. W. (2021). Chondroitin 6-sulphate is required for neuroplasticity and memory in ageing. *Molecular Psychiatry*, *26*(10), 5658–5668. https://doi.org/10.1038/s41380-021-01208-9

Yang, S., Hilton, S., Alves, J. N., Saksida, L. M., Bussey, T., Matthews, R. T., Kitagawa, H., Spillantini, M. G., Kwok, J. C. F., & Fawcett, J. W. (2017). Antibody recognizing 4-sulfated chondroitin sulfate proteoglycans restores memory in tauopathy-induced neurodegeneration. *Neurobiology of Aging*, *59*, 197–209. https://doi.org/10.1016/j.neurobiolaging.2017.08.002

Ye, Q., & Miao, Q.-L. (2013). Experience-dependent development of perineuronal nets and chondroitin sulfate proteoglycan receptors in mouse visual cortex. *Matrix Biology : Journal of the International Society for Matrix Biology*, *32*(6), 352–363. https://doi.org/10.1016/j.matbio.2013.04.001

Yu, P., Pearson, C. S., & Geller, H. M. (2018). Flexible Roles for Proteoglycan Sulfation and Receptor Signaling. *Trends in Neurosciences*, *41*(1), 47–61. https://doi.org/10.1016/j.tins.2017.10.005

Zernov, N., Bezprozvanny, I., & Popugaeva, E. (2022). CaMKIIβ knockdown decreases store-operated calcium entry in hippocampal dendritic spines. *IBRO Neuroscience Reports*, *12*, 90–97. https://doi.org/10.1016/j.ibneur.2022.01.001

Zhao, R.-R., Ackers-Johnson, M., Stenzig, J., Chen, C., Ding, T., Zhou, Y., Wang, P., Ng, S. L., Li, P. Y., Teo, G., Rudd, P. M., Fawcett, J. W., & Foo, R. S. Y. (2018). Targeting chondroitin sulfate glycosaminoglycans to treat cardiac fibrosis in pathological remodeling. *Circulation*, *137*(23), 2497–2513. https://doi.org/10.1161/CIRCULATIONAHA.117.030353

Zhou, J., Tracy, T. S., & Remmel, R. P. (2010). Bilirubin Glucuronidation Revisited: Proper Assay Conditions to Estimate Enzyme Kinetics with Recombinant UGT1A1. Drug Metabolism and Disposition, 38(11), 1907–1911. https://doi.org/10.1124/dmd.110.033829

Zhu, W., Cheng, S., Xu, G., Ma, M., Zhou, Z., Liu, D., & Liu, X. (2011). Intranasal nerve growth factor enhances striatal neurogenesis in adult rats with focal cerebral ischemia. *Compound Delivery*, *18*(5), 338–343. https://doi.org/10.3109/10717544.2011.557785

Zimmer, B. M., Howell, M. E., Ma, L., Enders, J. R., Lehman, D., Corey, E., Barycki, J. J., & Simpson, M. A. (2021). Altered glucuronidation deregulates androgen dependent response profiles and signifies castration resistance in prostate cancer. Oncotarget, 12(19), 1886–1902. https://doi.org/10.18632/oncotarget.28059

Zimmer, G., Schanuel, S. M., Bürger, S., Weth, F., Steinecke, A., Bolz, J., & Lent, R. (2010). Chondroitin sulfate acts in concert with semaphorin 3a to guide tangential migration of cortical interneurons in the ventral telencephalon. *Cerebral Cortex*, *20*(10), 2411–2422. https://doi.org/10.1093/cercor/bhp309

Zimmermann, D. R., & Dours-Zimmermann, M. T. (2008). Extracellular matrix of the central nervous system: from neglect to challenge. *Histochemistry and Cell Biology*, *130*(4), 635–653. https://doi.org/10.1007/s00418-008-0485-9

Chapter 9: Appendices

Appendix 1. FACE gels of disaccharide bands following compound treatment

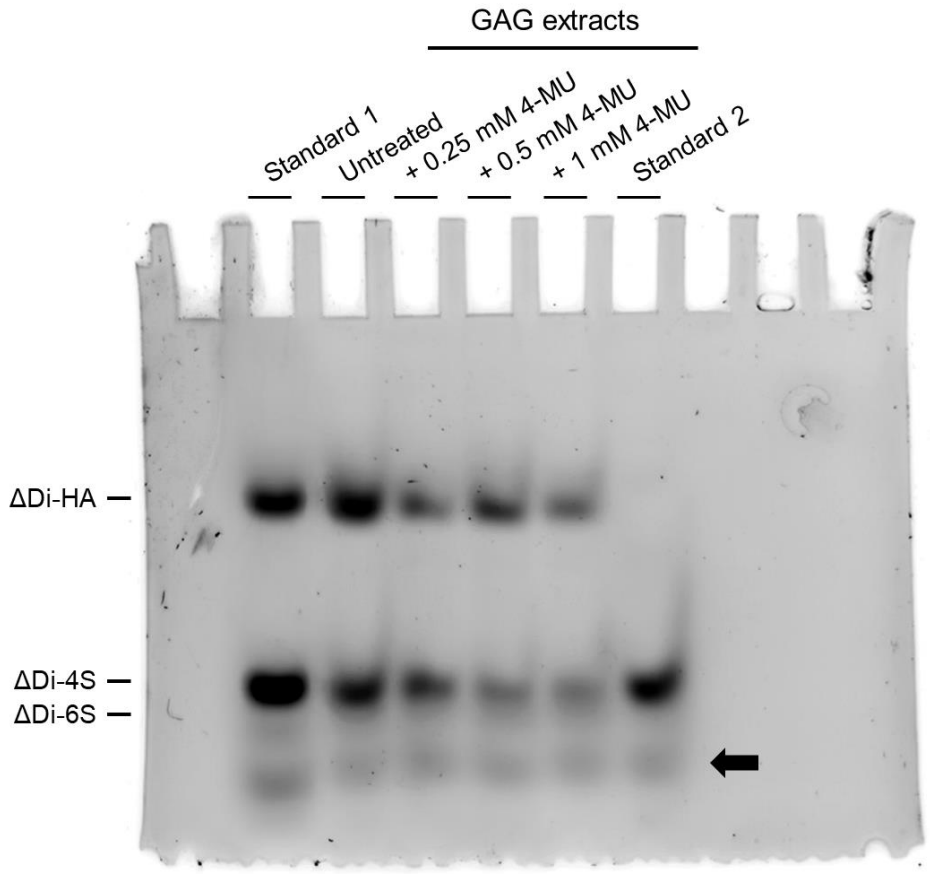

Figure 31. Full gel of disaccharide bands following 0.25 mM, 0.5 mM, and 1 mM of 4-MU. Distinct bands corresponding to the molecular weight of our standards were observed. The GAGs were digested into disaccharides using chABC and the resulting disaccharides were labelled with a fluorophore and electrophoresed in the FACE gel. ΔDi-HA combined with ΔDi-4S (standard 1) and ΔDi-6S (standard 2) were identified by comparing the migration of the band to standard disaccharides in the first two lanes. Treatment with increasing doses of 4-MU resulted in a significant decrease of ΔDi-HA band intensity and of ΔDi-4S or ΔDi-6S band intensities. Additionally, vague bands were observed consistently for every FACE experiment (arrow). These bands cannot be attributed to other types of low molecular weight CS-GAG disaccharides, given that these bands are also present underneath the disaccharide standards for HA and C4S/C6S, which were purchased from manufacturing companies (Sigma for HA and C4S, Biochemika for C6S) and should therefore be pure. Thus, these bands are likely artefacts due to 2-aminoacridone (2-AMAC) degradation.

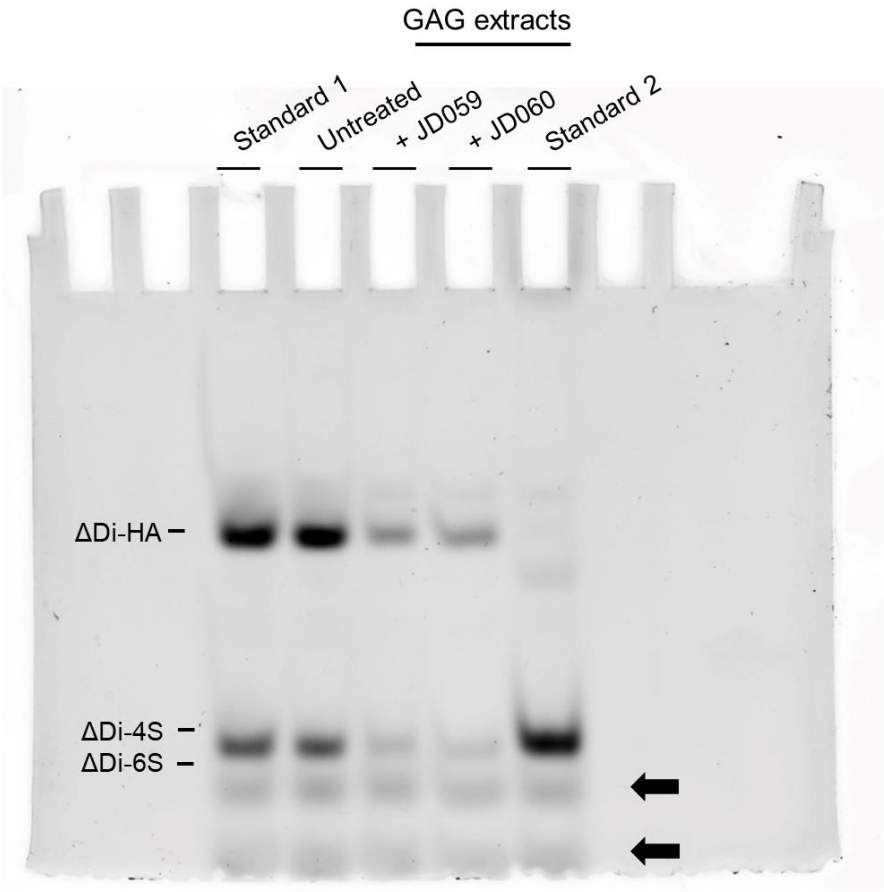

Figure 32. Full gel of disaccharide bands following 1 mM treatment of JD059 and JD060. Again, the GAGs were digested into disaccharides using chABC and the resulting disaccharides were labelled with a fluorophore and electrophoresed in the FACE gel. ΔDi-HA combined with ΔDi-4S (standard 1) and ΔDi-6S (standard 2) were identified by comparing the migration of the band to standard disaccharides in the first two lanes. Treatment with JD059 and JD060 resulted in an observable reduction of ΔDi-HA band intensity and of ΔDi-4S or ΔDi-6S band intensities. Additionally, vague bands were observed (arrows). As mentioned, these bands cannot be attributed to other types of low molecular weight CS-GAG disaccharides, given that these bands are also present underneath the disaccharide standards for HA and C4S/C6S, which were purchased from manufacturing companies (Sigma for HA and C4S, Biochemika for C6S) and should therefore be pure. Thus, these bands are likely artefacts due to 2-aminoacridone (2-AMAC) degradation.